CRANFIELD UNIVERSITY

S.J. LASKEY

A STUDY OF SINGLE AND TWO-PHASE FLOWS IN DEVICES WITH NARROW FLOW PASSAGES

SCHOOL OF ENGINEERING

PhD THESIS

CRANFIELD UNIVERSITY

SCHOOL OF ENGINEERING

PhD THESIS

S.J. LASKEY

A study of single and two-phase flows in devices with narrow flow passages

Supervisor: Dr H.C. Yeung

May 2002

This thesis is submitted in partial fulfilment of the requirements for the degree of Doctor of Philosophy

Abstract

In many industries, the depressurisation of gas-saturated solutions is controlled to regulate bubble formation. Carbonated drink dispensers need to depressurise solutions with minimum bubble formation, whereas dissolved air flotation nozzles need to produce the maximum number of micro-bubbles.

Four commercial carbonated drink dispensers were tested. The dispenser predicted to retain the most dissolved carbon dioxide at the outlet had a narrow annular gap of 0.1mm at the narrowest point. The pressure drop across this device varied linearly with water flow rate. When tested with two-phase air and water flow, the pressure drop decreased with increasing air flow at given water flowrates. This unusual behaviour was thought to be due to the narrow flow path. Carbon dioxide-saturated water tests supported these results as the pressure drop was found to be lower than the single-phase water tests. Thus under similar conditions, devices that create less turbulence would retain more dissolved gas.

Flow in coils was investigated, as they have flow characteristics that were potentially suitable for carbonated drink dispensing. Compared to straight pipes, flow in coils remained laminar until higher Reynolds numbers. The friction factors were also higher in coils than straight pipes. Coils made from 0.0025m internal diameter polyurethane tubing were tested, with coil diameters of 0.029m, 0.079m and 0.139m and lengths of 2, 3, 3.7, 5 and 7m. A method of estimating the friction factors in coils by treating them as a series of 90^{o} bends was proposed. The calculated results agreed with the present small tube experiments and with data from published literature for a range of tube diameters. At a given pressure drop, the shortest coil with the smallest coil diameter had the greatest dissolved gas concentration at the outlet and the highest flowrate. Furthermore, the concentration of dissolved gas at the coil outlet was greater than at the nozzle outlet.

Acknowledgements

In memory of my grandfather.

I am grateful to EPSRC, the department and Hoi Yeung for support. I am also grateful to SAW Technologies and especially Mike Scarffe for the supply of the carbonated drink equipment.

I would like to thank Craig Oliver, Jonathan Montgomery and Christian Omgba-Essama for continuous encouragement. I would also like to thank Janet Dare for her speedy proof reading and my parents for their amazing support that has been beyond the call of duty. I have also appreciated the support from my grandmother and brother.

I would finally like to congratulate a pupil from The Dame Alice Harpur School, Bedford for having a full understanding what research is about, at the age of 13. She said:

Q: What do research and kids on a long car journey have in common?
A: 'Are we nearly there yet?'

Notation

Abbreviations

atm - atmospheric
CFD - computational fluid dynamics
CO_2 - carbon dioxide
DAF - dissolved air flotation
H_2O - water
NV - needle valve
PT - pressure transducer (PT1 = pressure transducer 1…)
TC - thermocouple (TC1 = thermocouple 1…)

Nomenclature

A	- area	- mm^2
A	- factor in Friedel's equation, equation 2.3.2.6	
B	- velocity gradient of liquid, in equation 2.2.1.4	
c	- constant in equation 2.3.1.1	
C	- Chisholm constant	
C	- White's ratio of resistance in equation E.1.1.2	
C_G	- solubility of CO_2	- ($mgCO_2/mlH_2O$)
C_G^A	- solubility of CO_2 at atmospheric pressure and temperature	- ($mgCO_2/mlH_2O$)
C_G^R	- concentration of CO_2 dissolved at running pressure and temperature	- ($mgCO_2/mlH_2O$)
C_G^T	- solubility of CO_2 at trapped pressure and temperature	- ($mgCO_2/mlH_2O$)
d	- tube diameter	- mm
d_1	- tube diameter at atmospheric pressure, in section C.5.	- mm
d_2	- tube diameter under internal pressure, in section C.5	- mm
d_{av}	- mean bubble diameter	- mm
d_b	- bubble diameter	- mm
d_h	- hydraulic diameter	- mm
d_i	- annulus inner diameter	- mm
d_l	- laminar equivalent diameter	- mm
d_o	- annulus outer diameter	- mm
D	- coil diameter	- m
D_{av}	- average spiral diameter	- m
D_{min}	- minimum spiral diameter	- m
D_{max}	- maximum spiral diameter	- m
Dn	- Dean number	
e	- strain	
f	- Fanning friction factor	
fl	- factor in equation C.6.1	
F_d	- defined in equation E.2.1.5	
Fr	- Froude number	

g	- acceleration due to gravity	- m/s^2
G	- mass flowrate	- g/s
h	- wall thickness	- mm
h	- loss of pressure in equation 2.2.1.5	
Δh	- head loss	
k	- loss coefficient	
k_G	- gas density constant	
K_b	- loss coefficient of a bend	
K_c	- loss coefficient of a coil	
l	- length	- mm
l_1	- tube length at atmospheric conditions, in section C.5	- mm
l_2	- tube length under internal pressure, in section C.5	- mm
M	- molecular weight	
M_G^R	- total mass of CO_2 in system when running	- mg
M_G^T	- total mass of CO_2 in system when trapped	- mg
n	- flowrate index	
n_b	- number of 90^o bends	
N	- bubble concentration	
N_b	- number of bubbles	
p	- coil pitch	
P	- pressure	- bar
P_A	- absolute atmospheric pressure	- bar
P_c	- saturator (carbonator) pressure	- bar
P_R	- absolute Running Pressure	- bar
P_T	- absolute Trapped Pressure	- bar
P_v	- vapour pressure	- bar
ΔP	- pressure drop	- bar
ΔP_f	- frictional Pressure drop	- bar
Q	- volumetric flowrate	- ml/s
r	- radius	- mm
r_i	- inner radius of annulus	- mm
r_o	- outer radius of annulus	- mm
r^*	- annulus radius ratio	
R	- universal gas constant - 8314	- J/kmol K
Re	- Reynolds number	
Re^*	- modified Reynolds number defined in equation 2.3.4.2	
t	- temperature	- ^oC
t	- nozzle length	- mm
t_A	- atmospheric temperature	- °C
t_R	- running Temperature	- °C
t_T	- trapped Temperature	- °C
T	- time	- sec
u	- velocity	- m/s
V	- volume	- ml
V_1	- volume of water at atmospheric pressure, in section C.5	- ml
V_2	- volume of water when under internal pressure, in section C.5.	- ml

V_G	- volume of gas in tube at P_T (or P_R)	- ml
V_L	- volume of liquid trapped	- ml
V_S	- volume of gas in syringe	- ml
V_t	- total volume of trapping section	- ml
w	- width of plate	- mm
We	- Weber number	
x	- gas mass fraction	
X	- Lockhart and Martinelli parameter	
X_2	- defined as equation 2.3.2.19	
z	- distance in vertical direction	- mm
α	- void fraction	
β	- helix angle	- ^{o}
ε	- pipe roughness	- mm
ϕ	- two-phase multiplier	
λ	- liquid vol. fraction (Q_L/ (Q_L + Q_G))	
μ	- viscosity	- kg/m s
θ_b	- bend angle	- ^{o}
ρ	- density	- kg/m^3
ρ_G^A	- density of CO_2 at atmospheric conditions	- kg/m^3
ρ_G^R	- density of CO_2 at running pressure	- kg/m^3
ρ_G^T	- density of CO_2 at trapped pressure	- kg/m^3
σ	- surface tension	- N/m
σ_s	- stress	- N/mm^2
σ_c	- cavitation index	
ξ	- constant in equation 2.2.1.6	
ψ	- coefficient of effective collision of bubbles	

Additional subscripts

1	- inlet or before depressurisation
2	- outlet or after depressurisation
a	- annulus
c	- coil
G	- gas
H	- homogeneous
L	- liquid
s	- straight pipe
sc	- spiral coils
TP	- two phase

List of contents

List of figures

1 Introduction

1.1 Research background

This thesis is concerned with the depressurisation of single and two-phase flows, including gas-saturated liquids, which occur in several different industrial applications. Carbonated drinks dispensers are designed to depressurise carbon dioxide saturated water. The depressurisation should be controlled, so that as much carbon dioxide remains dissolved in solution as possible, to produce a supersaturated solution. If the gas is released prematurely, foam will form in the glass. Foam production means dispensing cannot be continuous, as the server has to wait for the foam to recede to fill the glass. This increases the dispense time and also makes the drink flat.

The dissolved air flotation (DAF) water treatment process uses the depressurisation of air saturated water to produce large numbers of bubbles. The process is outlined by Rees et al (1979), Zabel (1992) and Edzwald (1995). The depressurisation should be controlled to release all the dissolved air rapidly as microbubbles within a narrow size range (10-100μm). Particles in the water then attach to the bubbles so that the combined density is less than water. The agglomerates then float to the top of the tank, where they can be removed. Large bubbles are undesirable as they are wasteful and they disturb the sludge blanket at the top of the tank.

In beer dispensing the depressurisation is controlled to regulate the bubble formation and size of the foam 'head' on a beer. Beer dispensers can be made adjustable by combining a smooth restriction with turbulence generators, to produce the desired size of head. Examples of these are shown by Ash (1961a and b), Carnaghan (1964), Painter and Thomasson (1969) and Hildebrand and Yoakley (1972).

In a pump or piping system, cavitation bubbles form when the local pressure goes below the vapour pressure, which can be caused by pressure fluctuates due to turbulence. This is shown by Arndt (1981), Knapp et al (1970) and Brennen (1995). Rough surfaces or cracks and crevices also aid bubble formation. Extensive research has been conducted to design pump passages, while very little scientific investigation has been conducted on the flow passage of carbonated drink dispensers. From previous work on pumps and propellers it is clear that with carbonated drink dispensers, areas of turbulence should be avoided and the flow path should be as smooth as possible.

1.2 Depressurisation devices

Many different designs of carbonated drinks dispensers are commercially available. To maximise the number of customers served during busy periods, the flowrate through the device should be as high as possible without causing excessive turbulence. To minimise the release of the dissolved gas, the flow should ideally be

smooth and laminar. The nozzle, patented by Cornelius (1942, 1959 and 1960), alleged to have the best performance Scarffe (1997), appeared to comply with these considerations. It had a very narrow annular flow passage and was made of smooth plastic. However, this nozzle was relatively large. In another design the flow was depressurised through a series of small 1mm diameter passages. One more design had a series of chambers separated by perforated plates, and was very similar to devices used to generate microbubbles in DAF.

DAF nozzles aim to produce large amounts of microbubbles. For most DAF plants, 10% of the treated water is recycled to produce the air saturated water at around 5 bar to be reinjected into the DAF tank. As the production of gas-saturated water is costly, all the dissolved air should be released as microbubbles. Orifices and needle valves are the most commonly used devices. There are other more intricate designs that include impingement plates, a sudden enlargement and a directional change to create turbulence. These design principles have been investigated by Rykaart and Haarhoff (1995) and Jefferson (1997).

1.3 Factors affecting bubble formation

In order to evaluate and improve the performance of depressurisation devices, a good understanding is required of how bubbles are formed and what factors affect their formation in flowing liquid.

Brennen (1995) described how bubbles could be formed within a liquid by changing the thermodynamic or hydrodynamic conditions. When the pressure of a flowing liquid drops below the vapour pressure, at constant temperature, the liquid will cavitate. Turbulence and agitation can cause points of low pressure within the flow, resulting in bubble formation. Once the pressure is increased above the vapour pressure, the bubble will collapse. If the bubble collapse is near a solid surface, damage will be caused to the surface. Increasing the temperature of a liquid, at constant pressure can cause a liquid to boil. Unlike cavitation, once a bubble is formed, it usually continues to grow and rise in the liquid.

Bubbles can also be formed in a liquid saturated with dissolved gas, as with carbonated drinks. As the pressure of a liquid saturated with dissolved gas drops below a certain value, the excess dissolved gas will be released. This is because gas solubility increases with pressure. Solubility also increases as temperature decreases. Normally the release of dissolved gas occurs prior to cavitation or boiling. In contrast to cavitation and boiling, the bubbles contain the previously dissolved gas rather than gaseous liquid and are more stable. In the two industrial processes concerned in this thesis, i.e DAF and dispensing carbonated drinks, the bubbles are formed from dissolved gas.

Nucleation is the first stage of the bubble formation process. There are two main types of bubble nucleation outlined by Brennen (1995) and Whalley (1990). Heterogeneous nucleation requires a nucleation site for a bubble to form. This can be

an imperfection on a solid surface, a particle in the liquid, or a previously formed microscopic bubble in the liquid. Gas trapped in a scratch or crevice on a solid surface can also act as a site. In contrast, no pre-existing nucleation sites are required for homogeneous nucleation to take place. Random thermal motions of the liquid molecules can cause temporary microscopic voids that can act as the nuclei necessary to rupture the interface and to initiate bubble formation.

Fluid properties can have an influence on bubble formation. These include surface tension, viscosity, density and chemical composition. The hydrophobicity and roughness of a surface govern the size of the bubbles formed in heterogeneous nucleation. Ryan and Hemmingsen (1993) showed how a hydrophobic surface leads to surface 'de-wetting' and the formation of a contact base with the surface. The bubble contact base can grow up to 20 times the diameter of the initial cavity before detachment, resulting in relatively large bubbles. Bubbles are unable to 'de-wet' and make contact with a hydrophilic surface, releasing small bubbles earlier.

1.4 Flow behaviour in coils

In the search for a simple device suitable for the depressurisation of carbonated drinks, this thesis tests the suitability of coils. Coils are often used in heat transfer equipment. Previous researchers including Eustice (1910) and White (1929) found that coils have a greater pressure drop than straight pipes of the same diameter and length. Dean (1927) attributed the increase in pressure drop to secondary circulations present due to centrifugal forces. White (1929) found the flow in a coil remains laminar at higher Reynolds number than straight pipes. Due to the secondary circulation, the transition from laminar to turbulent flows is much less distinct than that of straight pipes. Here, it has been suggested that coils could create sufficient pressure drop and fit into a small amount of space, making them suitable for hand-held drinks dispensers.

Many authors have investigated single-phase flow behaviour in coils and there are many equations to calculate their friction factor, these are summarised by Srinivasan et al (1968) and Czop et al (1994). However, most of these works are for large diameter pipes. Very little information exists for diameters less than 6mm in single-phase flows, not to mention gas-liquid flows.

1.5 Objectives

The main objective of this work was to understand the mechanism of bubble formation when dispensing carbonated drinks, with the intention of designing a better drinks dispenser. The principles behind carbonated drink dispenser design have not been published in the literature but require the opposite principles to DAF. In contrast, the design principles of dissolved air flotation nozzles are well documented in the literature particularly by Rykaart and Haarhoff (1995) and Jefferson (1997). This information has been used to understand the factors that influence the gas release

and the requirements for controlling the concentration of dissolved gas in solution after depressurisation.

Preliminary experiments have been performed with four different commercially available carbonated drink dispensers. The nozzle designs were compared to find the nozzle with the smoothest pressure drop and the one most likely to retain the highest concentration of dissolved gas at the outlet.

The best presently available nozzle had a very narrow annular flow passage. Damianides and Westwater (1988), Triplett et al (1999) and Coleman and Garimella (1999) have found that narrow passages have different flow patterns and behave differently to larger diameter passages. Narrow annular passages have not been investigated before. Therefore the flow characteristics of single and two-phase flows within the annular nozzle were studied and compared to standard flow theories.

Coils have been found to have potentially suitable flow characteristics for dispensing carbonated drinks. Their suitability has been investigated in this thesis, the aim being to increase the concentration of dissolved carbon dioxide in solution after depressurisation, compared to the best presently available dispense nozzle. All previous research with coils has used tube diameters of greater than 6mm, which would be too big to fit into a drinks dispenser unit. Single and two-phase flows in 2.5mm diameter tube with coil diameters from 0.029 to 0.139m and a straight pipe have been investigated. The flow of gas-saturated water in coils has been researched for the first time.

The nozzle and coil performances and designs have been compared, to understand the most essential design features for carbonated drinks nozzles.

1.6 Research presented in this thesis

A review of published work from the literature is given in Chapter 2. It includes factors that affect bubble formation. This is followed by the different principles behind nozzle design for dissolved air flotation, soft drink and beer dispensers. Single and two-phase flow pressure drop theories are also detailed.

The results of preliminary experiments carried out on four presently used soft drink dispensers and a DAF needle valve can be found in Chapter 3. These experiments help to gain an insight into the depressurisation process and define the directions of subsequent work.

The experimental apparatus and methods used are detailed in Chapter 4. The experimental procedure and equipment varied slightly depending on the device being tested and the fluids being used. Two types of single-phase flow were tested: air and water. Two types of two-phase flows were tested: air and water and carbon dioxide saturated water.

Chapter 5 shows the experimental results of a test version of the soft drink dispenser that performed best in the preliminary experiments. The experimental results from flow in coils are shown in Chapter 6. The conclusions of this thesis are shown in Chapter 7.

2 Literature review

This chapter investigates the published research relevant to designing depressurisation devices for gas-saturated solutions. In order to understand the best designs to depressurise gas-saturated solutions, the principles of bubble formation must first be understood. Section 2.1 shows the various ways bubbles can be formed and their formation mechanisms. Section 2.2 looks at depressurisation devices, specific to dissolved air flotation, carbonated soft drinks and beer dispensers. The different principles behind dissolved air flotation nozzle design have been thoroughly investigated by various authors and are shown in Section 2.2.1. Details of various dissolved air flotation, carbonated soft drink and beer dispensers that are currently used or have been patented are included in Appendix B. Pressure drop principles and calculation methods for single and two-phase flows are shown in Section 2.3. Coils have been found to have greater pressure drops and maintain laminar flow to higher Reynolds numbers than equivalent lengths of straight pipe. The behaviour of flow in coils is detailed in Section 2.3.5.

2.1 Bubble formation

Bubbles occur in many different situations. They are desirable in some situations and hazardous in others. This section shows how bubbles can be formed and the mechanisms behind their formation.

2.1.1 Types of bubble formation

Various authors have studied bubble formation and dynamics. Brennen (1995) provided a good general overview of bubble dynamics. There are many different ways bubbles can be formed. Gas can be introduced into a liquid, or bubbles can be formed from within a liquid, by changing the thermodynamics or hydrodynamics. Increasing the temperature can produce vapour bubbles, as can a reduction in pressure or some combination of the two. If a constant temperature is maintained whilst decreasing the pressure below the saturated vapour pressure, a liquid can rupture by cavitation. In contrast, by increasing the temperature at a constant pressure, the liquid can rupture due to boiling. Bubbles can also be formed at ambient temperatures and pressures if a solution is supersaturated with dissolved gas, as with carbonated drinks. These different types of bubble formation are very similar and can often be difficult to distinguish. This research is primarily concerned with bubbles formed from the depressurisation of gas-saturated solutions.

2.1.1.1 Gas introduction into liquids

Forcing gas through a submerged device produces bubbles. Such devices can be orifices, perforated plates or porous sparging devices. The venturi effect can be used

to draw gas into a liquid from a porous stone, so the bubbles detach before they have a chance to grow. Bubbles from submerged orifices were studied by Clift et al (1978), Tsuge (1986) and Lin et al (1994). Kyriakides et al (1997) investigated various diameters of submerged nozzles. Rice and Howell (1987) looked at bubbles formed from submerged elastic holes. Flexible holes were found to reduce the complexities of fixed holes and produce large numbers of small bubbles, 100μm. Mechanical devices can also be used to create bubble dispersions, but are very energy intensive and produce bubbles of 100-400μm.

Electrolysis can be used to generate smaller bubbles with greater energy efficiency. The gas forms at nucleation sites on the electrodes, from which they grow and detach. Wilson and Hulme (1983) studied the bubbles attached to the electrode. Ptasinski et al (1995) found that by using a strong non-uniform electric field, electrolysis could produce bubbles with a mean diameter of 85μm.

2.1.1.2 Cavitation

Cavitation can occur in any liquid, when the pressure is reduced and maintained below the critical vapour pressure. The condition of the liquid and any contaminants present, gas or solid, and the pressure fields can all affect the occurrence of cavitation. The liquid properties can affect cavitation, including viscosity, surface tension and vaporisation characteristics. In flowing liquids, there are more variables that can affect the inception and subsequent character of cavitation including the absolute pressure and velocity and the critical pressure for a cavity to be formed and maintained. Cavitation also depends on the boundary geometry and surface conditions, including the cleanliness and the existence of crevices that might host undissolved gases. Detailed overviews of cavitation are given by Arndt (1981), Knapp et al (1970) and Brennen (1995). Plesset (1949) and Lehman and Young (1964) investigated the different stages of cavitation.

The 'cavitation index', calculated by equation 2.1.1, is a fundamental parameter for describing cavitation, shown by Arndt (1981) and Knapp et al (1970). If the cavitation index is less than the critical cavitation index, cavitation occurs.

$$\sigma_c = \frac{P - P_v}{\frac{1}{2}\rho u^2} \qquad \text{Equation 2.1.1}$$

σ_c - cavitation index
P - characteristic pressure
P_v - vapour pressure of liquid
u - characteristic velocity
ρ - density

Cavitation can interrupt the continuity of a liquid phase, displacing the liquid, modifying the flow pattern and altering the dynamic interaction between the liquid and its boundaries.

The collapse of cavities occurs when the pressure exceeds the vapour pressure. The violence of the bubble collapse can cause significant damage and erosion, creating noise and vibration. This can be devastating in the chemical industry by affecting machinery performance and modifying the flow hydrodynamics. Erosion can range from minor pitting after years, to disastrous structure failure over a short period of time. Cavitation can however also be a desirable and useful by-product, for example in the homogenisation of milk, industrial cleaning and in particular for cleaning false teeth. Fujikawa and Akamatsu (1983) looked at the shock waves caused by the collapse of bubbles. Plesset and Prosperetti (1977) attempted to solve the problem of the collapse of an empty cavity in liquids. Mitchell and Hammitt (1973) also studied bubble collapse.

Knapp et al (1970) described 4 main types of cavitation: travelling, fixed, vortex and vibratory. Travelling cavitation occurs at low pressure points in a flowing stream, along the solid boundary or in the bulk liquid. Fixed cavitation occurs in a flowing stream, when the liquid flow detaches from the rigid boundary of an immersed body. It appears as highly turbulent boiling on the surface and can extend well beyond the surface. Vortex cavitation occurs in areas of high shear, like a ship's propeller. It can also occur in a wake caused by a boundary separation, such as behind a sphere. Vortex cavitation can appear as fixed or travelling cavities and is steadier than other cavitation types. Vibratory cavitation occurs with no major flow, when the amplitude of the pressure from an oscillating pressure field goes below the vapour pressure. Vibrating submerged surfaces can set up pressure waves, causing cavities.

Cavitation has been studied in many different fluids. Lisle-Taylor (1997) studied cavitating hydrocarbons and Sarosdy and Acosta (1961) studied water and Freon. They both saw a visual difference between the cavitating fluids. Kamiyama and Yamasaki (1981), (1986) attempted to predict cavitation in various liquids.

Various authors have investigated the effect of cavitation around various different shaped objects. Ota et al (1992) researched cavitation effects around a rectangular cylinder. Katz (1984) looked at flat-faced cylinders and hemispherical headforms. Kubota et al (1992) looked at vortex cavitation on hydrofoils. Shimizu et al (1983) investigated cavitation of an annular type jet pump. The pressure on boundaries from cavitation bubbles was investigated by Ellis and Starrett (1983), Blake and Gibson (1987), Blake et al (1995) and Zhang et al (1993). Urata and Nakao (1993) looked at erosion induced by a cavitating jet from a V-shaped notch.

Turbulence and local pressure fluctuations have been shown to be fundamental to the occurrence of cavitation. This indicates that in order to reduce the number of bubbles formed during carbonated drinks dispensing, a smooth flow path and laminar flow may be required.

2.1.1.3 Boiling

In contrast to cavitation, boiling occurs when a body of liquid is heated under constant pressure to above the vapour pressure, producing bubbles. For boiling to occur there must be a small difference in temperature between the liquid and vapour. Once formed, the vapour bubbles then proceed towards the vapour phase above the liquid. Bubbles tend to nucleate on curved surfaces or irregularities on a surface. Whalley (1990) and Coulson and Richardson (1993) give general overviews of boiling.

To boil a liquid it must be superheated beyond its boiling point, as vapour bubbles at their boiling point are unstable and collapse spontaneously. Increasing the temperature of a pure liquid, above its boiling point decreases the surface tension and increases the vapour pressure, increasing the probability of nucleation. Blander and Katz (1975) tried to predict bubble formation. They found the rate of nucleation to be greatly dependent on the rate of growth and collapse of the bubbles. The rate of transfer of molecules between the liquid and bubble is slowest nearest its critical size.

There are three main types of boiling: interface, nucleate and film. Interface evaporation occurs when bubbles of vapour form on the heated surface and move to the vapour-liquid interface by convection. This exerts very little agitation on the liquid. Nucleate boiling occurs with a higher temperature difference when the bubbles form more rapidly with more centres of nucleation. The bubbles exert an appreciable degree of agitation on the liquid. Film boiling is only reached when a sufficiently high temperature difference is reached. In this case, the bubbles form so rapidly that they cannot escape from the hot surface and form a blanket over the surface, preventing the liquid from flowing on the surface.

2.1.1.4 Liquids saturated with dissolved gas

Gases are more soluble at high pressures and low temperatures. A liquid can become saturated with a dissolved gas at high pressures. Depressurisation of the solution causes the gas to be released and bubbles to form. The depressurisation can be controlled to minimise gas release so that a liquid is supersaturated at atmospheric pressure. The principle factors affecting bubble formation are similar to cavitation and boiling, but the saturator pressure also has an influence. This is discussed in more detail in Section 2.2. Ward et al (1986) modelled bubble formation in liquid-gas solutions near saturation value.

2.1.2 Bubble Nucleation

Brennen (1995) and Whalley (1990) both provided good overviews of general bubble nucleation. There are two main nucleation mechanisms: heterogeneous and homogeneous. Heterogeneous nucleation is the most common form of nucleation and requires a nucleation site for a bubble to form. Nucleation sites can be solid particles

or small bubbles, either suspended in the liquid or trapped in surface cavities after wetting. Bubbles will grow on the site until the liquid drag force sweeps the bubbles down stream. The nucleation rate depends on the fluid flowrate and the crevices on a solid. The size and number of bubbles produced at this stage will affect the total number of bubbles formed.

Homogeneous nucleation is an extreme case, where bubbles form without any pre-existing nuclei. Random thermal motions of the molecules within the bulk liquid can cause temporary microscopic voids that can act as the nuclei necessary for the interface to rupture and bubbles to grow. If no nucleation sites are present, a liquid can be superheated to well above its boiling point. Blander and Katz (1975) found that some liquids held at one atmosphere can be superheated to 88-90% of their critical temperature before boiling. For example, water can be heated to 250-275°C before boiling if no sites are present. Once growth is initiated it can be explosive, which can be a safety hazard in industry. The better the surface wetting the higher the probability that the nucleation will be homogeneous. Bisperink and Prins (1994) stated that for homogeneous nucleation to occur in gas-saturated solutions a dissolved gas supersaturation of 10^3 is required. However, carbonated drinks have a supersaturation of 5 times that at atmospheric pressure and hence in this case, bubbles are formed by heterogeneous nucleation.

Lubetkin (1995) and Brennen (1995) described an energy barrier to the nucleation process. In heterogeneous nucleation, the barrier height is influenced by the presence of a surface and its physiochemical properties. Both authors theoretically evaluated the barrier height for homogeneous nucleation, when no interface is present for bubble formation. Lubetkin used the well developed theory of nucleation of liquids from their vapour. It was applied to bubble nucleation with only minor modifications, with a reasonable degree of accuracy.

Jackson (1994) investigated energy effects on bubble nucleation, in water with dissolved air. It was found that some of the energy available went towards surface formation and bubble expansion, but the majority was used for nucleation. This energy could be provided by an increase in the system pressure. Low saturation pressures were found to produce many very small bubbles, whilst high gas concentrations produced an excess of large bubbles. Energy consumption was minimised using a low saturation pressure and pumping the liquid for higher transfer pressures. Nucleation in 'clean water' was found to require a higher level of energy, which resulted in only a few large bubbles being formed. The presence of impurities, particularly surface-active agents, increased the number of sites, lowering the nucleation energy, resulting in very large numbers of very small bubbles.

2.1.3 Theories of nuclei

Mesler (1986) described four different hypotheses to explain the stabilisation of gas nuclei in liquids. Two were dismissed experimentally. The most widely accepted model to describe possible sources of nuclei is the 'crevice model', also known as the

'Harvey model'. The model assumes a surface, like a wall or suspended solid particle, to be incompletely wet. Surfaces are known to have imperfections that can entrap gas, as a source of nuclei.

The second hypothesis for a possible source of nuclei, not dismissed experimentally by Mesler (1986), was the 'Varying permeability model'. The model assumes that bubble nuclei are stabilised in a liquid with a varying permeability skin. The formation of this skin on the bubble nucleus depends on the presence of surfactants. The skin is assumed to be permeable to gases until the ambient pressure is increased by a threshold amount. The skin is then impermeable to diffusion, until the pressure is lowered. Compression of the gas inhibits further decrease in the size of the nucleus and since the skin is impermeable, the gas cannot be dissolved.

The history of an experiment can influence the distribution and number of nuclei present. Mesler (1986) used high-speed pictures to show that when a bubble bursts from the liquid film, new bubbles can appear from where the bubble burst, creating new bubble nuclei. Mesler (1986) described three effective methods of removing gas nuclei, which are useful before performing homogeneous nucleation experiments. The first method involved subjecting a liquid to a high pressure for a short time. This increased the solubility of the gas and eliminated some of the nuclei. The second method suggested nuclei could be removed by degassing a liquid under vacuum and then leaving it to stand at atmospheric pressure. This allowed large nuclei to serve as nucleation sites, creating larger bubbles that rose to the interface and disappeared. Filtration was also used, using a filter with a pore size of 0.2 micrometers, so the larger nuclei would be unable to pass.

2.1.3.1 Heterogeneous nucleation sites

A classic example of heterogeneous nucleation sites is seen in a glass containing a carbonated drink. Bubbles can be observed originating from the same spot on the glass surface, even if the glass is emptied and refilled. If the glass surface is placed under a microscope, pits and cracks will be seen. Even after careful polishing, small imperfections will remain on the surface. If the liquid is pure and has no suspended particles, bubbles will not form in the bulk of the liquid. However, if a spoon of sugar is added to the drink, it will foam up rapidly, proving that bubbles need nucleation sites to form. This is similar to crystallisation when a crystal requires a nucleation site before it can start to grow. A site can be a rough surface, dirt or an another small crystal.

The stability and number of sites depends on the physical condition, properties and preparation of the surface and the properties of the liquid, e.g. surface tension. The number of sites is also influenced by how well the liquid wets the surface and how efficiently the liquid displaces air from the cavities. The poorer the wetting, the less violent the initial nucleation will be. Whalley (1990) stated that a typical cavity size is in the range of a micron, but a particular surface can have a wide range of sizes. The radius of a gas pocket in a wetted conical-shaped cavity has a minimum critical size

to allow bubble growth. Gas pockets smaller than the critical radius are thought to simply dissolve in the liquid. The critical radius is smaller at higher gas saturations. In theory, if the pressure is increased the critical radius will decrease.

The size and shape of a cavity mouth play a significant role in nucleation. Blander and Katz (1979) researched cavity shape and suggested an ideal shape to be conical with a circular opening. Coulson and Richardson (1993) showed that the nature of the surface makes a significant difference on a bubble's physical form and the contact area with the surface. Ryan and Hemmingsen (1993) showed that smooth hydrophobic surfaces produce far fewer bubbles than rough hydrophobic surfaces. The surface hydrophobicity effects the contact angle between the liquid and the nucleation site, as shown in Figure 2.1.1. A hydrophobic surface leads to surface 'de-wetting' and the formation of a contact base with the surface. This contact base can be up to 20 times the diameter of the cavity before detachment. With a hydrophilic surface, the bubble is unable to 'de-wet' the surface and make contact and is therefore released earlier, creating smaller bubbles. The bubble size with hydrophilic surfaces is independent of gas flowrate and a bubble will remain almost spherical. The addition of surfactant can be used to lower bubble size by reducing the surface tension.

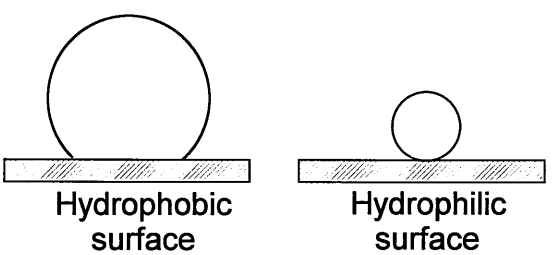

Figure 2.1.1 Diagram of the effect of hydrophobicity.

2.1.4 Bubble life after nucleation

Lubetkin (1995) split bubble evolution into five parts: nucleation, detachment (if heterogeneous), growth, rise and bursting. These processes run concurrently and are often difficult to separate experimentally.

Temperature, pressure, surface tension and inertial forces all affect the bubble growth rate. If dissolved gas is present, its concentration, solubility and degree of supersaturation influence the bubble growth. Bubbles continue to grow on a surface until the buoyancy and viscous drag forces overcome the surface tension. Szekely and Fang (1973) showed that inertia and surface tension control initial bubble growth but viscous forces slow the growth. The growth of a single bubble was modelled by Subramanian and Weinberg (1981). Epstein and Plesset (1950), Scriven (1959), Cooper and Chandratilleke (1981), and Cable and Frade (1987), (1988) also investigated bubble growth.

Once detached, bubbles continue to grow by coalescence, this decreases the total number of bubbles. The amount of coalescence depends on turbulence and the surface

chemistry. Prince and Blanch (1990) and Oolman and Blanch (1986) studied coalescence. Bubble growth can also be dependent on the presence of dissolved gas. Ishikawa et al (1986) experimented with carbon dioxide desorption in supersaturated solutions and looked at the mass transfer and drag coefficients of rising bubbles.

Jameson (1978) investigated how bubble shape can affect its rise velocity. The stability of a bubble at the liquid surface is dependent upon the rate of thinning of the liquid layer, on the upper surface of the bubble. Surfactants can be added to lengthen the bubble lifetime at the surface, so that very stable foams can be formed. In the absence of surfactants, bubble collapse is very rapid.

Many authors have found modelling the stages of bubble formation mathematically very complex. Plesset and Prosperetti (1977) attempted to theoretically model the different stages of bubble formation through to collapse. Matsumoto and Takemura (1994) modelled bubble motion numerically using conservation equations. Takemura and Matsumoto (1994) extended the work, comparing numerical and experimental results on the affects of internal phenomena on gas bubble motion. They predicted bubble radius well and experimentally detected light emission from a collapsing bubble that coincided with the calculated bubble collapse time. Takemura et al (1995) continued the work experimentally and numerically. Takahira et al (1994) looked at the theoretical dynamics of a bubble cluster. Rykaart and Haarhoff (1995) proposed a simple bubble growth model applied to DAF. Lisle-Taylor (1997) stated that it was almost impossible to produce an analytical solution for cavitation, due to its complexity.

2.1.5 Discussions

Many different factors effect when and where bubbles form. In cavitation, bubbles form in areas of low pressure, often caused by turbulence. There are several theories on how bubbles form, but some are still unproven. For heterogeneous nucleation, a nucleation site is needed for a bubble to form. A site can be a solid particle in solution or scratches and crevices on a surface. Gas bubbles in solution or trapped in surfaces can also aid bubble formation. A surface hydrophobicity and roughness can determine the size of bubbles formed. A hydrophilic surface produces small bubbles, as they are unable to de-wet the surface. Bubbles formed on hydrophobic surfaces, in contrast, can produce a large contact base with the surface and hence large bubbles. The fluid properties also influence bubble formation, including surface tension, viscosity, density and chemical composition. For gas-saturated solutions, bubble formation depends on the solubility of the dissolved gas and the saturator operating conditions, including the saturator pressure and efficiency and the degree of saturation of the solution.

2.2 *Depressurisation devices*

During the depressurisation of saturated water, the depressurisation device plays a large part in determining bubble formation. Descriptions of designs for DAF nozzles and drink dispensers are shown in this section and Appendix B.

Various design principles are used for the depressurisation of gas-saturated liquids, which depend on their purpose. Dissolved air flotation requires that all the dissolved gas be released as regular sized micro bubbles. This is achieved by creating large amounts of turbulence in the flow. In contrast, carbonated soft drink dispensers require a laminar flow, so that the gas remains dissolved in solution and the drink remains fizzy for longer. Beer dispensers require a controlled amount of turbulence, to produce the desired size of head on the beer.

2.2.1 Dissolved Air Flotation (DAF)

Flotation is a solid-liquid separation process. The process uses microbubbles to lift suspended particles out of water by floating them to the top of the tank. The particles attach to the bubbles so that their combined density becomes less than water and they float to the top of the tank together. The layer of sludge at the top of the tank is then scraped off and removed.

Flotation is used in preference to sedimentation to separate very small particles, with densities close to water, which would take a long time to settle. Heinänen et al (1995) and Casey (1993) compare sedimentation and dissolved air flotation (DAF). Bubbles suitable for flotation can be generated in different ways: dispersed air flotation, vacuum flotation, electroflotation and dissolved air flotation. Bratby and Marais (1986), Gochin (1990), Montgomery (1985), Zabel (1992), Rees et al (1979), Burns et al (1997) and Yoon (1993) discuss these processes. DAF is a viable method of producing small bubbles and is preferred in the water industry. Dissolved air flotation is has been discussed further in this thesis.

The depressurisation of the flow of air saturated water produces bubbles. The flow is saturated by pressurising air and water together in a saturator, dissolving the air. Upon release of the pressure, bubbles are formed. To achieve maximum flotation, the depressurisation must be controlled to produce a consistent bubble size. Optimum flotation is achieved with uniform sized bubbles with diameters of 10μm and 100μm. If the bubbles are too large, they use up a large proportion of the dissolved air. Large bubbles also interfere with the slow rising flocs and the stability of the sludge blanket at the top of the tank. In contrast, if the bubbles are too small, the combined particle and bubble density may be greater than water and the particles may sink.

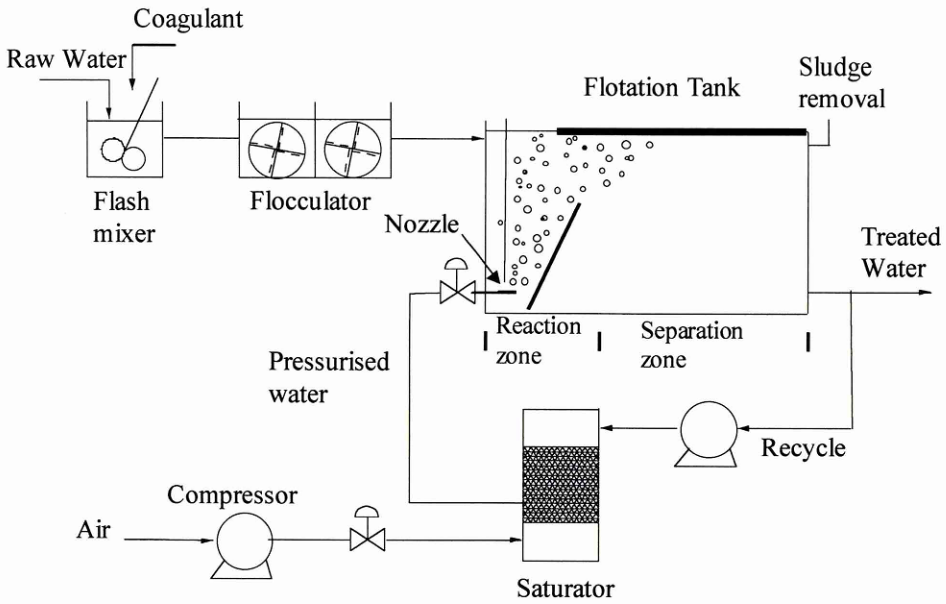

Figure 2.2.1 Schematic diagram of the DAF process.

A typical DAF process scheme is shown in Figure 2.2.1. The raw water is shown mixing with the coagulant in rapid mixers. The coagulated water is then flocculated by gentle agitation in a two-stage flocculator. The flocculated water then enters the flotation tank where it is combined with the depressurised saturated water, containing fine air bubbles. In the flotation tank, the bubbles attach to the flocs and the bubble-floc agglomerates rise to the top of the tank. Scrapers then remove the sludge blanket. Some of the treated water is then recycled back to the saturator.

Rees et al (1979), Zabel (1992) and Edzwald (1995) give good overviews of the complete DAF treatment process. Haarhoff and Vanvuuren (1995) and Edzwald (1995) surveyed the best design parameters for the process. Montgomery (1985) and Casey (1993) summarise the process design. Heinänen et al (1995) compared small and large plants. Gochin (1990) modelled the tank as a perfectly mixed flow cell. Rykaart and Haarhoff (1995) suggested a simple bubble growth model. Yoon (1993) demonstrated the hydrodynamics of bubble-particle interaction.

Careful saturator design is important because it uses about 12% of the capital cost and 50% of the operating cost of the total DAF process. A large saturator is needed with a pressure of at least 300kPa, as air is not very soluble in water. An efficiency of 90% can be reached with a packed saturator and 60-70% in an unpacked saturator. A packed saturator with a minimum packing depth of 0.3 - 0.8m, is most efficient. The following papers discuss the saturator design: Bratby and Marais (1975), Haarhoff and Rykaart (1995), Haarhoff and Steinbach (1997), Rees et al (1979), Zabel (1992) and Steinbach and Haarhoff (1997).

Bubble and particle attachment depends on whether the bubble 'sticks' to the particle. It only occurs if the water layer between the particle and bubble is ruptured during the

time they collide. If this does not happen, the bubble 'bounces' and attachment is not achieved. This is governed by the rules of thermodynamics and surface chemistry, and is not a rate process. Heinänen et al (1995) studied the effect of surface chemistry on attachment. Successful attachment requires a hydrophobic surface with low or no charge. Unfortunately, coagulation forms hydrophilic flocs but hydrophobicity can be encouraged with the addition of organics. Gochin (1990) and Edzwald (1995) investigated the effect of hydrophobicity on attachment. Air bubbles have a negative charge and hence, positive or zero charged flocs could attract air bubbles. Van der Waals forces also play a part. Liers et al (1996) studied bubble-floc attachment efficiency and the air-to-solids volume ratio. Fukushi et al (1995) modelled collision and attachment.

The main parameters that affect the efficiency of DAF are: the air-solids ratio, the hydraulic loading, the saturator characteristics and the injection nozzle performance. In this thesis the bubble formation and the performance of an injection nozzle are investigated.

2.2.1.1 Nozzle operating principles

The geometrical design and operating conditions of an injection nozzle can influence the size and distribution of the microbubbles produced. A DAF nozzle should reduce the saturation pressure and release all the dissolved gas as a mist of fine evenly sized microbubbles. Strong turbulence is needed within the nozzle, to knock all the dissolved gas out of solution. However, the outlet flow should have minimal turbulence and velocity so as not to disturb the flocs of the water to be treated.

There are many different types of nozzle in use. Some water companies use complex designs, but needle valves are also in common use. Even simple gate valves can be used. Nozzles can be fixed like an orifice or adjustable like a valve. Ideally nozzles should be made out of stainless steel as erosion can occur due to cavitation from the air release. Dead zones should be avoided to minimise the hold-up of bubbles and the possibility of coalescence.

Some authors suggested that the pressure drop should be rapid for an instantaneous gas release. However, the pressure should not go below the outlet pressure. Van Puffelen et al (1995) suggested that a gradual expansion of the flow area could lead to better bubble formation.

2.2.1.1.1 Nozzle positioning

Takahashi et al (1979) found that bubbles grew with height above the nozzle, until above 80cm when they did not appear to grow. At low saturator pressures, the bubble growth was remarkable as the vertical height from the nozzle outlet increased. Gochin (1990) suggested that multiple nozzle combinations could provide a better distribution of air bubbles. Van Puffelen et al (1995) stated that commercially

available nozzles have small capacities, meaning more nozzles are needed to provide an even distribution of the saturated water. N.V Dune waterworks of South Holland (DZH) is said by Van Puffelen et al to have shown improved flotation efficiency by pointing the saturation stream downwards, i.e. counter-current, which leads to better mixing and a higher residence time of the bubbles near the nozzles. Eades and Brignall (1995) investigated counter-current DAF and found that one redesigned nozzle was sufficient in the centre of a tank.

2.2.1.1.2 Effect of operating conditions

Different nozzle sizes require different flow and pressure combinations to deliver the same amount of air. The water temperature, hydrophobicity of the nozzle material and chemical constituents in the water, can all effect the bubble size. Urban (1978) tested three types of water: distilled, tap and evaporated tap. Each produced similar bubble numbers and rise times, which suggests that nuclei were not present in the bulk water. Jefferson (1997) found that increasing the surfactant concentration and altering the liquid gas interface properties significantly decreased the mean bubble size. Urban (1978) found that the addition of surfactant increased the number of bubbles and their rise time. Hemmingsen (1978) also investigated the addition of surfactants.

Further control of bubble size is possible by adjusting the saturation pressure. Takahashi et al (1979) and Wang and Ouyang (1994) both found that increasing the dissolved pressure, significantly increased the gas flowrate generated by the nozzle. However, an increase in saturator pressure also corresponded to an increase in the operating costs. Wang's experimental results, using dissolved carbon dioxide, are shown in Figure 2.2.2.

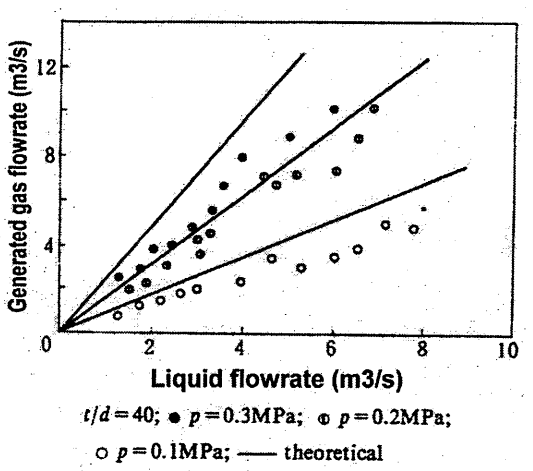

Figure 2.2.2 Effect of saturator pressure on generated gas flowrate. Wang and Ouyang (1994).

De Rijk et al (1994) and Takahashi both found the mean bubble size decreased with an increase in saturator pressure. De Rijk's results are shown in Figure 2.2.3. The bubble size was also found to decrease with an increased flowrate, but this became

less significant as the saturation pressure increased, until at 6.2bar where there was little difference.

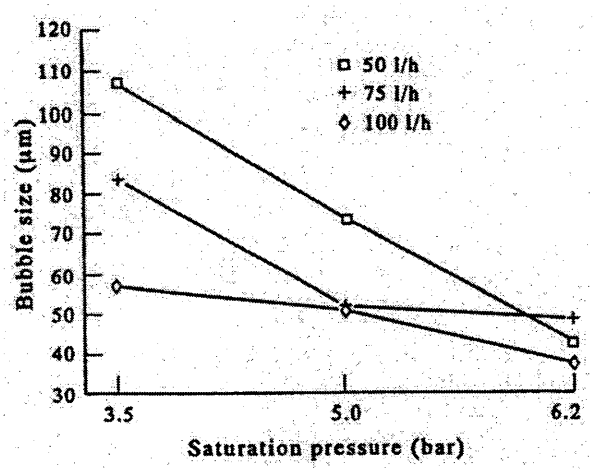

Figure 2.2.3 Relation between median bubble size and saturation pressure using a needle valve, with flowrates of 50, 75 and 100l/h. De Rijk et al (1994).

Rykaart and Haarhoff (1995) results contradicted other authors results and found no difference in the median bubble diameter for the saturator pressures of 200kPa and 500kPa. There was however, a significant increase in the macrobubble fraction of up to almost 10% at the higher pressure, compared to 3% at the lower pressure. The suggested theory for this was that the bubble growth was similar but more coalescence took place at the higher pressure. More coalescence was possible at the higher pressure because the velocity was greater producing larger eddies, when at the lower pressure there was less energy to be dissipated. Takahashi found the air flowrate increased with the liquid flowrate. The number of generated bubbles was strongly influenced by, and increased with, liquid flowrate and dissolved pressure.

Steinbach and Haarhoff (1997) studied the effect of the saturator pressure and efficiency on the air precipitation efficiency of the nozzle. The air precipitation efficiency is the amount of air available for flotation, calculated as the ratio between the actual air mass precipitated, and the maximum mass of air that could theoretically be precipitated. Increasing the saturator efficiency was found to increase the air precipitation efficiency, but was more significant at the low saturator pressure, 200kPa. Increasing the saturator pressure was also found to increase the air precipitation efficiency, which was more marked at the lower saturator efficiency. They found that the saturator efficiency and pressure had a greater influence on the air precipitation efficiency than the geometrical design of the nozzle.

2.2.1.2 Nozzle design principles

Many different types of depressurisation devices are utilised in DAF. Different geometric design principles are used to reduce the pressure and induce turbulence.

Needle valves are frequently used, as are simple orifices. Needle valves have definite disadvantages because they block easily and are difficult to clean. Other nozzle designs vary in the amount of intricacy with which the turbulence is created. Adjustable nozzles are advantageous, particularly if the adjustment can be automated. The adjustment means the ratio of saturated water to water being treated can be kept constant. Examples of DAF nozzle designs that are currently used are detailed in Appendix B.1. Urban (1979) found intricate designs were unable to create significantly more turbulence than a simple open device and had no significant advantages over the intricate designs.

The widely utilised WRC nozzle, shown in Appendix B.1, has been found to produce smaller bubbles than a needle valve. A combination of sections to reduce the pressure and induce turbulence can be used. Two orifice plates parallel to each other create a chamber. They are spaced apart so that the flow has a substantial change in direction and impinges on the walls of the chamber, creating strong turbulence. The inlet orifice is designed to control the flowrate and to drop a large proportion of the pressure, whilst releasing the majority of the dissolved gas into the chamber. A shroud member is located downstream of the second orifice to reduce the velocity of the water before it is mixed with the flocculated water, to reduce floc breakage.

The effectiveness of different nozzle design principles has been investigated by various authors and is shown in this section. These principles include the orifice dimensions, nozzle length, a change in direction, an impinging surface and diverging cones to decrease the velocity.

2.2.1.2.1 Orifice dimensions

Jefferson (1997) found that increasing the diameter of an orifice increased the coalescence, the mean bubble size and the number of bubbles with a diameter of more than 70μm. The results are shown in Figure 2.2.4. It was suggested that each stage of bubble formation could be affected by the change in orifice diameter.

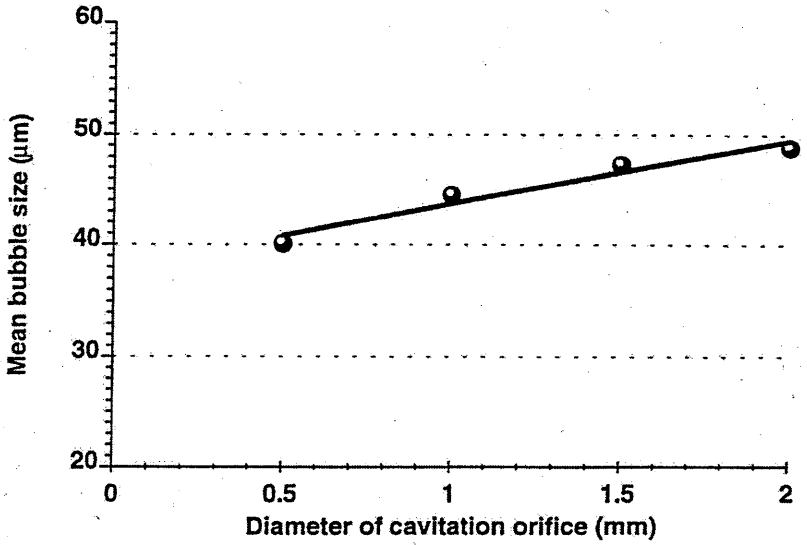

Figure 2.2.4 Effect of orifice diameter on the mean bubble diameter. Jefferson (1997).

Urban (1978) also found that increasing the diameter of an orifice for a given saturator pressure slightly increased the volume of gas liberated, but fewer and larger bubbles were produced. No trend on bubble formation was found when the effect of orifice thickness was tested with sharp-edged orifices with thicknesses of between 0.26mm to 5.35mm. This was attributed to the bubbles only forming on the top edge of the orifice.

Urban (1978) also tested multiple orifices on a single plate. From 1 to 7 orifices per plate were tested, with decreasing diameters, so that each plate produced the same flowrate as a single 1.4mm diameter orifice. No obvious trends were found at a high saturator pressure, 653 kPa or with surfactant present. At a lower saturator pressure, 377kPa, with no surfactant, it was found that with an increase in the number of holes, the number of bubbles produced increased. There was also a corresponding decrease in bubble diameter. This was possibly due to the increased circumference available for nucleation.

2.2.1.2.2 Impingement plates

Impingement plates are a common feature in DAF nozzles. They are used to control the size of bubbles formed by breaking them up. Rykaart and Haarhoff (1995) tested an impinging surface, as shown in Figure 2.2.5. The nozzle was 31mm long with a 2.5mm diameter nozzle channel. The surface was tested at 5, 10, 15 and 20mm from the nozzle. Two different saturator pressures were tested of 200kPa and 500kPa.

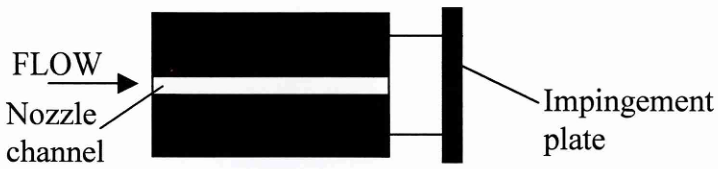

Figure 2.2.5 Experimental impinging surface, tested by Rykaart and Haarhoff (1995) and Steinbach and Haarhoff (1997).

At the low saturator pressure, 200kPa, the impinging surface was found to have no effect on the median bubble size and less than 3% of the bubbles were classified as macrobubbles. At a higher saturator pressure, 500kPa, with the surface close to the nozzle outlet, the median bubble size was significantly smaller. However, the macrobubble fraction increased linearly with the distance of the impinging surface to almost 10%. The macrobubble fraction results for both pressures are shown in Figure 2.2.6. The smaller median bubble size at the higher pressure was suggested to be due to fragmentation of the bubbles by the surface or additional nucleation sites being formed on impact. The increase in the macrobubble fraction with the distance of the plate, at the higher pressure was explained by energy dissipation in eddies. When the plate was close, very little of the energy could be dissipated by eddies at the nozzle outlet, but as it got further away, more of the energy could be dissipated in eddies, allowing for more coalescence. At the lower saturator pressure there was less energy to be dissipated and hence the effect of the impinging surface was less.

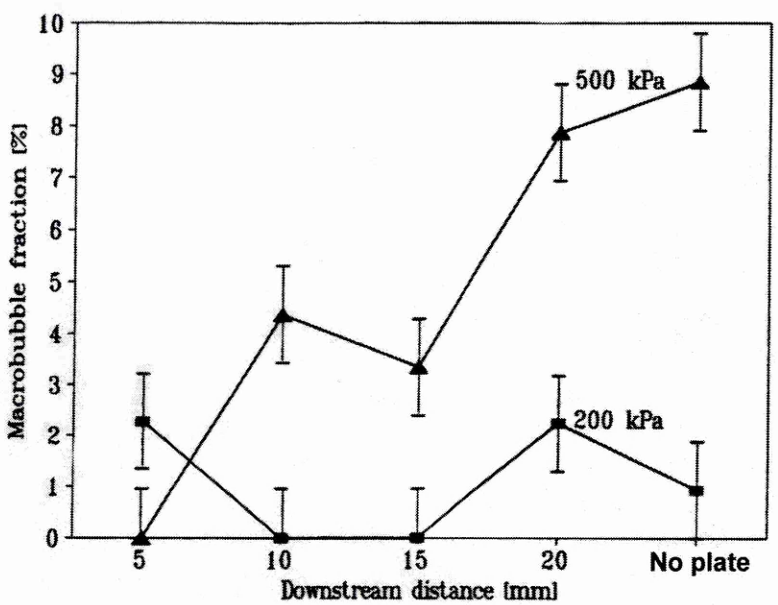

Figure 2.2.6 Effect of saturation pressure and downstream distance of the impinging surface, on the macrobubble fraction, with confidence intervals of 90%. Rykaart and Haarhoff (1995).

Jefferson (1997) also investigated the effect of the distance of an impingement plate on the mean bubble size. Figure 2.2.7 shows that the mean bubble size was only affected in his experiments when the impingement plate was between 1 and 5mm

away from the nozzle exit. A minimum mean bubble diameter was found when the plate was close to the nozzle, 3mm. The impact velocity at this distance would have been high and hence, there would have been a large force to aid bubble break up. It was also suggested that the plate could also reduce coalescence by slowing the velocity of the flow and reducing degree of turbulence.

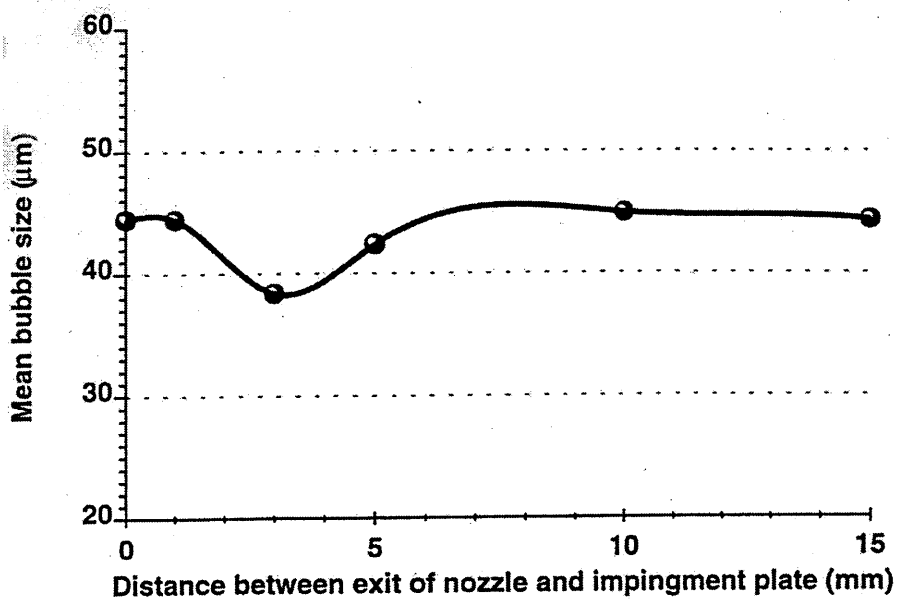

Figure 2.2.7 Effect of impingement plate on the mean bubble size. Jefferson (1997).

Steinbach and Haarhoff (1997) investigated the influence of an impinging plate using a similar nozzle to Rykaart. Two different channel diameters, 1 and 2 mm, were tested, both with a length of 5mm. Plate distances of 5 and 13mm from the nozzle exit were tested. They found that the presence of the impinging plate lead to a higher air precipitation efficiency. The effect was greater with the larger channel diameter. The plate distance was found to have no influence on the air precipitation efficiency. In most cases the air precipitation efficiency seemed to decrease with the increasing nozzle diameter, but this was not clear. The operating conditions, saturator pressure and efficiency were found to have a far greater influence on the air precipitation efficiency than the nozzle geometry.

2.2.1.2.3 Directional change

Rykaart and Haarhoff (1995) tested the effect of a sudden change in direction of the flow on bubble formation with two nozzles, one with and one without a bend. A diagram of the nozzle with the bend is shown in Figure 2.2.8. The bend was found to significantly reduce the macrobubble fraction, but made little difference to the median bubble diameter. This was attributed to bubbles breaking in the bend.

Figure 2.2.8 Test Nozzle as used by Rykaart and Haarhoff (1995) for change in direction.

2.2.1.2.4 Diverging outlet

The degree of turbulence in the bubbly flow before meeting the bulk flow can be reduced with a tapered outlet. Rykaart and Haarhoff (1995) tested a 33mm long, 3mm diameter nozzle with a 60mm long tapered outlet with a rectangular exit section measuring 40mm by 4. A diagram of the nozzle is shown in Figure 2.2.9. The presence of the tapering outlet was found to significantly reduce the median bubble diameter at the high saturator pressure, 500kPa. It also reduced the macrobubble fraction significantly at the high and low saturator pressures. The solid edges of the tapered outlet limited eddy formation and slowed the jet down with limited bubble coalescence. It was hypothesised that the large eddies formed at the interface between the edge of the jet and stagnant water, without the taper, could contribute significantly to bubble coalescence.

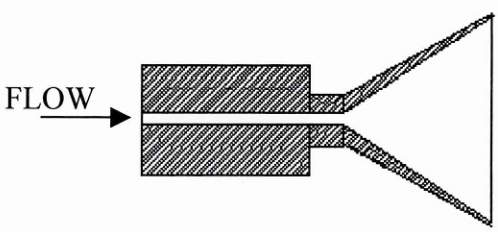

Figure 2.2.9 Tapered nozzle as tested by Rykaart and Haarhoff (1995).

Jefferson (1997) studied the effect of the angle of the diverging cone. The angle of the expanding jet was found to be 45°. The results, in Figure 2.2.10, show a decrease in the mean bubble size, with an increase in the cone angle, providing the cone angle was less than the natural angle of the expanding jet. A minimum bubble size was achieved at an angle of 45°, at this angle the flowpath was not affected, and turbulence was reduced. The figure also shows the affect of introducing an impinging plate after the diverging nozzle, which increased the mean bubble size. However the same mean bubble size of around 38μm was produced with the 45° tapered nozzle alone, as with a nozzle with an impingement plate 5mm away.

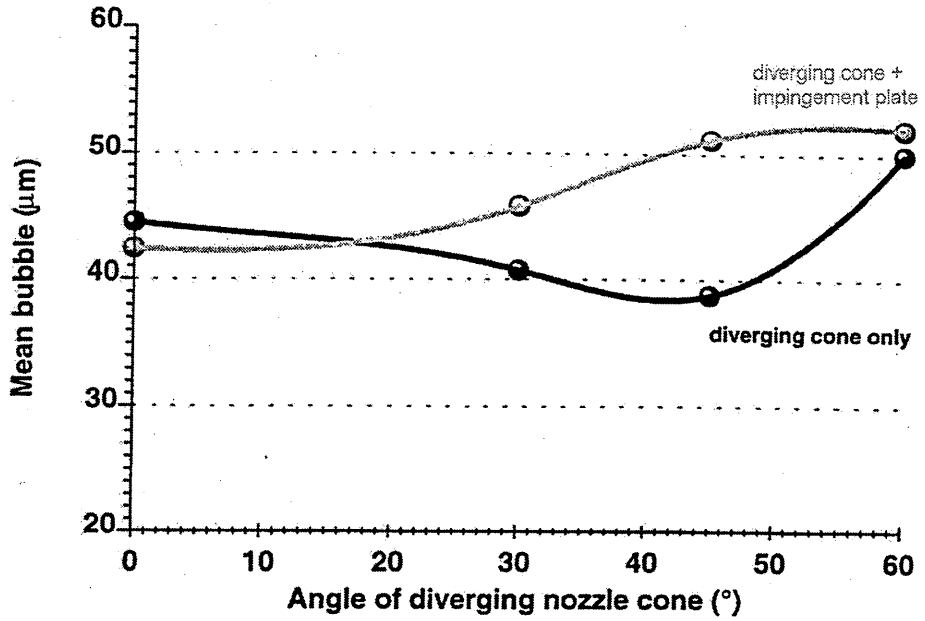

Figure 2.2.10 Effect of diverging cone on the mean bubble size. Jefferson (1997).

2.2.1.2.5 Nozzle length

Jefferson (1997) tested nozzle lengths of 0 to 20mm, with a 5mm diameter channel. He found the mean bubble size to increase with nozzle length, up to a maximum size, with an 11mm nozzle. The bubble size then decreased again with the 20mm long nozzle, to the smallest bubble size recorded. These results are shown in Figure 2.2.11. He also found the bubble concentration to increase with nozzle length. He suggested that nozzle length only affected the growth stage of bubble formation and any gas not released at this stage would have remained dissolved in solution and be wasted. A shorter nozzle may have had less time to release the excess gas, resulting in a reduction in the total number of bubbles. It was concluded that long nozzles were necessary for the maximum release of the dissolved air.

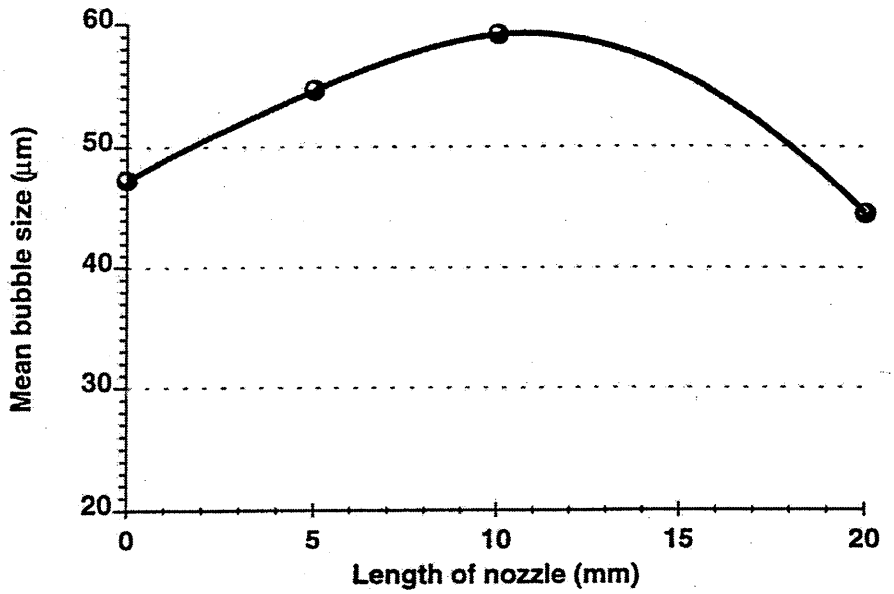

Figure 2.2.11 Effect of nozzle length on the mean bubble size. Jefferson (1997).

Takahashi et al (1979) tested smaller diameter nozzles of 0.2 to 0.4mm, with lengths of 2 to 50mm. They tested the ratio of nozzle length, t, to hole diameter, d, with eight different nozzles of the type shown in Figure 2.2.12. Figure 2.2.13 shows that the mean bubble diameter increased with nozzle length. This was particularly marked at low saturator pressures. It was also found that increasing the nozzle length decreased the generated air flowrate.

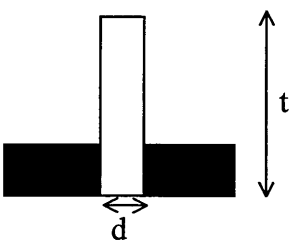

Figure 2.2.12 Type of nozzle tested by Takahashi et al (1979).

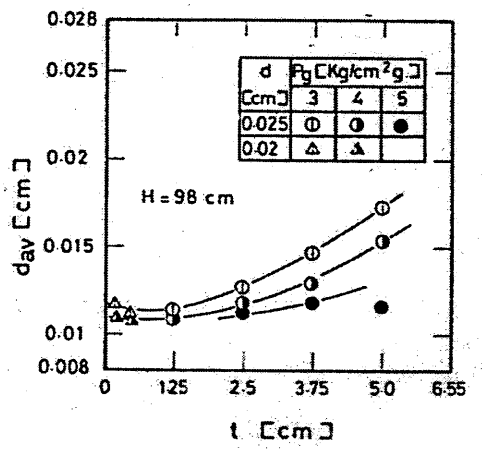

P_c - saturator pressure
d - nozzle diameter
t - nozzle length
d_{av} - mean diameter of bubble

Figure 2.2.13 Effect of nozzle length on generated bubble size. Takahashi et al (1979).

Takahashi et al and Jefferson both observed an increase in bubble size with short nozzle lengths, but Jefferson recorded a decrease in the bubble size with a 20mm nozzle, contradictory to Takahashi et al's results. Jefferson's nozzle diameter, 5mm, was however, significantly larger than Takahashi et al, which was 0.2-0.4mm. There was also a difference in the bubble size range, which was 40 to 60μm for Jefferson's experiment and 30 to 180μm from Takahashi et al.

Wang and Ouyang (1994) also studied the effect of the ratio of length, t, to diameter, d, ratio on the generated gas rate. They used nozzle lengths of 20 to 45mm and diameters 0.5 to 3mm. Figure 2.2.14 shows that increasing the ratio of t/d slightly decreased the generated gas flow. The bubble concentration was found to increase slightly with the t/d ratio, as shown in Figure 2.2.15. They suggested that a longer nozzle increased the intensity of turbulence of the liquid, releasing more dissolved gas. This is in agreement with Jefferson's results.

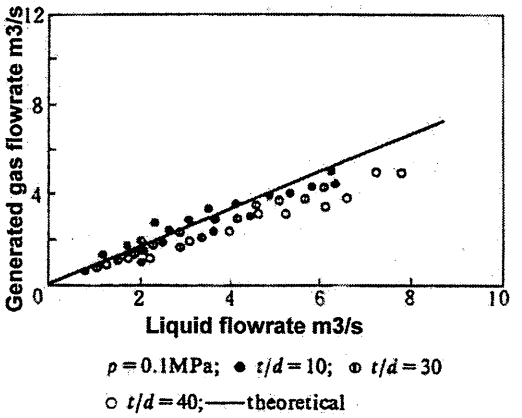

Figure 2.2.14 Effect of nozzle geometry on the generated gas flowrate P=0.1Mpa. Wang and Ouyang (1994).

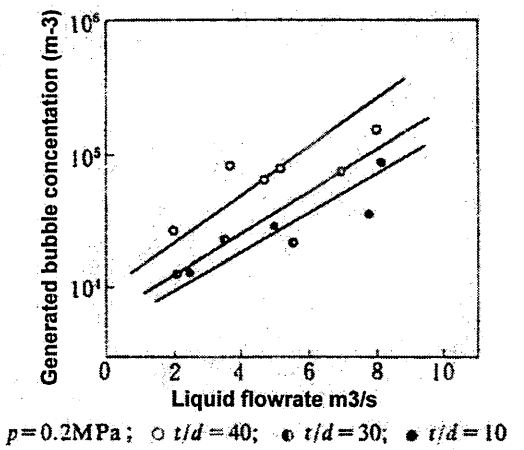

Figure 2.2.15 Effect of nozzle geometry on generated bubble concentration P=0.2Mpa. Wang and Ouyang (1994).

De Rijk et al (1994) investigated putting different lengths of tubes after a needle valve. The needle valve on its own produced 'good' bubbles, but the addition of the tube had a significant 'deteriorating' effect, increasing the bubble size. Figure 2.2.16 shows how the different sized tubes, placed after the needle valve, effected the bubble size distributions. Figure 2.2.16a shows the needle valve on its own and with two short tubes (100mm). Figure 2.2.16b shows the results of the longer tubes (600mm). The longest tubes produced the largest bubbles and reduced the bubble concentration. The experiment was scaled down so it may not produce the same result on a larger scale.

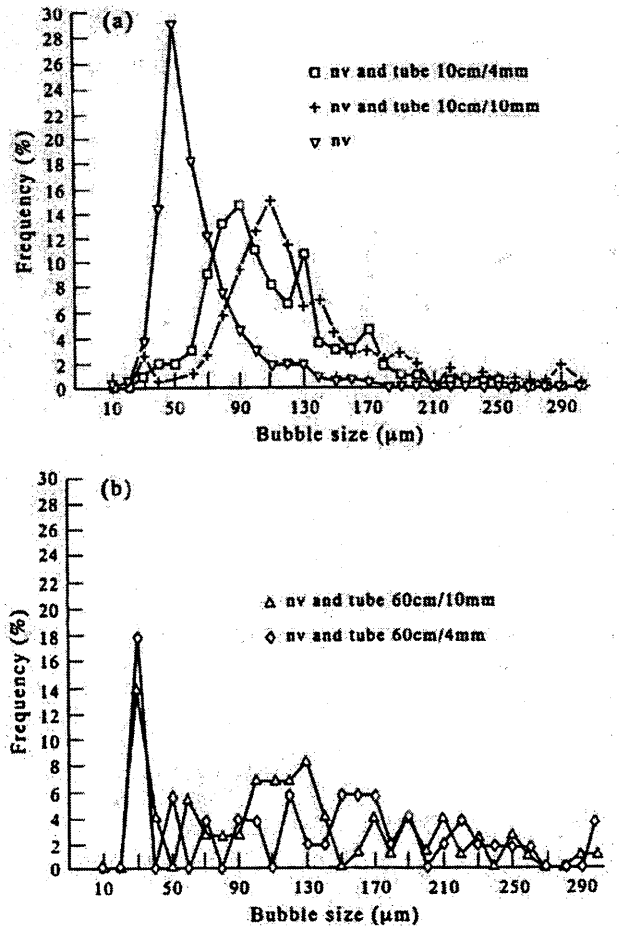

Figure 2.2.16 Frequency of various bubble sizes for different length tubes after a needle valve, from De Rijk et al (1994). a) shorter tubes and needle valve alone, b) longer tubes.

Takahashi et al (1979) correlated the nozzle geometry, dissolved pressure and liquid flowrate to produce equations to calculate the number of bubbles formed.

$$N_b = 0.45\times10^4\left(\frac{t}{d}\right)^{1/2}\left(\frac{P_c - P_A}{P_A}\right)^{3/2} Q^{1/2} \qquad 5\leq t/d\leq 20 \qquad \text{Equation 2.2.1.1}$$

$$N_b = 4.5\times10^4\left(\frac{t}{d}\right)^{-1/2}\left(\frac{P_c - P_A}{P_A}\right)^{2} Q \qquad 50\leq t/d\leq 200 \qquad \text{Equation 2.2.1.2}$$

N_b - number of bubbles
t - nozzle length
d - nozzle diameter
P_c - dissolved pressure
P_A - atmospheric pressure
Q - volumetric flow rate of liquid

They also produced equation 2.2.1.3 for the needle valve they tested.

$$N_b = 1\times10^4\left(\frac{P_c - P_A}{P_A}\right)^2 Q$$ Equation 2.2.1.3

The exponents of t/d, in equations 2.2.1.1 and 2.2.1.2 have reverse signs. This was suggested to have been due to the slower decrease in pressure in the longer nozzles. The dissolved pressure was proportional to the concentration of air. The exponent of the pressure term is larger than unity, while the increase in generated bubbles is more than the concentration of air.

Wang and Ouyang (1994) found that Smoluchowski's equation, shown as equation 2.2.1.4, fitted their experimental data well.

$$\frac{dN}{dT} = -\frac{2\psi B d_b^{\,3} N^2}{3}$$ Equation 2.2.1.4

where

N - bubble concentration
T - time
d_b - bubble diameter
ψ - Coefficient of effective collision of bubbles. The ratio of number of bubble coalescence to the number of bubble collision.
B - velocity gradient of liquid. Defined as equation 2.2.1.5.

$$B = \left(\frac{\rho g h}{\mu T}\right)^{\frac{1}{2}}$$ Equation 2.2.1.5

ρ - density of the solution
g - gravitation acceleration
μ - viscosity
h - loss of pressure. Defined as equation 2.2.1.6.

$$h = \left(f\frac{t}{d} + \xi\right)\frac{u^2}{2g}$$ Equation 2.2.1.6

t - length of nozzle
d - diameter of nozzle
f - Fanning friction factor
ξ - constant

The design of carbonated drink dispensers is not detailed in the literature. Hence, from this study of DAF nozzle design some of the opposite principles can be applied to carbonated drink dispensers. DAF nozzles are designed to create a high degree of turbulence with maximum disturbance to the flow. Therefore a smooth, careful pressure drop may minimise gas release in carbonated drink dispensing. Jefferson (1997) and Wang and Ouyang (1994) both suggested long nozzles may release more of the dissolved gas. Short nozzles may, therefore, be more suitable for dispensing carbonated drinks. However, orifices are used to rapidly release gas, so there may be an optimum nozzle length for carbonated drinks. The effect of coil length on dissolved gas concentration was investigated in Chapter 6.

2.2.1.3 Other possible flotation systems

So far all the nozzles described have been designed to depressurise a flow to produce a maximum number of fine bubbles. Kitchener and Gochin (1981) suggested that the efficiency of the process might be improved if the bubbles were to be nucleated within the flocs. This could be particularly useful as large bubbles waste air and rise too fast to collect the flocs. The mixing of the two streams also causes problems, as turbulence at the nozzle outlet can break up the flocs. Flocculation and flotation could be combined by introducing the recycled supersaturated water at or near the coagulant inlet, or by slightly pressurising all the water in the saturator with the coagulant. Kitchener and Gochin suggested three things that must be taken into account for the design of a 'floato-flocculator':

- Regions of higher shear, such as the edges of stirrer blades, must be avoided to reduce damage to flocs.
- All the materials – flocs, bubbles or aerated flocs – should be kept in suspension throughout the conditioning period in order to sweep up any smaller particles. Flotation must be confined to a separate, following vessel.
- To simulate batch ageing, the hydraulics should approximate plug flow through the unit; as any appreciable 'short circuiting' by 'young' suspension is bound to be detrimental to the clarity finally obtainable.

Ives (1990) also described the idea of 'bubble flocculation', where the flocculation and flotation processes are combined. The motion of bubbles rising through a suspension can create useful velocity gradients, which can be used for the flocculation. This is providing the bubbles can be kept fine.

Carbonated drink nozzles are designed to drop the saturation pressure, but to keep the gas dissolved in solution. This is the opposite principle to DAF nozzles as described in this section. Nozzles suitable for carbonated drinks dispensers could also be used for a 'floato-flocculator'. Carbonated drink dispensers are described in Section 2.2.2.

2.2.2 Drink dispensers

Bisperink and Prins (1994) stated that the gas dissolved in drinks could have a considerable effect on the appearance and flavour release of a drink. If there is too little gas dissolved, the drink can be tasteless and flat whilst if there is too much gas, the taste can be distorted. The quality of champagne is often related to the bubble size formed in the glass. When high numbers of bubbles are formed, bubble trains can be seen forming at sites on the wall.

2.2.2.1 Carbonated soft drinks

A carbonated soft drinks dispenser should be able to reduce the pressure used to dissolve the carbon dioxide into solution. The industry requires a high flowrate, to reduce the serving time. The depressurisation should be controlled to reduce bubble and foam formation. The foam is a sign of the carbon dioxide evolving from solution making the drink flat. Its formation also increases the dispensing time, as the server must wait for the foam to recede before topping up the container. Foam can also cause spills and loss of product. As gas solubility increases, as temperature decreases, the presence of ice in the target container can help to reduce foaming.

To reduce foam production, the drink should be dispensed with a flow that is undisturbed and as laminar as possible. This is because turbulence and agitation can cause excess gas release. Unfortunately, to add flavour to a drink, e.g. cola or lemonade, the carbonated water must be mixed with flavouring syrup. To achieve an even concentration of flavour throughout the drink, some degree of agitation is required. To combat this problem, some nozzles 'premix' the syrup before depressurisation, but this requires a different nozzle to be used for each flavour. 'Post-mix' nozzles, in contrast, mix the carbonated water and syrup after depressurisation. These nozzles are capable of integrating multiple syrup channels and a carbonated water channel within the same device. The ability to dispense a number of different flavoured drinks from the same device reduces the amount of space needed.

A nozzle should be designed so that it can be easily cleaned. If the drink is served cool, it is also important that the majority of the liquid is stored prior to the cooler and hence the flow volume within the nozzle should be as small as possible.

There are various patented nozzles available that use different designs to depressurise and dispense carbonated drinks. Two of these nozzles are described in Appendix B.2. The first is a premix nozzle with a narrow annulus that depressurises the flow smoothly, without any sharp bends or turns. This nozzle was tested in detail and the results are shown in Chapter 5. The other nozzle shown in the appendix uses narrow tubes to depressurise the flow and the syrup is added at the carbonated water outlet. A nozzle of a similar design was tested in the preliminary experiments, shown in Chapter 3.

2.2.2.2 Beers

Different beers, ales and stouts require different sized heads. The dispensing devices are designed to produce some degree of controlled turbulence and release some of the dissolved gas as bubbles to create the desired head. Since turbulence is generated, a beer dispenser is similar to a dissolved air flotation nozzle. The bubbles formed during dispensing affect the size and stability of the head. The qualities usually sought for a good head of beer as stated by Ash (1961a) are:

- Regularity - Consistent bubble size
- Fineness - Small bubbles up to 0.25mm average diameter
- Homogeneity - Continuity of bubble structure, without large irregular shaped random gaps
- Endurance - Ability of bubble structure, once poured and risen to the surface of the glass, to remain whether the drink is consumed quickly or slowly.

Rough, scratched patches are often etched to the bottom of beer glasses. These are designed as bubble formation sites, so bubbles continue to form, to maintain the head.

A device should not only control the head size but also be capable of providing an adequate liquid flowrate, for a rapid dispensing operation. Ash (1961b) states that the dispensing rate must be above 22ml/sec, with the ideal dispensing rate of 60ml/sec. At this rate, dispense of half a pint would take 5 seconds.

Ash (1961a) found that a greater head regularity and a more enduring head was achieved when a mixture of CO_2 and an inert gas dissolved in the beer, rather than with CO_2 alone. The inert gas should be nitrogen. No oxygen should be present, as the flavour of the beer can be affected. A carbon dioxide and nitrogen mixture is preferably used for dispensing fermented beers, stout and ales. Ash found that the head size varied with the partial pressure of carbon dioxide, whilst the head's appearance and endurance was controlled by the partial pressure of the nitrogen. The ideal partial pressure of carbon dioxide was found to be 0.8-1.4bar(g) and for nitrogen 0.3-2.8bar(g).

Various beer dispenser patents by Guinness are shown in Appendix B.3. Several of the designs are adjustable to regulate the turbulence and the head size. The adjustment was performed by combining flow through sections designed to produce turbulence or minimise turbulence. Painter and Thomasson (1969) described a nozzle that used a combination of a smooth restriction and cavitation holes. A plunger that moved within the nozzle changed the length of the restriction. Then when the smooth restriction length was at a maximum, the pressure drop was solely across the restriction. In this situation, the plunger was removed from the large hole in the centre of the perforated plate, decreasing the flow through the cavitation holes. When the restriction length was at its minimum, the pressure drop was solely across the cavitation holes and the large centre hole was closed.

Painter and Thomasson (1969) showed the approximate pressures at given positions within their dispenser nozzle. Figure 2.2.17 shows the approximate pressure distributions designed to produce both a maximum sized head, figure 2.2.17a and a minimum sized head, figure 2.2.17b. The minimum pressure to produce a significant gas release was referred to as the 'cavitation pressure'. Figure 2.2.17a shows that when the pressure drop was primarily across the cavitation holes, the pressure went below the cavitation pressure. Figure 2.2.17b shows the pressure distribution when the pressure drop was across the smooth restriction, with the flow through the

cavitation holes minimised. In this case, the pressure drop was insufficient for the gas to come out of solution and produce a head.

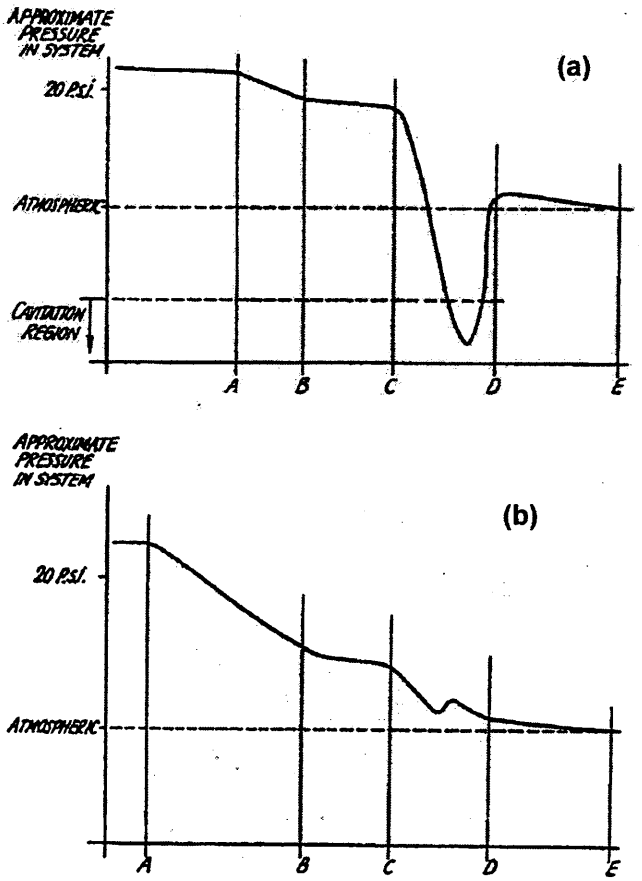

A - upstream input to the helix conduit
B - downstream output end of the helix conduit
C - upstream of cavitation holes
D - downstream of the cavitation holes
E - output end of spout

Figure 2.2.17 Pressure drop across Painter and Thomasson (1969) nozzle, a) to provide a head, b) to provide little or no head.

2.3 *Pressure Drops in pipes and coils*

This section reviews the present knowledge and equations for single and two-phase pressure drops. Pressure drop theories in different geometries have been reviewed, including annuli, narrow pipes, and coils.

2.3.1 Single-phase flow

A fluid flow in a pipe can have a change in momentum and pressure. The forces that effect momentum are:

Pressure force	- caused by a pressure gradient along the pipe's length.
Wall shear force	- from the shear stress at the walls
Gravitational force	- caused by acceleration due to gravity

The Bernoulli equation, equation 2.3.1.1, taken from Coulson and Richardson (1993), applies to an incompressible fluid. It relates the pressure, at a point in the fluid, to its position and velocity.

$$\frac{u^2}{2g} + \frac{P}{\rho g} + z = c \qquad \text{Equation 2.3.1.1}$$

u	- velocity
g	- acceleration due to gravity
P	- pressure
ρ	- density
z	- distance in vertical direction
c	- constant

Each term, in equation 2.3.1.1, represents energy per unit weight of fluid and has the dimensions of length. Each can be regarded as representing a contribution to the total fluid head. The terms represent the following:

$\frac{u^2}{2g}$	the velocity head
$\frac{P}{\rho g}$	the pressure head
z	the potential head

2.3.1.1 Frictional Pressure Drop

The majority of the pressure drop in a straight pipe is usually from frictional losses. The frictional pressure drop for single-phase, non-compressible flow in a straight pipe can be calculated from equation 2.3.1.2.

$$\Delta P_f = 4f \frac{l}{d} \frac{\rho u^2}{2} \qquad \text{Equation 2.3.1.2}$$

ΔP_f	- frictional pressure drop
f	- Fanning friction factor
l	- length
d	- diameter

Equation 2.3.1.2 varies in the literature, depending on the friction factor used. The Fanning friction factor, as used in equation 2.3.1.2, is used throughout this thesis. The friction factor can vary in value from half that of the Fanning friction factor, to four times the value. Friction factor is a function of Reynolds number and differs for laminar and turbulent flow. The Fanning friction factor for laminar flow is generally calculated by equation 2.3.1.3. For turbulent flow in smooth tubes, the Blasius equation, equation 2.3.1.4, is often used. Many other equations exist that can be used to calculate the turbulent friction factor. Other equations are shown in Bhatti and Shah (1987), Haaland (1983), Coulson and Richardson (1993), Perry (1984), Miller (1990), Ali and Seshadri (1971), Mori and Nakayama (1967b) and Lockin (1950). Alternatively, a friction factor chart, shown as Figure 2.3.1, can be used to extrapolate the friction factor for different roughnesses of pipes. The figure also shows the Blasius correlation.

Laminar flow	$f = 16/Re$	Equation 2.3.1.3
Turbulent Flow (Blasius)	$f = 0.079\ Re^{-0.25}$	Equation 2.3.1.4
$Re = \frac{\rho u d}{\mu} = \frac{Gd}{A\mu}$		Equation 2.3.1.5

Re - Reynolds number
μ - viscosity
G - mass flowrate
A - area

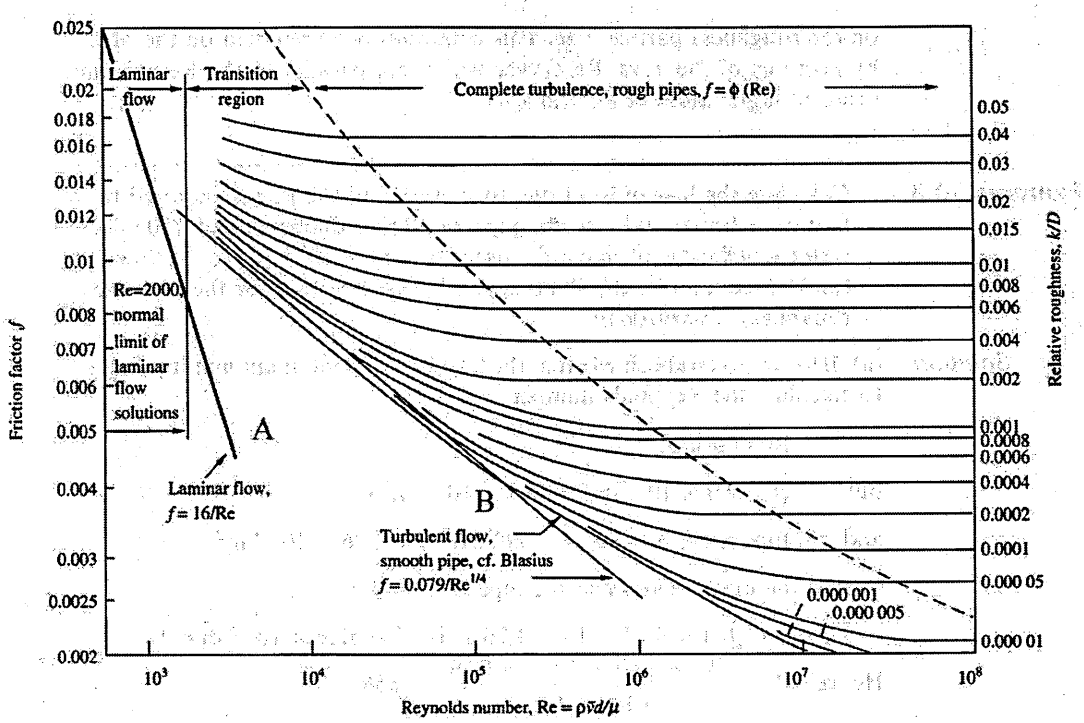

Figure 2.3.1 Friction factor chart. Douglas et al (1998).

Figure 2.3.1 shows different regions corresponding to different flow types. The straight line 'A' corresponds to laminar flow. The critical Reynolds number of 2000 represents the limit at which turbulent flow can be maintained once established. In the transition region between laminar and turbulent flow, the value of friction factor is considerably higher than in streamline flow. In this region, it is difficult to reproduce pressure drop results experimentally. Line B corresponds to turbulent flow through smooth tubes. At very high Reynolds numbers, the friction factor becomes independent of Reynolds number and depends only on the pipes relative roughness.

Extra losses can occur if a pipe is not straight or has any enlargements, contractions or additional fittings. Douglas (1995) showed the losses in expansions and contractions could be calculated by equations 2.3.1.6 and 2.3.1.7 respectively. The loss coefficient in the contraction equation was shown to vary from 0 for an area ratio, A_2/A_1, of 1 to 0.41 for an area ratio of 0.1.

$$h = \frac{u_2^2}{2g}\left(\frac{A_2}{A_1} - 1\right)^2 \qquad \text{Equation 2.3.1.6}$$

$$h = \frac{Ku_2^2}{2g} \qquad \text{Equation 2.3.1.7}$$

A_1 - inlet area
A_2 - Outlet area
u_2 - velocity in the outlet section
K - loss coefficient

In coils there is an additional loss due to the centrifugal forces. Fluid behaviour in coils is described in Section 2.3.5.

2.3.1.2 Compressible flow

Certain liquids and all gases are compressible. Hence they have a variable density and volumetric flowrate, that are functions of temperature and pressure. The mass flowrate, however, remains constant. In general, if there is a less than 20% change in pressure, the flow can be treated as incompressible. The equation for compressible flow, derived from the general energy equation, as shown in Coulson and Richardson (1993), is displayed as equation 2.3.1.6. The equation assumes the tube is straight and horizontal and that the flow is isothermal and an ideal gas.

$$\left(\frac{G}{A}\right)^2 \ln\frac{P_1}{P_2} + \frac{P_2^2 - P_1^2}{2Rt/M} + 2f\frac{l}{d}\left(\frac{G}{A}\right)^2 = 0 \qquad \text{Equation 2.3.1.6}$$

P_1 - Inlet pressure
P_2 - Outlet pressure
R - Universal gas constant = 8314 J/kmol K
t - Temperature
M - Molecular weight

2.3.2 Two phase flow

Multiphase flows are far more complex than single-phase flows. The flow behaviour depends on the component properties, their flowrates and the system geometry. It is important, in two-phase flow, to understand the nature of the interactions between the phases and the influence on the phase distribution across the pipe cross section. The components often travel at different velocities giving rise to slip between the phases, which can influence the hold up. The residence time of the two phases will often be different. The pressure drop depends on the relative velocities of the phases and their flow pattern.

In vertical flows of two-phase gas and liquid, the gas generally rises quicker, as it is the lighter phase. This gives rise to a slip velocity, which depends on the flow pattern in a complex way. Vertical pipe flow is symmetrical about the axis, whilst horizontal flow is not. Horizontal flow patterns are more complex due to the gravitational force acting perpendicularly to the pipe axis. This causes the denser phase to flow towards the bottom of the pipe. The pipe diameter, properties of the fluid and flowrate all influence horizontal flow patterns. All the experiments in this thesis were conducted horizontally. Figure 2.3.2 shows a flow pattern map, for horizontal flow in a pipe, produced by Chhabra and Richardson shown in Coulson and Richardson (1993). The divisions are approximate and based on subjective observations. The data relates to pipes with diameters of less than 42mm, but 205mm diameter pipes are also said to fit the diagram well.

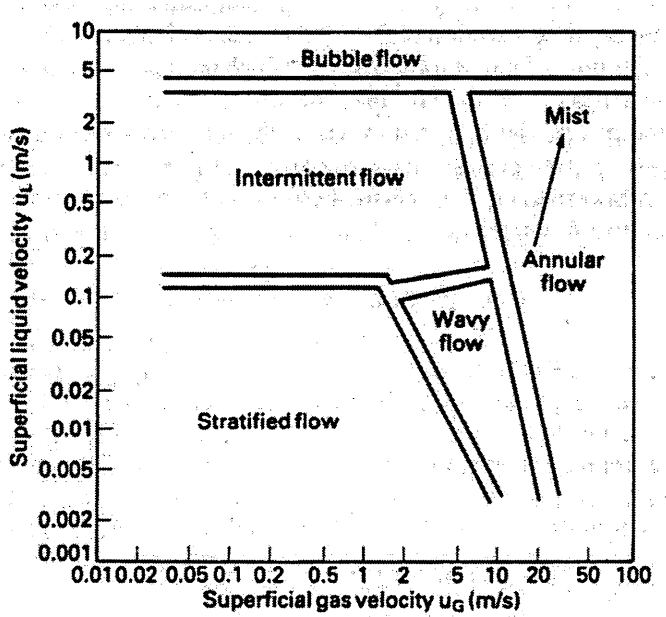

Figure 2.3.2 Flow pattern map. Coulson and Richardson (1993).

2.3.2.1 Pressure drop determination

The two-phase flow pressure drops are made up of three main losses: frictional, gravitational and acceleration. If the flow is horizontal, the gravitational losses can be neglected. Acceleration losses can be significant in two-phase flow due to the gas expansion, as the pressure is reduced. Dukler et al (1964) stated that Magiros found that for small pipes with characteristically large pressure drops, 50% of an experimental pressure drop could be due to acceleration.

Analytical solutions for two-phase pressure drops are difficult if not impossible, as it is difficult to specify the flow pattern and define the interaction between the phases. Rapid fluctuations in flow can occur and cannot easily be accounted for. Hence, design correlations have been derived experimentally and care should be taken when applying them outside of the experimental limits. Whalley (1990) described several practical correlations, by various authors, to calculate frictional pressure drop. Martinelli and Nelson (1948) were partially successful producing a graphical method to predict the pressure gradient in the flow of boiling water. Thom (1964) extended Martinelli and Nelsons work to calculate the pressure drop of steam-water flow, with reasonable results.

Lockhart and Martinelli (1949) produced the most widely used graphical method to calculate a two-phase frictional pressure drop. Dukler et al (1964) stated it was the best correlation they found when compared to a large data bank, but said it was far from perfect. The Lockhart and Martinelli correlation is an extension of single-phase pressure drop calculations. The two-phases are considered separately and the combined effect examined. This is known as the 'separated flow' model. The two-phase pressure drop can be calculated from either equation 2.3.2.1 or equation 2.3.2.2, for gas or liquid separated flow respectively. The graphical correlation uses a parameter X, shown as equation 2.3.2.3, calculated from the pressure drop for each phase if flowing alone.

$$\frac{-\Delta P_{TP}}{-\Delta P_G} = \phi_G{}^2 \qquad \text{Equation 2.3.2.1}$$

$$\frac{-\Delta P_{TP}}{-\Delta P_L} = \phi_L{}^2 \qquad \text{Equation 2.3.2.2}$$

$$X = \sqrt{\frac{-\Delta P_L}{-\Delta P_G}} \qquad \text{Equation 2.3.2.3}$$

$\phi_L{}^2$, $\phi_G{}^2$ - Two phase multipliers
$-\Delta P_{TP}$ - Two phase flow pressure drop
$-\Delta P_L$, $-\Delta P_G$ - Frictional pressure drop for liquid/gas flow alone
X - Lockhart and Martinelli parameter

The relationship between the Lockhart and Martinelli parameter X and the two-phase multipliers, ϕ_L and ϕ_G, was derived graphically and is shown as Figure 2.3.3. The figure shows four separate curves depending on whether each phase was laminar or

turbulent. The relationship was developed with tubes from 1.5mm up to 25mm in diameter, with flows of water, oils and hydrocarbons, with air. Perry (1984) found that the correlation could be applied to pipes up to 100mm in diameter, with a similar degree of accuracy. In general the predictions were high for stratified, wavy and slug flows and low for annular flow. Several investigators have studied flows in pipes and developed pressure drop correlations for their particular systems. However, a better general correlation has not been developed.

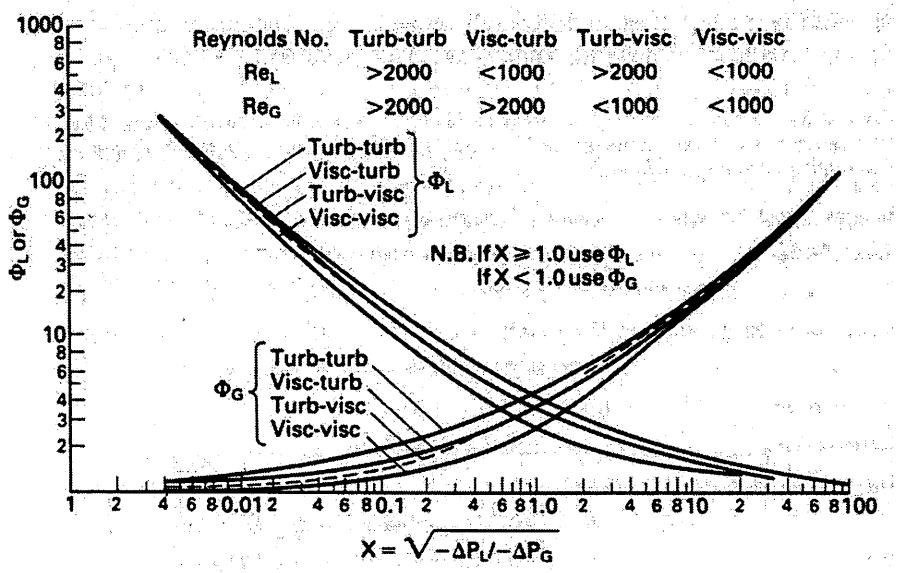

Figure 2.3.3 Lockhart and Martinelli correlation of X and ϕ. Coulson and Richardson (1993).

Chisholm and Laird (1958) and Chisholm (1967) extended the work of Lockhart and Martinelli, and derived an equation to calculate ϕ_L, in terms of X, shown as equation 2.3.2.4. The constant C, for two-phase air and water flow, depends on the type of flow that would occur if the liquid and gas phases were flowing independently.

$$\phi_L^2 = 1 + \frac{C}{X} + \frac{1}{X^2} \qquad \text{Equation 2.3.2.4}$$

C
- 20 turbulent / turbulent flow
- 10 turbulent liquid / streamline gas
- 12 streamline liquid / turbulent gas
- 5 streamline / streamline flow

Friedel produced equation 2.3.2.5, shown by Whalley (1990) for the liquid two-phase multiplier, from an extensive data bank. Whalley (1990) claimed this was the most accurate generally available correlation that was applicable to any fluid. However, the equation was not suitable when the viscosity ratio (μ_L /μ_G) became greater than 1000. Note equation 2.3.2.5 is misquoted in Triplett et al (1999a).

$$\phi_L^2 = A + 3.24x^{0.78}(1-x)^{0.224}\left(\frac{\rho_L}{\rho_G}\right)^{0.91}\left(\frac{\mu_G}{\mu_L}\right)^{0.19}\left(1-\frac{\mu_G}{\mu_L}\right)^{0.7} Fr_{TP}^{-0.0454} We_{TP}^{-0.035}$$

Equation 2.3.2.5

μ_G - gas viscosity
μ_L - liquid viscosity
ρ_G - gas density
ρ_L - liquid density
x - gas mass fraction or 'quality'

$$x = \frac{G_G}{G}$$

G - total (liquid + gas) mass flowrate
G_G - gas mass flowrate
Fr_{TP} - Froude number
We_{TP} - Weber number

where

$$A = (1-x)^2 + x^2 \frac{\rho_L f_G}{\rho_G f_L}$$

Equation 2.3.2.6

$$Fr_{TP} = \frac{G^2}{A^2 g d \rho_{TP}^2}$$

Equation 2.3.2.7

$$We_{TP} = \frac{G^2 d}{A^2 \sigma \rho_{TP}}$$

Equation 2.3.2.8

σ - surface tension

2.3.2.2 Homogeneous Flow

The two-phase homogeneous flow model assumes both phases are well mixed and flow at the same velocity. A homogeneous density and viscosity are used to calculate the pressure drop. The homogeneous density can be calculated from equation 2.3.2.9, as shown in Whalley (1990).

$$\frac{1}{\rho_H} = \frac{x}{\rho_G} + \frac{1-x}{\rho_L}$$

Equation 2.3.2.9

ρ_H - homogeneous density

Whalley showed three different equations to calculate the homogeneous viscosity. The simplest, by Isbin, is of the same form as the density equation and is shown as equation 2.3.2.10.

$$\frac{1}{\mu_H} = \frac{x}{\mu_G} + \frac{1-x}{\mu_L}$$

Equation 2.3.2.10

Whalley stated that the other equations were better than equation 2.3.2.10. However, Isbin's equation is stated more in the literature. Equation 2.3.2.11, was produced by Dukler et al (1964).

$$\mu_H = \mu_G \frac{x\rho_H}{\rho_G} + \mu_L \frac{(1-x)\rho_H}{\rho_L} \qquad \text{Equation 2.3.2.11}$$

Beattie and Whalley (1982) produced equation 2.3.2.13 as a hybrid of other equations specific to certain flow patterns, to apply for flow patterns, using the void fraction, α. The equation was said to be suitable in conjunction with the Colebrook-White equation for the friction factor, shown as equation 2.3.2.12, even when the flow was laminar.

$$\frac{1}{\sqrt{f}} = 3.48 - 4\log_{10}\left[2\frac{\varepsilon}{d} + \frac{9.35}{\mathrm{Re}\sqrt{f}}\right] \qquad \text{Equation 2.3.2.12}$$

$$\mu_H = \mu_G\alpha + \mu_L(1-\alpha)(1+2.5\alpha) \qquad \text{Equation 2.3.2.13}$$

ε - pipe roughness

Whalley derived an equation to determine the total pressure drop for homogeneous flow.

$$-\frac{\Delta P}{\Delta z} = \frac{2f_{L2}}{d\rho_H}\left(\frac{G}{A}\right)^2 + \rho_H g + \left(\frac{G}{A}\right)^2 \frac{d}{dz}\left(\frac{1}{\rho_H}\right) \qquad \text{Equation 2.3.2.14}$$

This can be integrated for the total pressure change from an inlet quality of zero to an outlet quality of x_o, assuming the quality varies with length.

$$-\frac{\Delta P}{\Delta z} = \frac{2f_{L2}l}{d}\left(\frac{G}{A}\right)^2\left[\overline{\frac{1}{\rho_H}}\right] + \overline{\rho}_H g l + \left(\frac{G}{A}\right)^2\left[\frac{1}{\rho_{H2}} - \frac{1}{\rho_L}\right] \qquad \text{Equation 2.3.2.15}$$

l - length

Where ρ_{H2} is the homogeneous density ρ_H when $x = x_2$. Equation 2.3.2.9 for the homogeneous density can be rearranged to produce equations 2.3.2.16-2.3.2.19.

$$\overline{\rho}_H = \rho_L \frac{\ln(1+X_2)}{X_2} \qquad \text{Equation 2.3.2.16}$$

$$\left[\overline{\frac{1}{\rho_H}}\right] = \frac{1}{\rho_L}\left(1 + \frac{X_2}{2}\right) \qquad \text{Equation 2.3.2.17}$$

$$\frac{1}{\rho_{H2}} - \frac{1}{\rho_L} = \frac{X_2}{\rho_L} \qquad \text{Equation 2.3.2.18}$$

Where

$$X_2 = x_2\left[\frac{\rho_L - \rho_G}{\rho_G}\right] \qquad \text{Equation 2.3.2.19}$$

x_2 - gas mass fraction at the outlet

Hence, the total pressure change in homogeneous flow can be written as equation 2.3.2.20.

$$-\Delta P = \left(\frac{2f_{L2}l}{d}\left(\frac{G}{A}\right)^2\frac{1}{\rho_L}\right)\left(1+\frac{X_2}{2}\right)+(\rho_L g l)\left(\frac{\ln(1+X_2)}{X_2}\right)+\left(\frac{G}{A}\right)^2\frac{X_2}{\rho_L}$$

A B C D E

Equation 2.3.2.20

A liquid-only frictional pressure change
B additional term because of two-phase flow
C liquid only gravitational pressure change
D additional term because of two-phase flow
E momentum pressure change.

2.3.3 Narrow channels

The hydrodynamics of two-phase flow within microchannels has been found to be different to that of larger channels. The main methods of predicting the two-phase characteristics in large channel diameters of at least several millimetres in diameter are not accurate for narrow channels. In narrow tubes, the surface tension can dominate and the velocity slip is small. Previous investigators of larger diameter tubes concluded that the effect of diameter and surface tension were negligible. Coleman and Garimella (1999) stated that the surface tension effect was negligible but this was for pipe diameters greater than 10mm. Microchannel flow patterns and momentum transfer processes are not well understood. The 'separated flow' model equations are not appropriate for narrow channels.

Mala and Li (1999) investigated water flow in 50-254μm diameter microtubes and found a significant increase in the experimental pressure drop at high Reynolds numbers compared to conventional flow theory, calculated by equation 2.3.1.2. The difference increased with a decrease in pipe diameter. This was explained to be due to an early transition from laminar to turbulent flow, at Reynolds numbers of approximately 500. The additional resistance from surface roughness was also investigated. The effect was calculated from a roughness-viscosity model that predicted the volumetric flowrate well.

Triplett et al (1999a) performed horizontal two-phase experiments with air and water, in transparent circular tubes with 1.1 and 1.45mm internal diameters. They also tested semi-triangular microchannels. Various void fraction models and pressure drop correlations were tested against their experimental data. The most accurate predictions of the void fraction, for bubble and slug flow, were from the homogeneous model. However, the model significantly over-predicted the void fraction in churn and annular flow, when there would have been significant slip. Other models over-predicted the velocity slip ratio and hence, underestimated the void fraction at low liquid velocities. The correlations tested were predominantly based on larger channels and underestimated the void fractions at low liquid

velocities. This suggested that velocity slip does not occur in microchannels. With annular flow, again each method over-predicted the void fraction, again indicating lower interphase slip in microchannels. The results showed that the gas-liquid interfacial friction phenomenon was significantly different in large channels compared to microchannels. Predictions were also shown from pressure drop correlations. Xu et al (1999) found that 0.6 and 1mm diameter rectangular channels had similar flow patterns to larger diameter tubes. However, in their 0.3mm diameter channel very different patterns were observed. Bubbly flow was never observed in the smaller diameter tube.

Most pressure drop correlations in the literature were for larger diameter tubes and were found not to be applicable to capillaries. Triplett et al (1999a) used Friedel's correlation and the homogeneous mixture model to calculate frictional two-phase pressure drops. Estimations of the pressure drop in microchannels found that the homogenous model predicted the bubbly and slug flow well at high Reynolds numbers, but deviated at low Reynolds numbers for slug annular and annular flow and slug flow. They found Friedel's equation less accurate than the homogeneous two-phase frictional pressure drop model. The pressure drop due to acceleration in microchannels was found to be significant, with high liquid and gas superficial velocities, due to the change in gas density.

Bao et al (1994) experimented with two-phase flow in channels with diameters of 0.74 to 3.07mm and compared the results to two-phase flow void fraction and pressure drop correlations. Correlations from Lockhart and Martinelli, CISE and Farooqi were used to predict the void fraction. Lockhart and Martinelli were found to predict the void fraction best, whilst Farooqi was not satisfactory. The void fraction results were found to be the same whether the flow was horizontal or vertical. Bao et al also tested frictional pressure drop equations from Lockhart and Martinelli, Chisholm, Friedel, Müller-Steinhagen and Beattie, for flow in narrow tubes. None of the correlations were particularly accurate for the whole range of conditions, but most methods predicted the pressure drop in turbulent conditions well. All of the correlations were poor at low liquid Reynolds numbers, except for Lockhart and Martinelli. However, the Lockhart and Martinelli correlation was very poor at predicting liquid-liquid flow of kerosene and water. The success of Lockhart and Martinelli could be due to them taking into account the state of the fluid flows. The best overall correlation was found to be the homogeneous correlation by Beattie. This correlation used the laminar friction factor at low Reynolds numbers, equation 2.3.1.3, and the Colebrook-White correlation, equation 2.3.2.12, to calculate the turbulent friction factor.

Barnea et al (1983), Suo and Griffith (1964), Fukano and Kariyasaki (1993), Triplett et al (1999b) and Coleman and Garimella (1999) looked at two-phase flow pattern maps for small diameter tubes. They all found that maps for larger tubes did not sufficiently predict the flow transitions. Surface tension was found to significantly effect the flow patterns, in small diameter tubes. The transition to stratified flow, in horizontal tubes was significantly different to the results from Taitel and Dukler (1976), for larger diameter tubes. Many authors were unable to produce stratified

flow in microchannels. Fukano and Kariyasaki (1993) found that decreasing the pipe diameter meant the film thickness became more uniform and axis-symmetric, regardless of the orientation of the pipe. The flow pattern was not effected by the direction of the flow, due to the surface tension effect. Damianides and Westwater (1988) tested tubes of diameters 1-5mm and were unable to achieve stratified flow in the 1mm tube. Triplett et al confirmed this result. However, Damianides and Westwater found that stratified flow could be achieved in their 2mm diameter tube. The transition to annular flow occurred by the liquid creeping up the tube wall. In contrast, the 3mm and larger diameter tubes changed from wavy to annular flow by liquid drops being deposited on the tube wall. The creeping of the liquid up the tube wall in the 2mm tube suggested that the surface tension was opposing gravity. This confirms that the surface tension had a significant effect in small diameter tubes.

Barnea et al (1983) stated that the surface tension in small diameter flows only affected the stratified-slug transition. However, they used larger diameter tubes with diameters of 4-12.3mm. A modified model to account for the effects of surface tension and gravity was suggested. Triplett et al (1999b) and Coleman and Garimella (1999) looked at narrower tubes, 1.1-1.45mm and 1.3-5.5mm respectively, and both found characteristics that were significantly different from larger diameter tubes. The flow characteristics were found to be independent of orientation. Coleman and Garimella studied the effect of the diameter and shape on the flow regime produced from air and water flow. The tube diameter was found to have a significant effect on the flow regime transitions. Decreasing the tube diameter meant the transition from plug-slug flow to dispersed flow occurred at progressively higher superficial liquid velocities. Coleman and Garimella concluded that the diameter, surface tension and the aspect ratio all play an important role in determining the flow regime of small diameter pipes.

Narrow noncircular tubes have also been studied. Pfund et al (2000) studied single-phase pressure drops in sandwich style 'microchannels', with one micro dimension of 128-521μm and found that an increase in the roughness significantly increased the laminar friction factor. The critical Reynolds number for the transition to turbulent flow was found to decrease with the depth of the microchannel. Fourar and Bories (1995) studied air and water flow between two plates, with a gap of 0.18-0.54mm. They found that the experimental pressure drop was higher than predicted, for annular flow using Lockhart and Martinelli. This was attributed to inertial forces. Zhao and Bi (2001) investigated air and water flow in narrow triangular channels and found the corners always contained liquid. This was attributed to surface tension, which also affected the flow regimes particularly with high gas void fractions. A new flow regime was found, called capillary bubble flow, which existed at low gas flowrates in a triangular tube with a hydraulic diameter of 0.886mm.

2.3.4 Flow in annuli

Ekberg et al (1999) investigated flow in two different sizes of narrow annuli, both with hydraulic diameters of 2.04mm. The flow pattern maps produced were different

from larger horizontal pipes and circular and rectangular microchannels. The void fraction correlation from Butterworth (1975), equation 2.3.4.1, was the most accurate for Ekberg et al's experimental data.

$$\frac{1-\alpha}{\alpha} = 0.28\left[\frac{1-x}{x}\right]^{0.64}\left(\frac{\rho_G}{\rho_L}\right)^{0.36}\left(\frac{\mu_L}{\mu_G}\right)^{0.07} \qquad \text{Equation 2.3.4.1}$$

However, it over-predicted the void fraction, to a degree that depended on the flow regime. They concluded that Friedel and the homogeneous model predicted the pressure drop best. Beattie (2001), however concluded that the Beattie and Whalley equation was more suited to Ekberg et al's data. Beattie and Whalley's calculations were based on a simpler 'lumped parameter' treatment rather than integration along the test section. Beattie and Whalley also used a larger friction factor as Bhatti and Shah (1987) stated a larger friction factor is needed for annuli.

Jones and Leung (1981) studied numerous sets of single-phase frictional pressure drop data obtained in concentric annuli and stated that the friction factor for concentric annuli can be significantly above those of smooth circular tubes. They produced a modified Reynolds number, using a laminar equivalent diameter, to calculate the friction factor in smooth concentric annuli, which can also be applied to circular tubes. The laminar equivalent diameter, d_l is calculated from the radius ratio and hydraulic diameter, as shown in equation 2.3.4.1.

$$\frac{d_l}{d_h} = \frac{1+r^{*2}+(1-r^{*2})/\ln r^*}{(1-r^*)^2} \qquad \text{Equation 2.3.4.2}$$

r^* - radius ratio = r_i/r_o
d_h - hydraulic diameter = $2(r_o-r_i)$

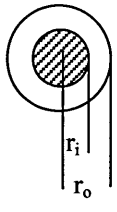

Figure 2.3.4 Dimensions of concentric annular duct.

The modified Reynolds number, shown as equation 2.3.4.2, can then be used to calculate the friction factor. Jones calculated the laminar friction factor from equation 2.3.1.3 and for turbulence by equation 2.3.4.3 from Colebrook.

$$\mathrm{Re}^* = \frac{\rho u d_l}{\mu} \qquad \text{Equation 2.3.4.3}$$

$$\frac{1}{\sqrt{f}} = 4.0\log_{10}\left(2\times \mathrm{Re}^*\sqrt{f}\right) - 1.6 \qquad \text{Equation 2.3.4.4}$$

Shah and Bhatti (1987) also produced an equation for the increased friction factor, f_a, for laminar flow in a concentric annular duct. This is shown as equation 2.3.4.4.

$$f_a = \frac{24r^{*0.035}}{\mathrm{Re}}$$ Equation 2.3.4.5

Bhatti and Shah (1987) produced equation 2.3.4.5 for the increased friction factor, for turbulent flow in concentric annular ducts. The equation is valid for Reynolds numbers in the range $5000 < \mathrm{Re} < 10^7$.

$f_a = (1+0.0925r^*) f$ Equation 2.3.4.6

The predictions from equation 2.3.4.5 are very similar to those determined by substituting d_l into a standard friction factor equation, equation 2.3.1.2.

A large annulus with a narrow gap could be classified as being like two parallel flat plates. The pressure drop for laminar flow between horizontal, parallel, flat plates can be calculated from equation 2.3.4.7, taken from Douglas et al (1995), when the plates are assumed to be sufficiently wide that the end effects are negligible.

$$\frac{\Delta P}{\Delta l} = \frac{12Q\mu}{d^3 w}$$ Equation 2.3.4.7

l - length of plate
d - diameter of gap
w - width of plate

2.3.5 Flow in coils

In this thesis, coils have been investigated as a potential new device to depressurise a gas-saturated solution. Single-phase flows in coils have been found to have a greater pressure drop than an equivalent length of straight pipe. The flow has also been shown to remain laminar to higher Reynolds numbers than straight pipes. Both of these factors are highly desirable for carbonated drink dispensers. With a higher pressure drop the solution can be depressurised in a smaller amount of space. Laminar flow is preferable, as bubbles have been found to form more readily in areas of turbulence.

2.3.5.1 Single-phase coil flow

Eustice (1910) found that in curved pipes, decreasing the coil diameter increased the flow resistance. Srinivasan et al (1968) stated that the effect of coil curvature on the friction factor was substantially less in turbulent than laminar flow. Eustice (1911) used dyes to study the flow path through curved glass tubes. The flow was found to change position continuously within the pipe, whilst exerting a 'scouring' action on the pipe walls. When a single filament of dye was introduced into the central plane, it split into two, leaving the central plane in opposite directions, forming a loop through the tube. An increase in the flow velocity was found to increase the curvature of the filament. Unlike streamline flow in straight pipes, the dye eventually mixed throughout the tube diameter.

Dean (1927) predicted the flow motion in coils to have two independent streamlines, in parallel planes going in opposite directions. This secondary circulation is shown in Figure 2.3.5. Dean's theory agreed with Eustice's experiments, showing why the motion in one half of the pipe was different to the other. White (1929) suggested that if complete slip existed at the boundary, the whole effect would cease. This secondary circulation in laminar flow causes a form of mechanical mixing, which can be beneficial to heat transfer.

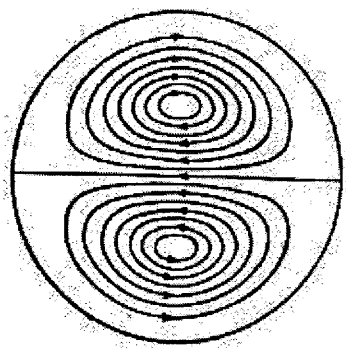

Figure 2.3.5 Circulation in the cross-section of a coiled pipe. Taylor (1929).

Taylor (1929) experimentally confirmed the presence of a secondary circulation by repeating Eustice's experiments. Coloured dye was slowly introduced through a small hole into the stream after one complete turn of the coil, so that the secondary circulation could be established. Eustice introduced the dye at the coil inlet and hence, the dye may have mixed with the flow whilst the secondary circulation was developing. Taylor found that the dye usually kept to one side of the tube. It first flowed inwards along the wall, until reaching the innermost point of the cross section, when it left the wall and moved across the middle section and towards the wall again. It was said that when the dye kept to one half of the cross section, it was visually quite striking. The dye occasionally crossed to the other side but this was explained to be due to imperfections in the uniformity of the helix. At a certain flowrate, the colour started to vibrate irregularly. It retained its identity for at least one helix turn, until the unsteadiness gave rise to diffusion by eddies with a rapid rise in resistance. After a further increase in the flowrate, turbulence was achieved and the colour dispersed.

Dean (1927) showed that for a given pressure gradient the ratio of mass flow through pipes with different curvatures is ruled by the Dean number. The Dean number can be calculated from equation 2.3.5.1.

$$Dn = \mathrm{Re}\left(\frac{d}{D}\right)^{1/2} \qquad \text{Equation 2.3.5.1}$$

Eustice (1910) found the transition from laminar to turbulent flow to be less defined in curved pipes than straight pipes. With coils, a gradual change in slope was seen, as opposed to a sharp change in motion seen in straight pipes. With laminar flow in straight pipes, pressure drop is proportional to velocity to the power of one. Eustice

found that for coils, the pressure drop was proportional to velocity to the power of 1.1-1.2. Dean (1928) explained that this was due to the flow in coils continuously changing position in the tube, even when streamline. Hence, the change in flow to turbulence is less distinct and the increase in resistance less rapid.

White (1929) investigated the flow in three different dimensions of coil and plotted the Dean Number versus the ratio of resistance, C, of a curved pipe f_c, to that of a straight pipe f_s. This produced a smooth curve as shown as Figure 2.3.6. Points that departed the main curve were found to be dependent on curvature and coincided with a change in motion from double helical streamline flow to turbulent flow. This point also indicated when Dean's theory was no longer applicable. The figure shows that the transitional Reynolds number increased, with the coil curvature ratio, d/D, when d was the tube diameter and D the coil diameter. A coil curvature ratio of 1/2050 was found to have a similar resistance to a straight pipe. A similar resistance to a straight pipe was also seen with a curvature ratio of 1/50, up to Reynolds numbers of 80. The resistance then increased up to 2.9 times that of a straight pipe, when turbulence occurred at a Reynolds number of 6000. With a curvature ratio of 1/15 the transition from laminar to turbulent flow, occurred at a Reynolds Number of 9000. White concluded that for large Reynolds numbers, the flow in small diameter coils was more stable than straight pipes. The additional resistance due to the pipe curvature was found to be less in turbulent flow than streamline, as secondary circulation was not possible in conjunction with turbulent eddy motion.

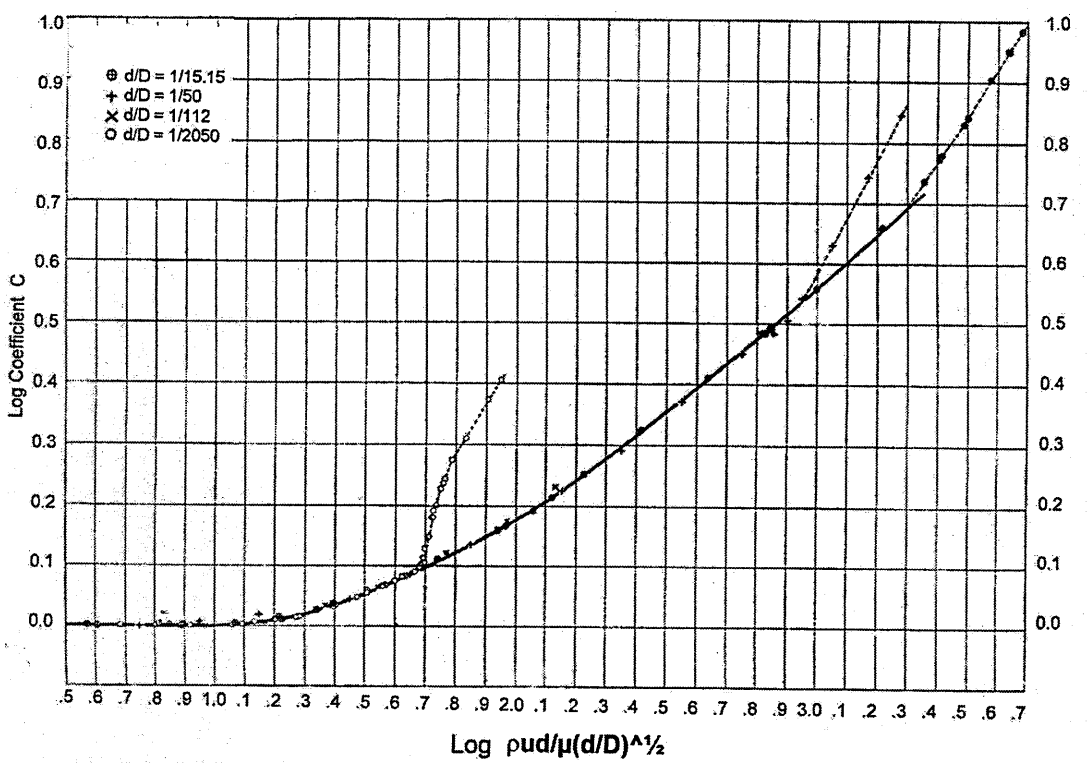

Figure 2.3.6 Increase of resistance due to curvature. White (1929).

Taylor (1929) found two points that define the transition from laminar to turbulent flow in coils: the lowest Reynolds number at which the flow appeared completely turbulent and the highest Reynolds number at which the flow was steady. The results were compared to the transitional values found by White and are shown in Figure 2.3.7. White predicted the transition to be higher than the lowest Reynolds number when the flow appeared completely turbulent from Taylor's results. Various other authors have produced equations to calculate the critical Reynolds number. Some of these are shown in Appendix E.

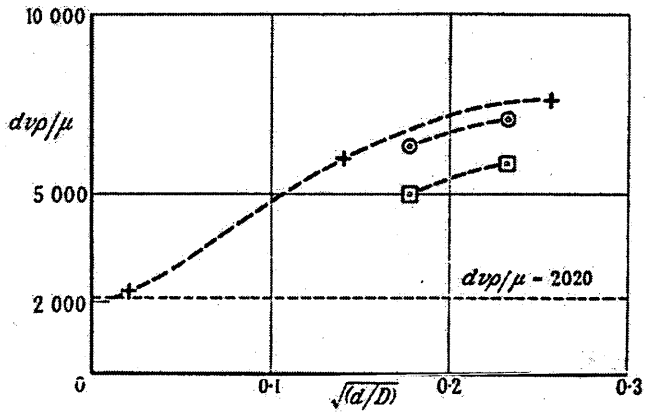

+ Speed at which White's curve indicates first appearance of turbulence.
◎ Lowest speed at which flow appears completely turbulent in a helical glass tube.
⊡ Highest speed at which flow is quite steady.

Figure 2.3.7 Critical Reynolds number. Taylor (1929).

Ito (1959) looked at turbulent flow in curved pipes and found the friction factor of large diameter coils coincided with straight pipe correlations, but a considerable increase in resistance was observed with smaller curve diameters. Another method to determine the transition to turbulence was found by plotting the Dean number against $f_c \sqrt{(D/d)}$, as shown in Figure 2.3.8. This proved clearer than the method shown by White in Figure 2.3.6. The numbered lines correspond to laminar flow equations from other authors, most of which are shown in Appendix E. A slight discrepancy between the experimental data from different authors was found, depending on whether the flow was disturbed before the coil inlet.

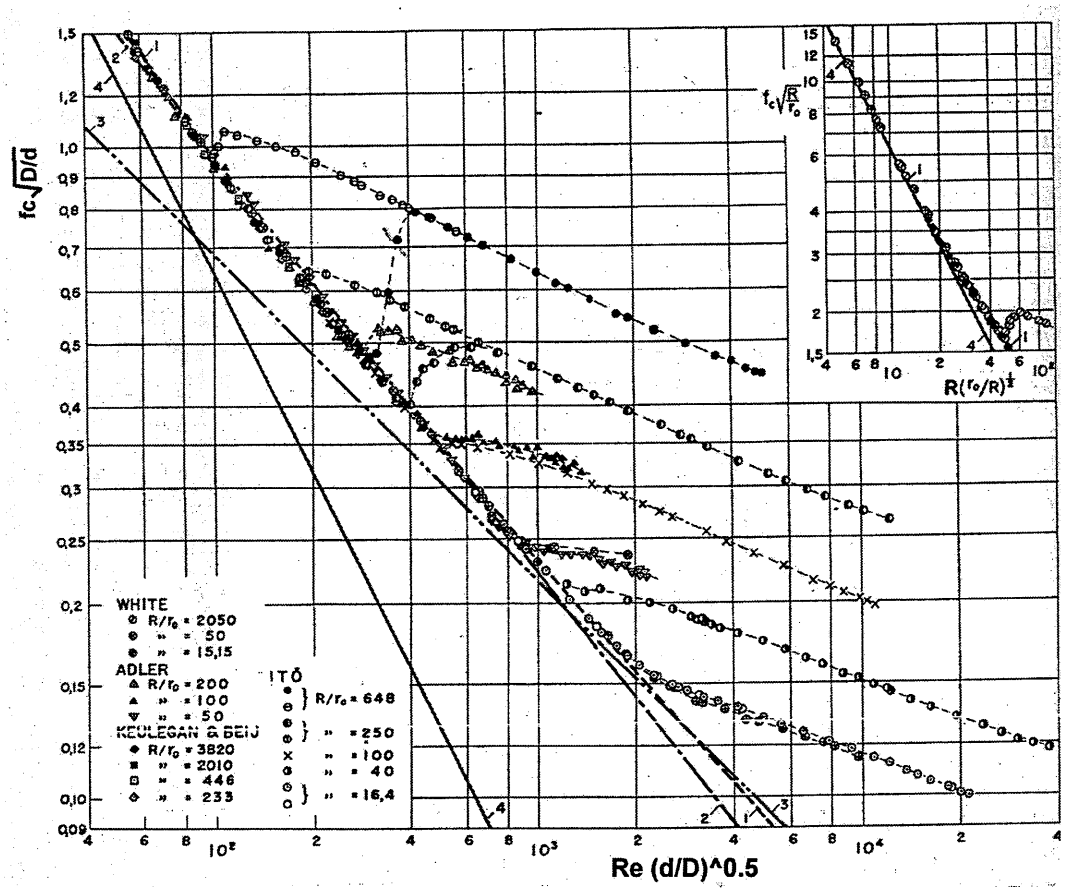

1. Whites empirical formula
2. Prandtls empirical formula
3. Adlers theoretical formula
4. Hagen-Poiseuille law

Figure 2.3.8 Transition from laminar to turbulent flow as shown by Ito (1959).

Various authors have produced correlations to calculate the friction factor in coils. Srinivasan et al (1968) provided an early summary of some of the coil correlations. An up to date summary of the most practical equations to calculate the friction factor in coils is shown in Appendix E. Srinivasan investigated the validity of some of the equations. Theoretically, when the coil diameter approaches infinity, the coil friction factor, f_c, should approach the friction factor of a straight pipe, f_s. Srinivasan found that for a number of equations this was not the case.

Mishra and Gupta (1979) and Liu et al (1994) investigated the effect of coil pitch. Mishra found that the friction factor decreased with an increase in coil pitch but the radius of curvature was the main factor responsible for an increased pressure drop. Kubair and Kuloor (1965) found that the friction factor for non-isothermal flow in coils was less than for isothermal flow. An equation was derived for the relationship between the friction factors for isothermal and non-isothermal flow in coils. Rogers and Mayhew (1964) also investigated the difference between isothermal and non-isothermal flow.

2.3.5.2 *Single-phase Spiral flow*

Significantly, less research has been performed with spirals than helical coils. Unlike coils that have a constant curvature ratio, the curvature ratio in spirals varies along its length. Spirals also have a greater pressure drop than an equivalent length of straight pipe. Ali and Seshadri (1971) studied the flow behaviour in archimedian spirals and found that the flow never became fully developed. This was due to a spiral having forward and reverse transitions between laminar and turbulent flow regimes. With the inlet at the inner most spiral turn, any initial turbulence from before the inlet became dampened. Towards the outer coils, as the intensity of the secondary circulation decreased and the diameter increased, a transition occurred back to turbulent flow. With the inlet on the outside of the spiral, turbulence from the outermost turns became dampened, as the intensity of the secondary circulation increased and a transition occurred to laminar flow. The pressure drop was found to be the same for a particular coil regardless of inlet position. This suggests that the transition lengths for forward and reverse transitions were the same.

Ali and Seshadri (1971) found two critical Reynolds numbers in spirals. The first critical number was suggested to be when turbulence was present in the outer coils. The second critical Reynolds number was presumed to be due to the inertia forces, being sufficient to overcome the damping effect of the secondary flows and having turbulence throughout the whole spiral. These critical points are shown on Figure 2.3.9. The first critical Reynolds number was found to vary with the maximum coil diameter, D_{max}. The second critical Reynolds number was found to be independent of D_{max} but varied with D_{min}. Both critical Reynolds numbers were found to be proportional to the pitch, p, and the tube diameter.

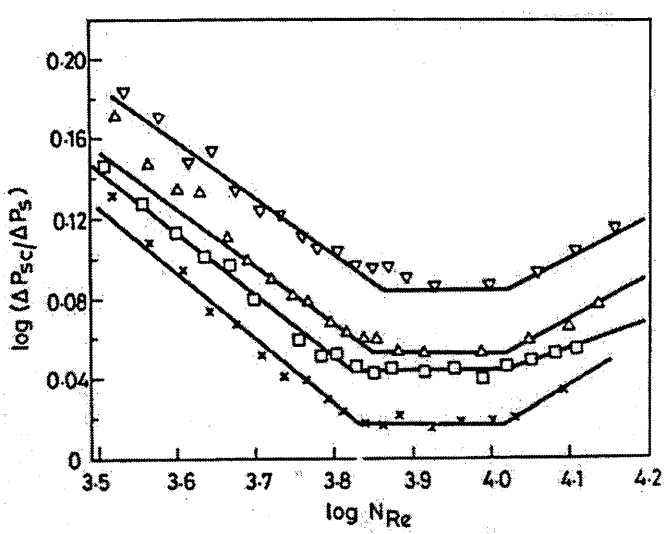

Figure 2.3.9 Critical Reynolds numbers prediction for spirals, with different D_{max}, and constant D_{min}, p and d. Ali and Seshadri (1971).

A limited number of equations were found in the literature to predict the friction factor and critical Reynolds number in spirals. These are shown in Appendix E. Kubair and Kuloor (1966) calculated the critical Reynolds number in a spiral by using the equations developed from coils and replacing the coil diameter with the average

spiral diameter. This was not really valid as the flow may have been laminar in the smaller diameter coils and turbulent in the larger coils. To ensure the flow was laminar in the entire spiral, it must be laminar in the largest coil diameter, as this is where the turbulence starts. Some of the equations used the diameters of the first and last turns of the spiral and hence they were independent of the conditions in-between.

2.3.5.3 Single-phase flow in other coil shapes

Xin et al (1997) studied the flow in annular helicoidal pipes and found the transition from laminar to turbulent flow to be very gradual over a wide range of Reynolds numbers. Oguri (1995) investigated the losses in a figure-of-eight shaped coil, and found the friction factor decreased with the tightness of the coil. Garimella and Christensen (1997) investigated the behaviour of spirally fluted annuli and found the transition from laminar to turbulence was again gradual but occurred at lower Reynolds number values than for straight pipes. Ishigaki (1996) investigated rotating curved pipes.

2.3.5.4 Two-phase coil flow

Significantly less research has been published for two-phase flow in coils. Unlike single-phase flow in coils, there is no significant increase in pressure drop between two-phase flow in straight pipes and coils. Rippel et al (1966) observed that the presence of two phases significantly reduced the Dean effect shown with single-phase flow in coils. This was attributed to the Lockhart and Martinelli parameters being ratios and the geometry not altering the ratio of two-phase to single-phase pressure drop. Rippel et al found the Lockhart and Martinelli relationship for straight pipes to accurately predict the two-phase pressure drop in coils. Rippel et al also correlated experimental data to produce different equations for different flow regimes. These are shown in Appendix E. At low liquid flowrates, the axial mixing was found to be greater than single-phase. Boyce et al (1969) found that calculating the two-phase friction factor in coils, using White's equation for laminar flow in coils and Ito's equation for turbulent flow, in conjunction with the Lockhart and Martinelli correlation proved as accurate at calculating the friction factor for two-phase flow in straight pipes.

The correlations shown in the literature to calculate the pressure drop of two-phase flow in coils are presented in Appendix E. Akagawa et al (1971) found that the two-phase frictional pressure drop in coils was 1.1-1.5 times that of straight pipes. Banerjee et al (1969) found that when both phases were turbulent in vertical coils, the pressure drop could be predicted reasonably well with the Lockhart and Martinelli correlation, using modified parameters. When both phases were laminar, the Lockhart and Martinelli relationship correlated the data well with the viscous liquid –turbulent gas correlation. It was assumed that irregular phase boundaries would destroy the secondary flow patterns in laminar flow, therefore the same friction factor as straight pipes was used. Awwad et al (1995a), (1995b) found that the Lockhart and Martinelli

correlation was not valid for horizontal coils, due to the water column accumulation in the coil. It was demonstrated that for horizontal coils the frictional pressure drop was strongly related to the flowrate as well as the Lockhart and Martinelli parameter. Xin et al (1996) showed that this was also true for vertical coils. Banerjee et al and Awwad et al both concluded that the helix angle had little effect on the pressure drop and hold-up. Awwad et al found that the effect of the coil diameter, D, decreased with an increase in Reynolds number. It appeared that by increasing the tube diameter, d, the pressure drop multiplier, ϕ_L, became independent of the coil diameter, D.

Banerjee et al (1969) found that the flow patterns in coils were adequately predicted by Baker's flow map for straight pipes. Banerjee et al (1969), Maddock et al (1974) and Whalley (1980) studied the liquid film in annular flow in coils and observed 'film inversion'. The film was expected to be thickest on the tube side furthest from the axis, due to centrifugal forces. However in certain cases it was thickest closest to the film axis. Chen and Guo (1999) investigated three-phase oil-air-water flow in coils.

2.3.5.5 Two phase flow in an annular coil

Xin et al (1997) studied the flow of water and air in annular helicoidal pipes. For vertical flow, the pressure drop multipliers were lower than predicted but the void fraction was well predicted. The pressure drop multipliers in horizontal flow were found to be dependent on the Lockhart and Martinelli parameter and liquid flowrate. The flowrate effect decreased with the pipe diameter. The equations shown in the literature are shown in Appendix E.

2.3.5.6 Discussions

Coils have been found to have a greater pressure drop than an equivalent length of straight pipe and the flow can remain laminar to higher Reynolds numbers than straight pipes. A secondary circulation has been found to exist in laminar single-phase coil flow. The transition from laminar to turbulent flow has been shown to be more gradual and far less marked. Many equations were shown in the literature to calculate the friction factor in coils, which are shown in Appendix E.

Less research has been performed for two-phase flow in coils. The presence of two phases appears to reduce the effect of the secondary circulation. It was shown that the pressure drop could be predicted well with a modified Lockhart and Martinelli correlation. The frictional pressure drop in two-phase flow was, however, a function of the fluid flowrates as well as the Lockhart and Martinelli parameter. Coils are primarily used for heat transfer purposes. No previous research was found for the flow of gas-saturated liquids through coils. This topic forms part of Chapter 6 of his thesis.

3 Preliminary experiments

3.1 Introduction

Carbonated drinks dispensers should be able to produce a flow of carbon dioxide-saturated water at a reasonable rate, whilst retaining as much gas dissolved in solution as possible, so that the drink remains fizzy for a long time. Whilst no published research was found on the flow behaviour in carbonated drink dispensers, the literature review suggested that the flow in a dispenser should be smooth and laminar. Preliminary experiments using four commercially available carbonated drink dispensers have been performed to verify this. A needle valve, commonly used in dissolved air flotation (DAF), was also tested. Carbon dioxide-saturated water, without the flavoured syrups, was used as the test fluid.

3.2 Preliminary experimental setup

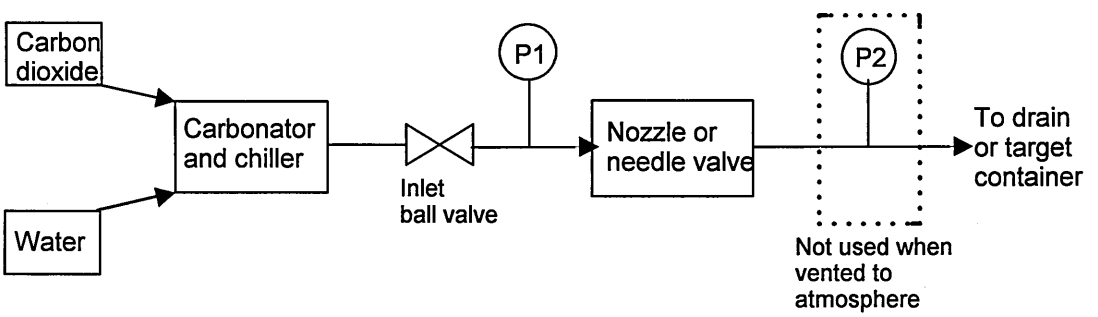

Figure 3.2.1 Preliminary experiment test rig layout.

The preliminary experiments were performed on the apparatus as shown in Figure 3.2.1. The carbon dioxide and water were pressurised together in a Whitlenge, Dorset EF Carbonator at 6.5bar(a) to produce the flow of gas-saturated water. The carbonator pressure was measured using a small 60mm diameter gauge supplied with the carbonation equipment. After carbonation, the gas-saturated water passed through the chiller before reaching the inlet ball valve that was used to adjust the flowrate. The pipe between the chiller and the inlet ball valve was 1m long, with a 10mm internal diameter. The pressure before the nozzle inlet was measured using a Budenberg standard test gauge, the calibration of which is shown in Appendix C.1. The inlet ball valve was connected to the nozzle, via the pressure tapping, with a 200mm length of 4mm internal diameter tubing. When the needle valve was tested, another Budenberg standard test gauge measured the outlet pressure. The needle valve was connected to the outlet pressure gauge by a 100mm long tube with an internal diameter of 4mm, before discharging to the atmosphere.

The effect of the different stages of closure of the needle valve was investigated. The valve had graduations on it, from 0 when closed to 6.5 when fully open. The mass flowrate of water was determined by weighing the amount of water that passed through the system over a given time.

3.3 Results

3.3.1 Carbonated drink dispenser nozzles

3.3.1.1 Nozzle designs

Carbonated drink dispensers should be designed to reduce the pressure and minimise bubble formation. However, the following sections shown that the four nozzles tested seemed to be based on different design principles.

3.3.1.1.1 Nozzle 1

Nozzle 1, patented by Cornelius (1959, 1960), had a very narrow annular gap as shown in Figure 3.3.1 and 3.3.2. The flow was directed around a bullet shaped central body within a casing. The nozzle was opened and closed with a plunger style valve at the nozzle outlet. When the plunger was pulled back a stopper blocked the outlet flow. The design is known to perform well, Scarffe (1997), and release a minimum amount of carbon dioxide during dispensing. A separate nozzle is required for each flavour of drink as the syrup is premixed with the saturated water before the nozzle.

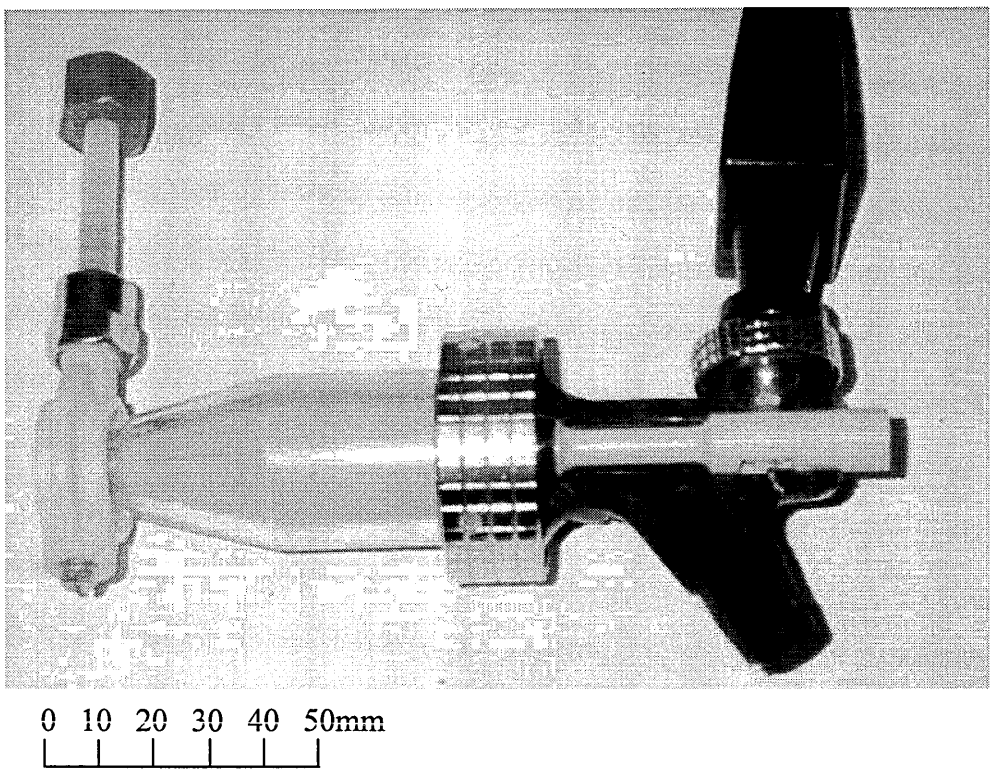

Figure 3.3.1 Photograph of the cross section of nozzle 1.

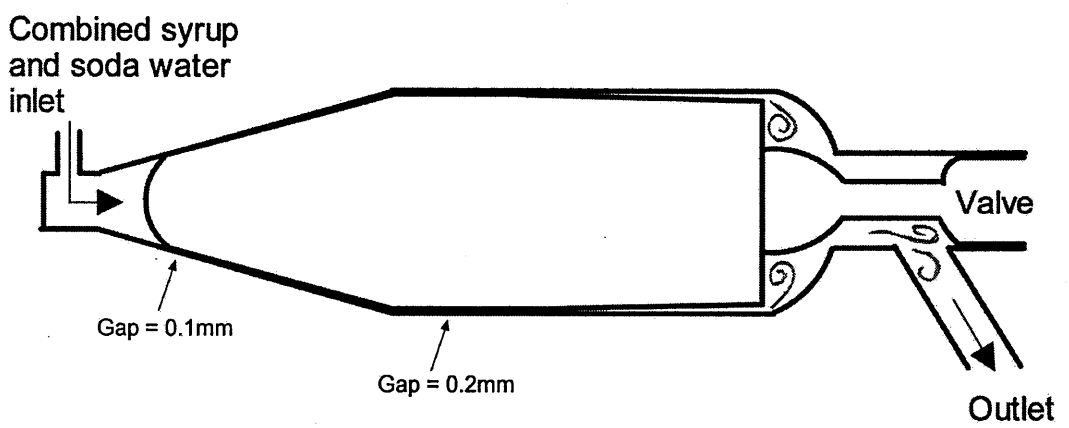

Figure 3.3.2 Diagram of the flow through nozzle 1.

The flow path was very narrow and gradually expanded from a 0.1mm gap. Hence, the majority of the pressure drop was likely to be due to frictional. The pressure drop was likely to be steady, but there may have been a limited amount of recirculation and turbulence near the outlet.

3.3.1.1.2 Nozzle 2

Nozzle 2 was a newer annulus design, which had a shorter flow passage than nozzle 1. It is shown in Figure 3.3.3 and 3.3.4. Figure 3.3.4 shows the flow path of the carbonated water and syrups, the two syrup paths are shaded. The annular gap between the casing and the central body was larger than nozzle 1 and was 0.8mm. The central body was hollow and was divided into two, with space for two different syrups. The syrups were mixed with the depressurised carbonated water at the nozzle outlet. This nozzle is known not perform as well as nozzle 1, Scarffe (1997).

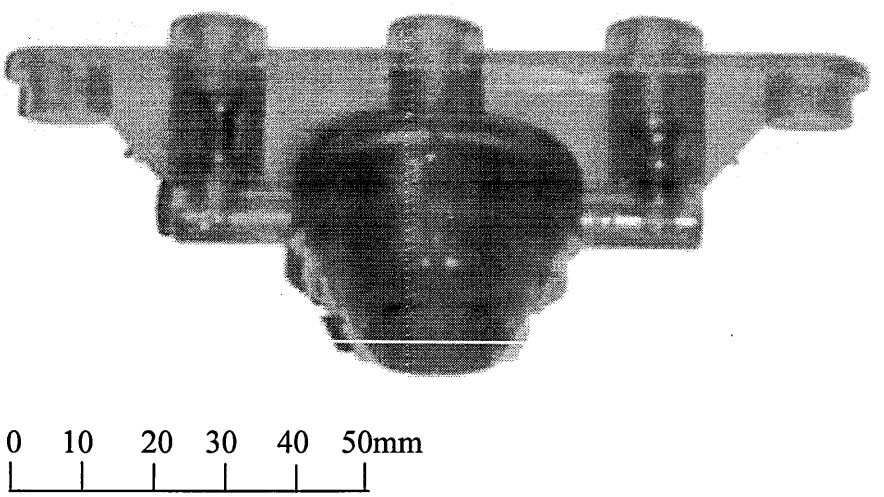

Figure 3.3.3 Photograph of nozzle 2.

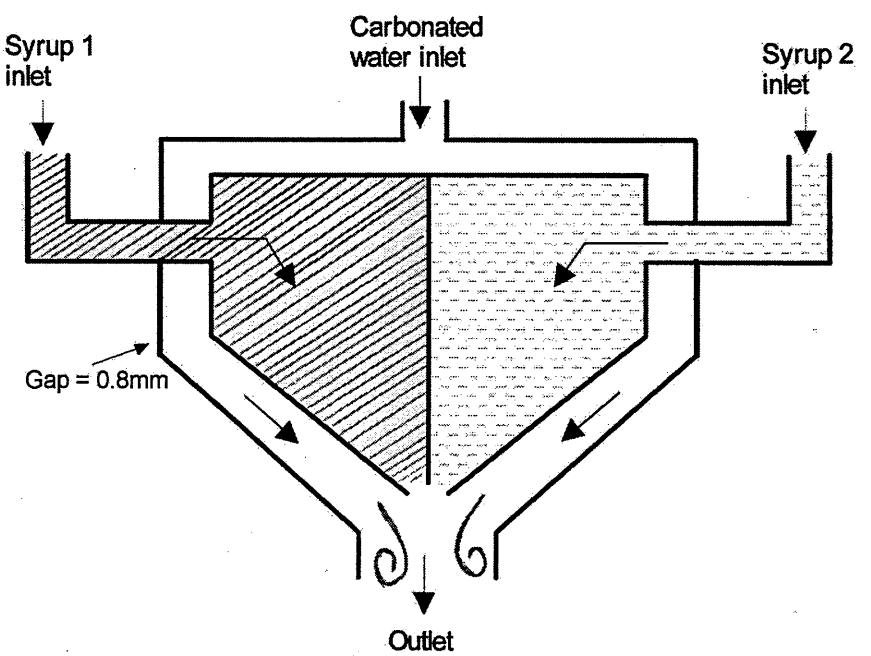

Figure 3.3.4 Diagram of nozzle 2 flow paths.

The changes in direction of the flow were more defined than in nozzle 1. Rykaart and Haarhoff (1995) found that sudden changes in direction were useful in DAF nozzle design and are probably not good for retaining dissolved gas. The 90° change in direction as the flow entered the nozzle and the mixing of the syrup and carbonated water at the outlet, could be areas prone to turbulence.

3.3.1.1.3 Nozzle 3

Nozzle 3 is shown in Figures 3.3.5 and 3.3.6. It depressurises the flow through ten 1mm diameter tubes, five of which are shown on Figure 3.3.6. The nozzle can be used to dispense several different syrups, as well as carbonated and still water individually. Buttons on the hand-held casing activate different combinations of valves that release different syrups and the carbonated water. The syrup is mixed with the depressurised carbonated water in a mixing chamber prior to exit.

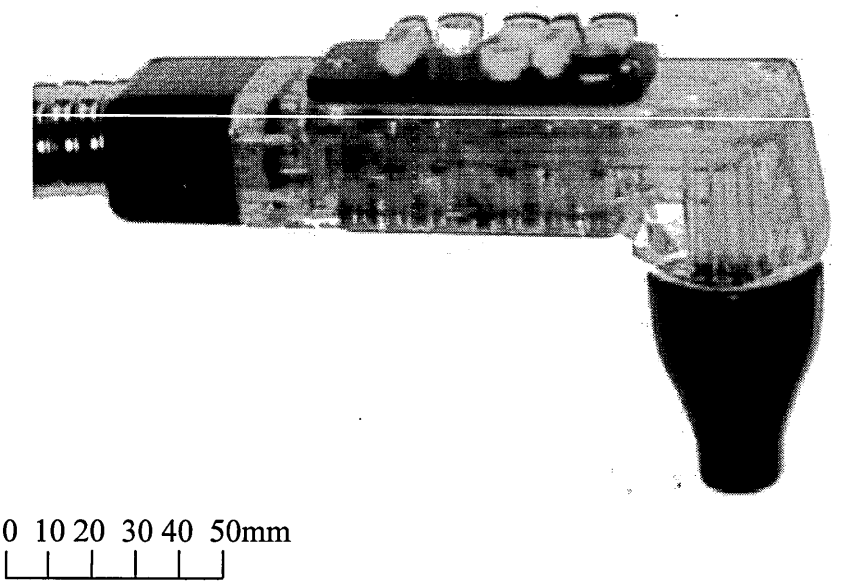

Figure 3.3.5 Photograph of nozzle 3.

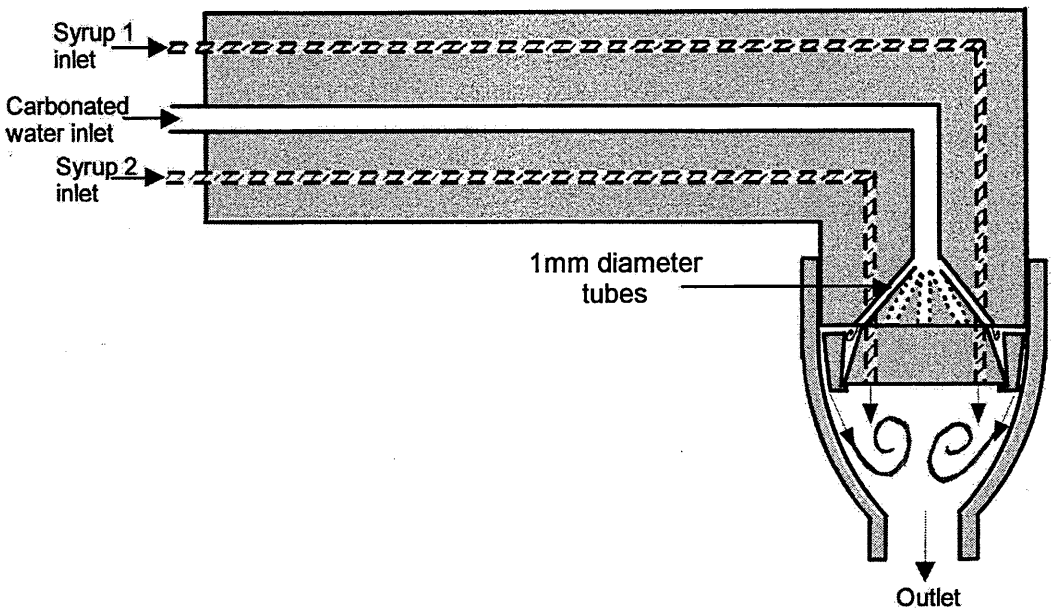

Figure 3.3.6 Simplified diagram of nozzle 3 flow paths.

Figure 3.3.6 shows a simplified flow diagram of the nozzle, with the carbonated water and syrup channels. Only two of the many syrup flow paths are shown, but the other syrups and still water follow similar paths. The end section of this nozzle has a mixing chamber and several changes in the flow direction, which are used in DAF nozzle design for releasing dissolved gas.

3.3.1.1.4 Nozzle 4

Nozzle 4, as shown in Figure 3.3.7 and 3.3.8, uses a baffle, two perforated plates and a chamber to depressurise the carbonated water. The syrup flows straight through a hollow spindle in the centre of the nozzle and is mixed with the water at the outlet. There is only one syrup pipe and hence, a new nozzle is needed for each flavour of drink.

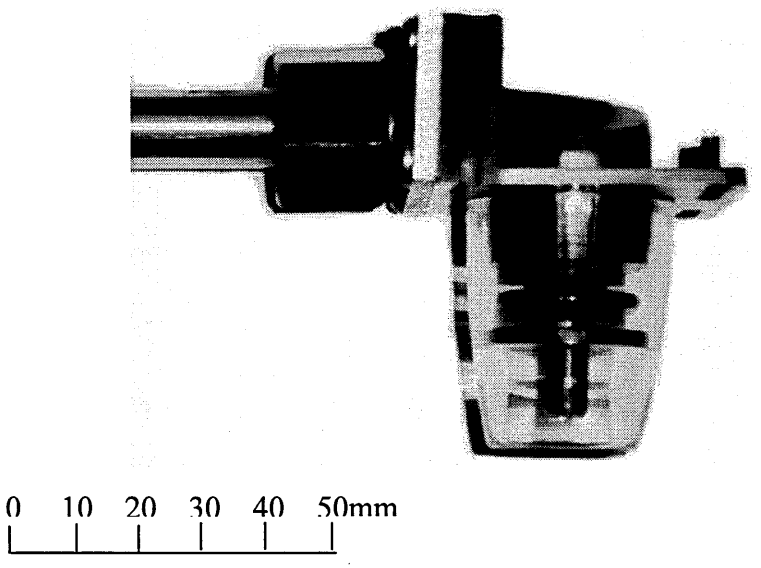

Figure 3.3.7 Photograph of nozzle 4.

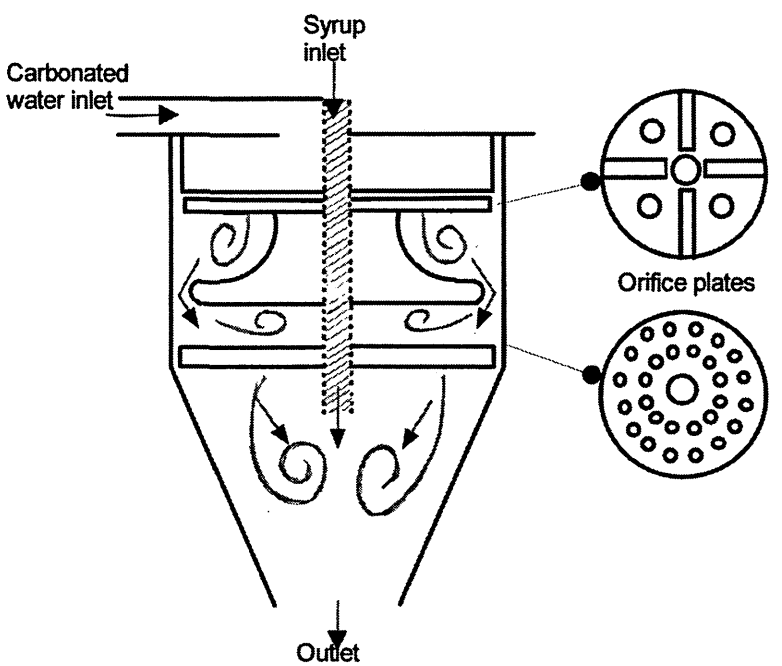

Figure 3.3.8 Nozzle 4 design layout.

This nozzle uses many of the principles utilised in DAF nozzle design. The chamber and changes in direction create ideal conditions for turbulence generation. Impingement surfaces have also been found useful for the release of dissolved gas, as shown by Rykaart and Haarhoff (1995), Steinbach and Haarhoff (1997) and Jefferson (1997). When dispensing Guinness, perforated plates are used to release bubbles to create the head, this was shown by Ash (1961a and b).

After studying the designs of these nozzles, nozzle 1 appears to have the smoothest flow path, whilst nozzle 4 appears to be designed like a DAF nozzle.

3.3.1.2 Pressure and flow characteristic results

The relationship between flowrate and pressure drop was found for each of the carbonated drink dispensers tested. The results are shown in Figure 3.3.9. Nozzles 1 and 3 performed similarly with low flowrates and high pressure drops. In contrast, nozzles 2 and 4 had high flowrates and low pressure drops.

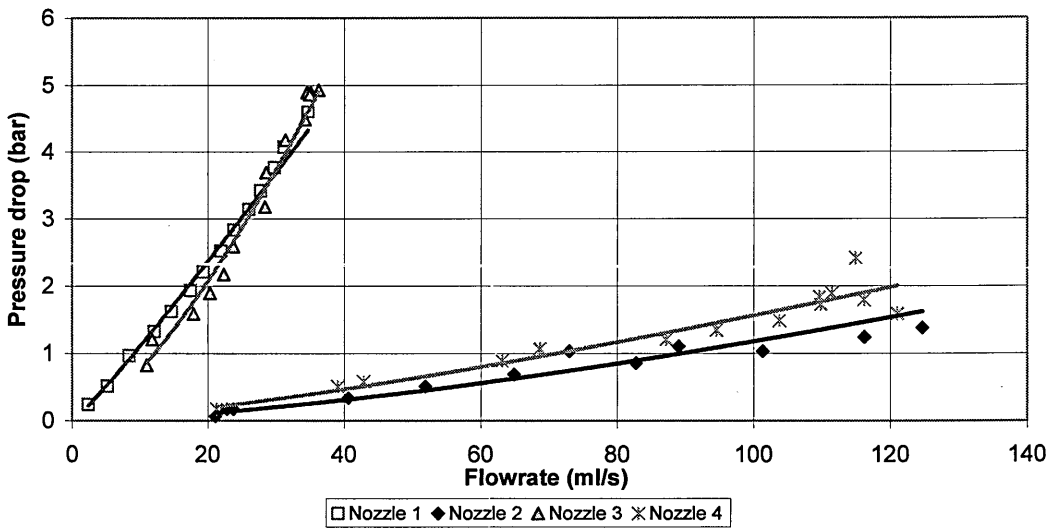

Figure 3.3.9 Pressure drop versus flowrate relationships of the four carbonated drink dispensers.

Ideally, the flowrate through each nozzle should be as high as possible, but not so much that excessive turbulence is induced. Nozzles 2 and 4 achieved flowrates of more than three times those of nozzles 1 and 3.

A carbonator pressure of 6.5bar(a) was used in the tests. The pressure was measured at the inlet of each nozzle. The outlet of each nozzle was discharged to atmosphere. Nozzles 1 and 3 were both able to drop the majority of the total pressure across the device. In contrast, even at the maximum flowrate, the inlet pressures of nozzles 2 and 4 were only 37% and 45% of the carbonator pressure respectively. The significant reduction in pressure prior to the device, meant that the flow resistance of the pipe work leading up to the nozzle was comparable to that of the nozzle itself. Hence, only a small proportion of the total pressure drop was across the device.

Ideally, the pressure drop should be solely across the nozzle, so that bubbles cannot form prematurely. When nozzles 2 and 4 were tested, 'bubble formation' noises could

be heard in the inlet valve, the inlet flow was also cloudy, indicating that the premature pressure drop was undesirable.

Turbulence is undesirable in carbonated drink dispensers as it can create local pressure fluctuations that can encourage bubble formation. To indicate the nature of the flows, calculations of the Reynolds numbers were made at the narrowest flow areas in each nozzle. In straight pipes Reynolds numbers of less than 2000 can indicate laminar flow. The calculations were performed at the maximum flowrate achieved. The fluid was assumed to be water, with a density of 1000kg/m^3 and viscosity of 0.001kg/m/s. For nozzle 1, at the narrowest 0.1mm gap, the Reynolds number at the maximum flowrate of 35ml/s would have been 2000. In nozzle 2, at the 0.8mm gap and the maximum flowrate of 120ml/s, the Reynolds number would have been 2500. In nozzle 3, the Reynolds number through the 1mm diameter tubes would have reached 4500, at the maximum flowrate of 36ml/s. Reynolds number calculations for nozzle 4 were very difficult, due to the change in size of the chambers. However, the flow was likely to have had large amounts of turbulence, as the flow went through a series of changes in direction and through perforated plates that could create large amounts of turbulence. From this analysis, nozzle 1 had the lowest Reynolds number, indicating that the flow may have been laminar.

The loss coefficient, k, was found for each nozzle by correlating the data in Figure 3.3.9, using equation 3.3.1, to produce a best-fit 'power' trendline. The R^2 residuals were between 0.95 and 0.99. A residual of 1 would indicate a perfect fit. These residual values indicate that the correlations fitted the data well.

$$\Delta P = k\, Q^n \qquad \text{Equation 3.3.1}$$

The flowrate index, n, was also used to indicate the nature of flow within the nozzle. In a straight pipe, with a solely frictional loss, n would equal 1 when the flow was laminar and increase to about 2 for fully turbulent flow. Table 3.3.1 shows the values of k and n calculated for each nozzle. It shows that nozzles 1 and 3 had the highest loss coefficients, suggesting that they had greater pressure drops than nozzles 2 and 4. Nozzle 1 also had the lowest flowrate index.

	k	**n**
Nozzle 1	0.0886	1.10
Nozzle 2	0.0038	1.31
Nozzle 3	0.0266	1.45
Nozzle 4	0.0015	1.45

Table 3.3.1 Summary of the nozzle loss coefficients.

The pressure drop versus flowrate relationships for different carbonator pressures through nozzle 1 were found to be very similar. In nozzle 1, bubbles could be seen forming on the small ridges of the nozzle and on scratches on the surface of the nozzle. When the inside of the casing was sprayed with WD40, coating the scratches,

fewer bubbles were formed because the oil had filled in the nucleation sites. The pressure versus flowrate relationship was unchanged

Nozzle's 1 and 3 seemed to have similar overall pressure and flowrate characteristics, and were able to drop the majority of the system pressure. The inlet pressure to both nozzles 1 and 3 was essentially the carbonator pressure. Therefore very little dissolved carbon dioxide would have come out of solution before the nozzle. However, nozzle 3 had a higher Reynolds number. It also had a mixing chamber before the exit where a high degree of turbulence would have present suggesting that its ability to retain the dissolved carbon dioxide would not be as good as nozzle 1.

3.3.2 Needle valve

A needle valve was tested as a direct comparison to the carbonated drink dispensers. The relationship between flowrate and pressure drop for each of the 6 different stages of opening of the needle valve (1= almost closed, 6= fully open), is shown in Figure 3.3.10.

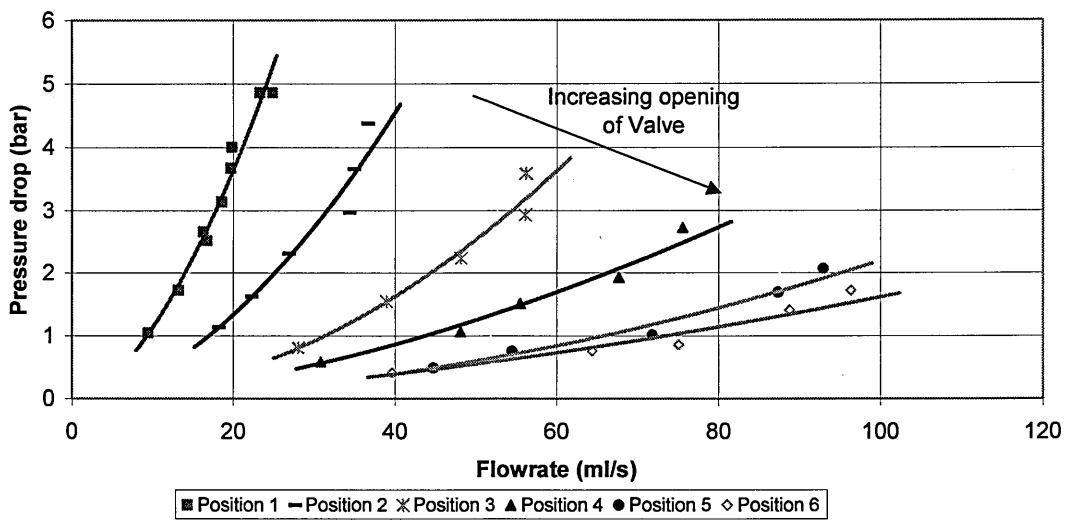

Figure 3.3.10 Effect of varying the opening of a needle valve.

When the needle valve was fully open, the inlet pressure to the valve was low and the pressure drop across it small. A substantial pressure also remained at the nozzle outlet, indicating that the most of the pressure drop occurred across the apparatus and that the valve had a negligible affect. When the valve was almost closed, the majority of the pressure was dropped across the valve.

The loss coefficient, k, and flowrate index, n, for each stage of opening of the needle valve were found by correlating the data in Figure 3.3.10 using a best-fit 'power' trendline with equation 3.3.1. The R^2 values were between 0.96 and 0.99, suggesting

a good fit. The results are shown in Table 3.3.2. The values of the flowrate index, n were high, indicating disturbed flow.

Opening position	k	n
1	0.023	1.6909
2	0.0067	1.7672
3	0.0011	1.9835
4	0.0019	1.6622
5	0.0004	1.8783
6	0.0012	1.5584

Table 3.3.2 The values of k and n for the needle valve.

The loss coefficient, k, calculated for each stage of opening is shown in Figure 3.3.11. The loss coefficient was greatest when the valve was almost shut. When the valve was at position 1, it had a similar loss coefficient to nozzle 3 but was 4 times less than nozzle 1.

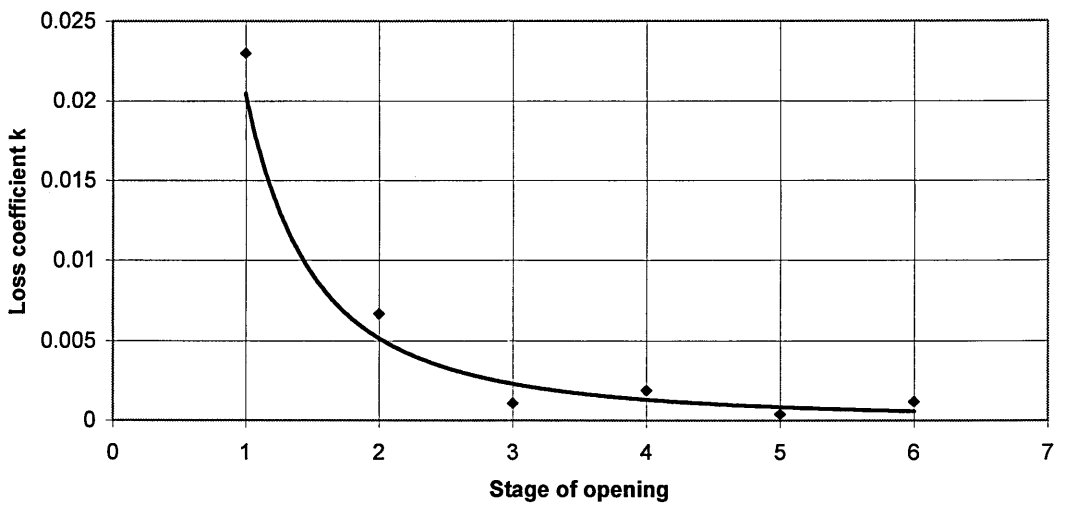

Figure 3.3.11 Variation of the loss coefficient in the needle valve with each stage of opening.

3.4 Discussions

3.4.1 Carbonated drink dispensers

	Maximum flowrate (ml/s)	Maximum pressure before nozzle (bar a)	Reynolds number (at narrowest gap)	Loss coefficient k	Index n
Nozzle 1	34.7	4.60	2000	0.0886	1.10
Nozzle 2	124.7	1.38	2500	0.0038	1.31
Nozzle 3	36.3	4.93	4500	0.0266	1.45
Nozzle 4	121.0	1.59	-	0.0015	1.45

Table 3.4.1 Summary results of the testing carbonated drink dispense nozzles.

A summary of the carbonated drink dispenser results is shown in Table 3.4.1. Nozzles 1 and 3 showed a similar pressure drop versus flowrate relationship. As each nozzle was discharged to atmosphere, the majority of the pressure drop for nozzles 1 and 3 was across the nozzle. Nozzles 2 and 4 could achieve higher flowrates but had low resistances, meaning a significant amount of the total pressure was dropped before the device. This was supported by the sounds of bubbles forming in the inlet valve before the nozzle. Nozzles 2 and 4 also had large areas where turbulence would occur, which is not desirable in carbonated drink dispensing.

For carbonated drink dispensing, a nozzle is required to drop a high pressure, with laminar flow. Based on the geometry, Reynolds number calculations and the flowrate index, it appeared that the flow through Nozzle 1 was likely to have been laminar. It also had a high pressure drop. Thus, it is suggested that out of the nozzles tested, nozzle 1 was the most likely to retain the highest amount of carbon dioxide dissolved in the solution, at the outlet.

Bubbles were observed forming on the scratches and ridges within nozzle 1. Coating the nozzle with WD40 appeared to give a more even bubble size distribution within the nozzle. This demonstrated the wetted surface effect of nucleation sites.

3.4.2 Needle valve

When the needle valve was fully open, it had a very low loss coefficient and low pressure drop, and hence the inlet pressure was low. On this occasion, the majority of the pressure drop occurred over the apparatus up and downstream of the valve and not across the valve. When the needle valve was nearly closed, it had a large loss coefficient and the pressure drop occurred solely across the valve.

3.5 *Modifications for detailed experiments*

Nozzle 1 was found the have all the characteristics to suggest it performed well as a carbonated drink dispenser. Hence, a test version of the nozzle was made so that measurements could be made before and after depressurisation. The measurements included the concentration of carbon dioxide dissolved in water, temperature and pressure were all measured, as well as the flowrate. Measurement of the concentration of dissolved carbon dioxide after depressurisation would give a clear measure of the nozzles performance. The test nozzle and fittings were made of transparent materials so that the formation of bubbles could be observed. All the connections were made as smooth as possible to cause minimal disturbance to the flow. The experimental set-up for the subsequent and main rig is described in Section 4.

3.5.1 Design of test nozzle

The test nozzle was designed to accurately imitate nozzle 1 and is shown in Figure 3.5.1. A complete set of engineering drawings for the test nozzle is shown in Appendix H. The outer casing of the nozzle was made of perspex so that any bubble formation could be visualised. An actual central body was used in the test nozzle. As the valve was removed in the test nozzle, an extra section was attached to the end of the central body to reproduce the geometry of the original nozzle. The ridges on the central body ensured the flow area was even around the annulus. An adjustable spacer was added so that the flow area of the annular gap at the start of the nozzle could be varied and hence too the flowrate. The test nozzle was made with connections in the axial direction at both the inlet and outlet, as shown in Figure 3.5.1. The nozzle was designed to withstand 7 bar. The outer casing was made in two sections to ease cleaning, so that any dirt or possible bubble nucleation sites could be removed. The surfaces were polished smooth to avoid crevices that would aid nucleation.

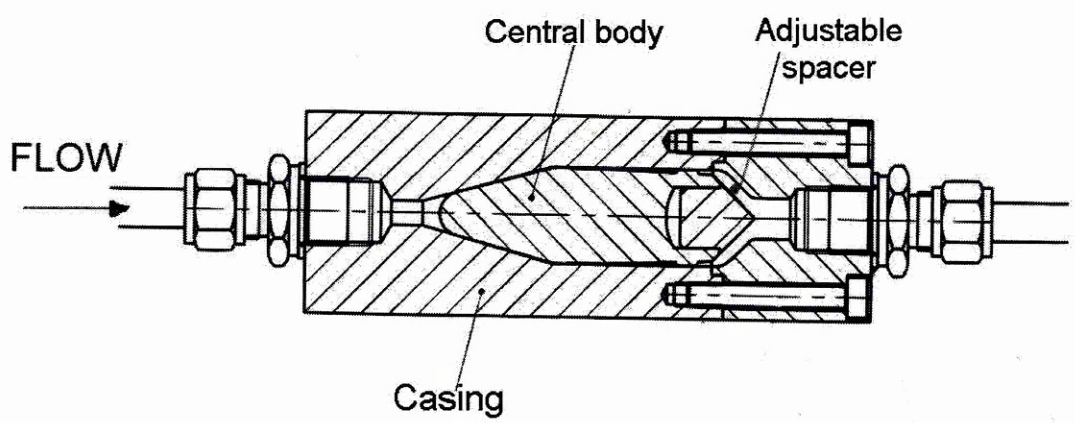

Figure 3.5.1 Design of test nozzle.

4 Experimental setup

4.1 Aim of the experiments

The test rig was designed and constructed to determine the performance of depressurisation devices. Coils and nozzles were both used to depressurise single-phase and two-phase flows. The test fluids used were:

Single-phase flow	- Water
	- Air
Two-phase flow	- Air and water
	- Carbon dioxide saturated water

Due to the compressibility of air, its volumetric flowrate would have increased as the pressure was reduced along the depressurisation device. With the two-phase flow of air and water, the volumetric flowrate of air would have increased along the device but the volumetric flowrate of water would have remained constant. The mass flowrates however, would have both remained constant. With the gas-saturated flow, the mass of gaseous carbon dioxide would have increased as the pressure was reduced, due to its solubility in water decreasing with pressure. The mass flowrate of water would have remained constant.

The performance of a device was evaluated by measuring the pressure and temperature of the flow before and after the device and the flowrate. In the gas-saturated water tests, the concentration of carbon dioxide dissolved in the water was also measured before and after the device. Pressure is a fundamental factor in bubble formation. Temperature is also critical, as carbon dioxide solubility increases as temperature decreases.

The rig was designed to minimise any disturbance to the flow and to ensure that the majority of the pressure drop was across the depressurisation device. The flow path was made as smooth as possible to minimise bubble formation. The equipment used is documented in Appendix A.

4.2 Overview

The rig consisted of three main parts: the flow supply section, test section and the flow measurement section, as shown in Figure 4.2.1.

There were two different flow supplies. The first was a carbonator unit, a Whitlenge, Dorset EF Carbonator, for the two-phase gas-saturated flow experiments. The second was for air and water, single or mixed two-phase experiments. After the flow supply section, the flow entered the test section.

Two types of depressurisation devices were studied: a nozzle for dispensing soft drinks and small diameter coils. In the test section, the temperature, pressure and carbon dioxide concentration (if applicable), were measured before and after the depressurisation devices. The concentration of carbon dioxide was determined by trapping the flow within a calibrated volume.

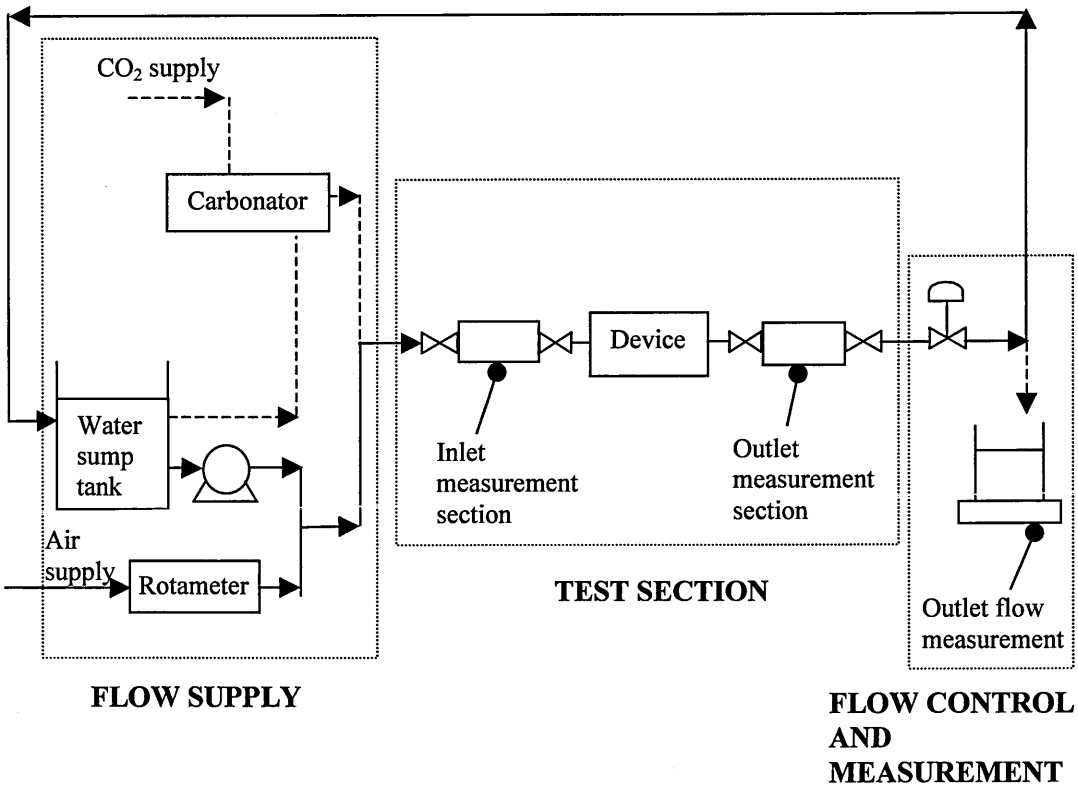

Figure 4.2.1 Overview of the experimental setup.

A valve, located downstream of the test section was used to control the flow. This was to ensure that any flow disturbance or cavitation did not affect the results of the device under test. At the outlet the water was either recycled to the water sump tank or directed to a weighing tank. Inline flow meters were not suitable for this study due to the two-phase nature of the flow.

4.3 Flow Supply

Water was drawn from a large sump tank. The laboratory temperature remained at between 23 and 25°C for all experiments, this meant the water had a constant inlet temperature for each test. The mass flowrate of water was determined by weighing the amount of water passing through the device in a measured time period. For the gas-saturated water experiments, the water flowrate was determined by timing the off/on cycle of the water pump to the carbonator. The water pump switched off when the water level in the carbonator reached a maximum and switched on when the minimum level was reached. The volume between the maximum and minimum water

level was 556g. Thus by timing the off/on cycle of the water pump, the water flowrate through the device could be calculated. This method was calibrated by weighing the amount of water that passed in a known amount of time. The uncertainty of the method was approximately 2% of the measurement. This calibration is detailed in Appendix C.4.

The space above the water in the saturator was occupied by carbon dioxide and the pressure regulator maintained the saturator pressure. The pressure at the outlet of the flow supply section was set to 5.3 bar absolute, which was the maximum operating pressure of the water pump.

4.3.1 Air and water supply

The air and water supply unit consisted of a water and air feed. These could be used independently to produce single-phase flows, or together to produce a flow of two-phase air and water.

The air was taken from the laboratory supply and regulated to a pressure of 5.4 bar absolute. This pressure was slightly higher than the water pressure, to ensure air was injected into the water flow for the two-phase air and water experiments. A Budenberg standard test gauge measured the air pressure. The calibration of which is detailed in Appendix C.1. The flowrate of air was measured using a Brooks Instrument, Model 1350, set of rotameters. The set consisted of a range of different sized tubes and floats for different flowrates. The calibrations of the rotameters can be seen in Appendix C.3. The air flowrate was controlled using the valve that was an integral part of the rotameter. A non-return valve was installed in the air-line prior to the air injection point, to ensure the rotameter remained dry.

In the two-phase air and water experiments, air was injected into the water over 100 pipe diameters upstream from the test section. This distance was chosen to ensure that the combined flow could stabilise before depressurisation. Between three and five different gas flowrates were investigated, for a range of water flowrates.

4.3.2 Carbonated water supply

The carbonated water supply consisted of a water and carbon dioxide feed to the Whitlenge, Dorset EF carbonator. The carbonator system, which is used commercially to dispense carbonated drinks, included a small pump to assist the water into the saturator. The carbon dioxide, taken from a compressed gas cylinder, and the water, were pressurised at 5.3 bar(a), within the small cylindrical saturator, to dissolve the gas into the water. The saturator had a diameter of 110mm and height of 270mm and was found to be 95% efficient, as shown in Appendix C.4. A diaphragm regulated the pressure within the carbonator. The pressure was displayed on a Budenberg standard test pressure gauge. The gas-saturated water from the carbonator was then directed to the test section.

The carbonator system was supplied with a chiller unit. The unit is used commercially to cool the carbonated water and syrups. As carbon dioxide solubility varies with temperature and the test section was not lagged, the chiller was not used. The laboratory temperature was always between 23-25°C, this ensured a constant temperature was maintained across the whole rig for all of the experiments.

It was impossible to measure the gaseous carbon dioxide flowrate directly. The amount of gas released into the flow before and after the device was found by trapping the flow in a known calibrated volume and measuring the volume of gas.

At very high flowrates there were large pulsations, due to large amounts of undissolved gas leaving the saturator. In this case, the water pump was unable to refill the saturator fast enough so gas was in the outlet flow with the water. The transition to pulsating flow was found to be approximately 100ml/s, as shown in Appendix C.4. The maximum flowrate achieved by the nozzle was 80ml/s and for the coil 25ml/s, well below the transition point.

4.4 Test section

The test section consisted of three main parts: the inlet measurement section, a depressurisation device and the outlet measurement section. All these were attached to a hinged wooden board. The board was orientated in the horizontal position whilst running the experiment and the vertical position to measure the volume of gas when trapped.

4.4.1 Inlet measurement section

The inlet section, situated before the depressurisation device, was identical for both the coil and nozzle experiments. The layout is shown in Figure 4.4.1 and the dimensions in Table 4.4.1. The flow was trapped in a calibrated 10mm internal diameter acrylic tube. The temperature and pressure of the flow were measured using a thermocouple and pressure transducer. The tappings for the pressure transducer and thermocouple were situated in a perspex block upstream of the acrylic tube. A 100ml gas-tight syringe was attached to a perspex block downstream of the tube. The flow path diameter through the perspex blocks was also 10mm. On either side of the blocks were the two 90° full bore ball valves. The tappings for the pressure transducers, thermocouple and syringe were made as small as practical and flush with the inside, to minimise any disturbance to the flow.

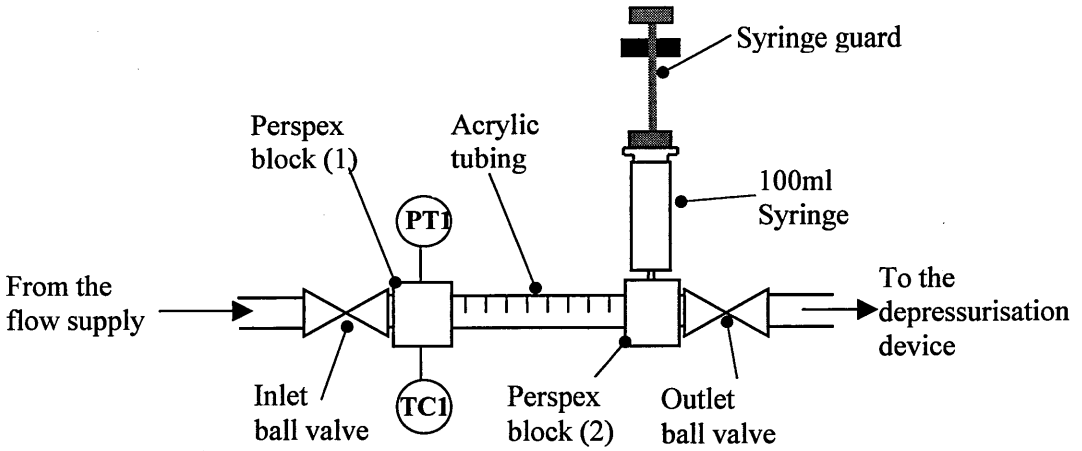

Figure 4.4.1 Inlet measurement section of the test section.

		d (mm)	l (mm)
Trapping tube		10	200
Ball valve (inlet and outlet)		10	20
Perspex block (1) + (2) (flow path in block)		10	5
Perspex block (1)	PT1 tapping	1	10
	TC1 tapping	2	10
Perspex block (2)	Syringe tapping	1	10

Table 4.4.1 Dimensions of the fittings in the trapping section at the device inlet.

Figure 4.4.2 shows the experimental equipment layout of the measurement section before the nozzle. No downstream ball valve is shown as it was removed, in later experiments, to minimise further disturbances to the flow. The inlet concentration was found to be the same for each experiment and was therefore not measured in the later experiments.

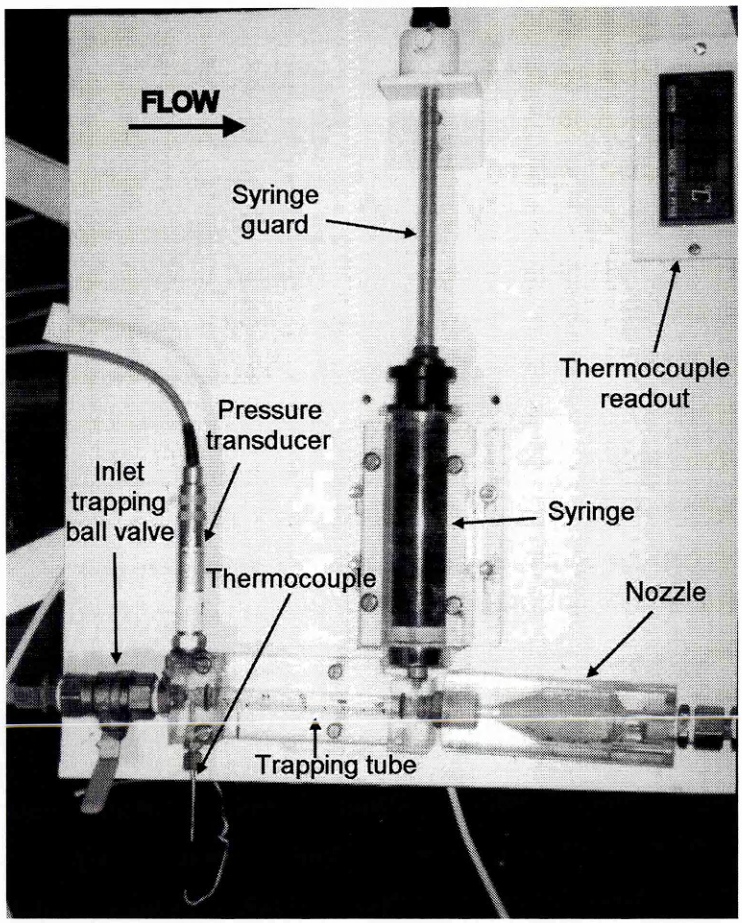

Figure 4.4.2 Experimental equipment of trapping section at nozzle inlet.

The pressure transducer, PT1, was a Keller series 3 piezoelectric pressure transducer with a working range of 0 to 10 bar absolute. The transducer was connected to a signal conditioning box, power supply and a voltmeter readout. The voltmeter readout for the pressure transducer was calibrated using a Druck DPI 601 digital pressure indicator. The calibration was linear and is shown in Appendix C.1. The temperature was measured with a PT100 PTFE insulated probe, TC1. It was calibrated against a digital thermometer and probe using a S1220 System Teknik AB calibration block. The calibration was linear and is shown in Appendix C.2.

When the two ball valves were closed, the trapped volume was found to be 19.6ml. The determination of this trapped volume is described in Appendix C.5. A syringe guard was used to keep the plunger in the 'fully closed' position when the system was running. After closing the trapping valves, the syringe guard was opened to depressurise the trapped fluid. The method used to determine the concentration of carbon dioxide in solution is described in Section 4.5.

In the coil tests, a transition block was used to reduce the diameter of the flow from 10mm to 2.5mm, the diameter of the coil. It was situated after the inlet measurement section and steadily reduced the diameter without creating excessive turbulence.

4.4.2 Depressurisation devices

Two types of depressurisation device were studied.

i) Carbonated drink dispenser nozzles

The preliminary experiments found Nozzle 1 to perform best, but it was designed to discharge freely to the atmosphere, making outlet measurements impossible. To study its behaviour in more detail, a test version of the nozzle was made. It was designed to enable standard pipe fittings to be attached at the inlet and outlet, so that the flow properties before and after depressurisation could be investigated. The engineering drawings for this nozzle are shown in Appendix H. The device was mounted to run horizontally. The outside casing of the nozzle was made of perspex, so that the flow and any bubble formation could be visualised. The same central body was used as the original nozzle but with an extra section attached to the outlet to imitate the valve that was excluded in the test nozzle design. The outer casing was made in two sections, held together by six screws so that it could be dismantled and easily cleaned. An adjustable spacer was used to vary the central body position within the casing and hence the flow area within the nozzle. The spacer was an adjustable nylon screw, situated at the back of the central body.

ii) Coils

Section 2.3.5 of the literature review found that the pressure drop, for a given flowrate, was higher in a coil than in an equivalent length of straight pipe. It also revealed that the flow in a coil could remain laminar to high Reynolds numbers, implying that coils may be suitable as a depressurisation device for carbonated drinks. Therefore, the flow behaviour in various coils was studied. The coils were made of flexible, polyurethane tubing, with an outside diameter of 4mm and an internal diameter of 2.5mm, wrapped around a plastic pipe. Two different sized plastic pipes were used to produce coil diameters, D, of 0.029m and 0.079m. Ten different coils were tested with 5 different lengths of tube, 2, 3, 3.7, 5 and 7m. The coils used are shown in Figure 4.4.3. A 5m long straight tube and 0.139m diameter coil were also tested with the single-phase water flow. The coils were run horizontally in all the experiments.

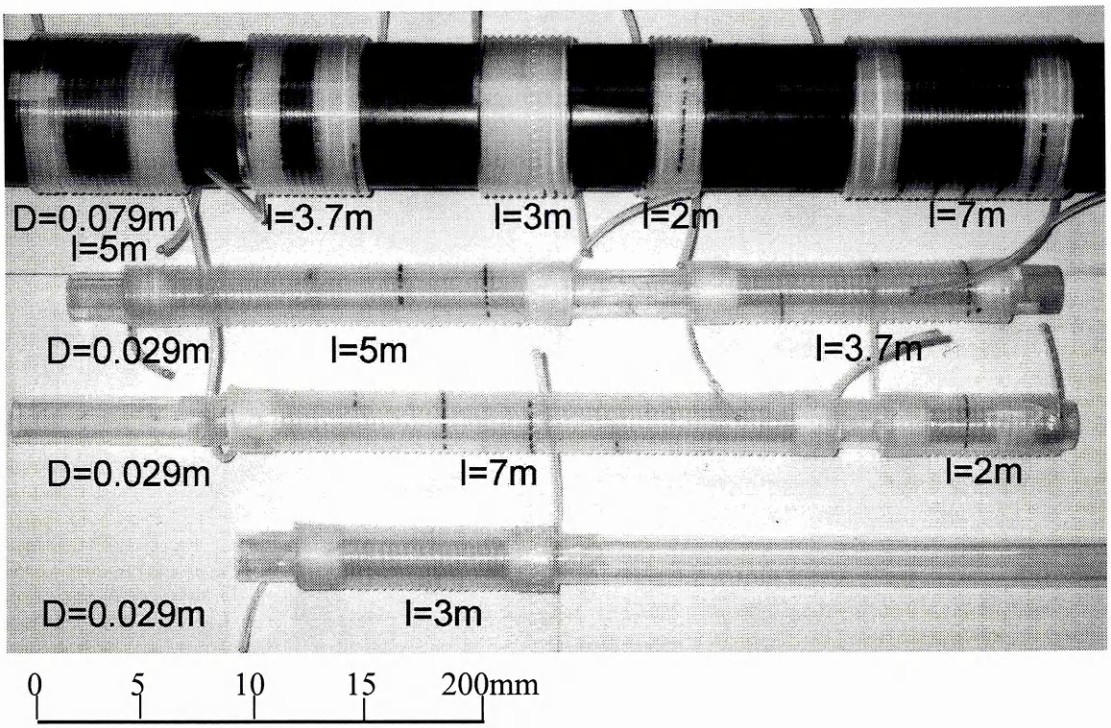

Figure 4.4.3 The coils used experimentally.

4.4.3 Outlet measurement section

The outlet measurement section, situated after the depressurisation device, varied slightly depending on whether the nozzle or a coil was being tested.

The nozzle measurement outlet section was identical to the inlet measurement section, as the nozzle's inlet and outlet diameter were both 10mm. This diameter was large compared to the minimum gap within the nozzle of 0.1mm, this ensured that the pressure drop across the fittings and the trapping section was negligible. The total trapped volume in the nozzle outlet measurement section was found to be 20.4ml. The determination of this volume is detailed in Appendix C.5. Sample calculations showed expansion of the tubing under pressure was negligible and hence the volume of the trapping tube remained constant. A piezoelectric pressure transducer, pressure transducer 2 (PT2), and a PT100 temperature probe (TC2), were used for the nozzle outlet measurement section. Part way through the project PT2 failed and was replaced with PT3. Both pressure transducer calibrations are shown in Appendix C.1. The probe calibration is shown in Appendix C.2.

The coil outlet trapping section was made of the same 2.5mm internal diameter polyurethane tubing as the coil. This was to ensure minimal disturbance to the flow with no sudden expansion that might encourage additional bubble formation and corrupt the results. The trapping tube was 300mm long with a total trapped volume of 1.99ml. This length was selected, so that the pressure loss across the trapping section was small in comparison to the depressurisation device but was long enough to trap a

reasonable volume of fluid. A diagram of the outlet trapping section for the coil experiments is shown in Figure 4.4.4. A photograph is shown in figure 4.4.5 and the dimensions are detailed in Table 4.4.2.

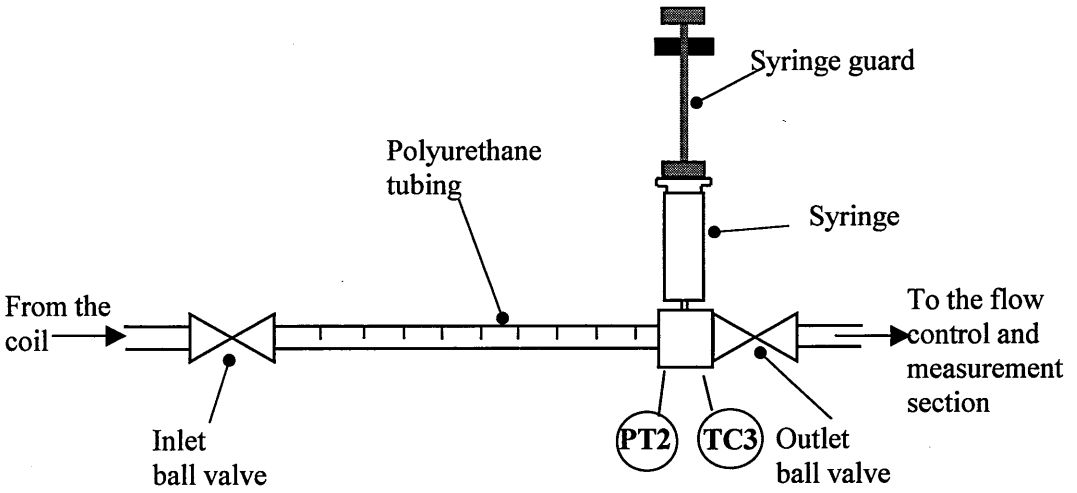

Figure 4.4.4 Outlet measurement section for the coil experiments.

		d (mm)	l (mm)
Trapping tube		2.5	300
Ball valve (inlet and outlet)		2.5	5
Perspex block (flow path in block)		2.5	20
Perspex block	PT2 tapping	1	10
	TC3 tapping	1	10
	Syringe tapping	1	10

Table 4.4.2 Dimensions of the fittings in the trapping section at the coils outlet.

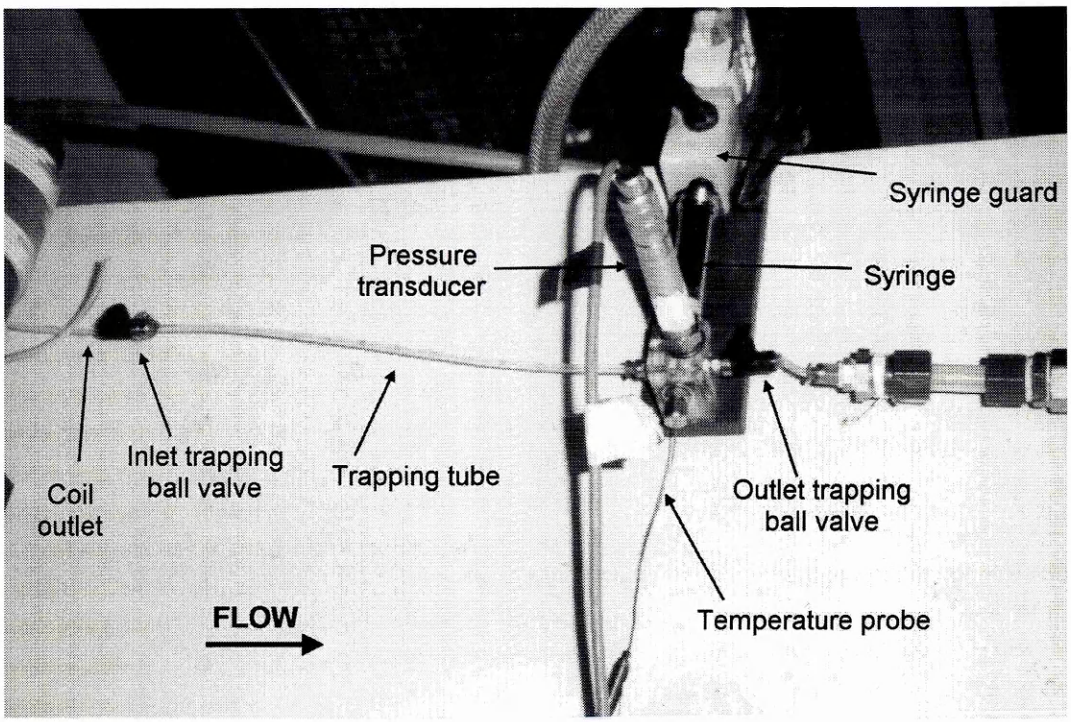

Figure 4.4.5 Experimental equipment of trapping section after the coil.

A single perspex block with a flow path diameter of 2.5mm was used to attach the pressure transducer, PT2, temperature probe, TC3, and syringe. This block was situated immediately after the trapping tube. A narrow type K industrial mineral insulated probe, with a 1mm diameter was used to minimise flow disturbance. The calibration is shown in Appendix C.2. A range of gas tight syringes, 2.5, 10 and 25ml were used, depending on how much dissolved gas remained in solution. Miniature ball valves with an internal diameter of 2.5mm, which had a simple snap fit mechanism, to connect to the tubing were used. The equipment used is detailed in Appendix A.

4.5 Carbon dioxide concentration measurement

In the gas-saturated water tests, the concentration of carbon dioxide dissolved in water was measured before and after depressurisation. Previous researchers have used various different methods determine the concentration of dissolved gas. Some of these methods are detailed in Appendix D. In this project two techniques were used to measure the dissolved gas content in the water. Both procedures involved trapping a known volume of flow in clear tubing by simultaneously closing two ball valves. The first method assumed an equilibrium pressure was reached in the system whilst trapped. This method was called the 'trapped method'. The other method involved releasing the pressure in the trapped section, using a syringe to measure the total volume of gas trapped. The carbon dioxide that remained dissolved in solution was also accounted for. This was known as the 'syringe method'. Both the trapped and syringe methods were incorporated into the experimental procedure.

After moving the test section to a vertical position, the volume of trapped water was read from the calibrated trapping tube. Once the volume of the liquid and the total volume of the trapping section were known, the volume of gas trapped could be calculated. This included the gas dissolved in the water at the trapping temperature and pressure. The polyurethane tubing used to trap the flow after the coils was found to expand under pressure. This affected the volume measurements and the concentration calculations if not corrected. The tube volume was found to increase by 4% at 4 bar(g). Calculation methods to allow for this expansion are shown in Appendix C.5.

$$V_t = V_L + V_G \qquad \text{Equation 4.5.1}$$

V_t - volume of trapping section
V_L - volume of liquid in the trapped section
V_G - volume of gas in the trapped section (at P_T and t_T)

In the coil tests, the volume of water in the outlet trapping tube was recorded, after lightly tapping the tube to ensure that no bubbles were trapped in the connections. Both methods assumed that the water was incompressible.

4.5.1 Trapped method

Consider a control volume with a flowing mixture of carbon dioxide bubbles in water, with a pressure P_R and temperature T_R. The volume of liquid flowing is V_L and the volume of gas flowing as bubbles is V_G. This is shown schematically in Figure 4.5.1. The concentration of carbon dioxide dissolved in the water in mg/ml is C_G^R.

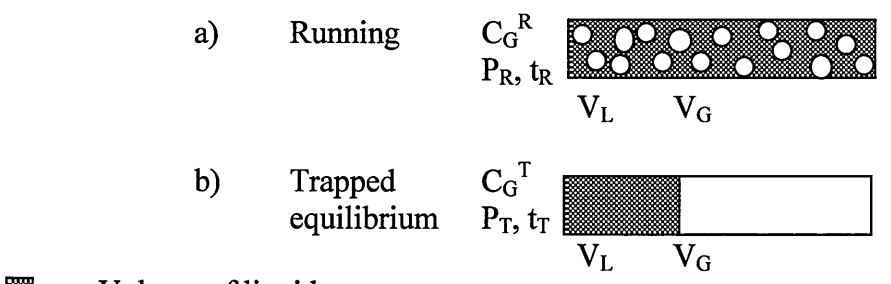

Figure 4.5.1 Trapped method system.

The total mass of carbon dioxide in the control volume when running can be calculated by adding the mass of carbon dioxide in the gas phase to the mass of carbon dioxide dissolved in the liquid.

$$M_G^R = V_G.\rho_G^R + C_G^R.V_L \qquad \text{Equation 4.5.1.1}$$

M_G^R - total mass of CO_2 when running
V_G - volume of CO_2 in gas phase in control volume
ρ_G^R - density of CO_2 at running pressure
C_G^R - concentration of CO_2 in water when running (mg/ml)
V_L - volume of water in the control volume

If this control volume is instantaneously trapped between two ball valves, as shown in Figure 4.5.1b, the mass of gas and volume of liquid in the section can be assumed to be the same as when flowing. This trapped volume was allowed to settle and reach equilibrium.

Assuming that water is incompressible, the volume can be assumed to remain unchanged. Therefore, the volume of gas in the trapped volume, before and after trapping, is also the same. The mass of carbon dioxide trapped in the controlled volume after reaching equilibrium is:

$$M_G^T = V_G.\rho_G^T + C_G^T.V_L \qquad \text{Equation 4.5.1.2}$$

M_G^T - total mass of CO_2 in system when trapped
ρ_G^T - density of CO_2 at trapped pressure
C_G^T - solubility of CO_2 at trapped pressure (mg/ml)

As equilibrium is assumed and that the liquid is saturated at temperature t_T and pressure P_T which are known, C_R^T can be obtained from the solubility equation, equation 4.5.1.3, which was derived from a table from Fogg and Gerrand (1991) and Quinn and Jones (1945). The derivation can be seen in Appendix C.6.

$$C_G = P_T^2 (0.0014152121\, t_T^2 - 0.1093249061 t_T + 3.302770923) \qquad \text{Equation 4.5.1.3}$$

P - pressure
t - temperature

The densities before and after trapping were calculated from equation 4.5.1.4, which is derived in Appendix C.7.

$$\rho = \frac{P}{0.00188t + 0.513} \qquad \text{Equation 4.5.1.4}$$

As the mass of CO_2 is conserved:

$$M_G^R = M_G^T \qquad \text{Equation 4.5.1.5}$$

$$V_G.\rho_G^R + C_G^R.V_L = V_G.\rho_G^T + C_G^T.V_L \qquad \text{Equation 4.5.1.6}$$

$$C_G^R(T) = \frac{V_G\rho_G^T + C_G^T V_L - V_G\rho_G^R}{V_L} \qquad \text{Equation 4.5.1.7}$$

4.5.2 Syringe method

In contrast to the trapped method, when the system reached an equilibrium pressure, the syringe method system was depressurised through a syringe to atmospheric pressure.

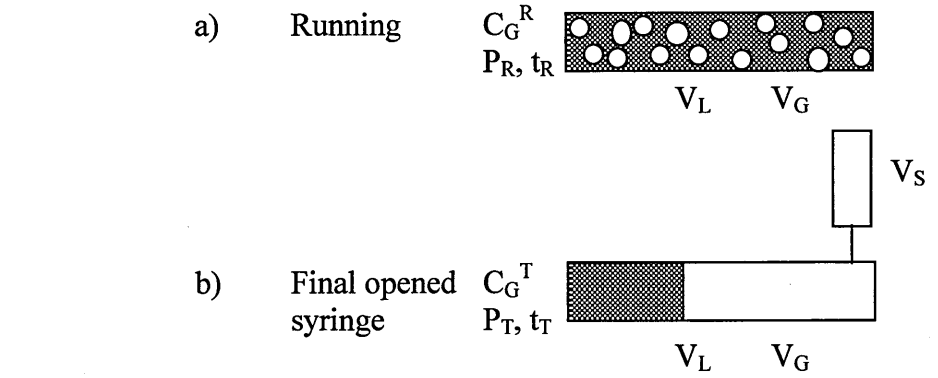

Figure 4.5.2 Syringe method system.

Figure 4.5.2a schematically shows the system when running, with a mixture of bubbles and liquid at Pressure P_R and temperature t_R. The mass balance of carbon dioxide over the controlled volume, when running, is therefore exactly the same as with the trapped method.

$$M_G^R = V_G.\ \rho_G^R + C_G^R.V_L \qquad \text{Equation 4.5.2.1}$$

After the two ball valves were shut simultaneously, the syringe was opened to depressurise the system to atmospheric pressure. This pressure was measured using the pressure transducer incorporated into the trapping section. The total volume of gas trapped in the system was calculated by adding the volume in the trapping section V_G and in the syringe V_s with the amount theoretically dissolved in solution at atmospheric conditions, $C_R^T V_L$. It is again assumed that the total mass of gas and the volume of liquid V_L in the section was the same when running and trapped and that water is incompressible.

$$M_G^T = \rho_G^A\ (V_G + V_S) + C_G^A.V_L \qquad \text{Equation 4.5.2.2}$$

M_G^T - total mass of gas in system when trapped
ρ_G^A - density of gas at atmospheric conditions
V_G - volume of gas in the tube
V_S - volume in syringe
C_G^A - solubility of gas dissolved in water at atmospheric conditions
V_L - volume of liquid in the tube

The syringe was 'pulled' to create a vacuum in the system to assist the release of the gas that was still dissolved in solution. The test board was also gently rocked to promote gas release. Before recording the syringe volume, the syringe was returned to atmospheric pressure and left to reach equilibrium. The volume of gas produced in the syringe varied depending on how hard the plunger was pulled and how long it was left after pulling. If the syringe was pulled too hard, all the gas dissolved at atmospheric pressure was released, making the apparent carbon dioxide volume too high. If however, the syringe was not pulled, the gas evolved too slowly. The test procedure was standardised to reduce these possible inaccuracies. To ensure the accuracy of the volume of gas measured, various methods of 'pulling' the gas out of solution were tested. This included keeping the syringe at vacuum overnight and then leaving it for 24 hours to reach equilibrium at atmospheric pressure. The system was also left for 3 days to determine the maximum volume of gas that could be released. After repeating the same experiment in excess of 15 times and leaving the syringe for different lengths of time under different conditions and studying the amount of gas released, a standard syringe method was produced. This standard method involved keeping the system at a vacuum of 0.6bar(a) for 15 minutes and then returning the plunger to atmospheric pressure for 5 minutes. This was found to produce accurate and reproducible readings.

The concentration of dissolved gas at atmospheric conditions was calculated from the solubility equation, equation 4.5.1.3. The densities before and after trapping were calculated using equation 4.5.1.4. As the mass of carbon dioxide is conserved:

$$M_G^R = M_G^T \qquad \text{Equation 4.5.2.3}$$

$$V_G.\rho_G^R + C_G^R.V_L = \rho_G^A (V_G + V_S) + C_G^A.V_L \qquad \text{Equation 4.5.2.4}$$

$$C_G^R(S) = \frac{\rho_G^A(V_G + V_S) + C_G^A V_L - V_G \rho_G^R}{V_L} \qquad \text{Equation 4.5.2.5}$$

Equations 4.5.1.7 and 4.5.2.5 both calculate the actual concentration of dissolved gas in $mgCO_2/mlH_2O$. This is not a clear representation nozzle performance. The concentration can also be stated as a percentage supersaturation, which is the extra amount of carbon dioxide dissolved at the outlet than would be dissolved at the outlet pressure. The percentage supersaturation can be calculated from equation 4.5.2.6.

$$\text{Percentage supersaturation} = \frac{\text{Calculated exit concentration}}{\text{Gas solubility at outlet pressure}} \times 100\% \qquad \text{Equation 4.5.2.6}$$

5 Experimental results and discussion – Nozzle

5.1 Introduction

This chapter presents the results of the detailed experiments for the test nozzle. It is divided into four parts.

Part 1: Single-phase flow - Water
Part 2: Single-phase flow - Air
Part 3: Two-phase flow - Air and water
Part 4: Two-phase flow - Carbon dioxide saturated water

The experimental test procedure used was outlined in Chapter 4. A diagram of the apparatus and fittings used is shown in Figure 4.4.1, with the dimensions shown in Table 4.4.1. The test nozzle was a model of nozzle 1, which was found to have the best flow conditions for a carbonated drinks dispenser, in the preliminary experiments. It consisted of a bullet shaped central body within a casing, which defined a variable flow area annulus. The central body was located in the middle of the casing with centralising ridges that ensured a uniform flow path. An adjustable back spacer was used to vary the axial position of the central body within the casing and hence, the geometry of the flow. The spacer was an adjustable nylon screw, situated at the back of the central body. Any minor adjustment in the length of the space adjuster contributed to a significant change in the flow area. The space adjuster length was measured to within ±0.02mm using callipers. A diagram of the nozzle, with the co-ordinates that define its shape, using the 3.23mm space adjuster, is shown in Figure 5.1.1. A space adjuster length of 3.23mm was used to test each flow type. In the gas-saturated water experiments three different space adjuster lengths were tested, 3.16, 3.23 and 3.50mm. The flow area along the nozzle for each central body position is shown in Figure 5.1.2. The area of the annulus gradually increased to minimise disturbance to the flow.

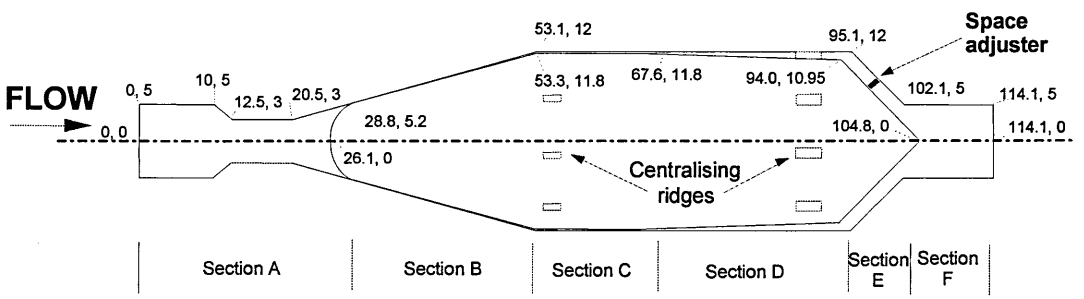

Figure 5.1.1 Diagram of the test nozzle, with the shape defining co-ordinates.

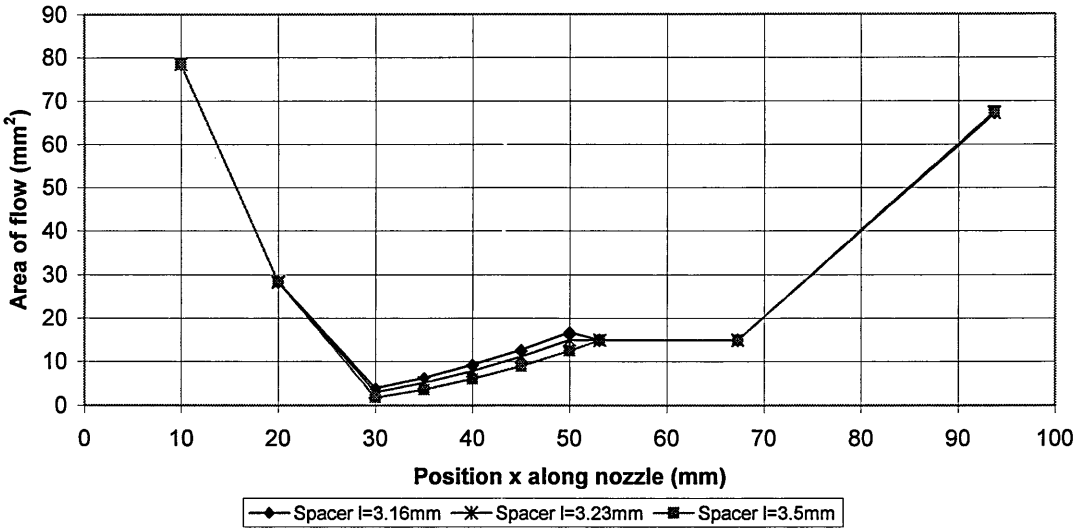

Figure 5.1.2 Variation of the flow area along the length of the nozzle, for three different central body positions.

5.2 *Single-phase flow – Water*

The pressure drop versus flowrate relationship for the single-phase water experiments in the nozzle is shown in Figure 5.2.1. The relationship is linear suggesting the possibility of laminar flow. A flowrate of up to 60ml/s was achieved through the nozzle, which is desirable in carbonated drinks dispensing.

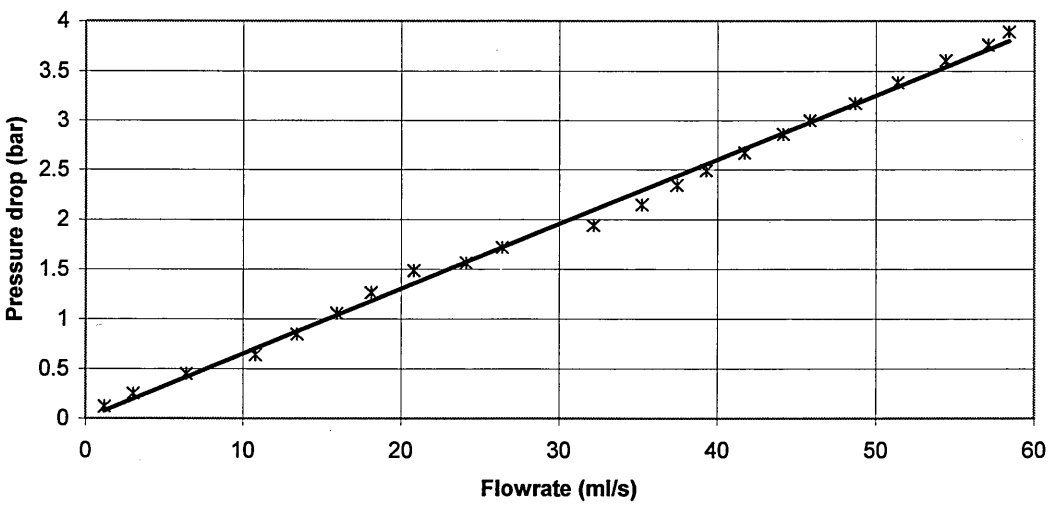

Figure 5.2.1 Pressure drop versus flowrate relationship for single-phase water flow through the test nozzle, with the 3.23mm space adjuster.

The Reynolds number was calculated at the maximum flowrate of 58ml/s, at various points along the nozzle, when the space adjuster was 3.23mm long. The density of water was taken to be 1000kg/m^3 and the viscosity 0.001kg/m/s. Figure 5.2.2 shows that the highest Reynolds number was calculated to be before and after the annulus section. The maximum Reynolds number in the nozzle was calculated to be 12,000, at the 6mm diameter section before the annulus section. However, once the flow reached the annulus section, the Reynolds number was significantly less, with the majority of the flow having a Reynolds number of less than 3000.

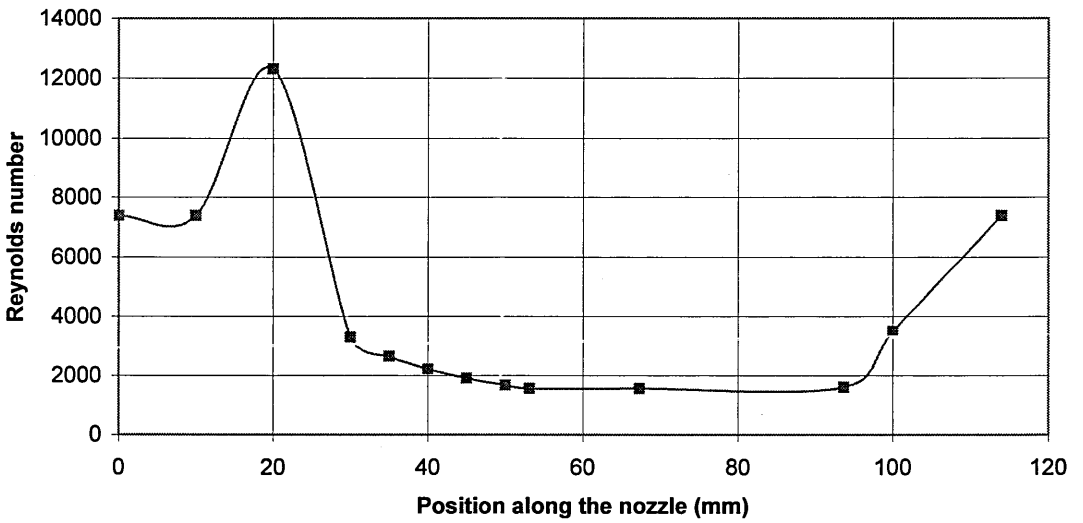

Figure 5.2.2 Variation of Reynolds number with position along the nozzle, at the maximum flowrate of 58ml/s, using the 3.23mm space adjuster.

The experimental results were compared to predictions of the pressure drop using equation 2.3.4.5 for an annulus. The result was also compared with the pressure drop equation for a flat plate, equation 2.3.4.7. This assumes that the annular gap is similar to the gap between two parallel plates, using the annulus circumference as the width of the plates.

$$f_a = \frac{24r^{*0.035}}{\mathrm{Re}} \qquad \text{Equation 2.3.4.5}$$

$$\frac{\Delta P}{\Delta l} = \frac{12Q\mu}{d^3 w} \qquad \text{Equation 2.3.4.7}$$

where

r^* - radius ratio, ($d_{inside}/d_{outside}$)

The nozzle was split into sections for the calculations. Section B, as shown in Figure 5.1.1, had the narrowest gap that dropped the majority of the pressure but it had a variable flow area. To simplify the calculations, this section was split into five parts of equal length, 5.1mm. Each part was then assumed to have a constant flow area and

the mean hydraulic diameter was used in the calculations. The density and viscosity of water were taken to be 1000kg/m^3 and 0.001kg/m/s.

There would have also been losses due to the contraction at the start of the annulus and the expansion at the outlet. The results of the calculations and experiments have been compared in Figure 5.2.3. The annulus and flat plate equations produced very similar results and predicted the pressure drop well.

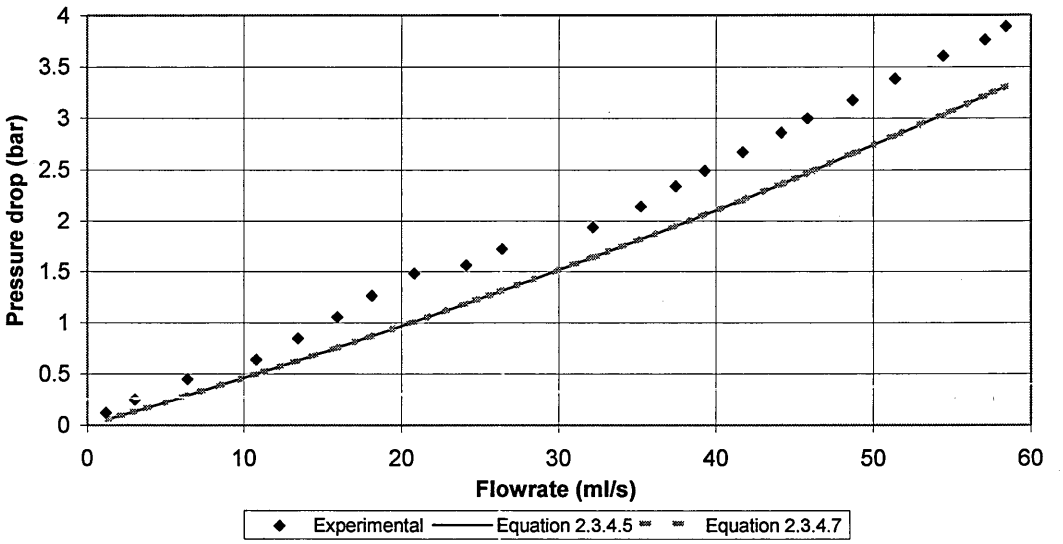

Figure 5.2.3 Predictions of the single-phase water pressure drop using equations 2.3.4.5 and 2.3.4.7, compared to the experimental results, using the 3.23mm space adjuster.

5.3 Single-phase flow – Air

The pressure drop versus mass flowrate relationship for single-phase air flow is shown in Figure 5.3.1 and is almost linear. The Reynolds number of the flow was calculated using the mass flowrate in equation 2.3.1.5, with a viscosity of 1.82x10^{-5}kg/m/s. At the highest flowrate through the narrowest gap, 0.1mm, the Reynolds number was calculated to reach over 10,000.

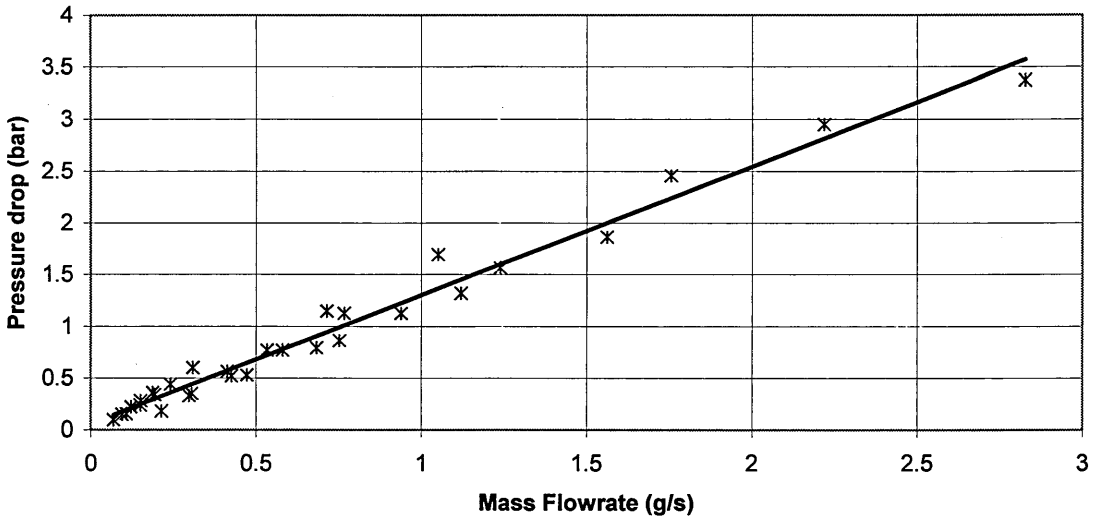

Figure 5.3.1 Flowrate versus pressure drop relationship for single-phase air flow in the test nozzle.

A large data scatter is seen on the figure, this was due to the inaccuracies created from measuring the air flowrate with the set of rotameters. A calibration computer program supplied by the rotameter manufacturers, Brooks Instrument, was used to determine the air flowrate. The rotameter outlet pressure used in the program was assumed to be the same as the nozzle inlet pressure. This was generally accurate, but at low flowrates, the pressure had dropped before the nozzle inlet. This was probably due to the restriction within the nozzle being insufficient. In this case some of the pressure may have dropped across the gap between the float and the tube of the rotameter or across the non-return valve. Any pressure losses that occurred between the rotameter outlet and nozzle inlet would have lead to the flowrate being underestimated. As this occurred at low flowrates, the correlation could have been more linear. An experimental calibration of the rotameters is shown in Appendix C.3. The accuracy of the rotameters decreased as the float moved into the lower part of the tube and was at worst ±10%.

A comparison of these experimental results, for single-phase air flow, with the annulus and flat plate equations would have proved difficult due to the complexity of the compressibility effects.

5.4 Two-phase flow – Air and water

The two-phase flow was produced, by introducing air into the water flow at a T-piece. The T-piece was situated 100 pipe diameters upstream of the nozzle, to ensure that the two-phase flow condition was established before the nozzle inlet. Tests were performed with a constant air flowrate whilst the water flowrate was varied. The experiment was repeated for five different air flowrates. The air flowrates were chosen to produce a range of results that covered the maximum gaseous carbon

dioxide flowrate at the outlet of the gas-saturated water experiments, shown in Section 5.5. The pressure drop versus water flowrate relationships, for different air flowrates, were linear and are shown in Figure 5.4.1. The air mass flowrates are shown alongside the volumetric flowrates at atmospheric pressure, with a density of $1.19kg/m^3$.

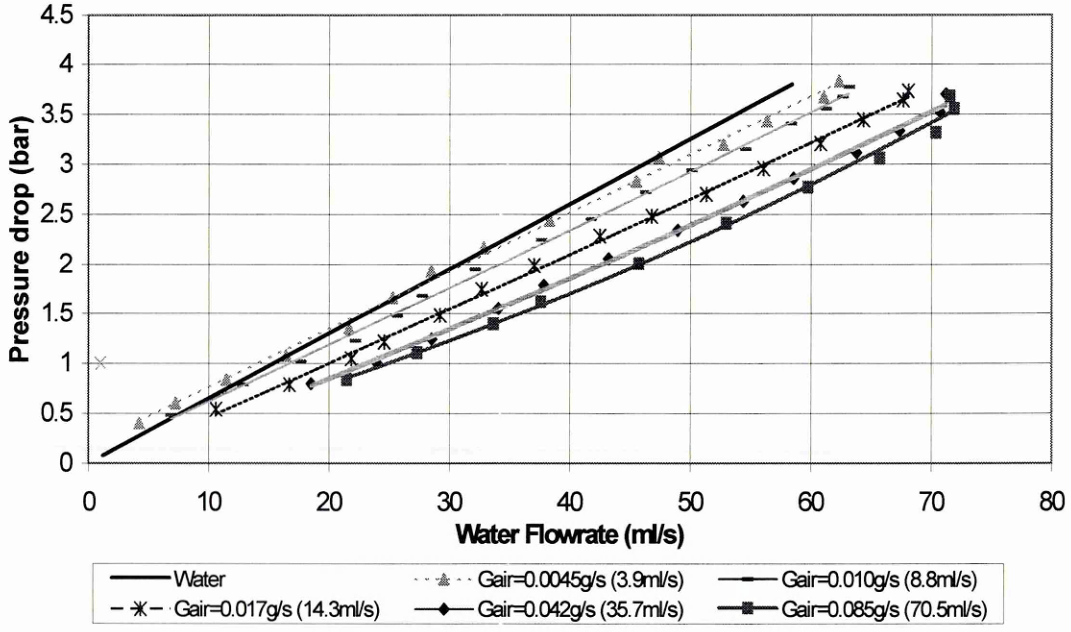

Figure 5.4.1 Pressure drop versus water flowrate relationship for two-phase air and water flow in the test nozzle, for various air flowrates, using the 3.23mm space adjuster.

The figure shows that, for a given water flowrate, an increase in the air flowrate reduced the pressure drop. This is contradictory to standard two-phase flow theories. A higher total flowrate would normally create a larger pressure drop. Figure 5.4.2 shows the same data but with the air flowrate against pressure drop for a range of water flowrates. Again, the pressure drop reduced with an increase in air flowrate. At a water flowrate of 10ml/s there was a slight reduction in the pressure drop at the lowest air flowrates but increasing the air flowrate reduced the pressure drop. The single-phase air results are also shown on Figure 5.4.2 and show a continuous increase in pressure drop with flowrate.

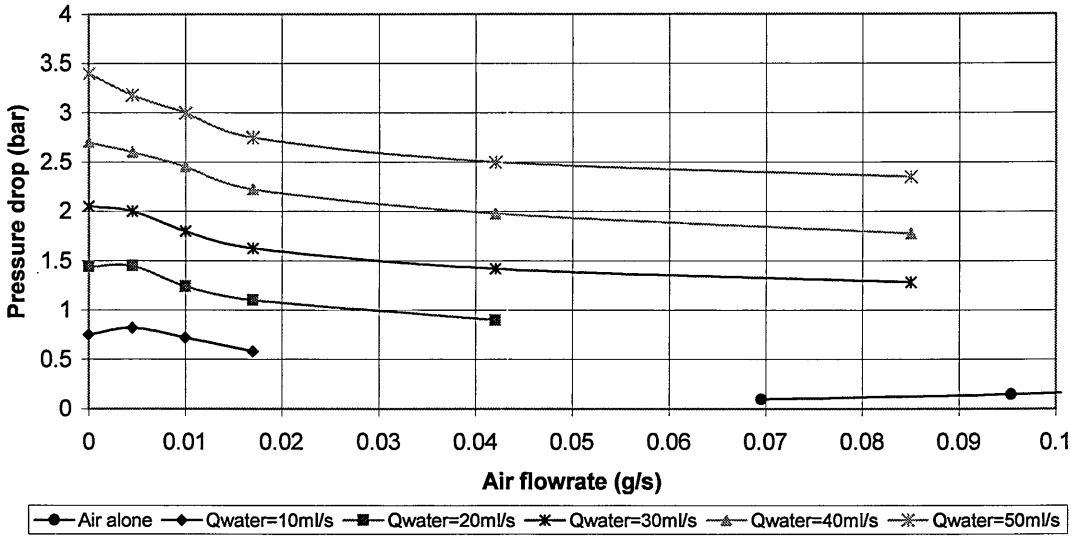

Figure 5.4.2 Pressure drop versus air flowrate relationship for two-phase air and water in the test nozzle, for various water flowrates, using the 3.23mm space adjuster.

The experimental data have been compared with various two-phase flow pressure drop correlations. The Lockhart and Martinelli parameter, X, as shown in equation 2.3.2.3 was calculated by correlating the single-phase experimental results for water and air, shown in Figure's 5.2.1 and 5.3.1, to produce equations 5.4.1 and 5.4.2 respectively. The two-phase pressure drop was then calculated using equations, 2.3.2.4 and 2.3.2.2.

$$\Delta P_{TP} = \phi_L^{\,2} . \Delta P_L \qquad \text{Equation 2.3.2.2}$$

$$X = \sqrt{\frac{-\Delta P_L}{-\Delta P_G}} \qquad \text{Equation 2.3.2.3}$$

$$\phi_L^{\,2} = 1 + \frac{C}{X} + \frac{1}{X^2} \qquad \text{Equation 2.3.2.4}$$

$$\Delta P \quad = 0.0651\ Q_{water} \qquad \text{Equation 5.4.1}$$

$$\Delta P \quad = 1.2856\ G_{air} \qquad \text{Equation 5.4.2}$$

The predictions of the pressure drop using the Lockhart and Martinelli correlation have been compared with the experimental results in Figure 5.4.3. The calculations are of the correct order, but the highest air flowrate was predicted to have the greatest pressure drop, contrary to the experimental results.

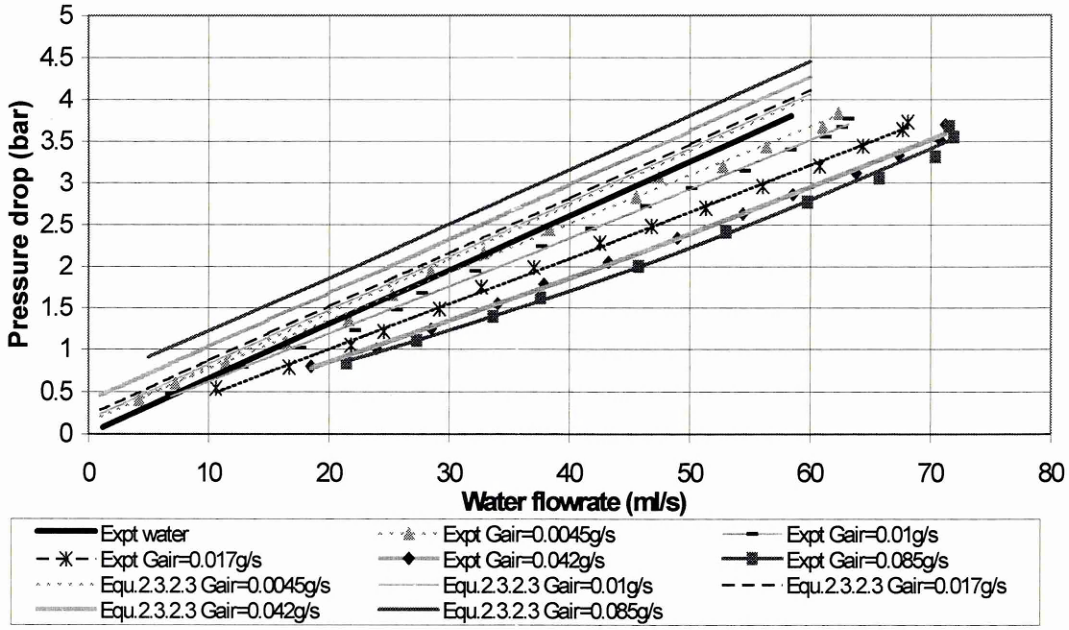

Figure 5.4.3 Comparison of the experimental pressure drop versus water flowrate relationship with the Lockhart and Martinelli correlation, for two-phase air and water flow in the test nozzle.

Friedel's correlation, equation 2.3.2.5 was also used to predict the pressure drop. The density and viscosity of water were taken to be 1000kg/m^3 and 0.001kg/m/s. The air density would have changed throughout the nozzle, due to its compressibility. Therefore a mean density of 3.6kg/m^3, corresponding to a pressure of 3bar, was used in this calculation. The viscosity was assumed to remain constant and a value of 1.82x10^{-5}kg/m/s was used. The results of these calculations have been compared to the experimental results in Figure 5.4.4. As with Lockhart and Martinelli, Friedel's equation predicted an increase in pressure drop with air flowrate, the opposite to the experimental results.

$$\phi_L^2 = A + 3.24x^{0.78}(1-x)^{0.224}\left(\frac{\rho_L}{\rho_G}\right)^{0.91}\left(\frac{\mu_G}{\mu_L}\right)^{0.19}\left(1-\frac{\mu_G}{\mu_L}\right)^{0.7} Fr_{TP}^{-0.0454} We_{TP}^{-0.035}$$

Equation 2.3.2.5

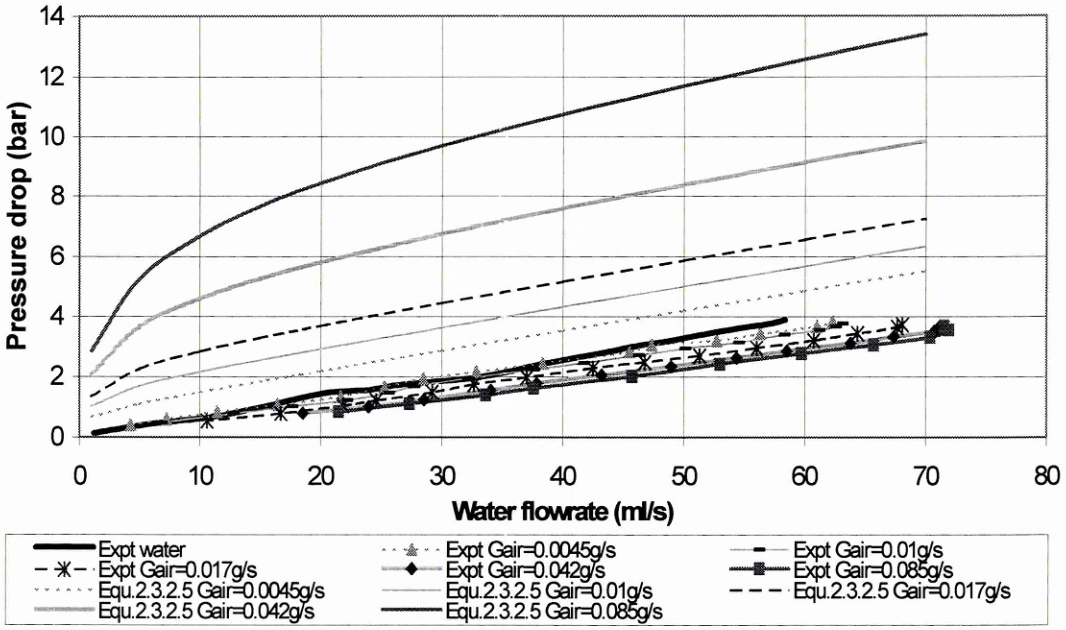

Figure 5.4.4 Comparison of experimental pressure drop versus water flowrate relationship, with Friedel's equation 2.3.2.5, for two-phase air and water flow in the test nozzle.

The two-phase pressure drop was also calculated by assuming homogeneous flow. Equation 2.3.4.7 for flat plates, showed that the pressure loss across a particular narrow gap in laminar flows is linearly dependent on the volumetric flowrate and fluid viscosity. In contrast, turbulent pressure drops depend on the square of the flowrate and the fluid density. The correlation of the single-phase water experimental results in the nozzle, equation 5.4.1, was rearranged to produce equation 5.4.3, to calculate the pressure loss in terms of viscosity and volumetric flowrate. The viscosity of water was assumed to be 0.001kg/m/s.

$$\Delta P = 65.1\ Q\mu \qquad \text{Equation 5.4.3}$$

Equation 5.4.3 was used to calculate the pressure loss assuming homogeneous flow, using the total flowrate and the homogeneous viscosity. Three different equations were used to estimate the two-phase homogeneous viscosity, namely equations 2.3.2.10, 2.3.2.11 and 2.3.2.13. A mean air density of 3.6kg/m^3 was used, which corresponded to a pressure of 3bar(a).

$$\frac{1}{\mu_H} = \frac{x}{\mu_G} + \frac{1-x}{\mu_L} \qquad \text{Equation 2.3.2.10}$$

$$\mu_H = \mu_G \frac{x\rho_H}{\rho_G} + \mu_L \frac{(1-x)\rho_H}{\rho_L} \qquad \text{Equation 2.3.2.11}$$

$$\mu_H = \mu_G\alpha + \mu_L(1-\alpha)(1+2.5\alpha) \qquad \text{Equation 2.3.2.13}$$

Figures 5.4.5, 5.4.6 and 5.4.7 show the calculation results using each equation to calculate the homogeneous viscosity. None of the correlations fitted the experimental

data well or were able to predict the reduction in pressure loss with increasing the air flowrate, as found experimentally. They all predicted an increase in pressure loss with air flowrate, at a given water flowrate, the opposite to the experimental results. However, using equation 2.3.2.13 to calculate the homogeneous viscosity, hardly any change in pressure drop was predicted, at different air flowrates. These equations were derived from experimental data and not theoretical considerations.

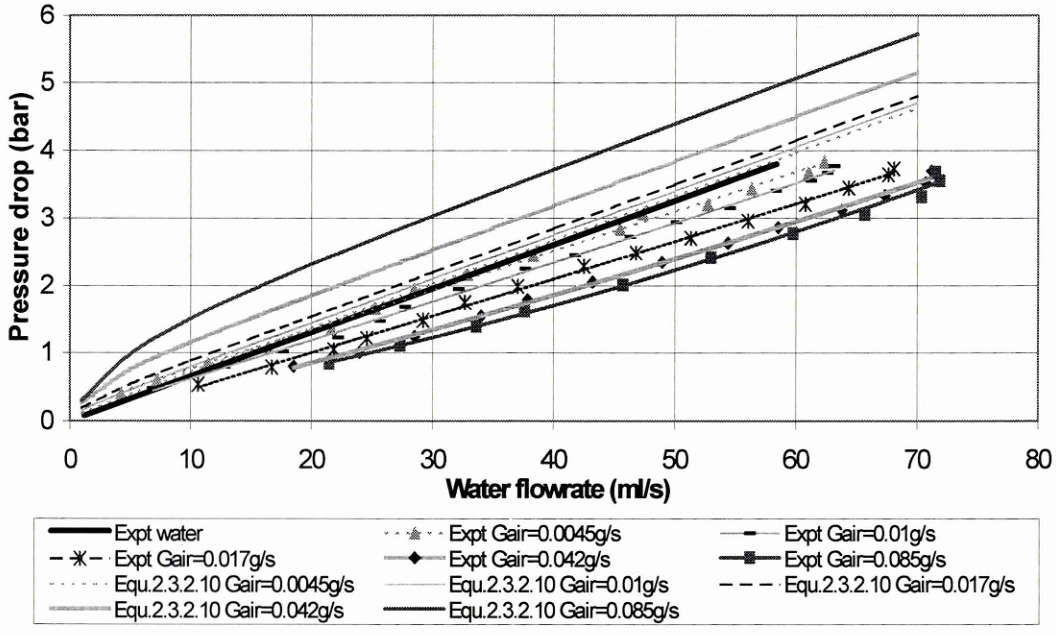

Figure 5.4.5 Comparison of experimental and calculated pressure drop using the homogeneous viscosity calculated from equation 2.3.2.10, for two-phase air and water flow in the test nozzle.

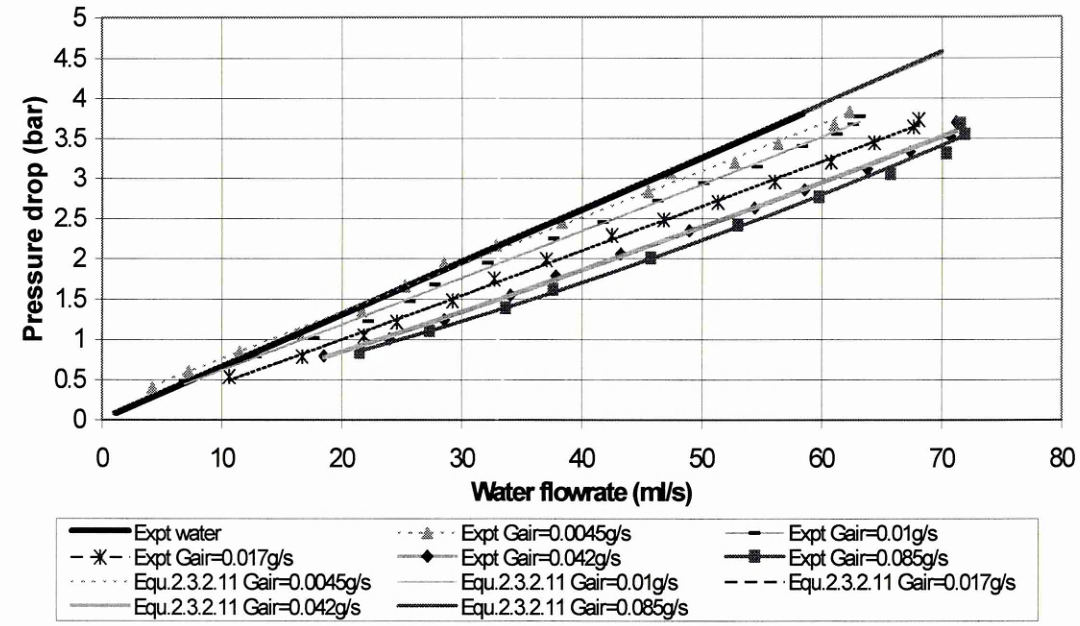

Figure 5.4.6 Comparison of experimental and calculated pressure drop using the homogeneous viscosity calculated from equation 2.3.2.11, for two-phase air and water flow in the test nozzle.

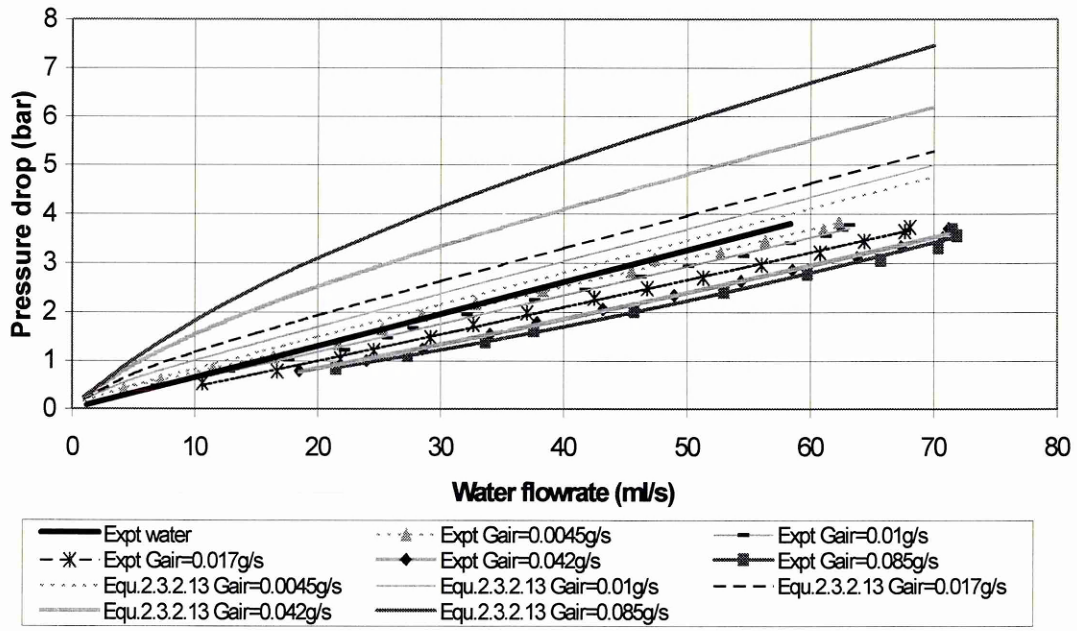

Figure 5.4.7 Comparison of experimental and calculated pressure drop using the homogeneous viscosity calculated from equation 2.3.2.13, for two-phase air and water flow in the test nozzle.

The homogeneous viscosity was also calculated by substituting the mass fraction in equation 2.3.2.10 for void fraction. This is shown as equation 5.4.4.

$$\frac{1}{\mu_H} = \frac{\alpha}{\mu_G} + \frac{1-\alpha}{\mu_L} \qquad \text{Equation 5.4.4}$$

Figure 5.4.8 shows that calculating the pressure loss using the volumetric weighted homogeneous viscosity, the reduction in pressure with increasing air flowrate, at a given water flowrate, was predicted. It was however, underestimated. This suggests that the fluid properties and the gas volume had significant effects on the two-phase air and water pressure loss in the nozzle.

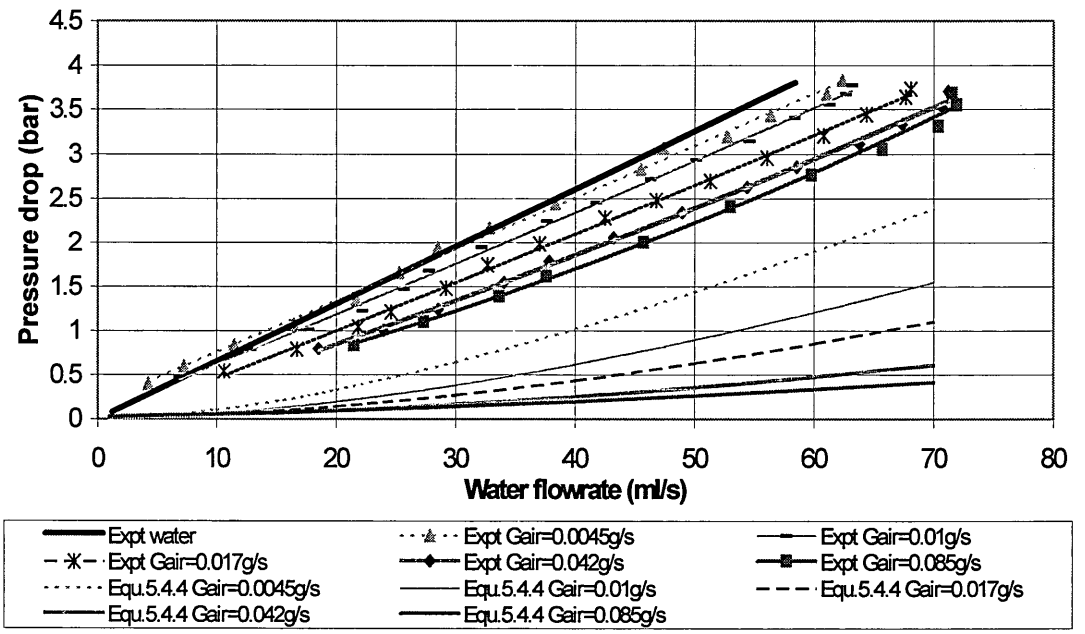

Figure 5.4.8 Comparison of experimental and calculated pressure drop using the homogeneous viscosity calculated from equation 5.4.4, using the void fraction, for two phase air and water flow in the test nozzle

It was also possible to plot the experimental data on a Lockhart and Martinelli style chart. The experimental two-phase multiplier ϕ_{TP}, was calculated from equation 2.3.2.2, using the experimental pressure drops of the two-phase air and water and the single-phase water. The experimental single-phase results for the water and air were used to calculate the experimental Lockhart and Martinelli parameter X, using equation 2.3.2.3. The results are shown on Figure 5.4.9 and are compared to Chisholm's correlation, equation 2.3.2.4, for streamline-streamline flow. The figure shows the two-phase multiplier ϕ_L went below 1. At low values of the Lockhart and Martinelli parameter, hence low liquid flowrates, the two-phase multiplier increased, with the experimental Lockhart and Martinelli parameter, when Chisholm's correlation decreased. This was particularly evident at high gas flowrates.

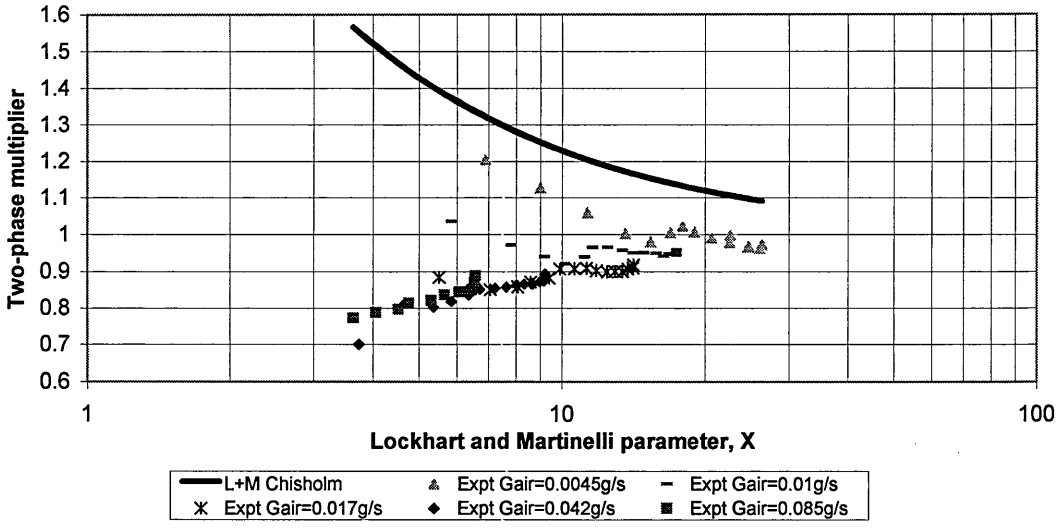

Figure 5.4.9 Comparison of the experimental Lockhart and Martinelli parameters with Chisholm's correlation, for two-phase air and water flow in the test nozzle.

The behaviour of the air and water flow through this small annulus could not be predicted by established two-phase flow correlations. The annular gap within the nozzle was however, very narrow and previous authors, including Triplett et al (1999), Coleman and Garimella (1999, found that correlations designed for two-phase flow in large diameter pipes were not suitable for narrow gaps. Most two-phase pressure drop research to date shows that the pressure drop should increase with the air flowrate, at a given water flowrate. The experimental results found a decrease in pressure drop.

Recent studies of two-phase flow in narrow tubes, including by Coleman and Garimella (1999) and Xu et al (1999), have found narrow tube flow patterns to be different to larger diameter tubes. Xu et al experimented with a circular vertical 0.3mm gap and found the flow patterns to be very different from their larger 0.6mm diameter tube. Bubble flow was found not to exist in the vertical 0.3mm tube. The narrowest gap in the nozzle tested here was 0.1mm, which is narrower than previous research.

The present experimental data can be plotted on a flow regime map, to determine the possible nature of the flow. The density of the water was assumed to be 1000kg/m^3. The density of air at the nozzle inlet, at a pressure of 5bar(a) was taken to be 5.9kg/m^3. The minimum superficial velocity range through the minimum gap of 0.1mm was calculated to range between 0.28 and 5.3m/s for the air and 2.96 and 7.4m/s for water. These would be higher at the outlet, when the air density would be less. When the present experimental data is plotted on a standard flow regime map for horizontal flow, from Coulson and Richardson (1993), shown as Figure 2.3.2, the

data was almost all within the bubbly flow region. Xu et al (1999) were unable to achieve bubbly flow in their vertical 0.3mm diameter channel.

Ekberg et al (1999) produced a flow regime map for flow in an annulus with a 1.02mm gap, shown as Figure 5.4.10. The map also shows the flow regimes found by Mandhane et al (1974) who used horizontal pipes with diameters of at least 12.7mm. According to the map the present experimental data appears to lie over the range of bubble, plug and slug flow. However, it was impossible to identify the flow regimes with the nozzle with the present experimental set up used.

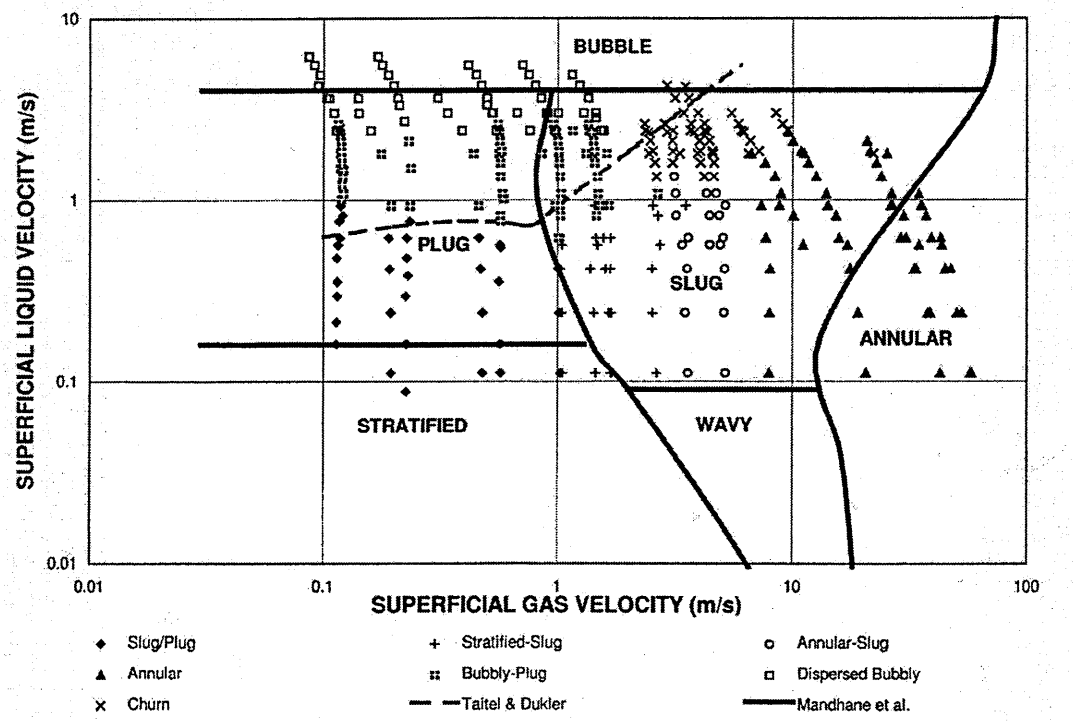

Figure 5.4.10 Flow pattern map for an annulus with an inner diameter of 6.6mm, outer diameter of 8.6mm and length 460mm. Ekberg et al (1999)

It is possible that the decrease in pressure drop found in the present investigation could have been due to how the air and water phases were distributed in the narrow annular space. The flow was unlikely to have been separated, because if both phases were to produce the same pressure drop, large interphase slip would have had to be present and Triplett et al (1999a) found that interphase slip was unlikely in narrow horizontal channels. Coleman and Garimella (1999) also stated that separated models are not appropriate for narrow horizontal channels.

Bannwart (2001) investigated heavy oil and water flow in vertical pipes. They were able to produce core-annular flow, where the water flowed in an annulus next to the wall and the oil occupied the centre of the tube. The pressure drop was comparable to water alone at the total volumetric flowrate. The fluids however, had similar densities and very different viscosities. With water and air both the viscosities and densities

were very different. If the air had formed a film next to the nozzle wall, the friction and hence, the pressure drop would have been reduced. The flow patterns could not be verified with the present set up. Hence, a more detailed investigation is needed.

5.5 *Two-phase flow – Carbon dioxide saturated water*

The water was saturated with carbon dioxide by pressurising the water and carbon dioxide together in a saturator. The saturator was found to be 95% efficient, as shown in Appendix C.4.2. The pressure drop versus flowrate relationship for the carbon dioxide-saturated water through the nozzle is shown in Figure 5.5.1. The figure shows the relationships for three different central body positions within the casing, which corresponded to space adjuster lengths of 3.16, 3.23, and 3.5mm. With the shortest space adjuster length, the central body was pushed to the back of the casing, increasing the flow area and flowrate. Each relationship on Figure 5.5.1 is linear.

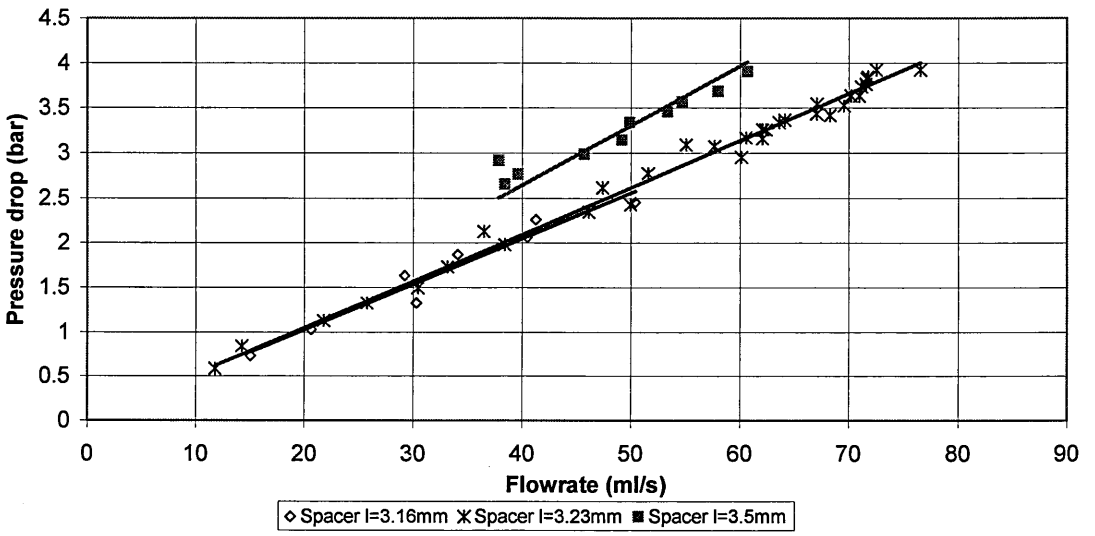

Figure 5.5.1 Pressure drop versus water flowrate relationship for carbon dioxide-saturated water, with the central body at different positions within the casing.

Figure 5.5.2 shows a comparison of the experimental results for the gas-saturated water and single-phase water flows, both with the 3.23mm long space adjuster. The dissolved gas flow had a lower pressure drop than the single-phase water flow. With the air and water experiments, it was found that, at a given water flowrate, the pressure loss was reduced by increasing the air flowrate. The pressure drop of the gas-saturated water flow was less than the single-phase water flow, indicating that some of the dissolved gas came out of solution. Visual observations, whilst performing the experiment, revealed that gas was released into the flow.

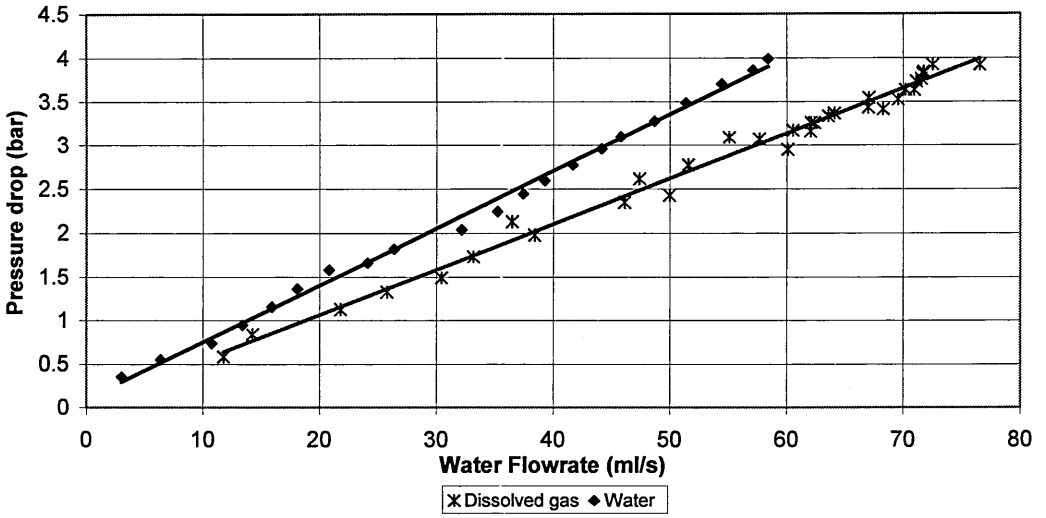

Figure 5.5.2 Comparison of the pressure drop versus flowrate relationships, for the single-phase water and dissolved gas flow in the nozzle, with a 3.23mm space adjuster.

An estimate of the volume of gas at the outlet has been calculated, using the exit concentration. At a water flowrate of 60ml/s, the exit concentration of carbon dioxide using the trapped method is shown on Figure 5.5.4 to be 5.68mg/ml. The initial concentration of dissolved gas, C_G, was found to be 7.5±0.3mg/ml, as shown in Appendix C.4. The amount of gas released was therefore:

7.5-5.68= 1.82mg/ml

The mass flowrate of carbon dioxide at the exit was therefore:

60 x 1.82 = 109.2 $mgCO_2/s$

Equation C.7.3, derived in Appendix C.7, was used to calculate the density of carbon dioxide at different temperatures and pressures. It was used to find the density of carbon dioxide at 24°C and atmospheric pressure,

$$\rho = \frac{P}{0.00188t + 0.513} \qquad \text{Equation C.7.3}$$

$$\rho = \frac{1.0133}{0.00188 \times 24 + 0.513} = 1.82 kg/m^3 = 1.82 mg/ml$$

Therefore the volumetric flowrate of gas at the outlet was calculated:

109.2 / 1.82 = 60 ml/s

This shows that the volume of gas at the outlet equalled the volume of liquid. At the inlet the gas flowrate would have been zero as the carbon dioxide would have all been dissolved. Table 5.5.1 shows a comparison of the measured pressure loss for the two types of two-phase flow, with the same water flowrate and similar gas flowrates at the

outlet. The pressure loss for the two-phase air and water experiments was only slightly less. This shows again that carbon dioxide was released in the nozzle.

	Air and water experiments	Carbon dioxide saturated water experiments
Water flowrate (ml/s)	60	60
Gas flowrate (ml/s)	70 (outlet)	0 (inlet)- 60 (outlet)
Pressure drop (bar)	2.8	3.1

Table 5.5.1 Comparison of water and gas flowrates and pressure drop for the two-phase experiments

5.5.1 Measurement of the dissolved gas concentration

The syringe and trapped methods were both incorporated into the experimental procedure in order to calculate the concentration of dissolved carbon dioxide at the nozzle outlet. The equations for the syringe and trapped methods and their derivations were shown in Chapter 4. Figure 5.5.3 shows a comparison of the syringe and trapped method results for the nozzle. It shows the exit concentration versus pressure drop calculated using both methods, with the 3.23mm space adjuster. The syringe method was found to produce consistently higher results.

Some air would have been dissolved in the water at atmospheric pressure before it was pressurised. As part of the syringe method, a vacuum was created in the system to 'pull' all the gas out of solution. During this process any gases dissolved at atmospheric pressure, including air and carbon dioxide, would have been released from solution. If this gas did not redissolve into solution when returned to atmospheric pressure, the syringe method would have overestimated the volume of gas and hence the concentration of gas dissolved in solution. Assuming that air and carbon dioxide were not dissolved at atmospheric pressure, the dissolved gas concentration, calculated by the syringe method, would have been 0.5-1.1mg/ml lower than the trapped method results. This indicates that the syringe method would require an additional correction factor to produce accurate results. The concentration of dissolved gas at the inlet was calculated to be 7.5±0.3mg/ml, as shown in Appendix C.4. Figure 5.5.3 shows the trapped method results approached a dissolved gas concentration of close to this value at zero pressure drop. The syringe method overestimates this value. Therefore, the trapped method has been used in this thesis. The uncertainty of the trapped method was approximately 5% of the calculated dissolved gas concentration.

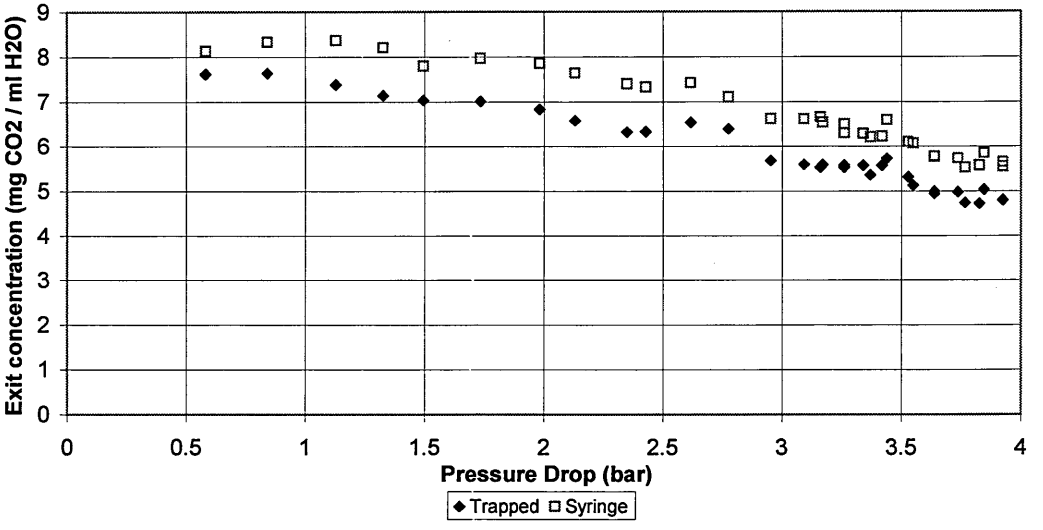

Figure 5.5.3 Comparison of the syringe and trapped methods results, with the 3.23mm central body space adjuster, showing the exit concentration versus pressure drop relationship.

Figure 5.5.4 shows the exit concentration versus flowrate results. It shows that, for a given flowrate, the lowest concentration of carbon dioxide in the outlet was seen with the longest space adjuster. The concentration can also be presented as the percentage supersaturation, which is the extra amount of carbon dioxide dissolved at the outlet than is theoretically dissolved at the outlet pressure. This calculation is shown in Chapter 4. The percentage supersaturation against flowrate is shown in Figure 5.5.5. This is a far clearer representation of performance, particularly at low flowrates, at which the pressure had not dropped and the solution was still saturated at close to the carbonator pressure. The figure shows that the highest percentage supersaturation occurred with the longest space adjuster length, 3.5mm, creating the narrowest restriction and greatest pressure drop, for a given water flowrate. The 3.23mm and 3.16mm space adjusters had similar lengths and hence, similar results.

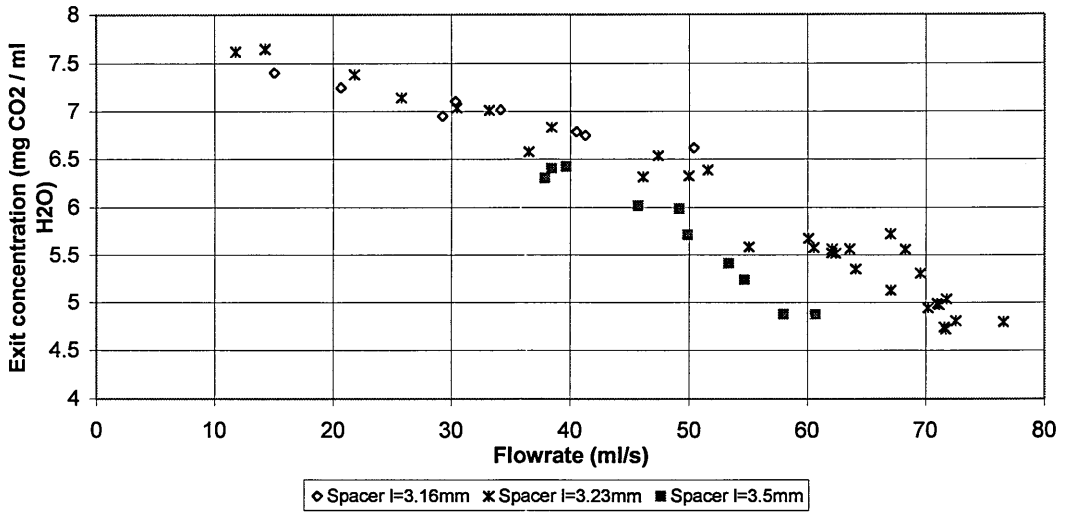

Figure 5.5.4 Exit concentration versus flowrate for the nozzle.

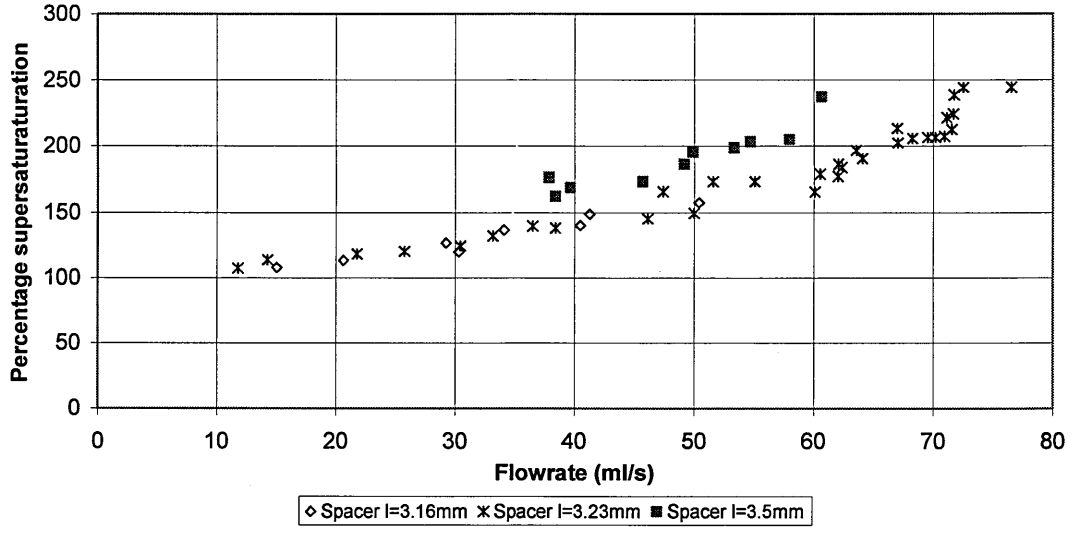

Figure 5.5.5 Percentage supersaturation versus water flowrate after the nozzle.

Figures 5.5.6 and 5.5.7 show the exit concentration and percentage supersaturation versus pressure drop for different space adjuster lengths. The relationships are very similar. This suggests that the restriction within the nozzle was not important and that, for a given pressure drop, the percentage supersaturation at the outlet was the same, regardless of the central body position. This may have been different if the flow was turbulent. The majority of the pressure would have dropped rapidly over the narrow gap at the start of the nozzle. As the pressure drop was so rapid the gap size may not have had a large influence. After the narrow gap, the flow area of the rest of the nozzle was virtually independent of the space adjuster length, indicating the effect

of the space adjuster to be minimal. Another possibility is that the percentage supersaturation was dependent on the amount of energy dissipated and not the gap size.

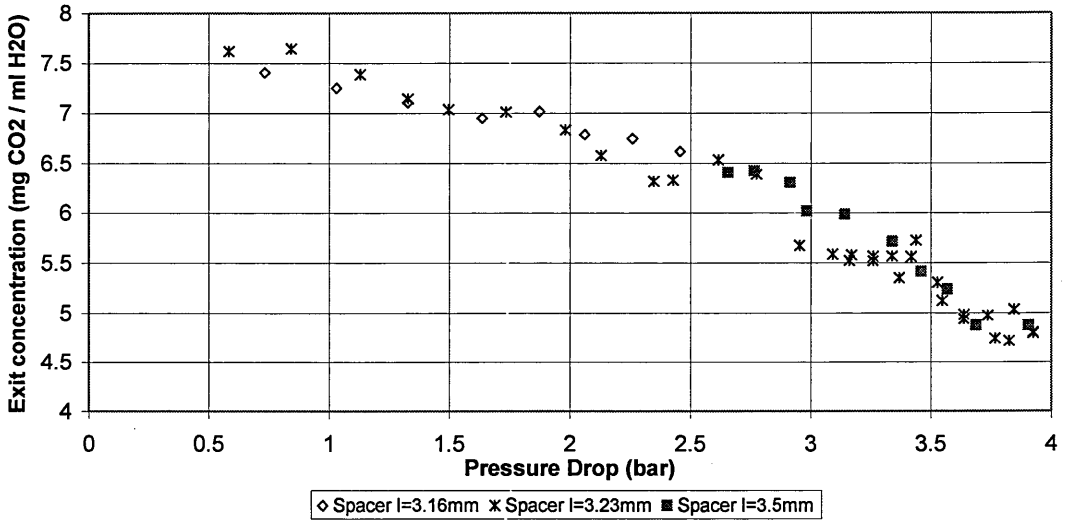

Figure 5.5.6 Exit concentration versus pressure drop of carbon dioxide at the nozzle exit.

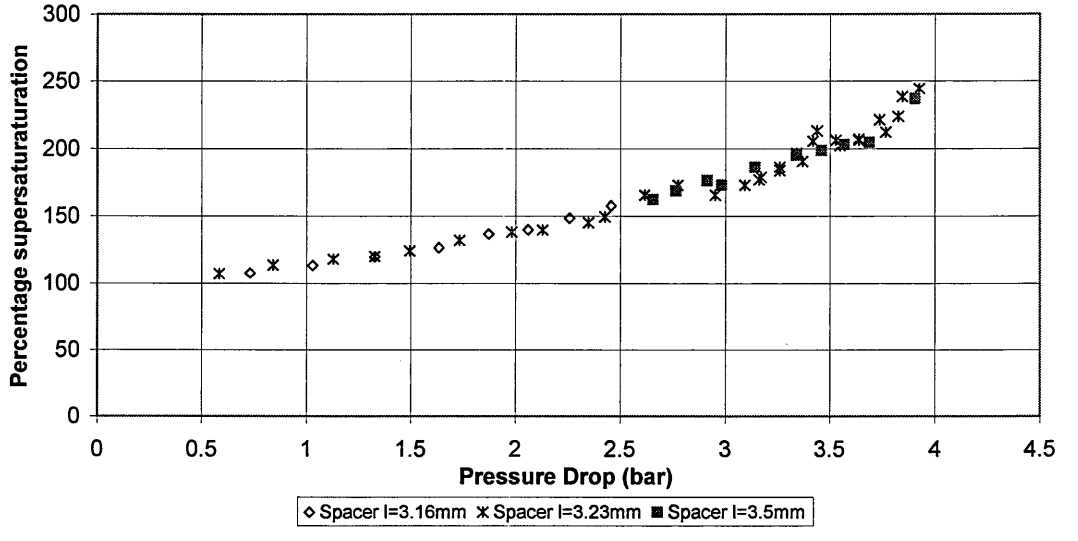

Figure 5.5.7 Percentage supersaturation versus pressure drop of carbon dioxide at the nozzle exit.

5.6 Computational Fluid Dynamics modelling

Computational Fluid Dynamics (CFD) can be used to model fluid behaviour and predict the velocity and pressure distributions within a system. Versteeg and Malalasekera (1995) gave an introduction to CFD. Finite difference methods calculate the flow behaviour from a grid created within the system geometry. CFD can be used to help to determine the areas of low pressure within the system, where bubble formation would be most likely with the gas-saturated flow. The literature review found no research that included CFD in nozzle design.

The geometry and grid were initially generated using PreBFC a basic grid generator, from Fluent Inc. Gambit also from Fluent Inc, was used for the majority of the computations, as it is a far more powerful tool to calculate meshes. Once the geometry was created, it was split into a series of sections, called faces. Each face was given a node distribution, from which a structured grid was generated. The grids generated had 49600 cells. As the nozzle was axisymmetrical, half of the annulus cross-section was drawn in 2D and an axis-symmetric model applied. Once the grid was generated, the boundary conditions were specified, which included the inlet, outlet, walls and line of symmetry.

The grid was then imported into the solver, Fluent 5.3, where the flow conditions were selected. So that the CFD results could be compared to the experimental results, the experimental inlet and outlet pressures were specified so that the flowrate could be calculated. Zero velocity was set at the wall and the walls were assumed to be perfectly smooth. The physical constants of water, including the density and viscosity were used.

Fluent gave the user options of a laminar and various turbulence models to solve the problem. These are detailed in the Fluent manual (1998). The nozzle experimental results of pressure drop versus flowrate were linear suggesting possible laminar flow. However, the laminar flow model is only appropriate when it is known that all the flow was laminar, as even small sections of turbulence would have confused the laminar model. Figure 5.2.2 showed that the Reynolds number before and after the annulus section of the nozzle was high. The flow at these points was likely to be turbulent. As part of the flow was calculated to be turbulent, a turbulent model was used. The turbulent model options included three types of k-ε model and Reynolds stress model. Different models were tested, which all produced similar results. The renormalization-group (RNG) k-ε turbulence model was the main model used.

5.6.1 Results

The single-phase water experimental results were used to set up the CFD model. The inlet and outlet gauge pressures were specified and CFD predicted the flowrate. The experimental results used are shown below, for a space adjuster length of 3.23mm.

Inlet Pressure (gauge) = 415909 Pa
Outlet Pressure (gauge) = 19579 Pa
Flowrate = 58 ml/s

The profiles of the local static pressure and the velocity magnitude along the nozzle, with a 3.23mm space adjuster, are shown in Figures 5.6.1 and 5.6.2, respectively. Figure 5.6.1 shows the static pressure at specific points along the grid. Despite the large number of grid points, the gap in the points is due to the pressure being dropped rapidly over a very small area. Figure 5.6.2 shows the maximum velocity in the centre of the flow path.

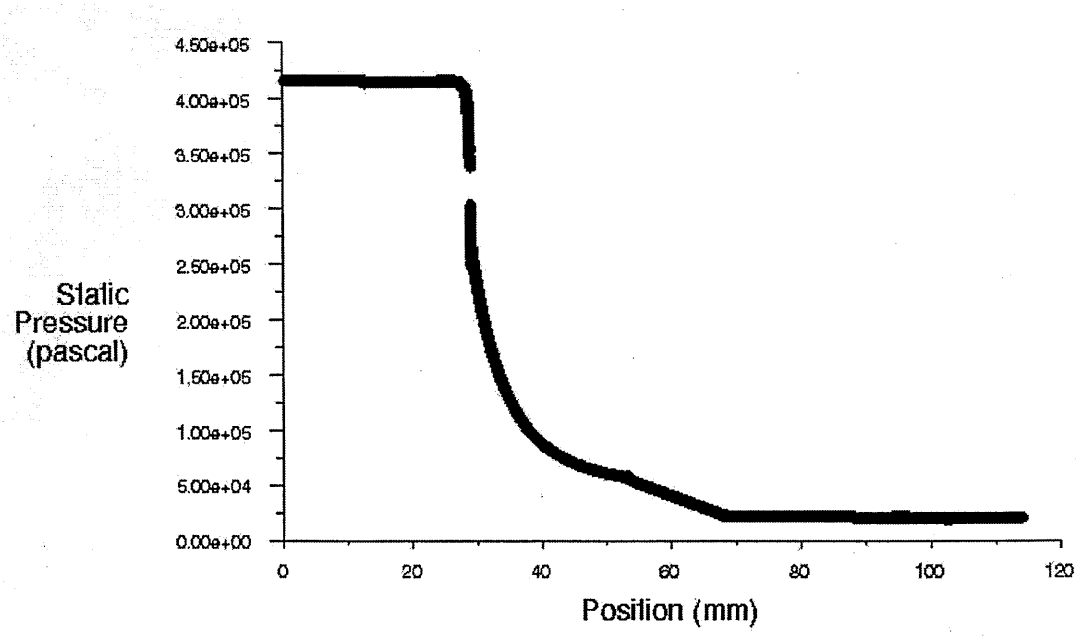

Figure 5.6.1 Static pressure along nozzle, with a space adjuster length of 3.23mm.

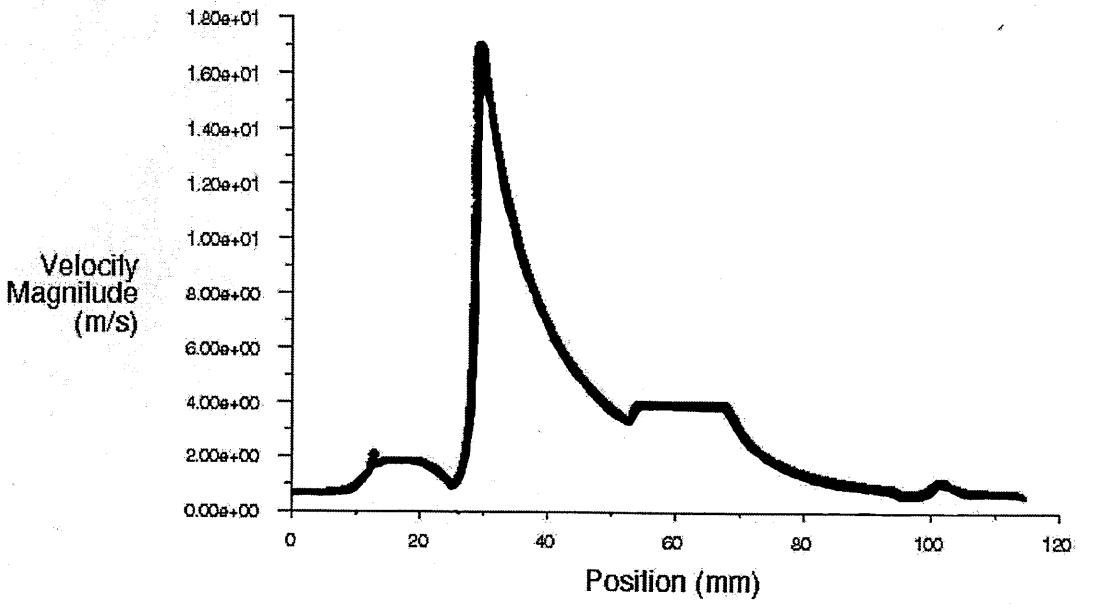

Figure 5.6.2 Velocity magnitude at the centre of the flow, along nozzle, with a space adjuster length of 3.23mm.

The static pressure reduced steadily through the nozzle. The total pressure showed a similar profile. The majority of the pressure drop occurred in section B, which had the narrowest gap, with a minimum size of 0.1mm. The velocity magnitude appeared to vary throughout the nozzle and reached a peak of 17m/s at 30mm along the nozzle, at the narrowest gap. A summary of the CFD and experimental results is shown in Table 5.6.1.

CFD		**3.23mm space adjuster**
Flowrate (ml/s)		44
Static Pressure (bar)	**min**	0.2
	max	4.16
Total Pressure (bar)	**min**	0.19
	max	4.26
Velocity(m/s)	**min**	0
	max	16.9
Experimental		
Flowrate (ml/s)		58
Pressure (bar)	**min**	0.2
	max	4.16
Velocity (m/s)	**min**	0
	max	21.2

Table 5.6.1 Summary of CFD and experimental results for the 3.23mm space adjuster.

The flowrate and maximum velocity, calculated by Fluent, were slightly lower than the experimental values but were of the correct order and seemed plausible. If the laminar model was used, the program had problems converging. With the turbulence models, results were very difficult to achieve as convergence took considerable time, and if stopped too early different results were obtained. The nozzle dimensions were very sensitive to any movement of the central body, which could be a reason for the discrepancy between the CFD and experimental results.

The majority of the pressure drop was predicted to occur at the start of the nozzle through the extremely narrow gap. With this in mind, it may be possible to omit the centre section of the nozzle, where there was minimal change in the flow area. A new shortened nozzle shape was also tested with CFD as shown in Figure 5.6.3. The figure shows the coordinates that defined the shape of the nozzle.

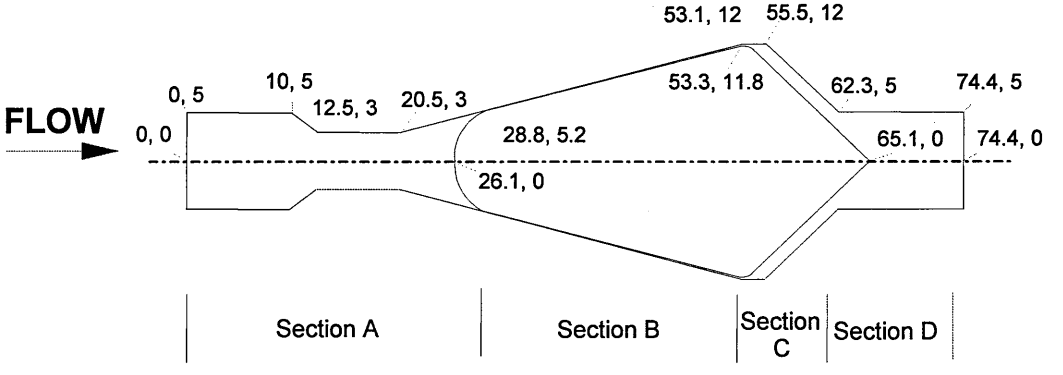

Figure 5.6.3 Diagram of the shortened version of the test nozzle, with shape co-ordinates.

Figure 5.6.4 shows the static pressure distribution along the shortened nozzle. The pressure appears to drop off more steadily than with the full nozzle. The velocity magnitude, as shown in Figure 5.6.5, appeared to drop very rapidly at a 55m along the nozzle, when the flow opened out. The distribution is, however, smoother than the full nozzle.

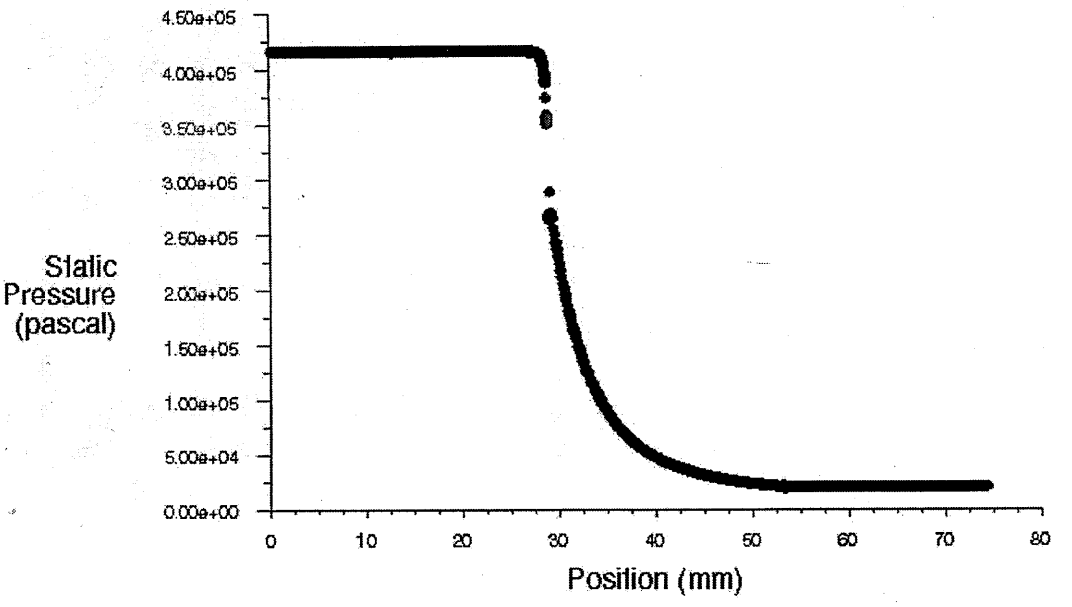

Figure 5.6.4 Static pressure in the shortened nozzle with a 3.23mm central body space adjuster.

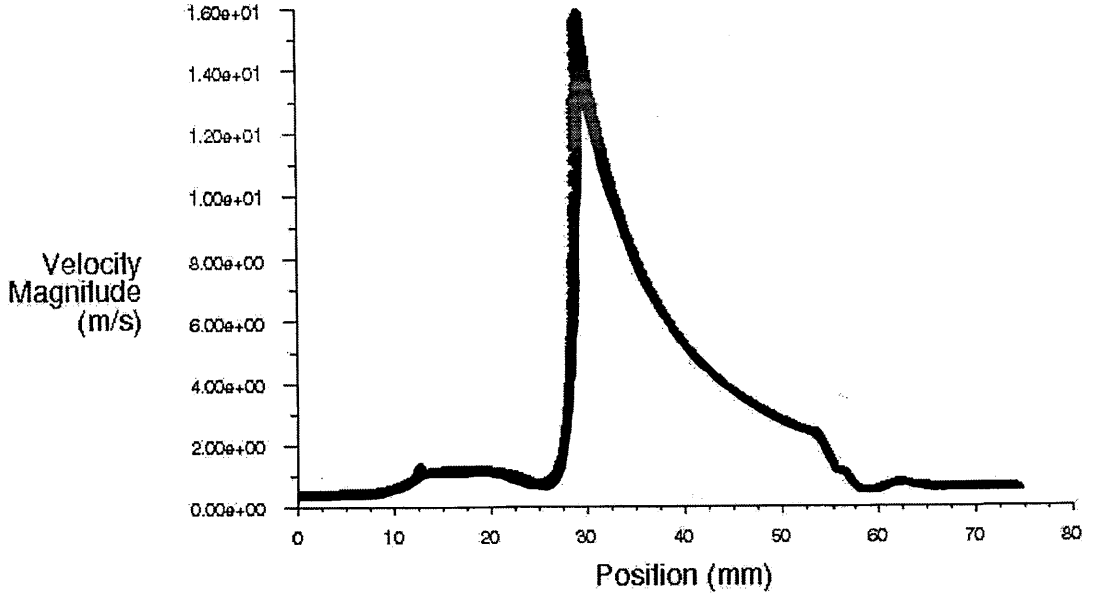

Figure 5.6.5 Velocity magnitude, at the centre of the flow, in the shortened nozzle with a 3.23mm central body space adjuster.

This simple change of shortening the nozzle demonstrates that further changes in the design could create smoother pressure drop and velocity profiles and improve its performance as a carbonated drink dispenser.

Further detailed research is needed to produce a nozzle design that reduces the pressure very steadily with a smooth velocity profile. The present nozzle is a premix nozzle that requires a different device for each flavour of drink. The new design could

be adapted to become a post-mix nozzle that includes the facility to dispense different flavoured syrups. The syrups could flow through the central body, as with nozzle 2 shown in Chapter 3. These design considerations could justify a further project.

5.7 Conclusions

In the preliminary experiments nozzle 1 was found to have the all flow characteristics most suitable for carbonated drinks dispensing. In this section, a test version of nozzle 1 was tested in further detail. The majority of the pressure was found to drop near the start of the nozzle, over sections B and C as shown on Figure 5.1.1. This was where the gap size ranged from 0.1 to 0.2mm. The pressure drop versus flowrate relationships for each of the single and two-phase flows were linear.

For the two-phase air and water experiments, it was found that for a given water flowrate, the pressure drop across the nozzle reduced with an increase in the air flowrate. This was contrary to standard two-phase flow theories. Various two-phase flow correlations were used to calculate the pressure drop but were unable to predict this behaviour. However, assuming homogeneous flow and using the void fraction in place of mass fraction in equation 2.3.2.10, to calculate the homogeneous viscosity, a decrease in pressure drop was predicted with an increase in air flowrate. This was the only equation to predict this, but the pressure drop was underestimated. This suggests that the fluid properties and gas volume of the two-phase air and water mixture had an influence on the pressure drop. The experimental data was plotted onto Lockhart and Martinelli's chart by calculating the experimental Lockhart and Martinelli parameter from the single-phase air and water experimental results. The liquid two-phase multiplier was determined from the experimental results of the single-phase water and two-phase air and water flow. The two-phase multiplier was calculated to be lower than 1 and overall it increased with the Lockhart and Martinelli parameter. This was the opposite of Chisholm's correlation. At low liquid and gas flowrates, the experimental data appeared to follow Chisholm's relationship more closely. If the air had formed some kind of layer on the nozzle surface, the friction would have decreased and hence, so would the pressure drop. This behaviour was unexpected and could justify a future project.

With the carbon dioxide-saturated water experiments, when space adjuster was at it's longest, 3.5mm, the pressure drop was greatest. The 3.23mm and 3.16mm space adjusters had comparable lengths and hence, produced similar results to each other. A comparison of the results for the single-phase water and gas-saturated water experiments, with a 3.23mm long space adjuster, showed that for a given water flowrate, the gas-saturated water flow had a lower pressure drop. In the two-phase air and water experiments, the pressure loss was found to decrease at a given water flowrate, with an increase in gas flowrate. It was suggested that the gas-saturated water flow had a lower pressure drop than the single-phase water, due to the carbon dioxide being released. With a water flowrate of 60ml/s, the gas-saturated flow was calculated to have a gas flowrate of 60ml/s at the outlet. At this water flowrate, the pressure drop of the two-phase air and water flow, with an air flowrate of 70ml/s, at

the outlet, was similar to the gas-saturated flow. As the dissolved gas flow was 95% saturated at the inlet, in order for it to produce a similar pressure drop, carbon dioxide would have to have been released in the nozzle.

The concentration of dissolved gas at the nozzle outlet was calculated using both the syringe and trapped methods. The syringe method results were consistently higher than the trapped method results and found to be less representative. The concentration of dissolved gas at the inlet was calculated using the solubility equation at the saturator pressure, assuming the saturator efficiency to be 95%, to be 7.5mg/ml. The trapped method results approached a dissolved gas concentration of close to this value at zero pressure drop. Hence, the trapped method was used.

For a particular flowrate the percentage supersaturation was highest, with the longest space adjuster length. As the flowrate increased, the percentage supersaturation in the outlet increased. Surprisingly it was found that, for a given pressure drop, the nozzle percentage supersaturation was the same irrespective of the central body position. Overall, it appears that the highest percentage supersaturation after depressurisation was achieved at the maximum flowrate, through the narrowest gap.

The CFD results were extremely sensitive to the nozzle dimensions and any slight variation produced different results. The flowrate and maximum velocity, predicted by CFD, were slightly lower than the experimental values but were of the correct order. The majority of the pressure drop was predicted to occur at the start of the nozzle. The calculations of the pressure drop for the single-phase water flow using the annulus and flat plate equations also showed this. As the majority of the pressure drop occurred over one region, a new shorter nozzle shape was proposed, where the pressure drop would occur over the majority of the nozzle. This possibility emerged as a result of the work in this thesis, and it would appear to justify a future project.

6 Experimental results and discussion – Coils

6.1 Introduction

This chapter presents the results of the experimental investigations with coils. It is divided into four parts.

Part 1: Single-phase flow - Water
Part 2: Single-phase flow - Air
Part 3: Two-phase flow - Air and water
Part 4: Two-phase flow - Carbon dioxide saturated water

The experimental procedure and description of the coils are shown in Chapter 4. The results for the coils have been compared with the results of previous coils research described in Chapter 2.3.5 and correlations shown in Appendix E. Most of the equations found in the literature were developed based on test results with larger diameter tubes. For the single-phase water experiments, a new method to estimate pressure loss was proposed and compared. No previous research was found with gas-saturated solutions in coils.

6.2 Single-phase flow - Water

6.2.1 Pressure drop and friction factor

The pressure drop versus flowrate relationships for single-phase water flow in the 0.029m and 0.079m diameter coils are shown in Figure 6.2.1.

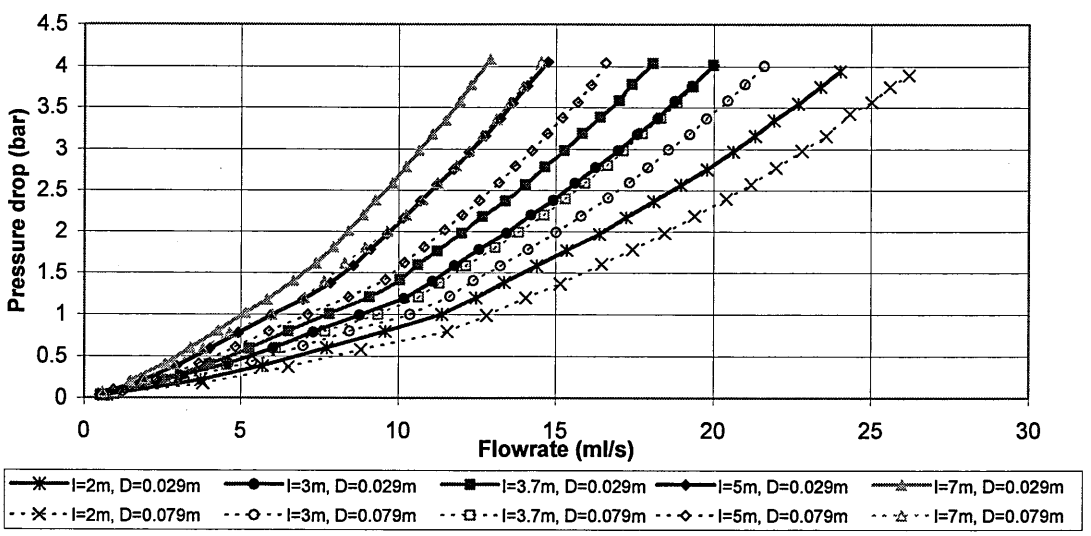

Figure 6.2.1 Pressure drop versus flowrate relationships for the coils, raw data, with single-phase water flow, D=0.029m and D=0.079m.

The experimental pressure drop, shown in Figure 6.2.1, included the pressure drop due to the fittings, as well as the coils. The fittings were the same for each coil experiment and could have contributed a significant pressure drop, particularly with the shorter coils. A diagram of the fittings is shown in Figure 4.4.5 and their dimensions are shown in Table 4.4.2. Their effects were removed by plotting the total pressure drop, due to the coils and fittings, versus coil length, for various flowrates. The equivalent pressure drop of the fittings, was given by the intercept, when the coil length was zero. Plotting the gradient e.g. pressure drop per unit length against flowrate enabled the friction factor of the coil alone to be determined. These calculations are detailed in Appendix F. The percentage of the total pressure drop attributable to the fittings was found to be up to 50% for the 2m coil and up to 20% for the 7m coil.

The pressure drop versus flowrate relationship for the coil alone is shown in Figure 6.2.2. The figure confirms the literature findings that, for a given flowrate, the longer and smaller diameter coils had the greatest pressure drops. The 7m long, 0.079m diameter coil had a similar relationship to the 5m long, 0.029m diameter coil. This suggests a shorter, smaller diameter coil had a similar pressure drop and flowrate to a longer, larger diameter coil. The 3.7m long, 0.079m diameter coil and 3m long, 0.029m diameter coil also had a similar relationship.

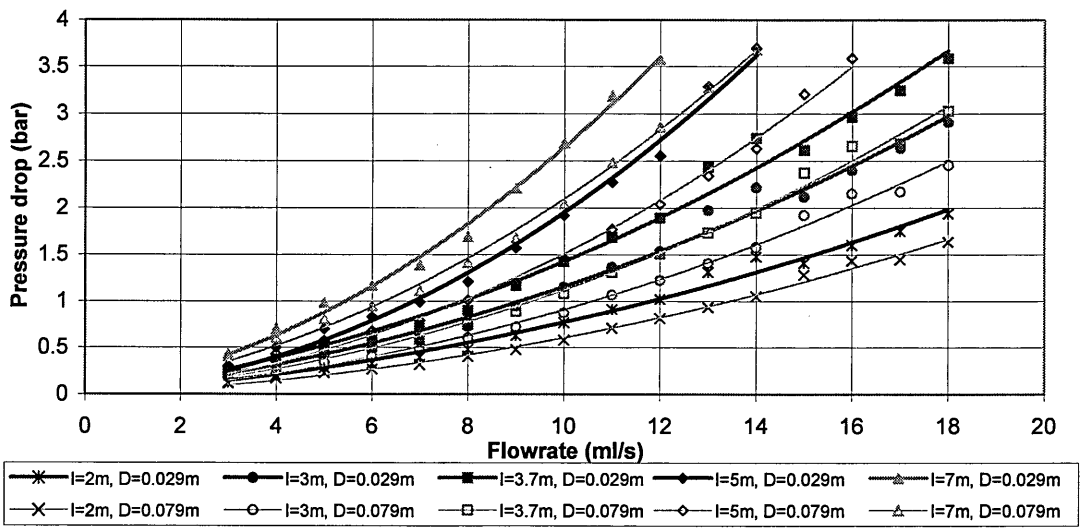

Figure 6.2.2 Pressure drop versus flowrate relationship for the coils, with the effects of fittings removed, for single-phase water flow, D=0.029m and D=0.079m.

A straight tube and a 0.139m diameter coil, both 5m long, were also tested. The percentage effects of the fittings were used to determine the proportion of the total pressure drop attributable to the 5m long coils, as outlined in Appendix F.2. Figure 6.2.3 shows the friction factor versus Reynolds numbers for the coils and the straight pipe. The laminar and turbulent (Blasius) friction factors for straight pipes are also shown on the figure. A marked increase in the friction factor with a decrease in coil diameter is shown. The straight tube results followed the laminar straight pipe equation well but the turbulent friction factor was lower than the value calculated

from the Blasius equation. This could be due to the Blasius equation overestimating the turbulent friction factor for smooth pipes at Reynolds numbers of less than 10^5. Figure 2.3.1 showed that the correlation for smooth pipes was lower than Blasius in this region.

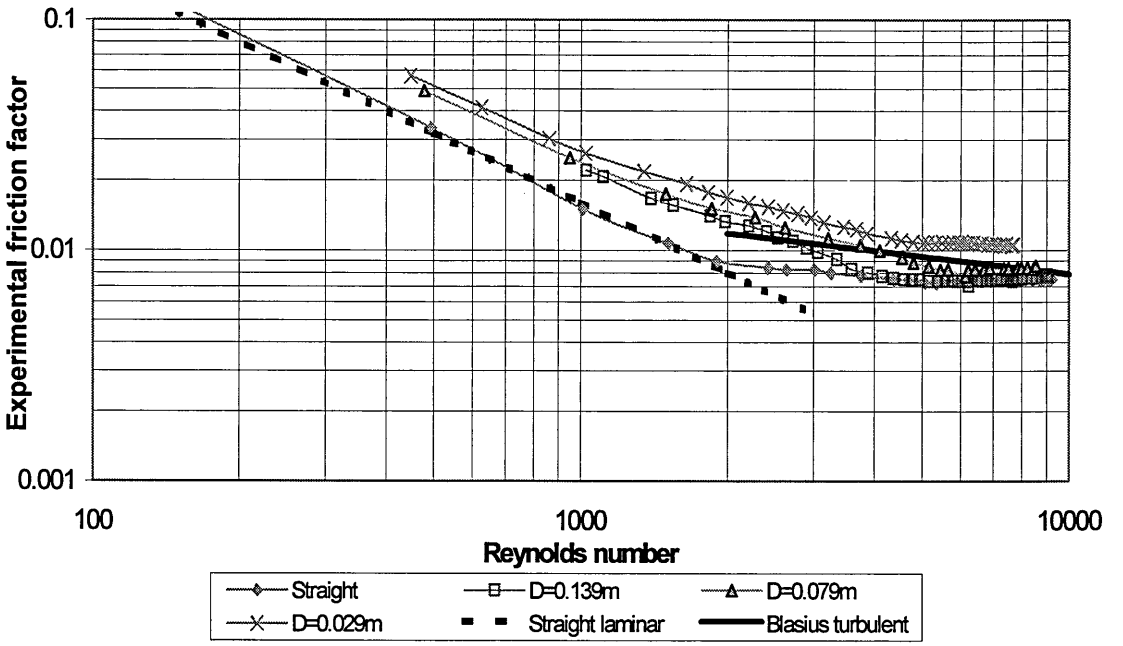

Figure 6.2.3 Friction factor chart for each coil diameter.

6.2.2 Comparison with friction factor relationships in the literature

Previous authors have produced a large number of equations to calculate the friction factor in coils. Equations have been produced for both laminar and turbulent regions. A summary of these equations is shown in Appendix E. Most of the equations were derived experimentally using coils with tube diameters in the order of 10mm. Mishra and Gupta (1979), Kubair and Varrier (1961-62), Kubair and Kuloor (1965), Das (1993), Schmidt (1967) and Lui et al (1994) all tested coils of less than 10mm. Lui used the smallest diameter tube of 4.4mm with the next smallest being 6mm. This is larger than the critical 3mm diameter straight tube, found by Damianides and Westwater (1988) to be the smallest tube diameter to behave like larger tube diameters. Narrow channel research for straight tubes is described in Section 2.3.3. The present experimental coils all had 2.5mm tube diameters.

The present experimental data have been compared to the equations from the literature. However, some of the equations were formulated with experiments performed at notably different conditions and were left out of the comparisons. Dean's (1928) equation E.1.1.1, for laminar flow was suited to Dean numbers of less than 50, when the experimental Dean numbers were between 75 and 3500. Dean's equation was therefore left out of the comparison. Ruffel's equation E.1.2.8, (referenced in Czop et al (1994)) for turbulent flow was for rough coiled tubes. Coulson and Richardson (1993) stated the absolute roughness of drawn tubing to be

0.0015mm e.g. smooth, hence, this equation was not considered. Figures 6.2.4 to 6.2.5 compare the equations for laminar and turbulent regions to the experimental

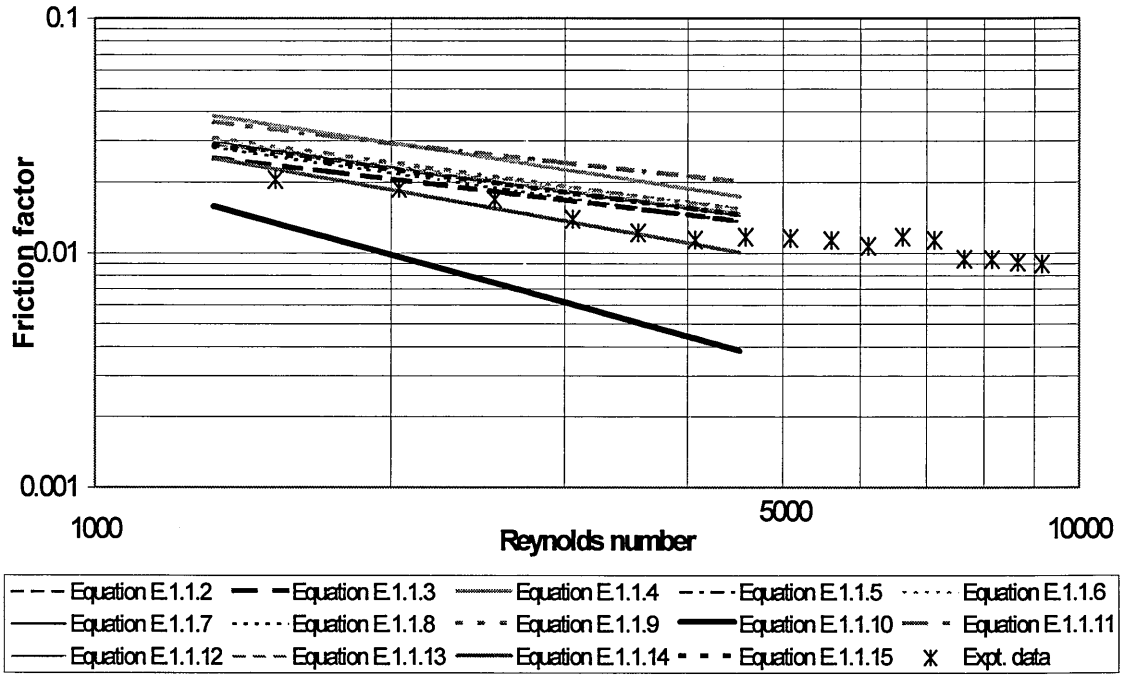

0.029m diameter coil results.

Figure 6.2.4 Comparison of the experimental data to the coil friction factor predictions in the literature, for the laminar region, when D=0.029m.

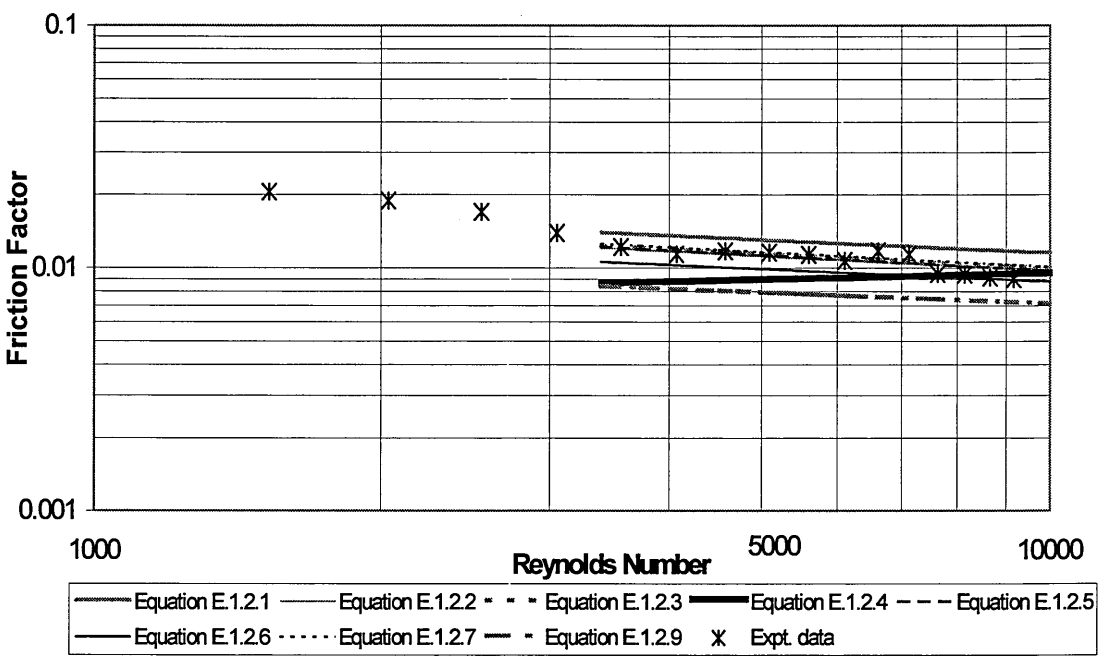

Figure 6.2.5 Comparison of the experimental data to the coil friction factor predictions in the literature, for the turbulent region, when D=0.029m.

The figures show that several of the equations fitted the experimental data well. The equations that fitted the experimental data best for each coil diameter and for laminar and turbulent flow are listed in Table 6.2.1. Van Dyke's (1978) equation fitted the laminar data best for both coil diameters. It was derived theoretically by extending Dean's theoretical equation. Various different equations fitted the turbulent experimental data well. For the smaller 0.029m diameter coil, Ito (1959) equations A and B, Mori and Nakayama (1967a) equation A and Mishra and Gupta (1979), fitted the data equally well. Ito's equations and Mishra and Guptas's equation were derived experimentally with 16-35mm and 6.2-19.05mm diameter tubes respectively. Mori and Nakayama's equations were produced theoretically. For the 0.079m and 0.139m diameter coils, Mori and Nakayama (1967) equation B and Czop et al (1994) fitted the turbulent experimental data well. Czop et al's equation was for a 19.8mm diameter tube.

Coil diameter	**Laminar**		**Turbulent**	
0.029m	Van Dyke (1978)	Equation E.1.1.14	Ito (1959)A Ito (1959)B Mori and Nakayama (1967a)A Mishra and Gupta (1979)	Equation E.1.2.2 Equation E.1.2.3 Equation E.1.2.5 Equation E.1.2.7
0.079m	Van Dyke (1978)	Equation E.1.1.14	Mori and Nakayama (1967a)B Czop et al (1994)	Equation E.1.2.6 Equation E.1.2.9
0.139m	Van Dyke (1978)	Equation E.1.1.14	Mori and Nakayama (1967a)B Czop et al (1994)	Equation E.1.2.6 Equation E.1.2.9

Table 6.2.1 Best equations from the literature for the experimental data.

6.2.3 Transitional Reynolds number

Previous research has found the critical Reynolds number for the transition from laminar flow to turbulent flow to be greater in coils than straight pipes. Previous authors produced equations E.1.3.1 to E.1.3.5, shown in Appendix E, to determine the transitional Reynolds numbers. These equations were used to calculate the approximate critical Reynolds number in the coils tested here. The minimum and maximum critical Reynolds numbers calculated from all of the equations are shown in Table 6.2.2.

The experimental transition from the laminar to turbulent region was estimated from the change in slope on Figure 6.2.3, for each coil diameter and is shown in Table 6.2.2. The transition was found visually by drawing lines along both the laminar and turbulent data and finding the intersection point. Ito (1959) showed a clearer method of determining the transition by plotting the Dean number against $f_c\sqrt{(D/d)}$, as shown

in Figure 6.2.6. The change in slope of the experimental data signified the transition. This critical Reynolds number was found visually by drawing lines along both the laminar and turbulent data and finding the intersection point. Table 6.2.2 shows the transitional Dean numbers with the equivalent Reynolds numbers.

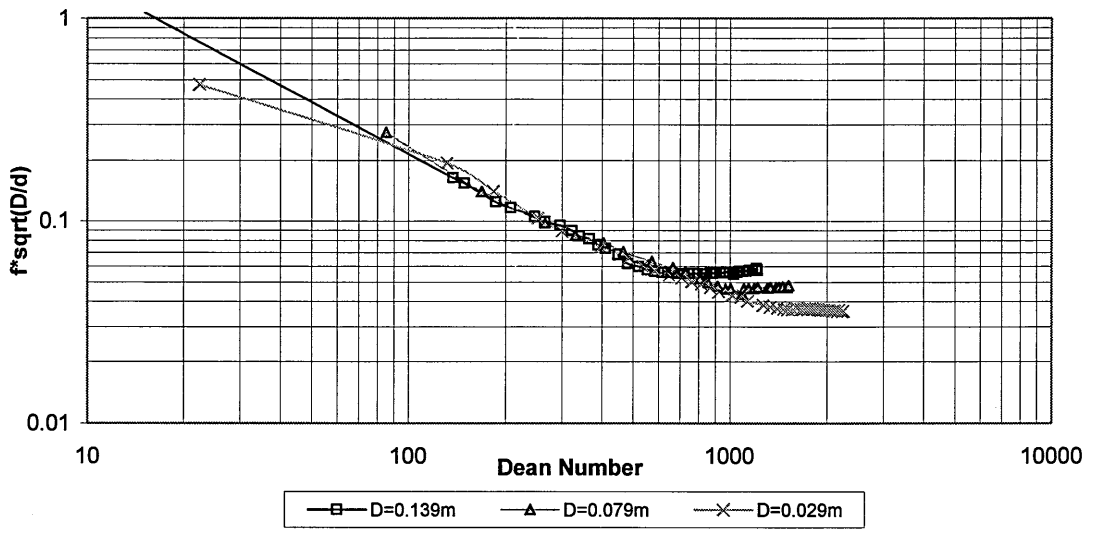

Figure 6.2.6 Determination of transition from laminar to turbulent flow in coils as detailed by Ito (1959).

	Equations from the literature, E.1.3.1- E.1.3.5		Re v f chart Figure 6.2.3	Dn chart Figure 6.2.6	
	Min Re	Max Re	Re	Dn	Re
Straight	2000	2500	2400	-	-
0.139	5400	6200	4300	580	4300
0.079	6400	6900	5000	920	5100
0.029	7800	9500	5000	1500	5100

Table 6.2.2 Critical Reynolds numbers calculated by equations in the literature and from the experimental results.

For each coil diameter, the transition from the laminar region appeared to occur at lower values than the equations from the literature predicted. It was impossible to determine an exact transition point, as the transition in coils is very smooth and gradual. During the winding of the coils, the tube may have become slightly oval and hence, the secondary effect may not have become fully developed. This is unlikely as the tube wall was thick compared to the tube diameter. The discrepancy could also be due to the experimental tube diameter being smaller than the coils tested in the literature. Consistent with this, Damianides and Westwater (1988) found that straight pipes under 3mm in diameter behaved differently to larger diameter pipes. The fittings were also likely to have disturbed the flow and may have upset any flow development.

The data on Figure 6.2.3 was split into laminar and turbulent regimes using the transitions found from Figure 6.2.6. From this, correlations were produced to calculate the experimental friction factor for each coil diameter, for the laminar and turbulent regions. The correlations are shown in Table 6.2.3. The laminar correlation for the straight pipe is in good agreement with the theoretical equation f=16/Re. The turbulent straight pipe equation does not match the Blasius equation but it was shown earlier that the experimental friction factor was less than Blasius.

	Straight	**D=0.139**	**D=0.079m**	**D=0.029m**
Laminar flow	$f = 15.175\ Re^{-0.9824}$	$f = 3.549\ Re^{-0.7346}$	$f = 3.1908\ Re^{-0.6991}$	$f = 2.7105\ Re^{-0.6596}$
Turbulent flow	$f = 0.0147\ Re^{-0.0765}$	$f = 0.0049\ Re^{0.0476}$	$f = 0.0089 Re^{-0.0072}$	$f = 0.0186\ Re^{-0.0634}$

Table 6.2.3 Correlations of friction factor versus Reynolds number for various Reynolds number ranges.

6.2.4 A method of estimating the friction factor in coils

A new procedure to calculate the friction factor of a coil, f_c, was formulated assuming a coil to be a series of 90° bends. The losses in bends and straight pipes are well documented in the literature, but not for coils. Therefore, the losses in a coil were estimated by adding the losses from the same length of a straight pipe and the losses in the number of 90° bends to create the coil. The number of turns of the coil was calculated by dividing the coil length by the circumference. This was multiplied by 4, to find the number of 90° bends. The method to determine the losses in a bend was taken from Miller (1990). Miller's loss data were for Reynolds numbers greater than 10^4. However, the method was found to also apply to lower Reynolds numbers. The derivation of the equation, 6.2.1, is shown in Appendix G. Similar results were obtained using a series of 180° bends. If other loss data references were to be used equation 6.2.1 could be different.

The friction factor for straight pipes, f_s, was calculated using f=16/Re for laminar flow. For turbulent flow equation 6.2.2, taken from Miller and converted to Fanning friction factor was used. The roughness of the polyurethane tubing used in this thesis was taken from Coulson and Richardson (1993) for drawn tubing, to be 0.0015mm.

$$f_c = f_s + \left(\mathrm{Re}^{-0.1653} \frac{d}{D} \left(-0.1727 \ln\left(\frac{d}{D}\right) + 0.02 \right) \right) \qquad \text{Equation 6.2.1}$$

$$f_s = \frac{0.0625}{\left[\log\left(\varepsilon/3.7d + 5.74/\mathrm{Re}^{0.9}\right)\right]^2} \qquad \text{Equation 6.2.2}$$

Figure 6.2.7 shows the new equation compared to the experimental data for the 0.029m diameter coil. The equations found in section 6.2.2 that matched the experimental data best are also shown. The new method using the laminar equation fitted the experimental data well. This was surprising as Miller's loss coefficient was

derived for Reynolds numbers greater than 10^4. The turbulent version of the bends equation was less accurate and overestimated the experimental friction factor. The new equation for laminar flow matched the experimental turbulent data better than the turbulent version of the equation. The correction factor used to account for the bend-bend interaction may not have been accurate for the turbulent flow. The correction factor used was for a bend radius versus tube diameter of 3 but the experimental coils had a value greater than this. The results were similar if a coil was treated as a series of 180^o bends.

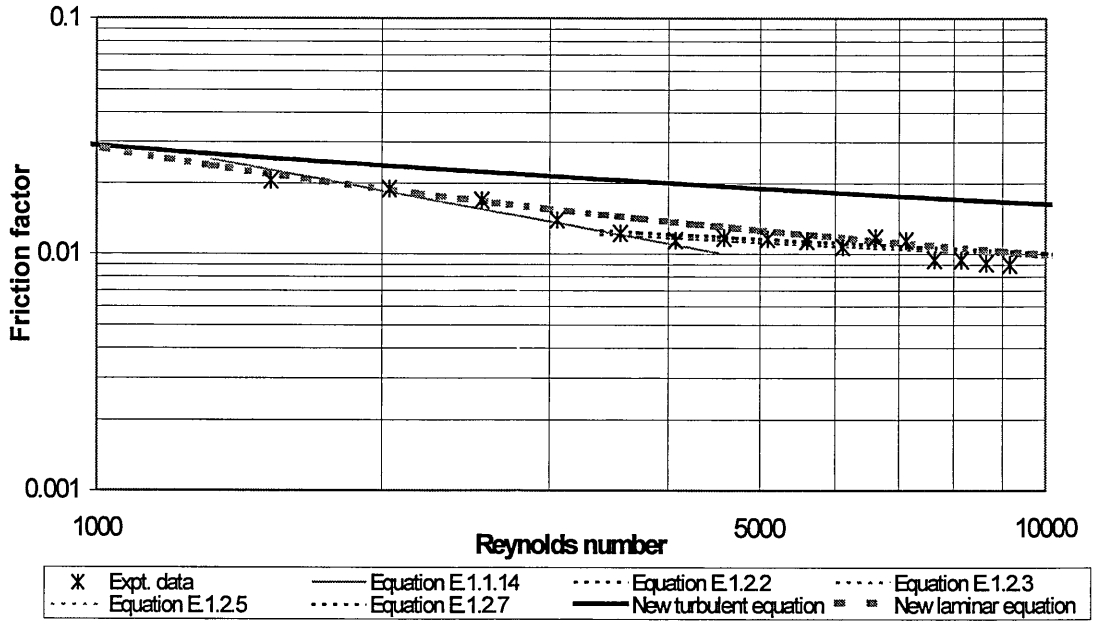

Figure 6.2.7 Comparison of the new equation and the best previously reported equations for laminar and turbulent regions and the experimental data, for the 0.029m diameter coil.

Figure 6.2.8 shows a comparison of the new equation with the results obtained by White (1929) for 3 different values of d/D: 1/15.15, 1/50 and 1/2050. White used lead pipes for which an absolute roughness of 0.15mm was used. The new equation fitted the experimental data well for both laminar and turbulent flow.

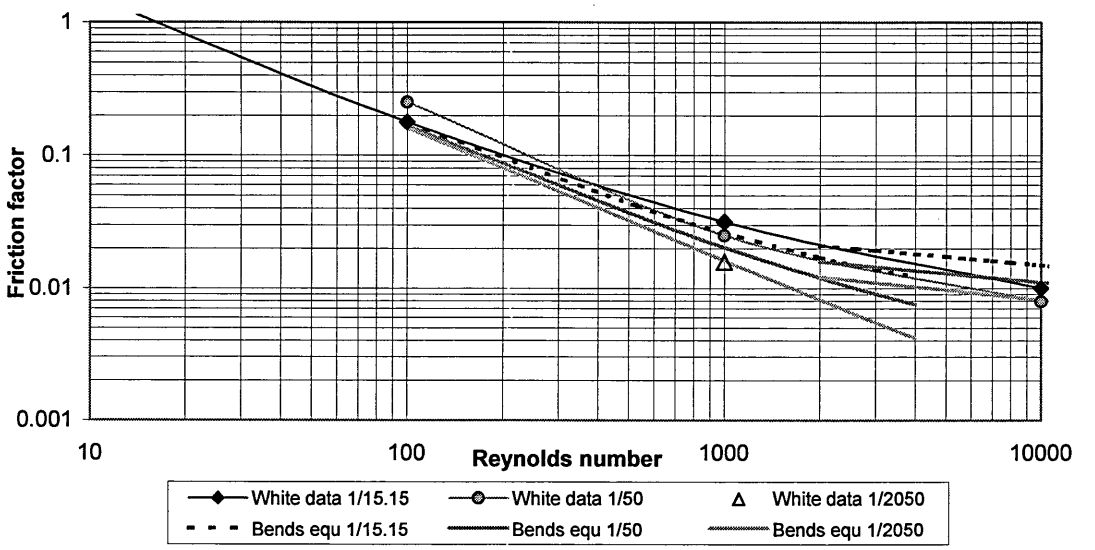

Figure 6.2.8 Comparison of the new equation with White's results.

In summary, these single-phase water experiments have confirmed the finding shown in the literature that the friction factor in coils increases with a decrease in coil diameter. The flow also appeared to remain laminar to higher Reynolds numbers in coils than in straight pipes. Several of the correlations produced for larger diameter coils, fitted the present experimental data well, despite the tube diameter of the coils tested here being smaller than previously tested. The laminar version of the new approach to estimate the friction factor in coils, predicted the experimental laminar and turbulent results well. The turbulent version of the equation overestimated the experimental pressure drop. The new method also predicted White's experimental data well for the laminar and turbulent regions.

6.3 Single-phase flow - Air

Single-phase air flow experiments were performed in the 0.029m and 0.079m diameter coils. The air flowrate was measured using a set of rotameters, for which the calibrations are shown in Appendix C.3. Figure 6.3.1 shows the air mass flowrate versus pressure drop. The mass flowrate is shown as the volumetric flowrate varied with pressure. The longest and smallest diameter coils are shown to have had the greatest pressure drops.

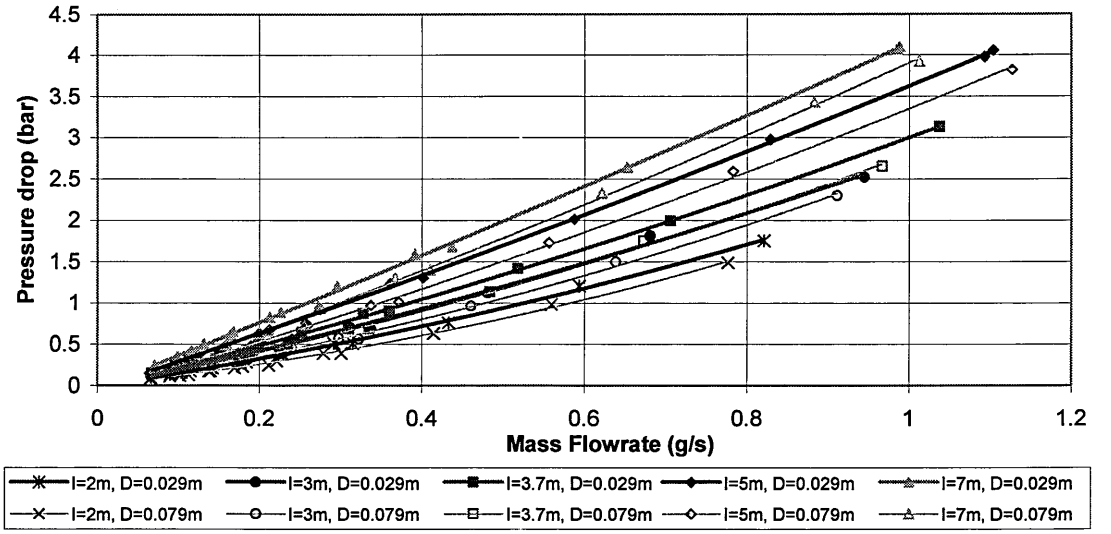

Figure 6.3.1 Pressure drop versus mass flowrate relationship for the coils, with single-phase air flow, D=0.029m and D=0.079m

With single-phase air flow, it would have been virtually impossible to accurately remove the effect of the fittings due to the complexity of the compressibility effect. Appendix F shows that the effects of the fittings would have been minimised with the 7m long coil, with at least 80% of the total pressure drop being due to the coil. The experimental friction factor for the 7m coil was calculated using the compressible flow equation, equation 2.3.1.6. The Reynolds number was calculated with the mass flowrate from equation 2.3.1.5, with a viscosity of 1.82×10^{-5}kg/m/s. For a given Reynolds number, the smaller diameter, 0.029m coil was calculated to have the higher friction factor. Ito (1959) showed that plotting $f_c\sqrt{(D/d)}$ versus Dean number was a clear method of determining the possible transition point from laminar to turbulent flow in coils. This has been plotted for the 7m coils in Figure 6.3.2. The equations produced from the single-phase water experiments to calculate the coil friction factors, as shown in table 6.2.3, are also shown on the figure. The single-phase air laminar friction factors were slightly higher than with the single-phase water flow, but if the effects of the fittings were removed, the friction factor would decrease. Therefore the equations to calculate the coil friction factors derived from the experimental single-phase water would seem appropriate for single-phase air flow.

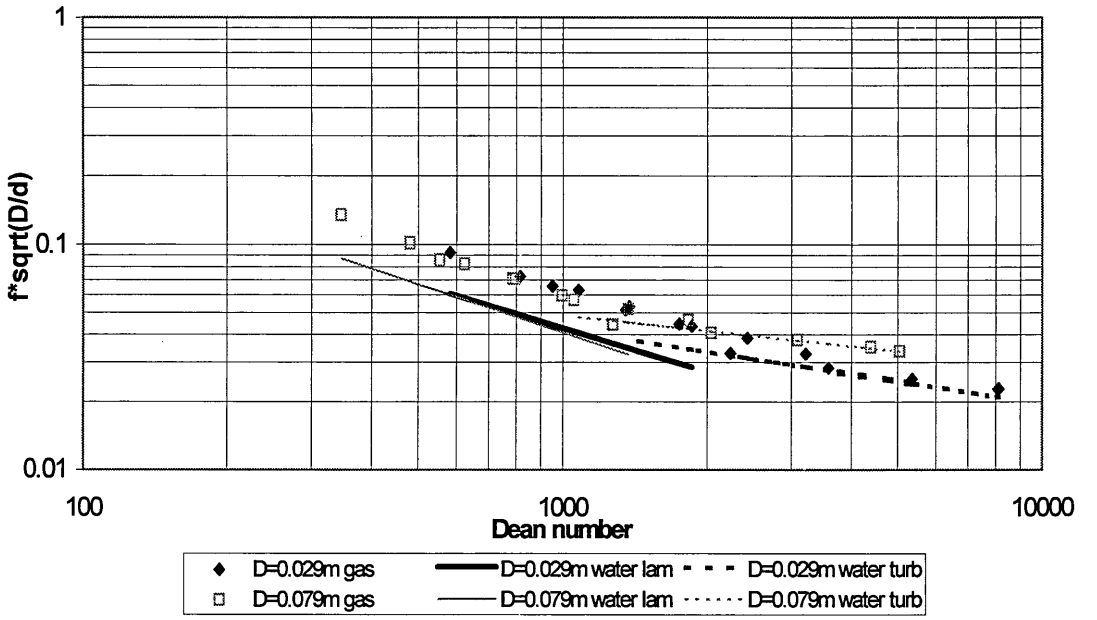

Figure 6.3.2 Determination of transition from laminar to turbulent flow in coils as detailed by Ito (1959) for single-phase air flow in the 7m coils

6.4 Two-phase flow - Air and water

6.4.1 Pressure drop

The two-phase flow of air and water was investigated in the 0.029m and 0.079m diameter coils. The tests were performed by varying the water flowrate whilst the air flowrate remained constant. Three different air flowrates were investigated 0.017, 0.011 and 0.0045g/s. Figure 6.4.1 illustrates the relationship between the water flowrate and the pressure drop for an air flowrate of 0.0045g/s. The figure shows that for a given water flowrate, the smallest diameter and longest coils had the greatest pressure drops. The removal of the effects of the fittings was not possible with the flow type due to its compressibility.

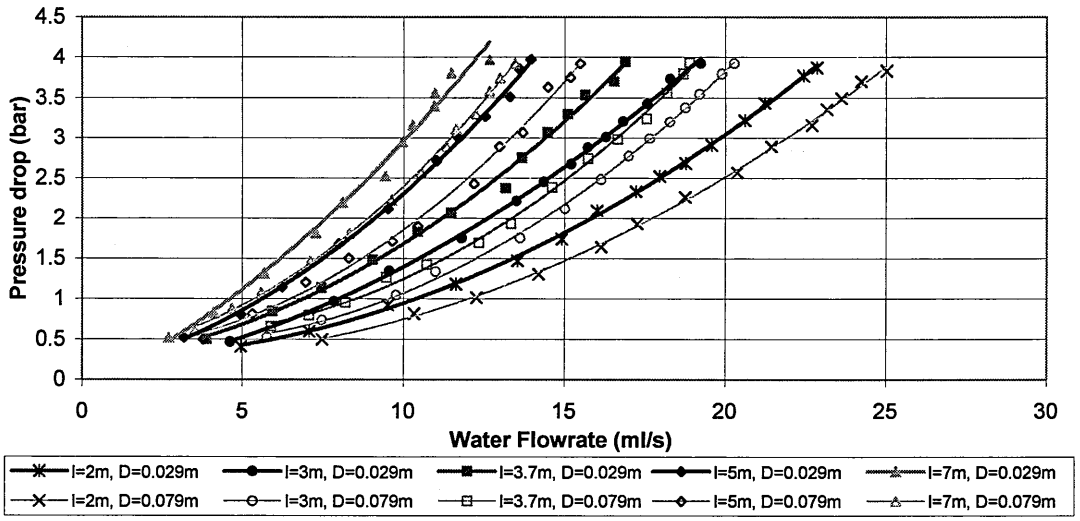

Figure 6.4.1 Pressure drop versus water flowrate for different lengths and diameters of coil. For an air mass flowrate of 0.0045g/s.

Figure 6.4.2 shows the pressure drop versus mass flowrate relationships for the three different air flowrates in the 2m and 7m, 0.029m diameter coils. The volumetric air flowrates at atmospheric pressure, with a density of 1.19kg/m^3, are also indicated. The figure also shows the single-phase water flow relationship for each coil. For a given water flowrate, it is shown that the higher the air flowrate, the greater the pressure drop, as expected.

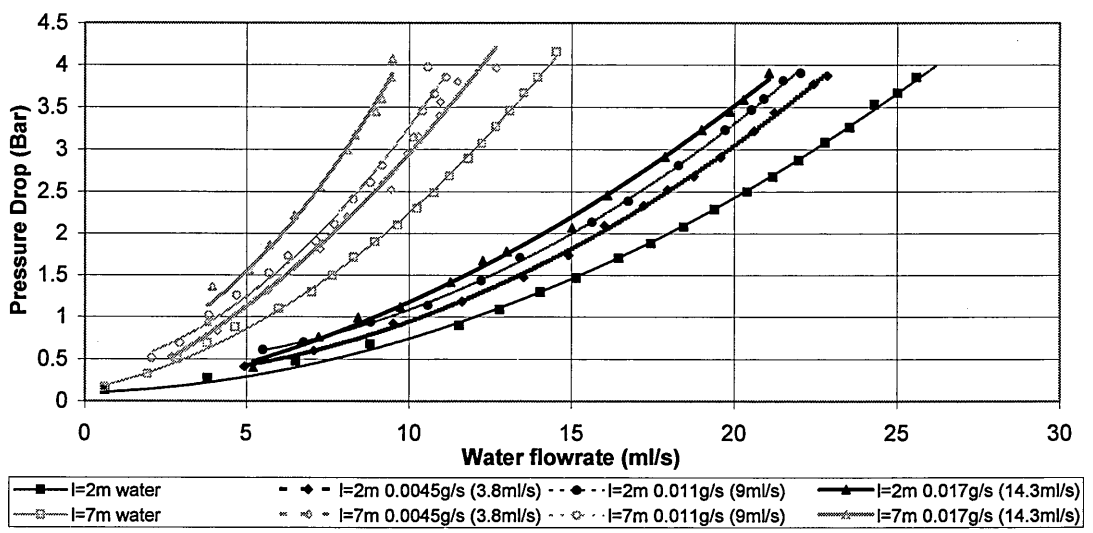

Figure 6.4.2 Pressure drop versus water flowrate for the 2m and 7m long, 0.029m diameter coils, for 3 different air flowrates.

6.4.2 Comparison with friction factor relationships in the literature

Previous researchers have produced a limited number of correlations to calculate the pressure drop of two-phase gas and liquid flows in coils. These equations are shown in Appendix E.2. Most of the correlations use modified versions of the Lockhart and Martinelli correlation, shown by equations 2.3.2.2, 2.3.2.3 and 2.3.2.4 Boyce et al (1969) used the Lockhart and Martinelli correlation, and calculated the single-phase friction factors of water and air using the equations for coils shown in the literature. To compare the results to the experimental data, Van Dyke's (1978) equation, E.1.1.14 for laminar was used as it was found to fit the experimental data well, see Table 6.2.1. For turbulent flow Ito's (1959) equation, E.1.2.2 was used as it also fitted the experimental data well.

$$\frac{-\Delta P_{TP}}{-\Delta P_L} = \phi_L{}^2 \qquad \text{Equation 2.3.2.2}$$

$$X = \sqrt{\frac{-\Delta P_L}{-\Delta P_G}} \qquad \text{Equation 2.3.2.3}$$

$$\phi_L{}^2 = 1 + \frac{C}{X} + \frac{1}{X^2} \qquad \text{Equation 2.3.2.4}$$

$$\frac{f_c}{f_s} = 0.47136 Dn^{1/4} \qquad \text{Equation E.1.1.14}$$

$$f_c = 0.076 \mathrm{Re}^{-0.25} + 0.00725\left(\frac{d}{D}\right)^{0.5} \qquad \text{Equation E.1.2.2}$$

The pressure drop of single-phase water was calculated using equation 2.3.1.2 for straight pipes, with the friction factors calculated from equation E.1.1.14 or E.1.2.2 depending if the flow was calculated to be laminar or turbulent. The density and viscosity of water were taken to be 1000kg/m^3 and 0.001kg/m/s respectively.

$$\Delta P_f = 4f \frac{l}{d} \frac{\rho u^2}{2} \qquad \text{Equation 2.3.1.2}$$

The Reynolds number of air was calculated using the mass flowrate in equation 2.3.1.5, with a viscosity of 1.82x10^{-5}kg/m/s. The maximum Reynolds number of air was calculated to be 500, therefore laminar correlations were applied. The friction factor calculated from equation E.1.1.14 was substituted into the compressible flow equation, equation 2.3.1.6, with the known inlet pressure, P_1, of 5.3bar(a), to determine the single-phase air pressure drop.

$$\mathrm{Re} = \frac{Gd}{A\mu} \qquad \text{Equation 2.3.1.5}$$

$$\left(\frac{G}{A}\right)^2 \ln\frac{P_1}{P_2} + \frac{P_2{}^2 - P_1^2}{2Rt/M} + 2f\frac{l}{d}\left(\frac{G}{A}\right)^2 = 0 \qquad \text{Equation 2.3.1.6}$$

In order to calculate the two-phase multiplier, ϕ_L, values of 10 or 5 were used for the constant, C, in equation 2.3.2.4, depending if the flows were calculated to be

turbulent or laminar. The two-phase pressure drop calculated from equation 2.3.2.2 is compared to the experimental data, for the 7m, 0.029m coil, in Figure 6.4.3. The results fit the experimental data well.

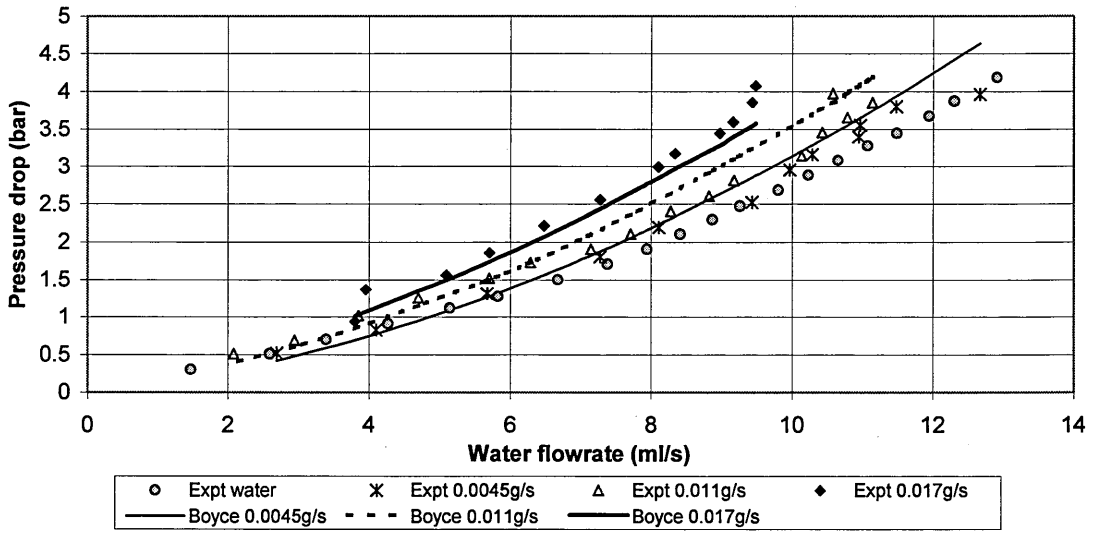

Figure 6.4.3 Comparison of the experimental results with Boyce et al's theory, with the D=0.029, l=7m coil.

Akagawa et al (1971) produced equation E.2.1.2, to calculate the two-phase pressure drop within a coil. The single-phase water friction factor was calculated using Ito's equation, E.1.2.2, for turbulent flow in coils. The Reynolds number of air was calculated using the mass flowrate, in equation 2.3.1.5, with a viscosity of 1.82×10^{-5}kg/m/s. To calculate the Reynolds number of the water, the density and viscosity of water were taken to be 1000kg/m^3 and 0.001kg/m/s. The results from this equation have been compared to the experimental data in Figure 6.4.4.

$$\frac{\Delta P_{TP(coil)}}{\Delta P_{L(straight)}} = \frac{f_{L(coil)}}{f_{L(straight)}} + 9.63\left(1+1.7\frac{d}{D}\right)\left(\frac{\mathrm{Re}_G}{\mathrm{Re}_L}\right)^{0.747} \mathrm{Re}_L^{-0.019} \quad \text{Equation E.2.1.2}$$

Czop et al (1994) developed equation E.2.1.3 to calculate the Lockhart and Martinelli parameter, X. The density and viscosity of water were taken to be 1000kg/m^3 and 0.001kg/m/s. A mean air density was used as it would have varied along the tube. The density at 3bar pressure of 3.6kg/m^3 was used. The viscosity was assumed to have been constant at 1.82×10^{-5}kg/m/s. Once the Lockhart and Martinelli parameter, X was found, the two-phase pressure drop was calculated in the same manner as Boyce et al, described above. The experimental data has been compared to these results in Figure 6.4.5.

$$X = \left(\frac{1-x}{x}\right)^{0.924}\left(\frac{\mu_G}{\mu_L}\right)^{-0.07585}\left(\frac{\rho_G}{\rho_L}\right)^{0.5} \quad \text{Equation E.2.1.3}$$

Xin et al (1996) produced equation E.2.1.7b to calculate the two-phase multiplier, ϕ_L. The equation applies for F_d, greater than 0.1, which is defined in equation E.2.1.5.

The Lockhart and Martinelli parameter and hence the two-phase pressure drop was calculated in the same manner as Boyce et al's method. The results of the calculations are compared with the experimental data in Figure 6.4.6.

$$\frac{\phi_L}{\left(1+20/X+1/X^2\right)^{1/2}} = 1+\frac{X}{434.8F_d^{1.7}}$$ Equation E.2.1.7b

$$F_d = \frac{u_L^2}{gd}\left(\frac{d}{D}\right)^{0.1}$$ Equation E.2.1.5

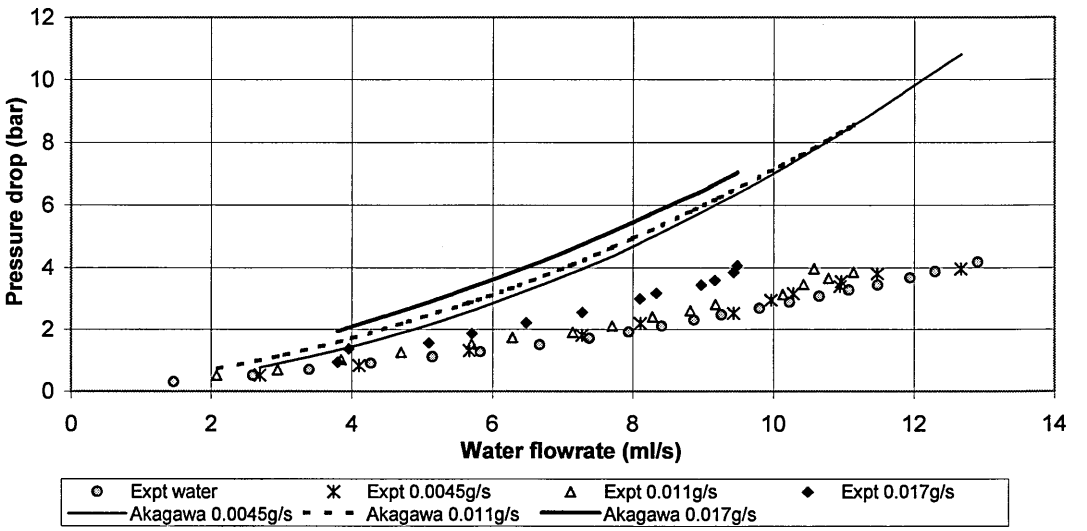

Figure 6.4.4 Comparison of the experimental results with Akagawa et al's equation, E.2.1.2, with the D=0.029, l=7m coil.

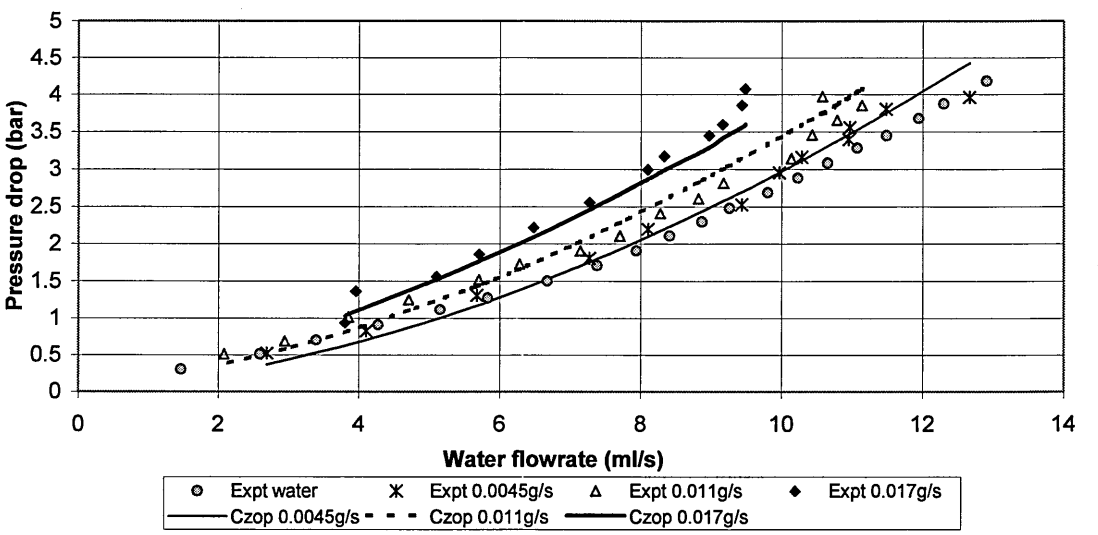

Figure 6.4.5 Comparison of the experimental results with Czop et al's equation, E.2.1.3, with the D=0.029, l=7m coil.

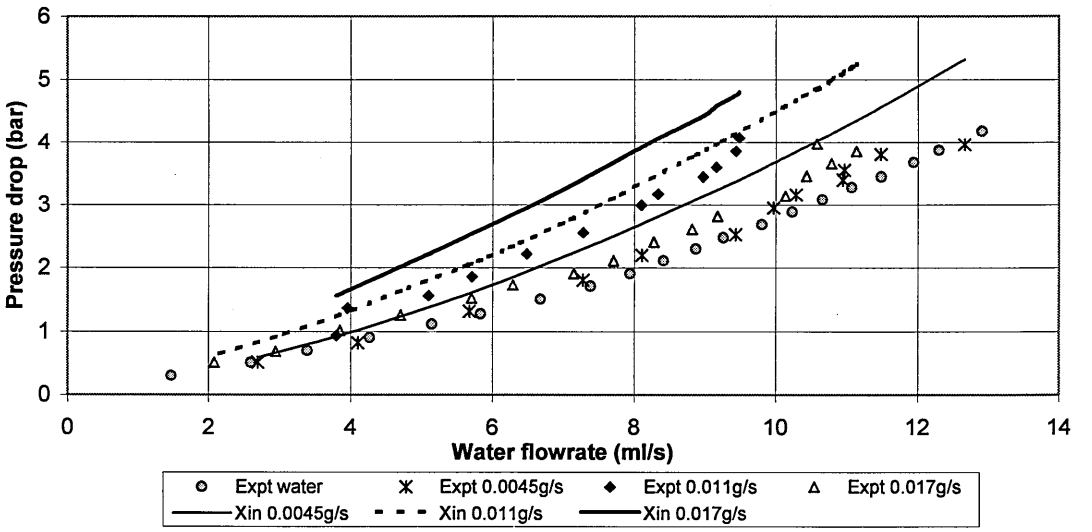

Figure 6.4.6 Comparison of the experimental results with Xin et al's equation, E.2.1.7, with the D=0.029, l=7m coil.

Boyce et al's method and Czop et al's equation, equation E.2.1.3, were found to predict the pressure drop particularly well.

In summary, despite these coils have smaller tube diameters than have previously been tested, the equations from the literature for two-phase flow in coils fitted the new experimental data well. Increasing the air flowrate, at a given water flowrate, resulted in an increase in pressure drop, as expected. This is the opposite effect as seen with the nozzle.

6.5 Two-phase flow - Carbon dioxide saturated water

A carbonated drink dispenser should be capable of reducing the pressure used to saturate the water with carbon dioxide, whilst releasing a minimum amount of gas. A high flowrate is desirable, to reduce the serving time. The depressurisation of carbon dioxide saturated water was investigated in the 0.029m and 0.079m diameter coils. The gas-saturated water was produced by pressurising the water and carbon dioxide in a saturator, at 5.3 bar absolute. The concentration of dissolved carbon dioxide entering the device was determined using the inlet trapping section to the device. Appendix C.4 shows that the inlet concentration of dissolved gas was found to be 7.5±0.3mg/ml and the flow was 95% saturated. The concentration of gas that remained dissolved in solution after depressurisation was measured using the method as described in Chapter 4.

6.5.1 Pressure drop and friction factor

The flowrate versus pressure drop relationships for the gas-saturated flow in the coils are shown in Figure 6.5.1. As with both the single-phase flows and the two-phase air and water flow, the longest and smallest diameter coils had the greatest pressure drops. The gas-saturated flow was assumed to have the same properties as water, with a density of 1000kg/m^3 and viscosity of 0.001kg/m/s, the minimum Reynolds number at the lowest experimental flowrate was found to be not quite 2000. For the 2m, 0.079m diameter coil, the maximum Reynolds number was over 12000.

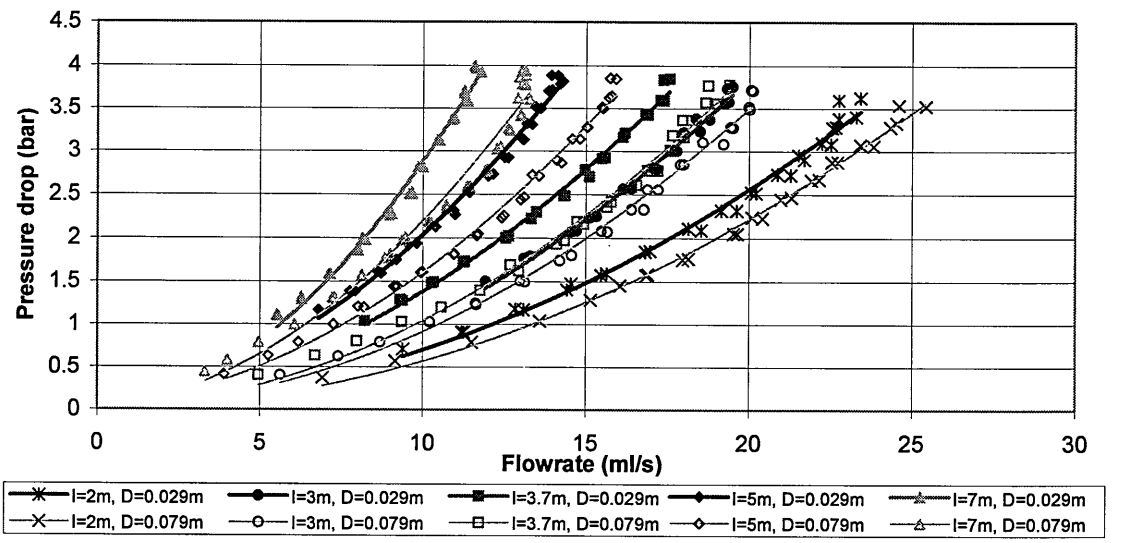

Figure 6.5.1 Pressure drop versus flowrate relationship for the coils, with gas-saturated water flow, D=0.029m and 0.079m.

The fittings would have had a significant effect on these results. However, it was not possible to determine the pressure losses due to the coil alone, because of the compressible nature of the flow, especially at the outlet. The effect of the fittings would have been minimised with the 7m coil, when it was estimated that at least 80% of the pressure drop would have been due to the coil, see Appendix F.2.

The pressure drop versus flowrate relationships of the single-phase water and the carbon dioxide-saturated water flows were compared for the 7m long, 0.029m and 0.079m diameter coils. Theoretically, if no gas were evolved from the gas-saturated flow, the relationships would be the same. The comparisons are shown in Figure 6.5.2. The relationships were similar until a flowrate of approximately 10ml/s, after which the pressure drop of the gas-saturated flow increased more rapidly, suggesting that bubbles began to affect the flow. As with the two-phase air and water coil experiments, the pressure increased with gas flowrate, at a given water flowrate. The figures appear to show that the larger diameter coil released the gas at a higher flowrate, however the difference was minimal.

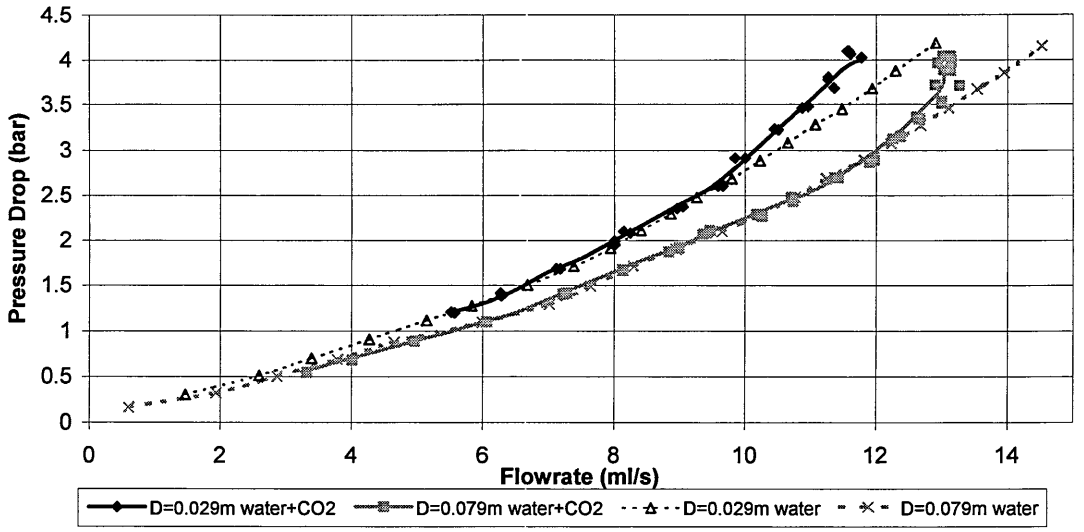

Figure 6.5.2 Comparison of the pressure drop versus water flowrate relationships for the single-phase water and carbon dioxide saturated water for the 7m coils.

The experimental friction factor was calculated for the 7m long coils. The smaller diameter coil was again calculated to have a higher friction factor. Ito (1959) showed that plotting $f_c\sqrt{(D/d)}$ versus Dean number was a clear method of determining the possible transition point from laminar to turbulent flow in coils. This has been plotted for the gas-saturated flow in the 7m coils in Figure 6.5.3. The single-phase water results using the friction factors shown in Table 6.2.3 are also shown on the figure.

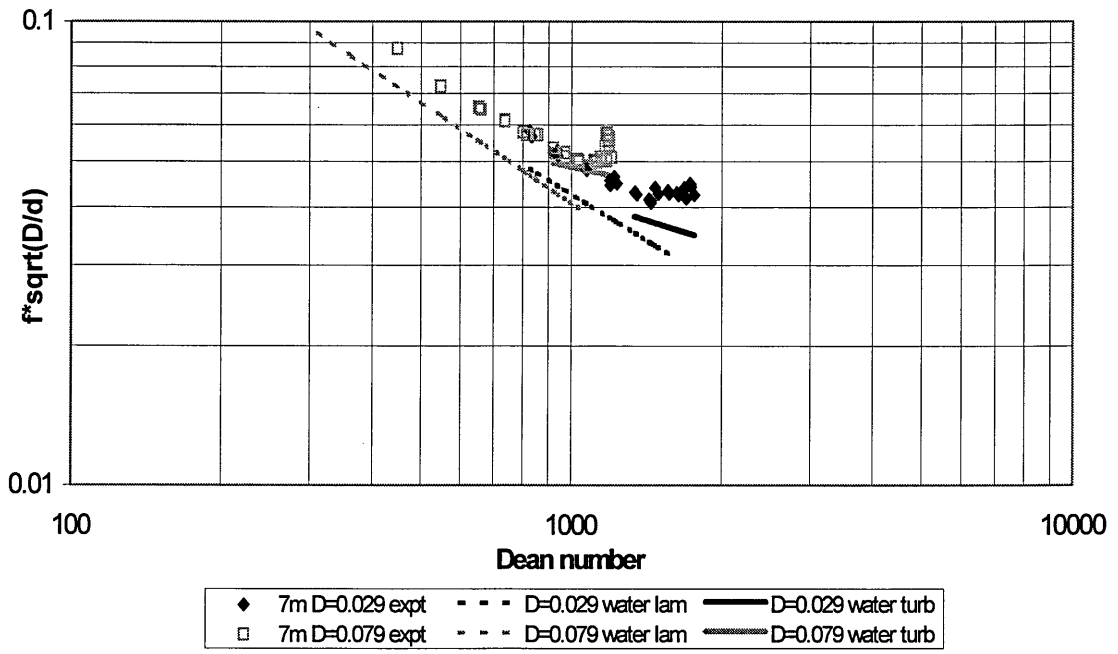

Figure 6.5.3 Determination of transition from laminar to turbulent flow in coils as detailed by Ito (1959) for gas-saturated water flow, in the 7m coils

The difference between the gas-saturated water and single-phase water results could be accounted for by the fittings. From visual inspection it appears that the transition from laminar to turbulent flow occurred at a Dean number of approximately 1500 for the 0.029m diameter coil, which corresponded to a Reynolds number of 5100. For the 0.079m diameter coil the transition appeared to occur at a Dean number of 1000 corresponding to a Reynolds number of 5600. These values are similar to the single-phase water results. With the 0.079m diameter coil, there was a marked increase in the friction factor at Dean numbers greater than 1000. This could have been due to the carbon dioxide coming out of solution.

6.5.2 Measurement of the dissolved gas concentration

Both the syringe and trapped methods were incorporated into the experimental procedure, to determine the concentration of dissolved gas at the outlet. The trapped method was found to produce the most accurate results for the test nozzle experiments, as shown in Section 5.5. This was also the case for the coil results. Hence, the trapped method has been used to present the dissolved gas concentration results.

Figure 6.5.4 shows the flowrate against exit concentration, for the 0.029m diameter coils. The figure confirms that the 2m coil had the highest flowrate. The actual concentration when there was little or no pressure drop was high, but the solution would still have been saturated at almost the saturator pressure. Figure 6.5.5 illustrates the equivalent chart showing the outlet percentage supersaturation. This gives a clearer picture of the performance of a depressurisation device, as it is a measure of the extra amount of gas dissolved at the outlet pressure. A high percentage supersaturation means that more gas will be dissolved in solution so that the drink will remain fizzy for longer. For a given flowrate, the longer coils had the highest percentage supersaturation at the outlet, but they were unable to produce as high a flowrate.

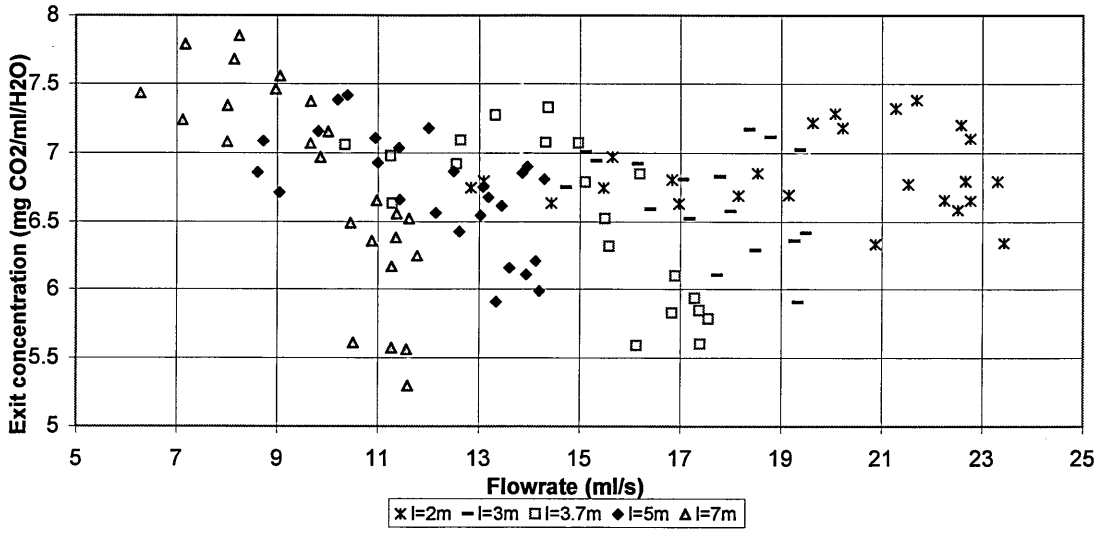

Figure 6.5.4 Exit concentration versus flowrate for the 5 different lengths of the 0.029m diameter coil.

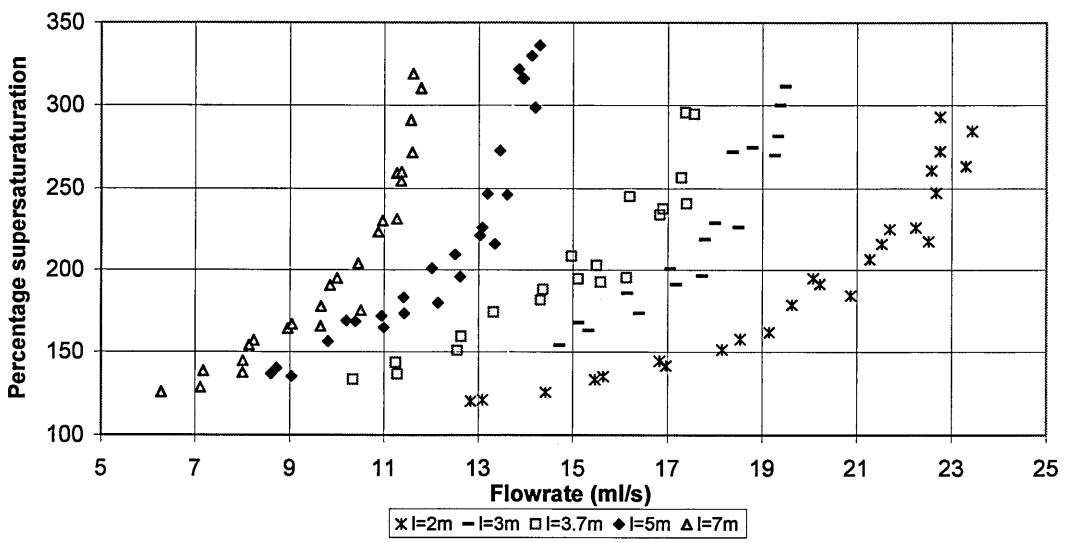

Figure 6.5.5 Percentage supersaturation versus flowrate for the 5 different lengths of the 0.029m diameter coil.

The exit concentration versus pressure drop is shown in Figure 6.5.6 for the 0.029m diameter coils. It shows that the longest, 7m coil had the highest exit concentration at low pressure drops, but at the higher pressure drops the shorter coils appeared to have a higher exit concentration. Figure 6.5.7 shows the equivalent chart illustrating the percentage supersaturation. The figure shows clearly that for a given pressure drop, the shortest coil had the highest exit concentration. A shorter tube and faster flowrate would suggest the fluid would have had less contact time with the tube walls and with any nucleation sites. These results are in agreement with Jefferson (1997) and Wang and Ouyang (1994) who found that long nozzles were required for DAF to release the

maximum amount of gas. Hence a shorter device would be more suitable for carbonated drinks dispensing.

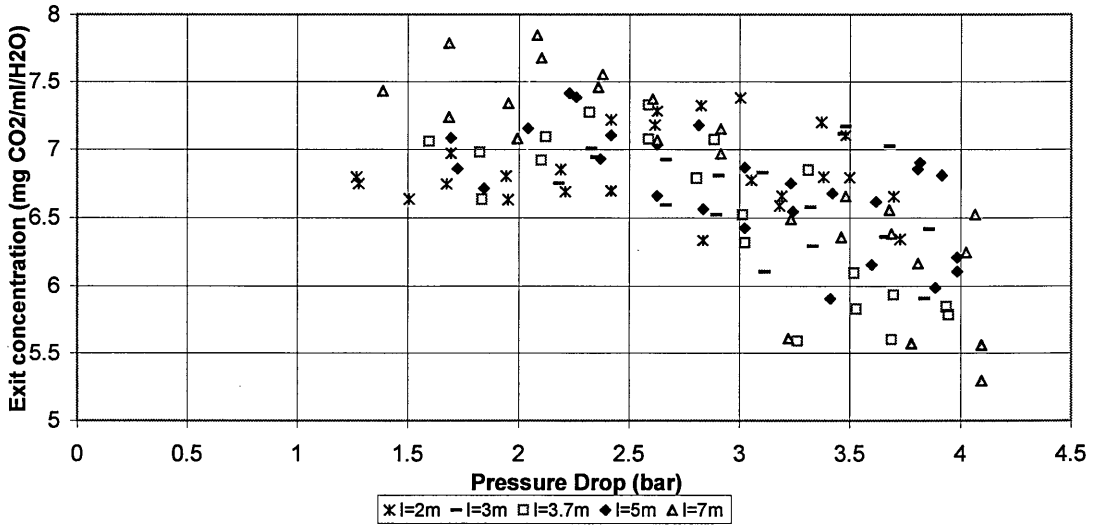

Figure 6.5.6 Exit concentration versus pressure drop for the 5 different lengths of the 0.029m diameter coil.

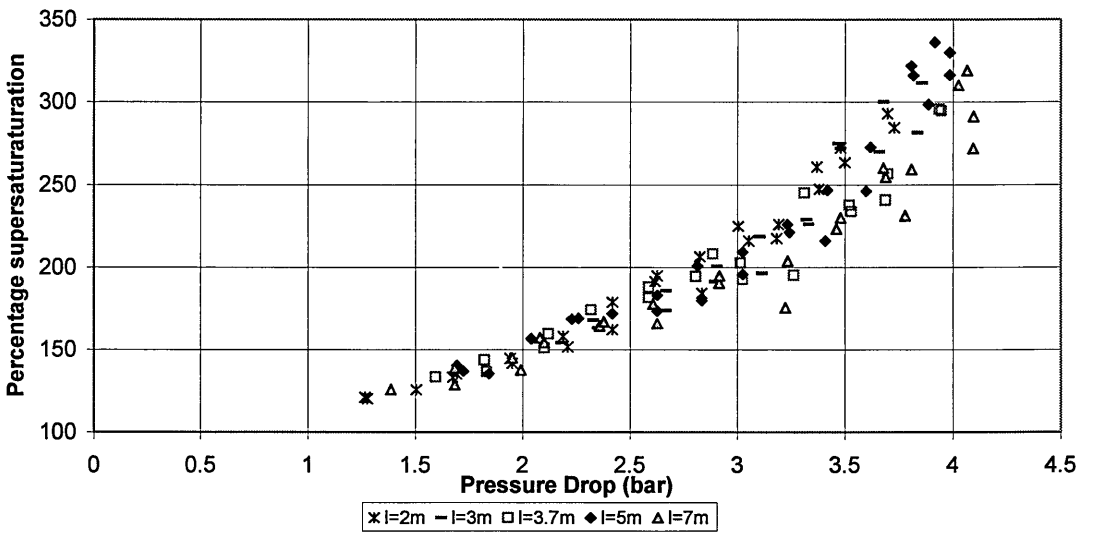

Figure 6.5.7 Percentage supersaturation versus pressure drop for the 5 different lengths of the 0.029m diameter coil.

The results so far have only shown the 0.029m diameter coil. Figures 6.5.8 and 6.5.9 compare the 2m and 7m coils, for the 0.029m and 0.079m diameter coils. The figures show the exit concentration and percentage supersaturation versus pressure drop, respectively. They appear to show that, for a given pressure drop, both coil diameters had similar concentrations of dissolved gas at the outlet.

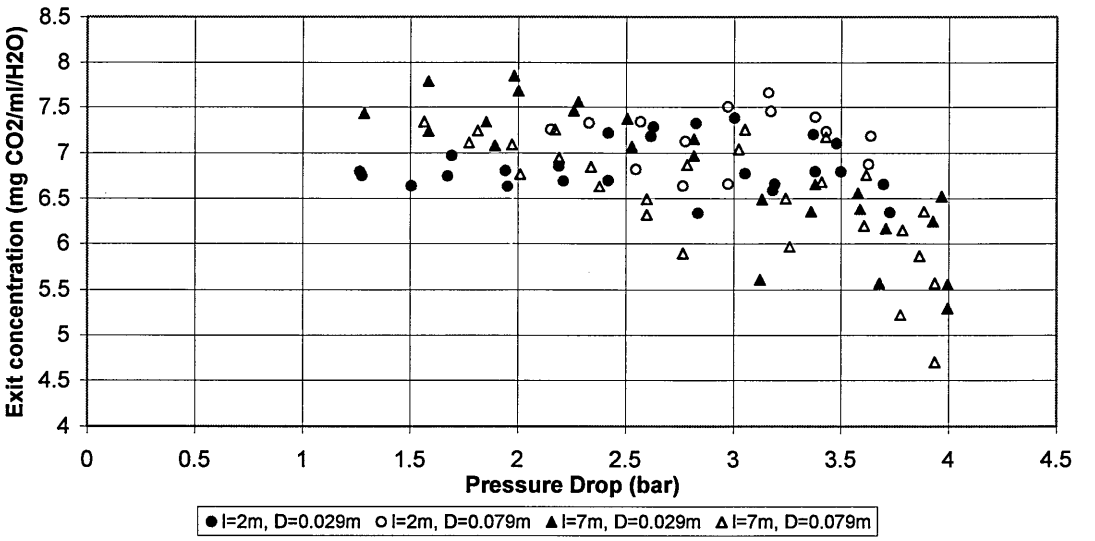

Figure 6.5.8 Exit concentration versus pressure drop for the 2m and 7m coils.

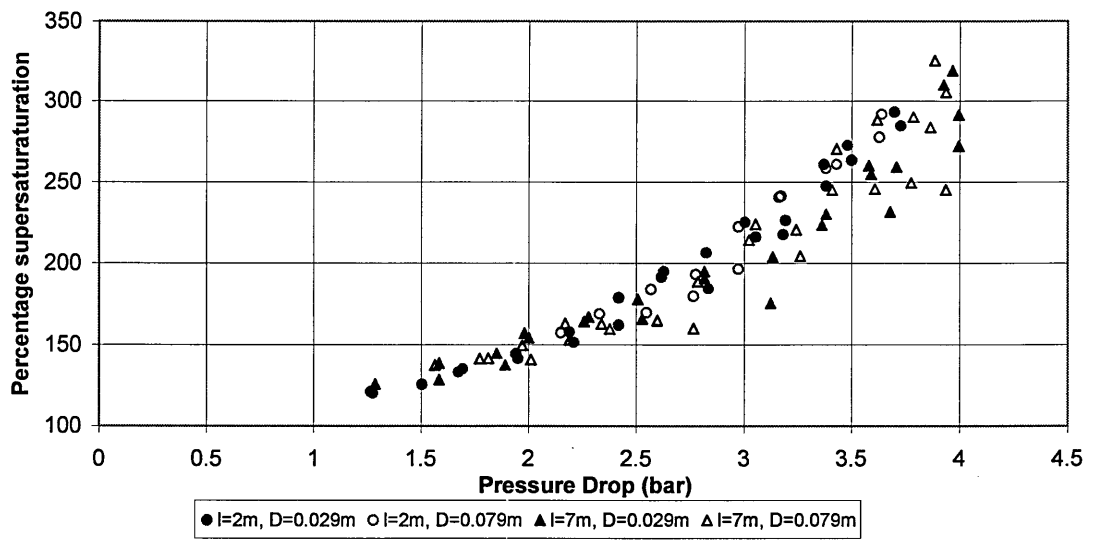

Figure 6.5.9 Percentage supersaturation versus pressure drop for the 2m and 7m coils.

For a clearer overall picture of the results, Figure 6.5.10 shows the percentage supersaturation versus flowrate at three different pressure drops. For each line in the figure an increase in flowrate corresponds to a decrease in coil length. For a given pressure drop, an increase in flowrate corresponded to an increase in percentage supersaturation. Hence, the shortest coils had the highest degree of supersaturation at the outlet. The figure also shows that, for a given pressure drop and flowrate, the smaller diameter, 0.029m, coils had a higher percentage supersaturation at the outlet. Hence, to achieve the highest percentage supersaturation in the outlet flow a short, small diameter coil is recommended.

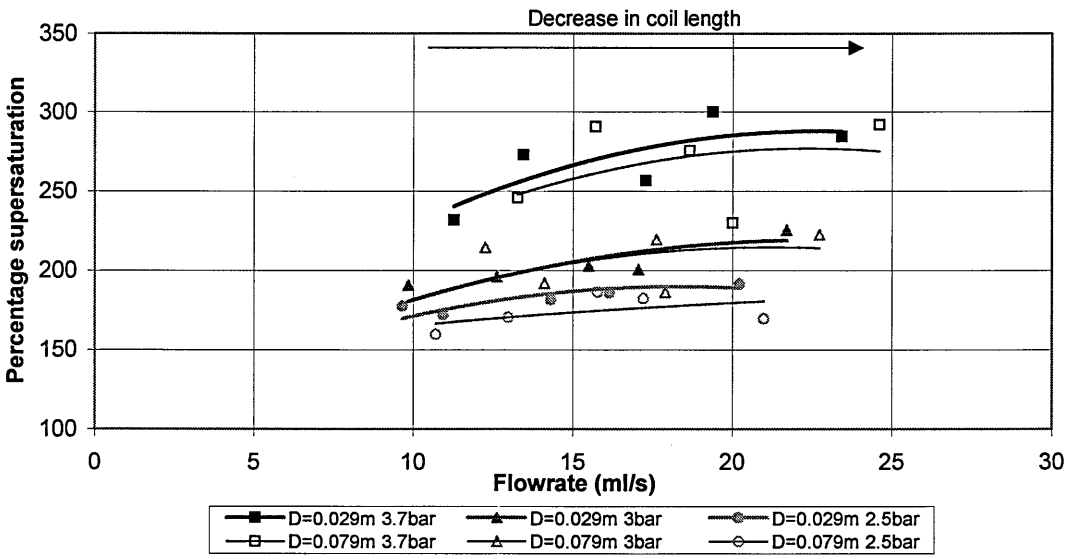

Figure 6.5.10 Percentage supersaturation versus flowrate for constant pressure drop across each of the coils.

It is possible that the optimum coil length is shorter than the minimum coil length tested of 2m. An infinitely short coil would resemble orifices, which are used in DAF nozzles to release dissolved gas. In order for a very short coil to drop the carbonator pressure, the flowrate would have to be very high, and probably more turbulent, suggesting more gas would be released. Hence, the optimum coil length would be between zero and 2m. However, coils shorter than 2m could not be tested with the present experimental set up as the pressure losses due to the fittings would have been greater than the coil itself.

6.6 Discussions

For each flow type, it was found that at a given flowrate the longest and smallest diameter coils had the highest pressure drops. The shorter coils however had the higher flowrates. It was found that a short, small diameter coil had the same pressure drop, at a given flowrate as a longer, larger diameter coil. The transition from laminar to turbulent flow in coils was found to occur at higher Reynolds numbers than the straight pipe. The transition occurred at higher Reynolds numbers as the coil diameter increased. This was in agreement with the work of previous researchers using larger

tube diameters. The transition between laminar and turbulent flow was found to be lower than the equations from the literature review suggested. This could have been due to the small tube diameter or to the fittings upsetting the flow development.

The experimental pressure drop included the pressure drop of the fittings, as well as the coil. A method was developed to quantify and eliminate the effects of the fittings to determine the pressure loss of the coil alone. This was done by plotting the total pressure drop due to the fittings and coil against coil length. The intercept indicated the pressure drop due to the fittings. With the 2m coil up to 50% of the total pressure drop was found to be attributable to the fittings. With the 7m coil up to 20% of the total pressure drop was due to the fittings. Equations were derived to calculate the experimental friction factor for each coil diameter in both the laminar and turbulent regions.

The literature review uncovered a large number of equations to calculate the single-phase friction factor in coils. The following equations fitted the experimental data best:

For laminar flow:	Van Dyke (1978)
For turbulent flow:	Mishra and Gupta (1979), Ito (1959) equations A and B, Czop et al (1994), Mori and Nakayama (1967a) equations A and B

A new method to calculate the friction factor of a coil was formulated by treating a coil as a series of 90° bends. The laminar version of the method predicted the experimental friction factor well for both the laminar and turbulent data. The new bends equation also predicted the pressure drop of White's (1929) experimental results well, for laminar and turbulent flow. Treating the coil as a series of 180° bends produced similar results. The advantage of the proposed approach is that no testing is required and the method can be applied to estimate the pressure losses in coils with any geometry.

With two-phase air and water flow, the pressure drop was found to increase with air flowrate, at a given water flowrate. The pressure drop was predicted well by two-phase flow coil correlations from Boyce et al (1969) and Czop et al (1994).

The pressure drop versus flowrate relationships for the gas-saturated and single-phase water flows were compared. The relationships were very similar at low water flowrates, but at high flowrates the pressure drop for the dissolved gas experiments increased more rapidly, signifying the release of dissolved gas.

The percentage supersaturation at the outlet was found to increase with flowrate and pressure drop. It was shown that for a given pressure drop and flowrate, the highest degree of supersaturation at the outlet was achieved with the shortest and smallest diameter coils. The shortest coils also had the highest flowrates. The higher percentage supersaturation at the outlet of the shorter coils could be attributed to the flow having passed over less surface area and hence fewer nucleation sites for bubbles to form. The higher percentage supersaturation at the outlet of the smaller diameter coil, 0.029m diameter, was likely to be due to the flow remaining laminar

until higher Reynolds numbers than the larger diameter coil. Hence, giving the bubbles less chance to form.

Coils shorter than 2m could not be tested with the apparatus used, as the fittings would have had a significant effect on the results. An infinitely short coil would resemble orifices, which are used in DAF to release dissolved gas. This suggests that the coil length, to maintain the highest concentration of dissolved gas at the outlet, should be between zero and 2m. Further definition of the optimum coil length was not feasible with the experimental set up used. Of the coils tested, the 2m long, 0.029m diameter coil would be the most suitable as a carbonated drinks dispenser.

6.7 Comparison of the nozzle and coils

The carbonated drinks industry is interested in finding the ultimate depressurisation device to dispense carbonated drinks. In the preliminary experiments, nozzle 1 was found to be the best device presently available, as it created a large pressure drop with probable laminar flow. It is however, large and a different device is required for each flavour of drink. Ideally a device should be small so it takes up minimal space. Coils were found to have properties that could be potentially useful for carbonated drink dispensing. In this section the test nozzle and coil experimental results have been compared.

The overall results for the coils and nozzle were similar. However, with the two-phase air and water flow, an opposite effect was seen with the pressure drop and flowrate relationship for the devices. The coil pressure drop was predicted well by correlations from the literature. For a given water flowrate the pressure drop increased with air flowrate. In contrast, the nozzle pressure drop could not be predicted by present correlations. For a given water flowrate in the nozzle a reduction in pressure was seen with an increase in air flowrate. This appears to be due to the narrow restriction within the nozzle.

The concentration of dissolved gas after depressurisation was investigated for both the nozzle and coils. With the nozzle, the highest degree of supersaturation at the outlet was achieved with the longest space adjuster, 3.5mm, which had the narrowest gap. For the coils, the shortest, 2m, and smallest diameter, 0.029m, coil was found to maintain the highest concentration of carbon dioxide dissolved in the water after depressurisation. This coil has been compared to the nozzle to see if it could be used as an alternative depressurisation device to increase the amount of dissolved gas at the outlet.

Figure 6.7.1 shows the flowrate versus pressure drop relationships for the 2m and 7m coils, and the nozzle with space adjuster lengths of 3.23 and 3.5mm. The nozzle is shown to have achieved significantly higher flowrates. However, three intertwined coils could be used to produce the same flowrate as the nozzle, and have a higher percentage supersaturation at the outlet.

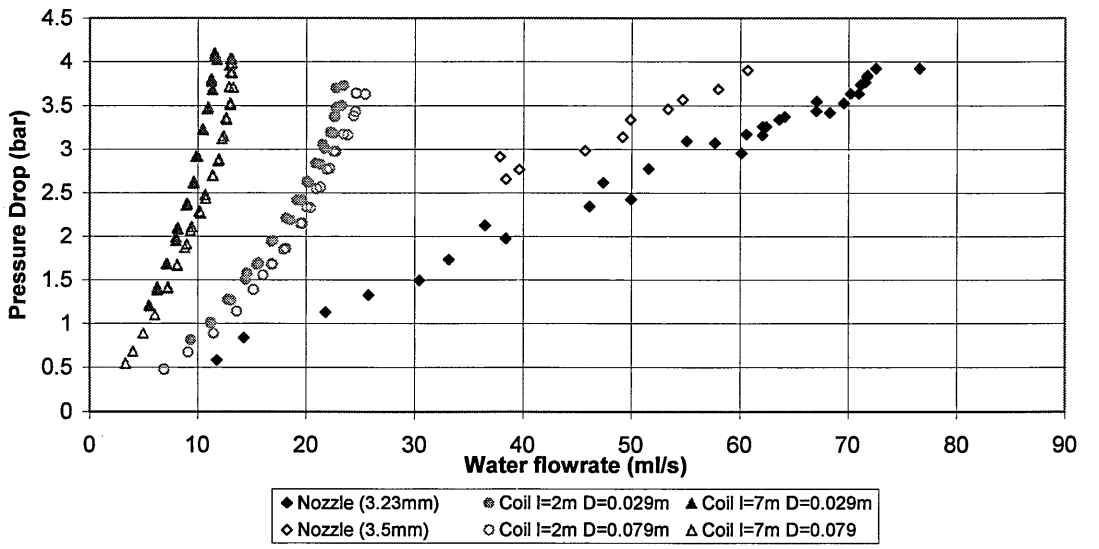

Figure 6.7.1 Pressure drop versus flowrate relationships for both devices.

Figure 6.7.2 shows the percentage supersaturation of carbon dioxide at different flowrates. Figure 6.7.3 shows the percentage supersaturation against pressure drop. It clearly shows that for a given pressure drop the coils, in particular the 2m coil, had the highest percentage supersaturation at the outlet.

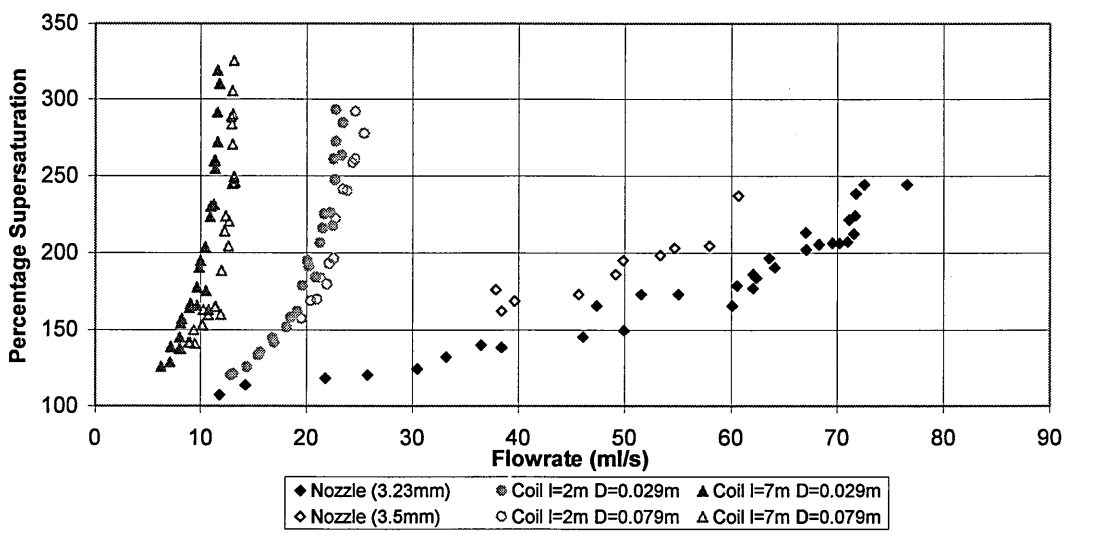

Figure 6.7.2 Percentage supersaturation versus flowrate relationship for both devices.

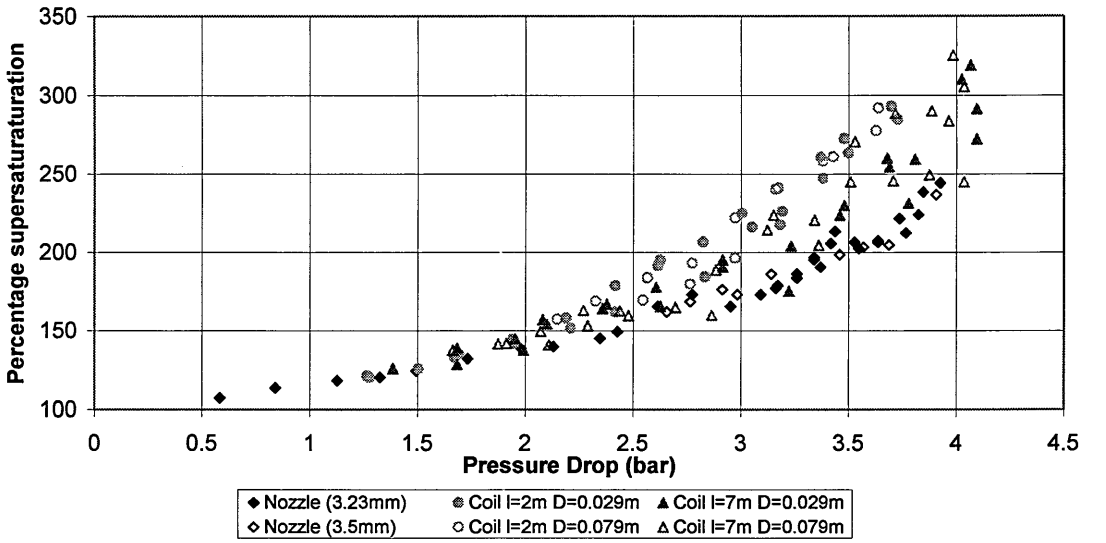

Figure 6.7.3 Percentage supersaturation versus pressure drop relationship for both devices.

Figure 6.7.4 shows how the percentage supersaturation varied with flowrate for given pressure drops in the coils and nozzle. It shows that the nozzle had a higher flowrate than the coil. However, the coil had a far greater concentration of dissolved carbon dioxide in the outlet. The nozzle results for a spacer length of 3.23mm are shown, as more results were produced for this position. This is appropriate, as it was found that for a given pressure drop the outlet concentration was similar for each central body position.

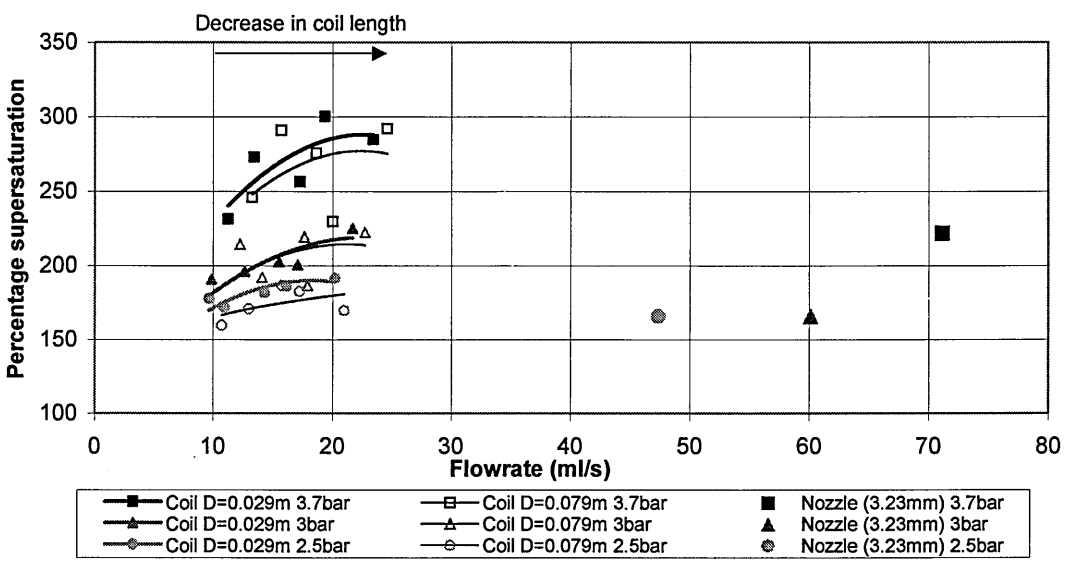

Figure 6.7.4 Comparison of the percentage supersaturation versus flowrate relationship for the nozzle and coil, at specific pressure drops.

When comparing the pressure drop versus flowrate relationships for single-phase water and gas-saturated flows in the nozzle and coil, they were found to be very different. Figure 5.5.2 for the nozzle showed a marked difference between the pressure drops for the two flow types, even at low flowrates. In contrast, Figure 6.5.2 for the coils showed the pressure drops of the two flow types to be similar until a flowrate of 10ml/s when the presence of gas would have increased the pressure drop of the gas-saturated flow. This again suggests that more gas were evolved from the nozzle.

The surface areas of the nozzle and coil were found to be similar, $0.0101m^2$ and $0.0157m^2$ respectively. The volume of the depressurisation section of the nozzle was calculated to be 24.16ml and for the coil 9.82ml. If the number of coils were increased to produce the same flowrate as the nozzle, the volumes would be comparable. The residence times were also similar 0.345 and 0.377sec for the nozzle and coil respectively. The local pressure distribution within the devices was however, very different. Figure 6.7.5 shows the local pressure distribution within the 2m, 0.029m diameter coil and nozzle against the percentage of the total distance along the device. The pressure distribution within the nozzle was calculated from the flat plate equation, equation 2.3.4.7. A similar pressure distribution in the nozzle was found with the CFD results in Figure 5.6.1. The pressure drop in the coil was steady, whilst the majority of the pressure drop in the nozzle was at the start over a small proportion of the device. These differences in local pressure distribution could be the reason for the higher dissolved gas concentration at the coil outlet.

Another advantage of the coil is that it would take up less space on the bar top, as the length of the coil when wound was only 87mm compared to 114mm of the nozzle. The coils could be developed so that the syrups would flow down the centre of the coil so that different flavours of drinks could be dispensed from the same device. The coils would also be significantly cheaper to manufacture.

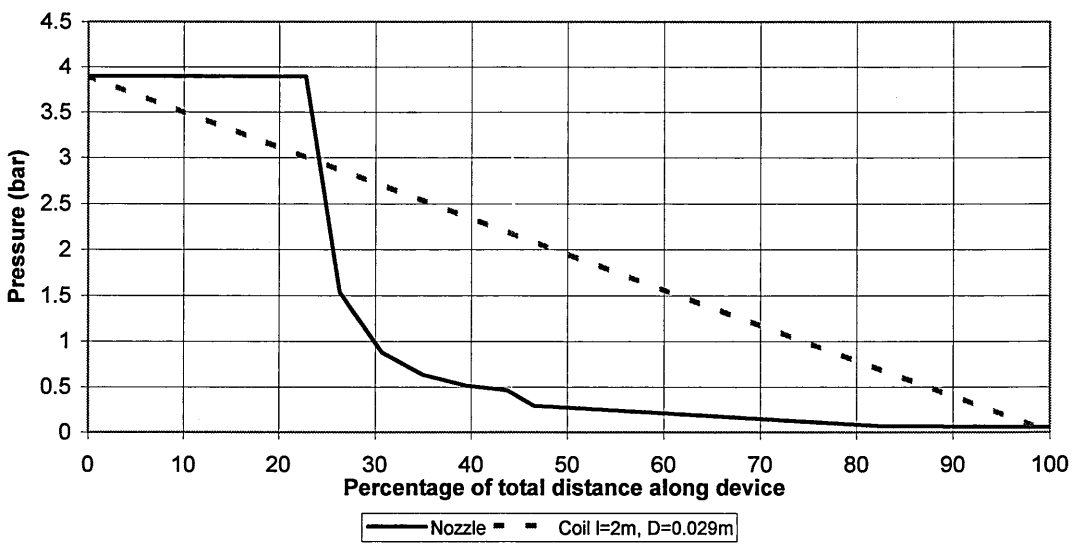

Figure 6.7.5 Pressure distribution in the nozzle and coil.

In conclusion, it has been found that coils were capable of maintaining a greater concentration of carbon dioxide dissolved in solution after depressurisation than the best currently available nozzle tested. The highest percentage supersaturation at the outlet was achieved with the shortest, 2m, coil with the smallest diameter 0.029m. If three of these coils were intertwined together, they would deliver the same flowrate, and provide superior performance to currently used nozzles.

7 Conclusions

1. The main objective of this work was to understand the mechanism of bubble formation when dispensing carbonated drinks, with the intention of designing a better drinks dispenser. The design of a device used to depressurise a gas-saturated solution can affect the concentration of dissolved gas after depressurisation. Different design factors influence whether bubbles form or not. Bubbles will form when the local pressure goes below the vapour pressure, which can occur with pressure fluctuations due to turbulence. The quality of the surface and potential nucleation sites can also influence whether bubbles form.
   - The dissolved air flotation water treatment process requires a depressurisation nozzle to release all the dissolved gas from solution as regular sized microbubbles. The gas can be released by creating turbulence within the nozzle using sudden expansions, directional changes and impingement plates.
   - In contrast, the carbonated drinks industry requires a device that keeps the gas dissolved in solution, so that a drink remains fizzy for a long time. From a combination of preliminary experiments with commercially available carbonated drink dispensers and a review of the literature, it was concluded that smooth, laminar flow is most suitable in carbonated drink dispenser design. However, some of the drink dispensers tested appeared to be based on different design principles.

2. The flow characteristics of a current carbonated drink dispenser known to perform well were investigated. Preliminary experiments found the nozzle to have a high pressure drop that varied linearly with flowrate. The nozzle had a narrow annular flow path that was formed between a bullet shaped central body within a casing. The annulus had a variable flow area and a minimum gap of 0.1mm.
   - In the nozzle the majority of the pressure was dropped across the very narrow gap at the start of the annulus. The pressure drop across the device was found to increase linearly with flowrate, with each flow type tested. At the maximum flowrate, the Reynolds number was calculated to be high before and after the annulus, up to 12,000, but less than 3000 around the annulus. The single-phase water pressure drop was predicted well using equations for laminar flow in annuli and between flat plates.
   - With two-phase air and water flow in the nozzle, the pressure drop was reduced with an increase in air flow, at a given water flowrate. This behaviour was unexpected, as most two-phase works to date show an increase in pressure drop. However, these works are related to pipes and devices with much larger flow passages. Recent research has shown that the flow patterns in micro-channels with diameters of less than 3mm are quite different from large channels. For example, interphase slip and normal bubble flow were found not to occur in narrow channels. The decrease in pressure drop found in the present investigation could have been due to the way the air and water phases were distributed in the narrow annular space. It is possible that there may have been some kind of layer of air next to the nozzle surface that would have reduced the friction and lead to a lower pressure drop.

- When comparing the gas-saturated and single-phase water results in the nozzle at a given water flowrate, the gas-saturated flow had a lower pressure drop. This indicated that gas was evolved and supported the two-phase air and water results, showing that increasing the gas flowrate in the nozzle, at a given water flowrate, reduced the pressure drop.
- Three different central body positions were tested in the nozzle. The highest percentage supersaturation at the outlet was achieved, for a given gas-saturated water flowrate, when the central body was furthest forward in the casing, creating the narrowest gap. However, at a given pressure drop, the central body position seemed to have no effect on the percentage supersaturation.
- CFD simulations of the nozzle showed that the static pressure dropped rapidly at the start of the nozzle. The velocity profile was not smooth and did not decrease steadily as the annular flow path expanded. A shortened version of the nozzle was modelled using only the section that dropped the majority of the pressure. This created smoother local pressure and velocity profiles within the nozzle, suggesting it might retain more dissolved gas at the outlet.

3. There were two main reasons for examining the flow behaviour of small diameter coils. First, from the literature many authors have found that the friction factors of coils are higher than in equivalent straight pipes of the same length and diameter. Second, it has also been reported that, the flow in coils can remain laminar to higher Reynolds numbers than in an equivalent straight pipe. Both reasons are desirable in carbonated drinks dispensing. All previous works are for tube diameters of greater than 6mm, which are too big to fit into a drinks dispenser unit. Therefore, coils made up of 2.5mm diameter tubes were tested with coil diameters from 0.029 to 0.139m and lengths of 2 to 7m. A straight tube was also tested.
   - The friction factors of the coils tested were found to be greater than the straight pipe and to increase with a decrease in coil diameter. The transition from laminar to turbulent regions was much smoother in the coils than the straight tube. The turbulent region was reached at higher Reynolds numbers as the coil diameter decreased.
   - Van Dyke's (1978) laminar friction factor equation for coils fitted the laminar region of the present single-phase experimental data well. The equations of Mishra and Gupta (1979), Czop et al (1994), Ito (1959) equations A and B and Mori and Nakayama (1967a) equations A and B all agreed well with the experimental data in the turbulent region.
   - Coil friction factors are not normally detailed in hydraulic data books but straight pipes and bends are well documented. A new method of determining the friction factor of a coil was formulated by treating a coil as a series of 90^{o} bends. This new approach was found predict the friction factor of the present experimental results well, particularly when using the laminar version. The new method predicted White's (1929) experimental data well, in the laminar and turbulent regions. The simple approach is useful, as it minimises the need for testing and can be applied to tubes with any geometry and roughness.

- With two-phase air and water flow in coils, it was found that for a given water flowrate, the pressure drop increased with air flowrate. Equations shown in the literature to determine the two-phase friction factor in coils predicted the experimental results well. The simplest correlations from Boyce et al (1969) and Czop et al (1994) were particularly good and could be applied to coils with small tube diameters of 2.5mm.
- The pressure drop versus flowrate relationships for the single-phase water and gas-saturated water were similar until a flowrate of approximately 10ml/s. After this the gas-saturated water had a higher pressure drop, indicating the presence of a gas phase.
- For a given pressure drop and flowrate, the shortest 2m coil was found to have the highest percentage supersaturation of dissolved gas at the outlet. This could have been because the flow had to pass over less surface area and hence, less nucleation sites. The smallest diameter, 0.029m, coils were found to have the highest percentage supersaturation at the coil outlet. This was possibly because the flow remained laminar to higher Reynolds numbers, giving bubbles less chance to form.

4. The performance of the nozzle and coils were compared to determine if coils could improve on the nozzle's performance as a carbonated drink dispenser.
   - For a given pressure drop the 2m long, 0.029m diameter coil had a greater percentage supersaturation of carbon dioxide at the outlet than the test nozzle. The nozzle had a higher flowrate than the coils. However three intertwined coils would produce the same flowrate as the nozzle and would have a higher percentage supersaturation at the outlet than the nozzle.
   - The increased concentration of dissolved gas at the outlet of the coil may have been due to its steady pressure drop. In contrast, the pressure drop in the nozzle was very rapid with the majority of the pressure drop at the start of the annulus.
   - For a particular device, the difference between the pressure drop versus flowrate relationships of the single-phase water and gas-saturated water flows, indicated the presence of a gas phase with the gas-saturated flow. The relationships for the coil were very similar at flowrates of less than 10ml/s but became separated at higher flowrates. With the nozzle there was significant difference between the relationships even at low flowrates. This suggests that more gas was evolved when using the nozzle.
   - The coil had a higher percentage supersaturation at the outlet than the nozzle and could be used as an improved carbonated drinks dispenser. Syrups could flow down the centre of the coil so that different flavours of drinks could be dispensed from the same device. Coils would also be simpler to manufacture.

7.1 Recommendations for future work

1. The pressure drop within the test nozzle was not smooth. This may have been why it had a lower percentage supersaturation at the outlet than the coil. A shorter version of the test nozzle was modelled with CFD and was found to have a

smoother pressure drop and velocity profile. Further research could be performed to find the best design to create the smoothest pressure drop. The present nozzle is a premix nozzle and requires a different device for each flavoured drink. The new nozzle could become a post-mix nozzle to include the facility to dispense different flavoured syrups, possibly within the central body.

2. Further investigation of two-phase air and water flow in narrow annuli is needed to understand why that for a given water flowrate, the pressure drop was reduced with an increase in air flowrate. Recent research has found the flow behaviour in narrow channels to be significantly different to larger diameter pipes however, this particular behaviour has not been reported before. The behaviour may be particular to annuli or to the geometry of the nozzle. To ascertain if this behaviour is particular to annuli, tests could be performed with cylinders with different sized inserts to create different sized annuli. The research could also determine if the orientation has an influence.

3. The experiments were performed with coil lengths of between 2 and 7m. The shortest 2m coil was found to have the highest percentage supersaturation of dissolved carbon dioxide at the outlet. The optimum coil length may be less than 2m, but will be greater than 0m, as this is would resemble an orifice. Testing coils shorter than 2m would enable the ideal coil length to be found. This was not possible with the apparatus used, as the effect of the fittings would have been too great. To perform tests with coils shorter than 2m, a shorter trapping tube would have to be used. However, this would decrease the accuracy of the trapped volume measurements. The pressure losses from the temperature probe and pressure transducer fittings would have also been very significant when testing a shorter coil. An alternative method to determine the concentration of dissolved gas would have to be used.

4. Carbonated drink dispensers are required to be as small as possible. A coil with a smaller tube diameter would have a larger pressure drop in less space. However, smaller tube diameters were impossible to test on the apparatus used, as the smallest ball valve commercially available had an internal diameter of 2.5mm. Using a valve with a diameter different to the tubing would have caused significant disturbances to the flow. An alternative method of trapping the flow would have to be used, that would minimise disturbance to the flow.

8 References

ADLER, M. *Strömung in gekrümmten rohren.* Z. Agnew. Math. Mech, 14(5), 1934, 257-275.

ALI, S. and SESHADRI, C.V. *Pressure drop in archimedian Spiral Tubes.* Industrial and engineering chemistry. Process design and development, 10(3), 1971, 328-332.

AKAGAWA, K; SAKAGUCHI, T and UEDA, M, *Study on a gas-liquid two-phase flow in helically coiled tubes,* Bulletin of the JSME, 14(27), 1971, 564-571.

ARNDT, R.E.A. *Cavitation in fluid machinery and hydraulic structures.* Annual review of fluid mechanics, 13, 1981, 273-328.

ASH, M.E. *Improvements in a method of dispensing beverages containing gas in solution.* Patent specification GB 876628, January 1961a.

ASH, M.E. *Improvements in means for dispensing liquids containing gases in solution.* Patent specification GB 876629, September 1961b.

AWWAD, A.; XIN, R.C.; DONG, Z.F.; EBADIAN, M.A. and SOLIMAN, H.M. *Flow patterns and pressure drop in air/water two-phase flow in horizontal helicoidal pipes.* Transactions of the ASME- Journal of fluids engineering, 117, December 1995a, 720-726.

AWWAD, A.; XIN, R.C.; Dong. Z.F.; EBADIAN, M.A. and SOLIMAN, H.M. *Measurement and correlation of the pressure drop in air-water two-phase flow in horizontal helicoidal pipes.* International journal of multiphase flow, 21(4), 1995b, 607-619.

BANERJEE, S.; RHODES, E. and SCOTT, D.S. *Studies on cocurrent gas-liquid flow in helically coiled tubes.* The Canadian journal of chemical engineering, 47, October 1969, 445-453.

BAO, Z.Y.; BOSNICH, M.G. and HAYNES, B.S. *Estimation of void fraction and pressure drop for two-phase flow in fine passages.* Transactions of the institution of chemical engineers, 72(A) September 1994.

BANNWART, A.C. *Modeling aspects of oil-water core-annular flows.* Journal of petroleum science and engineering, 937, 2001.

BARKER, G.S.; JEFFERSON, B. and JUDD,S. *Measuring techniques for the determination of CO_2 in beverages.* IN: CAMPBELL, G.M.; WEBB, C.; PANDIELLA, S.S. and NIRANJAN, K (ed), Proceedings of an international conference. Bubbles in food, June 1998, Manchester UK.

BARNEA, D.; LUNINSKI, Y.; and TAITEL, Y. *Flow pattern in horizontal and vertical two phase flow in small diameter pipes.* The Canadian journal of chemical engineering, 61, October 1983, 617-620.

BAROCZY, C.J. *A systematic correlation for two-phase pressure drop.* Chemical engineering progress symposium series. heat transfer – Los Angeles, 64(62), 1966, 232-249.

BARUA, S.N. *On secondary flow in stationary curved pipes.* Quarterly journal of mechanics and applied mathematics, 16, 1963, 61-77.

BEATTIE, D.R.H. *Gas-liquid two-phase pressure losses in narrow horizontal annuli.* Nuclear engineering and design, 203, 2001, 107-109.

BEATTIE, D.R.H. and WHALLEY, P.B. *A simple two-phase frictional pressure drop calculation method.* International journal of multiphase flow, 8(1), 1982, 83-87.

BERGER, S.A.; TALBOT, L. and YAO, L.S. *Flow in curved pipes.* Annual review of fluid mechanics, 15, 1983, 461-512.

BHATTI, M.S. and SHAH, R.K. *Turbulent and transition flow convective heat transfer in ducts.* Chapter 4. IN: KAKAÇ, S.; SHAH, R.K. and AUNG, W. (Eds) *Handbook of single-phase convective heat transfer.* John Wiley and sons, inc. 1987.

BISPERINK, C.G.J. and PRINS, A. *Bubble-growth in carbonated liquids,* Colloids and surfaces A-Physiochemical and engineering aspects, 85(2-3), 1994, 237-253.

BLAKE, J.R. and GIBSON, D.C. *Cavitation bubbles near boundaries.* Annual review of fluid mechanics, 19, 1987, 99-123.

BLAKE, J.R.; HOOTON, M.C. and ROBINSON, P.B. *Pressures on a rigid boundary due to the motion of a collapsing cavitation bubble.* Cavitation and multiphase flow, FED-Vol. 210, ASME, 1995.

BLANDER, M. and KATZ, J.L. *Bubble nucleation in liquids.* AIChE Journal, 21(5), 1975, 833-848.

BOYCE, B.E.; COLLIER, J.G. and LEVY J. *Hold-up and pressure drop measurements in the two-phase flow of air-water mixtures in helical coils.* IN; RHODES, E and SCOTT, D.S. (ed), Proceedings of the international symposium on research in concurrent gas and liquid flow, 1969, Plenum Press, New York. 203-231.

BRATBY, J. and MARAIS, G.V.R. *Flotation.* IN: PURCLAS, D.B. and WAKEMAN, R.J. (ed). Solid/liquid separation equipment scale up, 2nd revised edition. 1986.

BRATBY, J. and MARAIS, G.V.R. *Saturator performance in dissolved air (pressure) flotation.* Water research, 9, 1975, 929-936.

BRENNEN, C.E. *Cavitation and bubble dynamics.* Oxford engineering science series 44, Oxford university press. 1995.

BURNS, S.E.; YIACOUMI, S. and TSOURIS, C. *Microbubble generation for environmental and industrial separations.* Separation and purification technology, 11, 1997, 221-232.

BUTTERWORTH, D. *A comparison of some void fraction relationships for co-current gas-liquid flow.* International journal of multiphase flow, 1, 1975, 845-850.

CABLE, M. and FRADE, J.R. *Diffusion-controlled growth of multi-component gas bubbles.* Journal of materials science, 22, 1987, 919-924.

CABLE, M. and FRADE, J.R. *The influence of surface tension on the diffusion-controlled growth or dissolution of spherical gas bubbles.* Proceedings of the Royal Society of London A, 420, 1988, 247-265.

CALLISTER, W.D. Jr. *Materials science and engineering, An introduction.* John Wiley and sons, inc. 1994.

CARNAGHAN, D.W.B. *Improvements in means for dispensing liquids particularly beverages containing gases in solution.* Patent specification GB 956901. April 1964.

CASEY, T.J. *Unit treatment processes in water and wastewater engineering.* Wiley and sons. 1993.

CHEN, X. and GUO, L. *Flow patterns and pressure drop in oil-air-water three-phase flow through helically coiled tubes.* International journal of multiphase flow, 25, 1999, 1053-1072.

CHISHOLM, D. *A theoretical basis for the Lockhart-Martinelli correlation for two-phase flow.* International journal of heat and mass transfer, 10, 1967, 1767-1778.

CHISHOLM, D. and LAIRD, A.D.K. *Two-phase flow in rough pipes.* Transactions of the ASME. February 1958. 276-286.

CLIFT, R.; GRACE, J.R. and WEBER, M.E. *Bubble, drops and particles.* New York academic press. 1978.

COLEMAN, J.W. and GARIMELLA, S. *Characterization of two-phase flow patterns in small diameter round and rectangular tubes.* International journal of heat and mass transfer, 42, 1999, 2869-2881.

COLLINS, W.M. and DENNIS, S.C.R. *The steady motion of a viscous fluid in a curved tube.* Quarterly journal of mechanics and applied mathematics, 28, 1975, 133-156.

COOPER, M.G. and CHANDRATILLEKE, T.T. *Growth of diffusion-controlled vapour bubbles at a wall in a known temperature gradient.* International journal of heat and mass transfer, 24(9), 1981, 1475-1492.

CORNELIUS, R.T. *Faucet.* U.S. patent 2,270,932. January 27th 1942.

CORNELIUS, R.T. *Foam control device in liquid dispensing apparatus.* U.S. patent 2,924,238. February 1960.

CORNELIUS, R.T. *Liquid dispensing apparatus.* U.S. patent 2,899,170. August 1959.

COULSON, J.M. and RICHARDSON, J.F., *Chemical engineering. Volume 1 (Fluid flow, heat transfer and mass transfer)*, 4th Edition, Pergamon. 1993.

CZOP, V.; BARBIER, D. and DONG, S. *Pressure drop, void fraction and shear stress measurements in an adiabatic two-phase flow in a coiled tube.* Nuclear engineering and design, 149, 1994, 323-333.

DAMIANIDES, C.A. and WESTWATER, J.W. *Two phase flow patterns in a compact heat exchanger and in small tubes.* Proceedings of second U.K. National conference on heat transfer, Vol II. Glasgow, Scotland. 1988. 1257-1268.

DAS, S.K. *Water flow through helical coils in turbulent condition.* The Canadian journal of chemical engineering, 71, December 1993, 971-973.

DEAN, W.R. *Note on the motion of fluid in a curved pipe,* Philosophical magazine, 4, 1927, 208-231.

DEAN, W.R. *The streamline motion in a curved pipe.* Philosophical magazine, 5, 1928, 673-695.

DE RIJK, S.E.; VAN DER GRAAF, J.H.J.M. and DEN BLANKEN, J.G. *Bubble size in flotation thickening.* Water research, 28(2), 1994, 465-473.

DOUGLAS, J.F.; GASIOREK, J.M and SWAFFIELD, J.A. *Fluid mechanics.* 3rd Edition. Longman Singapore publishers ltd. 1998.

DUKLER, A.E.; WICKS, M. and CLEVELAND, R.G. *Frictional pressure drop in two-phase Flow: A. A comparison of existing correlations for pressure loss and holdup.* AIChE. Journal, 10(1), January 1964, 38-43.

EADES, A. and BRIGNALL, W.J. *Countercurrent dissolved air flotation filtration.* Water science and technology, 31(3-4), 1995, 173-178.

EDZWALD, J.K. *Principles and applications of dissolved air flotation.* Water science and technology, 31 (3-4), 1995, 1-23.

EKBERG, N.P.; GHIAASIAAN, S.M.; ABDEL-KHALIK, S.I.; YODA, M and JETER, S.M. *Gas-liquid two-phase flow in narrow horizontal annuli.* Nuclear engineering and design, 192, 1999, 59-80.

ELLIS, A.T. and STARRETT, J.E. *A study of cavitation bubble dynamics and resultant pressures on adjacent solid boundaries.* Cavitation. IMechE; C190/83: 1983.

EPSTEIN, P.S. and PLESSET, M.S. *On the stability of gas bubbles in liquid-gas solutions.* The journal of chemical physics, 18(11), 1950, 1505-1509.

EUSTICE, J. *Experiments on steam-line motion in curved pipes.* Proceedings of the Royal Society of London, Series A, 85, 1911, 119-131.

EUSTICE, J. *Flow of water in curved pipes.* Proceedings of the Royal Society of London, Series A, 84, 1910, 107-118.

FLUENT 5, *Users guide*, Volumes 1-3. Fluent incorporated. July 1998.

FOGG, P.G.T and GERRAND, W. *Solubility of gases in liquids.* John Wiley and Sons, 1991, 20-29.

FOURAR, M. and BORIES, S. *Experimental study of air-water two-phase flow through a fracture (narrow channel).* International journal of multiphase flow, 21(4), 1995, 621-637.

FUJIKAWA, S. and AKAMATSU, T. *Some recent aspects of bubble dynamics.* Cavitation. IMechE, C194/83, 1983, 31-40.

FUKANO, T. and KARIYASAKI, A. *Characteristics of gas-liquid two-phase flow in a capillary tube.* Nuclear engineering and design, 141, 1993, 59-68.

FUKUSHI, K.: TAMBO, N. and MATSUI, Y. *A kinetic-model for dissolved air flotation in water and waste-water treatment.* Water science and technology, 31(3-4), 1995, 37-47.

GARIMELLA, S. and CHRISTENSEN, R.N. *Performance evaluation of spirally fluted annuli: Geometry and flow regime effects.* Heat transfer engineering, 18(1), 1997, 34-46.

GOCHIN, R.J. *Flotation.* Solid–liquid separation. Edited by Svarovsky, L. Third edition. Butterworths, London. 1990.

GREEN, T.S. *Soft drink dispensing head.* United States patent. US 5,526,959. 18th June 1996.

HAALAND, S.E. *Simple and explicit formulas for the friction factor in turbulent pipe flow.* Journal of fluids engineering. 105, 1983, 89-90.

HAARHOFF, J. and RYKAART, E.M. *Rational design of packed saturators.* Water science and technology, 31 (3-4), 1995, 179-190.

HAARHOFF, J. and STEINBACH, S. *A comprehensive method for measuring the air transfer efficiency of pressure saturators.* Water research, 31(5), 1997, 981-990.

HAARHOFF, J. and VANVUUREN, L.R.J. *Design parameters for dissolved air flotation in South Africa.* Water science and technology, 31 (3-4), 1995, 203-212.

HALL, R.W. and CORLETT, A.E. *X-ray visualisation and dissolved gas quantification: Multiphase flow research and development at NEL.* North sea flow measurement workshop. 1997.

HARVEY, J.F. *Theory and design of pressure vessels.* Van Nostrand Reinhold Company, New York. 1985.

HAYWARD, T.J. *Two new instruments for measuring the air content of oil,* Journal of the institute of petroleum, 47(447), March 1961, 99-106.

HEINÄNEN, J. *Use of dissolved-air flotation in potable water treatment in Finland.* Aqua fennica, 18(2), 1988.

HEINÄNEN, J.; JOKELA, P. and ALAPEIJARI, T. *Use of dissolved air flotation in potable water-treatment in Finland.* Water science and technology, 31(3-4), 1995, 225-238.

HEMMINGSEN, E.H. *Effects of surfactants and electrolytes on the nucleation of bubbles in gas-supersaturated solutions.* Z. Naturforsch, 33a, 1978, 164-171.

HILDEBRAND, S.H. and YOAKLEY, F.G. *Device for use in dispensing beverages containing gas in solution.* Patent specification GB 1280240. July 1972.

HYDE, R.A.; MILLER, D.G.; PACKHAM, R.F. and RICHARDS, W.N. *Water clarification by flotation.* Journal of the American water works association, 69, 1977, 369-374.

HYDE, R.A.; RICHARDS, W.N. and BURLEY, M.J. *A method of clarifying impure water.* Patent specification. GB 1444026. July 1976a.

HYDE, R.A.; RICHARDS, W.N. and BURLEY, M.J. *A nozzle for introducing gas into liquid.* Patent specification GB 1444027. July 1976b.

ISHIGAKI, H. *Laminar flow in rotating curved pipes.* Journal of fluid mechanics, 329, 1996, 373-388.

ISHIKAWA, H.; MIKI, T.; OKAMOTO, M. and HIKITA, H. *Gas desorption from liquids: Mass transfer and drag coefficients for single bubbles in free rise through newtonian fluids.* Chemical engineering science, 41(9), 1986, 2309-2319.

ITO, H. *Friction factors for turbulent flow in curved pipes.* Transactions of the ASME- Journal of basic engineering, 81, June 1959, 123-134.

ITO, H. *Laminar flow in curved pipes.* Z. Angew. Math. Mech. 49. 1969. 653-663.

ITO, H. *Pressure losses in smooth pipe bends.* Transactions of the ASME. Journal of basic engineering, 82, March 1960, 131-143.

IVES, K.J. *Coagulation and flocculation. Part II – Orthokinetic flocculation.* Solid – liquid separation. Edited by Svarovsky, L. Third edition. Butterworths, London. 1990.

JACKSON, M.L. *Energy effects in bubble nucleation.* Industrial and engineering chemistry. Research, 33(4), 1994, 929-933.

JAMESON, G.J. *Physics and hydrodynamics of bubbles.* The scientific basis of flotation, Nato advanced study series. Sijthoff and Noordhoff, Alphen aan den Rijn, The Netherlands. (ed Ives K.J.) 1978. 53-77.

JEFFERSON, B. *Mechanisms of particle capture in dissolved air flotation.* PhD thesis. Loughborough University, Leics. LE11 3TU. August 1997.

JONES Jr., O.C. and LEUNG, J.C.M. *An improvement in the calculation of turbulent friction in smooth concentric annuli.* Transactions of the ASME. Journal of fluids engineering, 103, December 1981, 615-623.

JUELL, F. *Method and device for separating solid substances from suspensions.* Patent specification. U.S. 2,330,589. 28th September 1943.

KAMIYAMA, S. and YAMASAKI, T. *Critical condition of cavitation occurrence in various liquids.* Transactions of the ASME, 108, December 1986, 428-432.

KAMIYAMA, S. and YAMASAKI, T. *Prediction of gaseous cavitation occurrence in various liquids based on two-phase flow analogy.* Journal of fluids engineering, 103, December 1981, 551-556.

KATZ, J. *Cavitation phenomena within regions of flow separation.* Journal of fluid mechanics, 140, 1984, 397-436.

KITCHENER, J.A. and GOCHIN, R.J. *The mechanism of dissolved air flotation for potable water - basic analysis and a proposal.* Water research, 15(5), 1981, 585-590.

KNAPP, R.T.; DAILY, J.W. and HAMMITT, F.G. *Cavitation.* McGraw-Hill book company. 1970.

KROFTA, M. *Apparatus for purification of unclarified waste water.* Patent specification U.S. 3,307,701. March 7th 1967.

KUBAIR, V and KULOOR, N.R. *Heat transfer to newtonian fluids in coiled pipes in laminar flow.* International journal of heat and mass transfer, 9, 1966, 63-75.

KUBAIR, V. and KULOOR, N.R. *Non-isothermal pressure drop data for liquid flow in helical coils.* Indian journal of technology, 3, January 1965, 5-7.

KUBAIR, V. and VARRIER, C.B.S. *Pressure drop for liquid flow in helical coils.* Transactions of the IIChE, 14, 1961-1962, 93-97.

KUBOTA, A.; KATO, H. and YAMAGUCHI, H. *A new modelling a cavitating flows: a numerical study of unsteady cavitation on a hydrofoil section.* Journal of fluid mechanics, 240, 1992, 59- 96.

KYRIAKIDES, N.K.; KASTRINAKIS, E.G.; NYCHAS, S.G. and GOULAS, A. *Bubbling from nozzles submerged in water: transitions between bubbling regimes.* Canadian journal of chemical engineering, 75(4), 1997, 684-691.

LARRAIN, J. and BONILLA, C.F. *Theoretical analysis of pressure drop in the laminar flow of fluid in a coiled pipe.* Transactions of the society of rheology, 14(2), 1970, 135-147.

LEHMAN, A.F. and YOUNG, J.O. *Experimental investigations of incipient and desinent cavitation.* Journal of basic engineering, June 1964, 275-284.

LIERS, S.; BAEYENS, J. and MOCHTAR, I. *Modeling dissolved air flotation.* Water environment research, 68(6), 1996, 1061-1075.

LIN, J.N.; BANERJI, S.K. and YASUDA, H. *Role of interfacial-tension in the formation and the detachment of air bubbles. 1. a single hole on a horizontal plane immersed in water.* Langmuir, 10(3), 1994, 936-942.

LISLE-TAYLOR, S.C. *Cavitation performance of pumped hydrocarbons.* PhD Thesis. School of mechanical engineering, Cranfield university, BHR. 1996-7.

LIU, S.; AFACAN, A.; NASR-EL-DIN, H.A. and MASLIYAH, J.H. *An experimental study of pressure drop in helical pipes.* Proceedings of the Royal Society of London A, 444, 1994, 307-316.

LOCKHART, R.W. and MARTINELLI, R.C. *Proposed correlation of data for isothermal two-phase, two-component flow in pipes.* Chemical engineering progress, 45(1), 1949, 39-48.

LOCKIN, D.W. *Energy losses in 90-degree duct elbows.* Transactions American society of heating and ventilating engineers, 56, 1950, 479-502.

LUBETKIN, S.D. *The fundamentals of bubble evolution.* Chemical society reviews. 1995; 243-250.

MADDOCK, C.; LACEY, P.M.C. and PATRICK, M.A. *The structure of two-phase flow in a curved pipe.* Institute of Chemical Engineers Symposium. Series No.38, Multiphase flow systems. March 1974.

MALA, G.M. and LI, D. *Flow characteristics of water in microtubes.* International journal of heat and fluid flow, 20, 1999, 142-148.

MANDHANE, J.M.; GREGORY, G.A. and AZIZ, K. *A flow patterns map for gas-liquid flow in horizontal pipes.* International journal of multiphase flow, 1, 1974, 537-553.

MANLAPAZ, R.L. and CHURCHILL, S.W. *Fully developed laminar flow in a helically coiled tube of finite pitch.* Chemical engineering communications, 7, 1980, 57-78.

MARTINELLI, R.C. and NELSON, D.B. *Prediction of pressure drop during forced-circulation boiling of water.* Transactions of the ASME, August 1948, 695-702.

MATSUMOTO, Y. and TAKEMURA, F. *Influence of internal phenomena on gas bubble motion. (Effects of thermal diffusion, phase change on the gas-liquid interface and mass diffusion between vapor and noncondensable gas in the collapsing phase)* JSME international journal, Series B, 37(2), 1994, 288-296.

MESLER, R. *Bubble nucleation,* Encyclopaedia of fluid mechanics, ed. Cheremisinoff, N.B., Vol. 3, Gas-liquid Flows, 1986. 191-232.

MILLER, D.S. *Internal flow systems,* 2nd Edition, BHRA The fluid engineering centre. 1990: 205-225.

MISHRA, P. and GUPTA, S.N. *Momentum transfer in curved pipes. 1. Newtonian fluids.* Industrial and engineering chemistry. Process design and development, 18(1), 1979, 130-137.

MITCHELL, T.M. and HAMMITT, F.G. *Asymmetric cavitation bubble collapse.* Journal of fluid engineering, March 1973, 29-37.

MONTGOMERY, J.M. *Water treatment, principles and design.* Consulting engineers Inc. Wiley and Sons, 1985.

MORI, Y. and NAKAYAMA, W. *Study on forced convective heat transfer in curved pipes. (1st report, laminar region).* International journal of heat and mass transfer, 8, 1965, 67-82.

MORI, Y. and NAKAYAMA, W. *Study on forced convective heat transfer in curved pipes. (2nd report, turbulent region).* International journal of heat and mass transfer, 10, 1967a, 37-59.

MORI, Y. and NAKAYAMA, W. *Study on forced convective heat transfer in curved pipes. (3rd report, theoretical analysis under the condition of uniform wall temperature and practical formulae.* International journal of heat and mass transfer. 10, 1967b, 681-695.

MUNDAY, A.J. and FARRAR, R.A. (Edited by) *An Engineering data book.* The Macmillan Press Ltd. 1979.

OGURI, Y. *Hydraulic losses of tubular pipe coiled continuously in an 8-shape.* JSME international journal, Series B, 38(1), 1995, 45-50.

OOLMAN, T.O. and BLANCH, H.W. *Bubble coalescence in stagnant liquids.* Chemical engineering communications, 43, 1986, 237-261.

OTA, T.; KAGA, T.; KAMATA, S. and KOBAYASHI, N. *Cavitating flow around a rectangular cylinder.* FED-Vol.135, Cavitation and multiphase flow forum, ASME, 1992.

PACKHAM, R.F. and RICHARDS W.N. *The determination of dissolved air in water.* Treatment division, Water research centre, technical memorandum TM106, March 1975.

PAINTER, A. and THOMASSON, P.G. *Improvements in means for dispensing liquids particularly beverages containing gases in solution.* Patent specification GB 1150609. April 1969.

PERRY, R.H. *Perry's chemical engineers handbook,* Sixth edition, McGraw-Hill international editions, 1984.

PFUND, D.; RECTOR, D.; SHEKARRIZ, A.; POPESCU, A. and WELTY, J. *Pressure drop measurements in a microchannel.* AIChE Journal, 46(8), August 2000, 1496-1507.

PLESSET, M.S. and PROSPERETTI, A. *Bubble dynamics and cavitation.* Annual review of fluid mechanics, 9, 1977, 145-185.

PLESSET, M.S. *The dynamics of cavitation bubbles.* Journal of applied mechanics. September 1949, 277-282.

PRANDTL, L. *Essentials of fluid dynamics.* Blackie and son limited, London and Glasgow, 1954.

PRINCE, M.J. and BLANCH H.W. *Bubble coalescence and break-up in air-sparged bubble columns.* AIChE Journal. 36(10), October 1990, 1485-1499.

PTASINSKI, K.J.; GEURTS, F.L.S.; STARING, A.J.P.M.; VAN HEESCH, E.J.M. and KERKHOF, P.J.A.M. *Formation of small bubbles in an electric field.* Separation science and technology, 30(10), 1995, 2127-2144.

QUINN, E.L. and JONES, C.L. *Carbon dioxide,* Reinhold publishing corporation, New York, 1945.

REES, A.J.; RODMAN, D.J. and ZABEL, T.F. *Dissolved air flotation for solid/ liquid separation.* Water research centre, January 1979.

REES, A.J.; RODMAN, D.J. and ZABEL, T.F. *Evaluation of dissolved- air flotation saturator performance.* Water research centre. Technical report, TR 143, July 1980.

RICE, R.G. and HOWELL, S.W. *Bubble formation from elastic holes.* Chemical engineering communications, 59, 1987, 229-241.

RIPPEL, G.R.; EIDT, C.M. Jr. and JORDAN, H.B. Jr. *Two phase flow in a coiled pipe. (Pressure drop, holdup, and liquid phase axial mixing).* Industrial and engineering chemistry. Process design and development, 5(1), Jan 1966, 32-38.

ROGERS, G.F.C. and MAYHEW, Y.R. *Heat transfer and pressure loss in helically coiled tubes with turbulent flow.* International journal of heat and mass transfer, 7, 1964, 1207-1216.

RYAN, W.L. and HEMMINGSEN, E.A. *Bubble formation in water at smooth hydrophobic surfaces.* Journal of colloid and interface science, 157, 1993, 312-317.

RYKAART, E.M. and HAARHOFF, J. *Behaviour of air injection nozzles in dissolved air flotation.* Water science and technology, 31(3-4), 1995, 25-35.

SAROSDY, L.R. and ACOSTA, A.J. *Note on observations of cavitation in different fluids.* Journal of basic engineering. September 1961, 399-400.

SCARFFE, M. Private communication. 1997

SCHMIDT, E.F. *Wärmeübergang und druckverlust in rohrschlangen.* Chemie ingenieur technik, 39(13), 1967, 781-789.

SCRIVEN, L.E. *On the dynamics of phase growth.* Chemical engineering science, 10(1-2), 1959, 1-13.

SEBAN, R.A. and McLAUGHLIN, E.F. *Heat transfer in tube coils with laminar and turbulent flow.* International journal of heat and mass transfer, 6, 1963, 387-395.

SHAH, R.K. and BHATTI M.S. *Laminar convective heat transfer in ducts.* Chapter 3. (In) KAKAÇ, S.; SHAH, R.K. and AUNG, W. (Eds) *Handbook of single-phase convective heat transfer.* John Wiley and sons, Inc, 1987.

SHIMIZU, Y.; KUZUHARA, S. and NAKAMURA, S. *Studies on the cavitation characteristics of annular type jet pump.* Cavitation. IMechE, C200/83, 1983.

SRINIVASAN, P.S.; NANDAPURKAR, S.S. and HOLLAND, F.A. *Pressure drop and heat transfer in coils.* The chemical engineer, CE113-CE119, May 1968.

STEINBACH, S. and HAARHOFF, J. *Air precipitation efficiency and its effect on the measurement of saturator efficiency.* IN: Dissolved air flotation, international conference. The chartered institution of water and environmental management, April 1997, London.

SUBRAMANIAN, R.S. and WEINBERG, M.C. *Asymptotic expansions for the description of gas bubble dissolution and growth.* AIChE Journal, 27(5), 1981, 739-748.

SUO, M. and GRIFFITH, P. *Two-phase flow in capillary tubes.* Transactions of the ASME, Journal of basic engineering, September 1964, 576-582.

SZEKELY, J. and FANG, S.D. *Non-equilibrium effects in the growth of spherical gas bubbles due to solute diffusion - II. The combined effects of viscosity, liquid inertia, surface tension and surface kinetics.* Chemical engineering science, 28, 1973, 2127-2139.

TAITEL,Y. and DUKLER, A.E. *A model for predicting flow regime transitions in horizontal and near horizontal gas-liquid flow.* AIChE Journal, 22(1), January 1976, 47-55.

TAKAHASHI, T.; MIYAHARA, T. and MOCHIZUKI, H. *Fundamental study of bubble formation in dissolved air pressure flotation.* Journal of chemical engineering of Japan, 12 (4), 1979, 275-280.

TAKAHIRA, H.; AKAMATSU, T. and FUJIKAWA, S. *Dynamics of a cluster of bubbles in a liquid (theoretical analysis).* JSME international journal, Series B, 37(2), 1994, 297-305.

TAKEMURA, F. and MATSUMOTO, Y. *Internal phenomena in bubble formation.* Bubble dynamics and interface phenomena, 1994, 467-474.

TAKEMURA, F.; MATSUMOTO, Y.; TSUBOTA, M. and TOMITA, Y. *Effects of the internal phenomena on bubble motion in liquid nitrogen.* FED-Vol.210, Cavitation and multiphase flow ASME, 1995, 187-192.

TAYLOR, G.I. *The criterion for turbulence in curved pipes.* Proceedings of the Royal Society of London, Series A, 124, 1929, 243-249.

THOM, J.R.S. *Prediction of pressure drop during forced circulation boiling of water.* International journal of heat and mass transfer, 7, 1964, 709-724.

TRIPLETT, K.A.; GHIAASIAAN, S.M.; ABDEL-KHALIK, S.I,; LEMOUEL, A. and McCORD, B.N. *Gas-liquid two-phase flow in microchannels. Part II: void fraction and pressure drop.* International journal of multiphase flow, 25, 1999a, 395-410.

TRIPLETT, K.A; GHIAASIAAN, S.M.; ABDEL-KHALIK and SADOWSKI, D.L. *Gas-liquid two-phase flow in microchannels. Part I: two-phase flow patterns.* International journal of multiphase flow, 25, 1999b, 377-394.

TSUGE, H. *Hydrodynamics of bubble formation from submerged orifices.* IN: CHEREMISINOFF, N.B. (ed). Encyclopaedia of fluid mechanics, Gas-liquid flows, Vol. 3, 1986, 121-129.

URATA, E. and NAKAO, Y. *Erosion by high-water-content fluid flowing from a V-notch.* JSME international journal, Series B, 36(2), 1993, 252-260.

URBAN, M. *Aspects of bubble formation in dissolved air flotation.* PhD thesis. University of London, 1978.

VAN DYKE, M. *Extended stokes series: laminar flow through a loosely coiled pipe.* Journal of fluid mechanics, 86(1), 1978, 129-145.

VAN PUFFELEN, J.; BUIJS, P.J; NUHN,; PNAMPNAM and HIJNEN, W.A.M. *Dissolved air flotation in potable water-treatment - the Dutch experience.* Water science and technology, 31(3-4), 1995, 149-157.

VAN VUUREN, L.R.J. and PRINSLOO, J. *Forming of gas bubbles in a liquid.* South African patent. SA-83/7720, 17th October 1983.

VERSTEEG, H.K. and MALALASEKERA, W. *An Introduction to computational fluid dynamics. The finite volume method.* Longman scientific and technical, 1995.

WANG, L.X. and OUYANG, F. *Hydrodynamics of the process of depressurization of saturated water.* Chinese journal of chemical engineering, 2(4), 1994, 211-218.

WARD, C.A.; TIKUISIS, P. and TUCKER, A.S. *Bubble evolution in solutions with gas concentrations near the saturation value.* Journal of colloid and interface science, 113(2), 1986, 388-398.

WHALLEY, P.B. *Air-water two-phase flow in helically coiled tube.* International journal of multiphase flow, 6, 1980, 345-356.

WHALLEY, P.B. *Boiling, condensation and gas-liquid flow.* Oxford university press. Oxford engineering science Series 21, 1990.

WHITE, C.M. *Fluid friction and its relation to heat transfer.* Transactions of the institute of chemical engineers, 10, 1932, 66-86.

WHITE, C.M. *Streamline flow through curved pipes.* Proceedings of the Royal Society of London A, 123, 1929, 645-663.

WILLIAMS, P.G.; VAN VUUREN, L.R.J. and VAN DER MERWE, P.J. *Dissolved air flotation upgrades a conventional plant treating eutropic water.* 11th International convention of the Australian water and wastewater association. Melbourne, Australia, 1985, 189-196.

WILSON, S.D.R. and HULME, A. *The effect of bubbles attached to an electrode on electrical resistance and dissolved gas concentration.* Proceedings of the Royal Society of London A, 387, 1983, 133-146.

XIN, R.C.; AWWAD, A.; DONG, Z.F. and EBADIAN M.A. *An experimental study of single-phase and two-phase flow pressure drop in annular helicoidal pipes.* International journal of heat and fluid flow, 18(5), October 1997, 482-488.

XIN, R.C.; AWWAD, A.; DONG, Z.F.; EBADIAN, M.A. and SOLIMAN, H.M. *An investigation and comparative study of the pressure drop in air-water two-phase flow in vertical helicoidal pipes.* International journal of heat and mass transfer, 39(4), 1996, 735-743.

XU, J.L.; CHENG, P. and ZHAO, T.S. *Gas-liquid two-phase flow regimes in rectangular channels with mini/micro gaps.* International journal of multiphase flow, 25, 1999, 411-432.

YOON, R.H. *Microbubble flotation.* Mineral engineering, 6(6), 1993, 619-630.

ZABEL, T.H.F. *Flotation in water treatment.* P.Mavros and K.A. Matis (eds.), Innovations in flotation technology, 1992, 431-454

ZHANG, S.; DUNCAN, J.H. and CHAHINE, G.L. *The final stage of the collapse of a cavitation bubble near a rigid wall.* Journal of fluid mechanics, 257, 1993, 147-181.

ZHAO, T.S. and BI, Q.C. *Co-current air-water two-phase flow patterns in vertical triangular microchannels.* International journal of multiphase flow, 27, 2001, 765-782.

APPENDICES

A Equipment list

Piezoelectric pressure transducers PT1, PT2, PT3
- Keller series 3
- Working range 0-10bar absolute

Thermocouple TC1, TC2
- PTFE insulated
- PT 100 probe
- RS components - 158-985

Thermocouple TC3
- Farnell – 707-8110
- Industrial mineral insulated probes - Type K
- Probe diameter 1mm, length 150mm
- -40'C to 1100'C

Polyurethane tubing
- 100m clear tubing
- SMC pneumatics ltd.- TU0425C-100
- i.d. 2.5mm, o.d. 4mm

Pressure gauge
- Standard test gauge
- Budenberg gauge co. ltd, Broadheath
- Serial no. FeN005M

Tubing connectors
- Male connector – KQH04-U01
- SMC pneumatics ltd

Gas tight syringes
- Birisilicate glass, Teflon (PTFE) plunger tips
- Volume conformance of ±1% traceable to international standards
- Removable luer lock
- 2.5MDR-GT (2.5ml)
- 10MDR-LL-GT (10ml)
- 100MR-LL-GT (100ml) (2 off)

Syringe connector
- Syringe-valve connector

- SGE europe ltd – 030930 -

Miniature quick action shut-off valves
- Lever-operated ball valves
- Farnell
- For tubing i.d. (mm) 4
- Nominal size 2.5mm
- Pressure range –0.75 to +10bar
- QH-QS-4-1-1/8 (1 off)
- QH-QS-4 (2 off)

Rotameters
- Brooks instrument.
- Fisher-rosemount.
- Sho-rate® flowmeters,
- Model 1355.

B. Depressurisation devices

This section describes designs of depressurisation nozzles presently in use or patented for dissolved air flotation, carbonated soft drinks and beer.

B.1 Present DAF Nozzles

Many different types of depressurisation device are utilised in DAF. A simple orifice can be used, whilst needle valves are commonly used. Needle valves have definite disadvantages as they are easily blocked and are difficult to clean. Other nozzle designs varying in the amount of intricacy, with which the turbulence is created, are detailed in this section.

B.1.1 Orifices and venturis

Kitchener and Gochin (1981) found that orifices appear to be incapable of yielding only microbubbles and saw macro bubbles emerging above the jets. This was seen clearly in glass jets that had slowly circulating eddies near the orifice. They also studied venturi tubes, which produced micro-bubble clouds when fed with water under sufficient pressure to induce cavitation in the throat. When cavitation occurred, a region of opalescent vapour was seen just down-stream of the throat with a distinctive 'sizzling' sound. There were no large bubbles present but any microbubbles formed near the jet grew in the expanding stream beyond the jet. Larger bubbles were eliminated at lower jet pressures (0.7barg) but the bubble density was also reduced. Urban (1979) tested a venturi and orifice with equal throat diameters and found fewer bubbles were formed by the venturi.

B.1.2 Needle valve

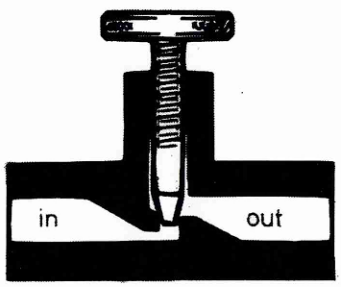

Figure B.1.1 Typical needle valve.

Needle valves are commonly used in DAF and can successfully decrease a pressure and regulate the flow. They use a screw down stop valve, with a needle that restricts the flow, as shown in Figure B.1.1. Careful adjustment is needed, according to the conditions, to create the desired bubbles. This is not easy, particularly when multiple

valves are used. In practise they are usually not set accurately. Needle valves are very sensitive to fouling and erosion. They cannot be simply cleaned, and are costly to repair. They are more expensive than orifices but orifices cannot be adjusted.

Van Puffelen et al (1995) referenced needle valve experiments performed by Kiwa. In the direct vicinity of the outlet there was found to be a large amount of agglomeration and coalescence of bubbles. Bratby and Marais (1975) tested two different designs of needle valve. The performance of both valves was almost identical, with nearly all the air precipitated from solution. Maddock et al (1976) tested five different needle valves and found they each had different efficiencies. Two had a complete release of dissolved gas, whilst the others had lower efficiencies. The most efficient valves had the more convoluted flowpaths. De Rijk et al (1994) compared a 'Econosto' needle valve and the smallest 'normal' valve available and found that at 5 bar and 50 l/h the needle valve produced 25% larger bubbles. It was found that any increase in the pressure or flowrate lead to a higher bubble concentration in a needle valve.

B.1.3 WRC Nozzle

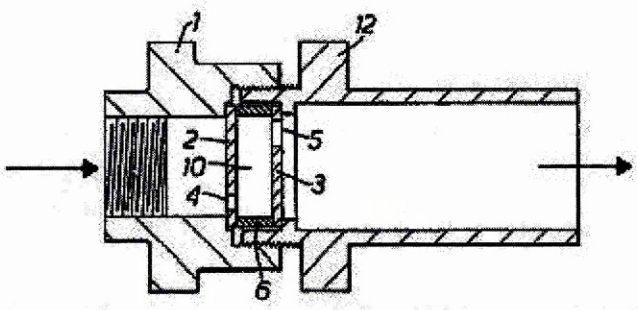

4 - inlet orifice
5 - outlet orifice
10 - chamber
12 - shroud

Figure B.1.2 WRC Nozzle.

The WRC (Water research centre) nozzle was patented by Hyde et al (1976a, b and 1977). It is widely used and referenced. A diagram of the nozzle is shown in Figure B.1.2. The nozzle has a cylindrical bore with two orifice plates that define a chamber, followed by a shroud section. The combination of sections reduces the pressure and induces turbulence, with a change in direction, impinging plate and shroud.

The orifice plates are parallel to each other, creating a chamber, but spaced apart so that the flow has a substantial change in direction and impinges on the walls of the chamber, creating strong turbulence. The inlet orifice is smaller than the outlet, so that the majority of the pressure is dropped and the gas released in the chamber. The inlet orifice also controls the flowrate. There is an additional reduction in the pressure across the outlet orifice, causing a further release of gas. The position of the orifices is not critical and it is possible to have more than one inlet or exit orifice. The orifice discs are easily replaceable for maintenance and cleaning. The shroud member is

provided downstream of the second orifice to reduce the velocity of the water, before mixing with the flocculated water, to reduce floc breakage.

The nozzle has significant advantages over a needle valve, as it is constructed simply and cheaply and is easily maintained without frequent adjustment. It is less likely to block and easier to clean than a needle valve. It is made of two metal parts that screw together and clamp the discs and spacer in place. A picture of the bubbles produced from the nozzle is shown in Figure B.1.3.

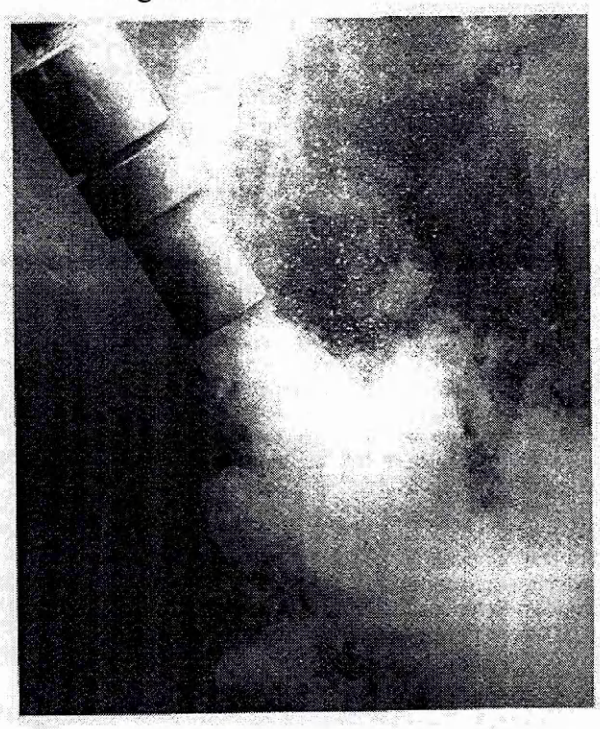

Figure B.1.3 WRC Nozzle in action. Hyde et al (1977).

Rees et al (1979) compared the WRC nozzle and a needle valve. The bubble size distribution results are shown in Figure B.1.4. It was found that at a saturator pressure of 485kPa, slightly larger bubbles were produced by the needle valve. Both nozzles produced 95% of the bubbles in the range of 10-120μm. Figure B.1.5, from Rees et al (1980), shows that the air release efficiency was the same for the WRC nozzle and the needles valve. Rees et al also tested different sizes of orifice in WRC nozzle, at different operating pressures. Each variation produced 95% of the bubbles in the range 10-120μm.

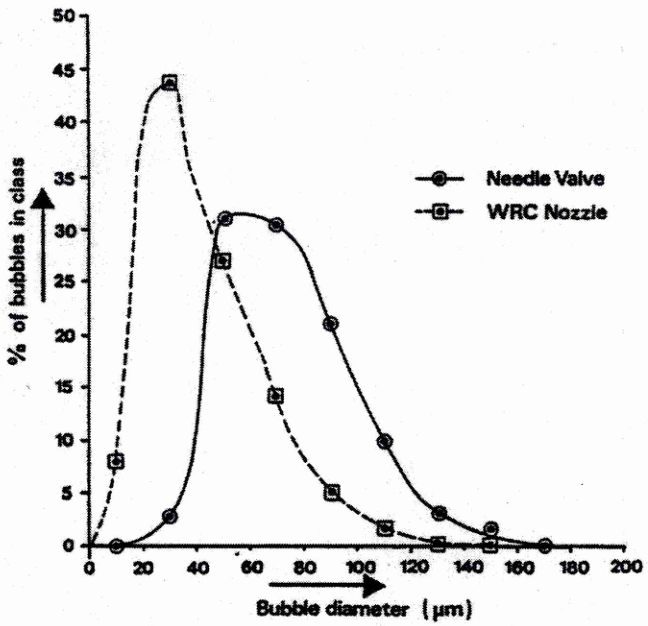

Figure B.1.4 Bubble size distributions produced by needle valve and WRC nozzle. Rees et al (1979).

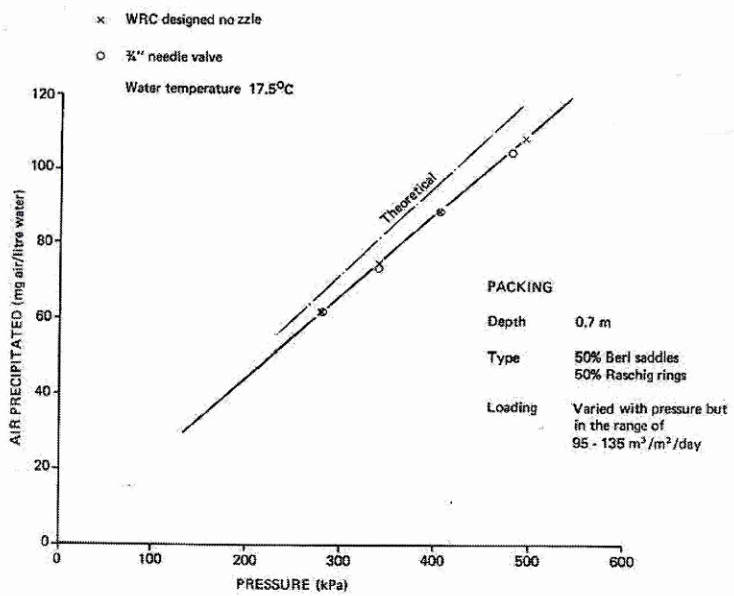

Figure B.1.5 Comparison of the air release efficiency of a needle valve and the WRC nozzle. Rees et al (1980).

Zabel (1992) also compared the WRC nozzle to a needle valve. The results were similar to those reported by Rees et al (1979), with more than 95% of the bubbles with a diameter of 10-120µm, and a mean of 40µm. Zabel found that the nozzle produced smaller bubbles than the needle valve, but they both produced a similar quality of treated water.

B.1.4 RICTOR nozzle

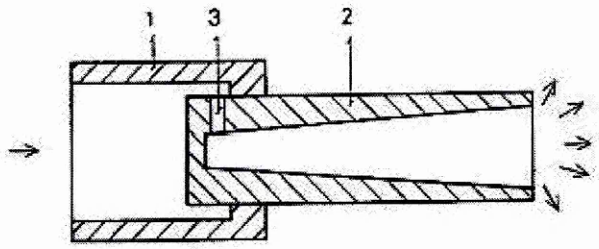

Figure B.1.6 RICTOR Nozzle.

Heinänen et al (1995) reported the RICTOR nozzle to be the most popular nozzle in use in Finland. The design is shown in Figure B.1.6. The nozzle uses an orifice followed by a sudden change in direction, to depressurise and induce turbulence in the flow, followed by a tapered section. It can be made from brass, but PVC and stainless steel are now used, as they are more corrosion resistant. It is designed to give the right flowrate without on-site adjustment. The only way to adjust the flowrate is to adjust the saturator pressure or number of nozzles. Heinänen (1988) reported that most plants had 1-22 nozzles per metre along the clarification basin side, with an average of nine per metre. The main complaints from operators about this nozzle are the difficulty in cleaning and adjustment. Needle valves are also in use in Finland, which are adjustable and cost less. One site compared needle valves and a Rictor nozzle and clearly preferred the latter.

B.1.5 NIWR Nozzle

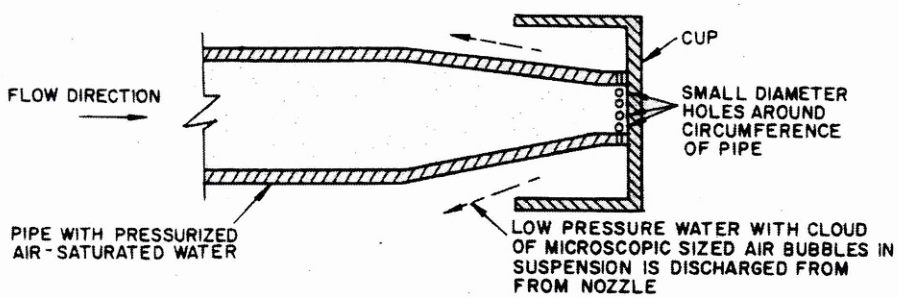

a) Basic nozzle design

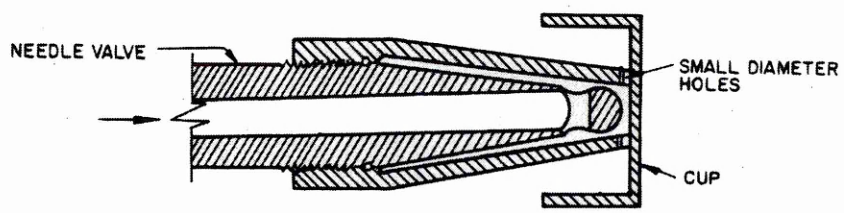

b) Nozzle with needle valve

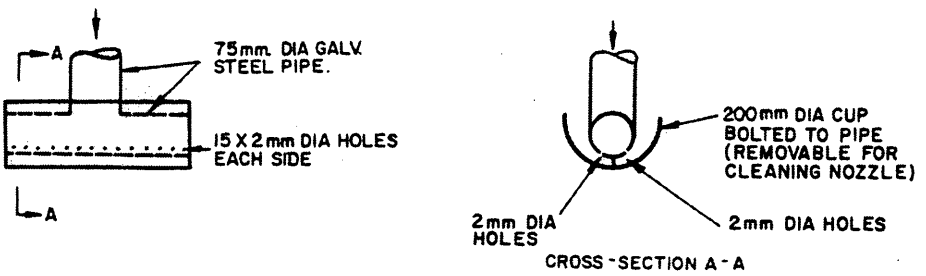

c) Nozzle used at Schoemansville

Figure B.1.7 NIWR Micro bubble nozzle as shown in Williams et al (1985).

The South African NIWR (National Institute for water research) nozzle, patented by Van Vuuren and Prinsloo (1983), is shown in Figure B.1.7. Orifices in combination with a change in direction, impingement and turbulence create a rapid pressure drop and induce turbulence. A tapered spigot is blanked at the small end, with a number of orifices that are directed radially outwards through the wall. The orifices outlets project into a cup and impinge on the walls, changing the flow direction towards an annular outlet.

The basic nozzle shown in Figure B.1.7a, has a tapered spigot that is blanked off at the small end, with a number of orifices that are directed radially outwards through the wall. The orifices outlets project into a cup and impinge on the walls, changing the flow direction towards an annular outlet. The nozzle is thought to be successful due to the rapid reduction in pressure (within 0.01sec) and the turbulence in the cup. The pressure should not be reduced before the cup or the premature release of air can produce larger bubbles. Figure B.1.7b shows how the flowrate can be regulated by the use of a needle valve, within the nozzle. Adjusting the number of holes in the nozzle can also regulate the flowrate. The Schoemansville nozzle, shown in Figure B.1.7c, again uses the same principle but the nozzle itself restricts the flowrate to the required rate to simplify the plant operation. From experiments, the optimum diameter for the hole was found to be 2mm.

The nozzle is said to be capable of creating a pressure drop of greater than 200 kPa, in less than 0.1 seconds, creating bubbles with a diameter of less than $2x10^{-4}$m. It was found that, in a $0.5m^3$ tank, with a water flowrate of 15 l/min, milky white clouds could be generated in a few seconds. The entire tank could be filled in minutes.

Van Vurren and Prinsloo (1983) suggested an alternative form of the original nozzle. The alternative form is shown in Figure B.1.8. It has an untapered cylindrical pipe with a row of orifices spaced along its length. The jets from the orifices project onto the wall of an outer pipe, which encloses the other pipe. On the opposite side of the enclosure is a longitudinal slit, which extends axially to form the outlet. The nozzle is said to perform very similarly to the RICTOR nozzle.

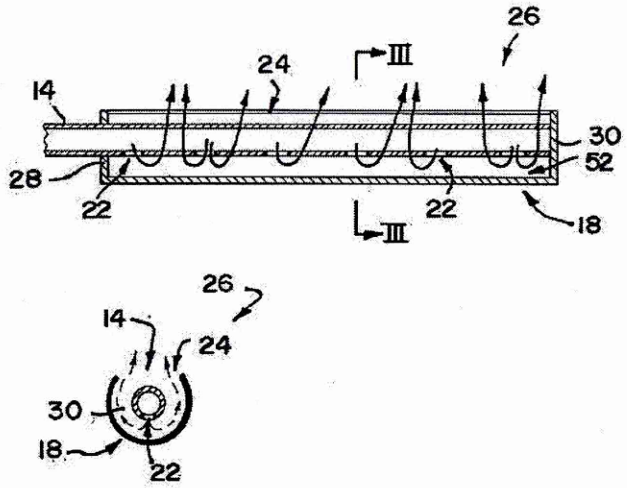

Figure B.1.8 Alternative nozzle suggested by Van Vuuren and Prinsloo (1983).

B.1.6 Krofta Nozzle

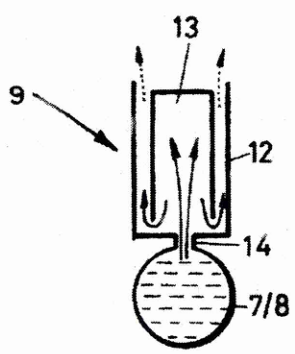

7/8 'air charged' waste water
9 dispersing nozzle
12 upright sleeve
13 inverted sleeve
14 short connecting piece to the bottom orifice

Figure B.1.9 Krofta dispensing nozzle. Krofta (1967).

The Krofta (1967) system uses two superimposed planes of pipes with 'air charged' water, each with many dispersing nozzles, as shown in Figure B.1.9. The higher plane contains wastewater that is pressurised. The lower plane is used to float particles that did not attach to the bubbles from the higher plane. The Krofta nozzle uses two 'sleeves', to depressurise the flow and create turbulence. A small sleeve is inverted over the pipe outlet, to redirect the flow, creating an annulus. The 'air charged' water is deflected to produce fine dispersed air bubbles from the annular space between the sleeves. There are no data on the bubbles formed from this nozzle.

B.1.7 Juell Nozzle

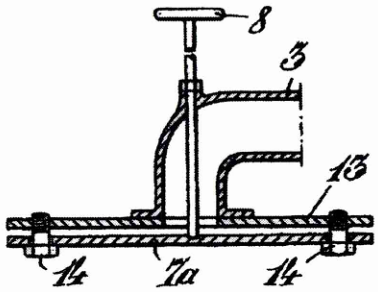

3 Tube with pressurised water
7a Bottom disc
8 Spindle
13 Top disc
14 Stud bolts

Figure B.1.10 Juell Nozzle (1943).

Juell (1943) described an early nozzle as shown in Figure B.1.10. It is a diffuser style design and very different to all the other nozzles. The saturated flow goes through a pipe with a blanking flange at the end. The flow impinges on the flange, which is mounted loosely to produce a small gap. The flow escapes radially from the blanking flange, sucking the flange closer. The pressurised solution flows outwards from a central point, enlarging the area of flow and abruptly reducing the velocity. The pressure is momentarily reduced below atmospheric pressure, forming a stream of minute bubbles. The vacuum lifts the bottom plate, restricting the flow. It is said to be very simple, inexpensive and reliable. A spindle is used to control the height of the plate and hence, the flowrate. There are no data for the size or number of bubbles released from this device. The pressure is encouraged to go below atmospheric, which is not recommended by other authors.

B.1.8 Other nozzles

Other nozzles are mentioned in the literature. Rykaart and Haarhoff (1995) described the DWL, the 'Hague Nozzle' and the 'improved Hague nozzle', from the Netherlands, which are both adjustable. Diagrams of the nozzles are shown in Figure B.1.11. They use a directional change and tapered section to depressurise the flow. De Rijk et al (1994) found that this nozzle produced generally smaller bubbles than a needle valve.

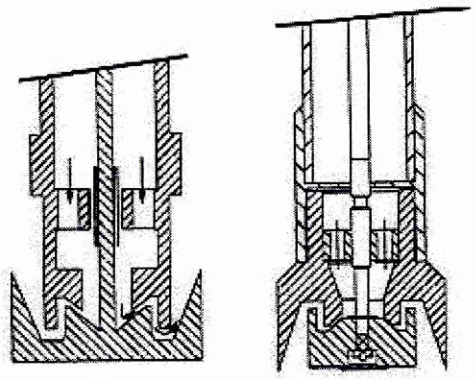

a) b)

Figure B.1.11 a) DWL 'The Hague Nozzle'
b) Improved 'The Hague Nozzle'.

The Leidse Nozzle is shown in Figure B.1.12. A disadvantage of the Leidse Nozzle is that they are not easily adjusted. The original nozzle is not adjustable but the improved nozzle can be adjusted after dismantling.

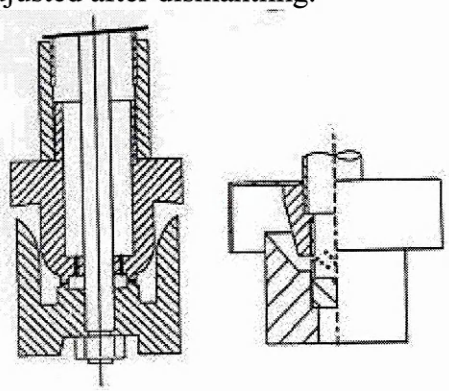

a) b)

Figure B.1.12 a) Leidse Nozzle
b) Improved Leidse Nozzle.

The VERKO nozzle, from Finland, uses a sudden change in direction during depressurisation. The AKA nozzle, from the Netherlands, uses a diverging cone to decrease the flow velocity.

B.2 Soft Drink dispensers

There are many different designs of nozzles available and in use, designed to depressurise and dispense carbonated drinks. This section describes two patented nozzles. One uses a narrow annulus to carefully depressurise the flow. This is the same design as the test nozzle, investigated in Chapter 5. The other uses several narrow tubes to depressurise the flow.

B.2.1 Cornelius nozzle

Cornelius (1942, 1959 and 1960) designed and patented a premix nozzle to control the depressurisation and foam produced when dispensing carbonated liquids. The nozzle is shown in Figure B.2.1. The performance of this nozzle was tested experimentally in this thesis. In my preliminary experiments, Chapter 3, it was known as Nozzle 1. It was also tested in greater detail in Chapter 5.

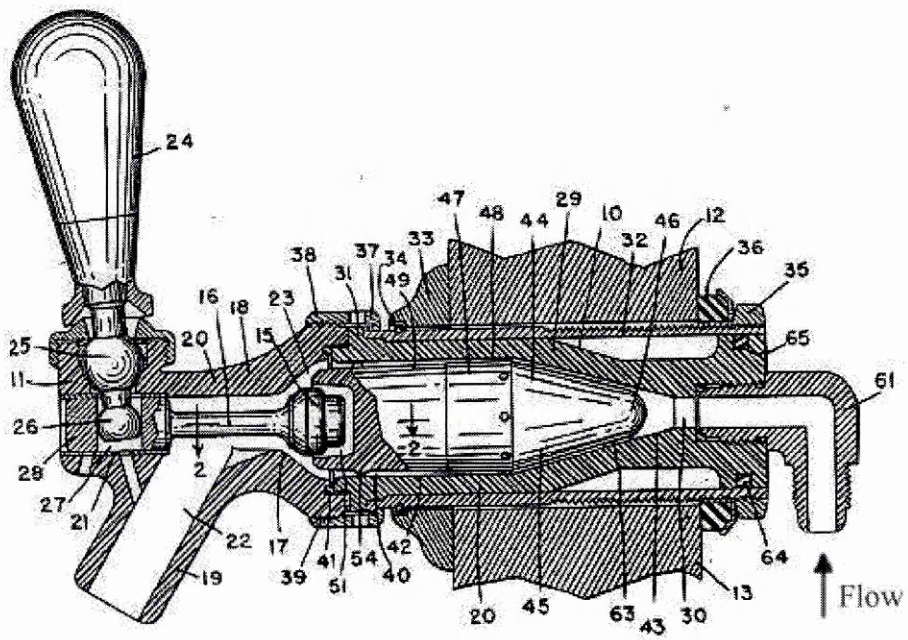

Figure B.2.1 Cornelius carbonated drink dispenser nozzle. Cornelius (1959).

The nozzle claims to have a simple and practical construction, that is easy to operate and can be easily disassembled for cleaning and repair. It depressurises a liquid, through a narrow annular restriction, without sharp bends or turns. It is said to reduce the tendency of foaming. The restriction is created by a bullet shaped central body within a bore casing. The casing tapers outwards from the inlet towards a cylindrical section. This is followed by a valve arrangement. The central body also tapers from the inlet at the same angle as the casing. This is followed by a cylindrical section with a diameter slightly less than the casing. Another narrow-angled tapered section of the central body follows the cylindrical section, increasing the cross sectional area of the flow towards the outlet. There are two sets of protuberances on the central body. These accurately align the central body within the casing, without affecting the flow through the device and maintain the annular passageway. At the central body outlet, a flange receives the plunger from the valve.

The central body can move longitudinally within the casing to vary the degree of restriction and cross-sectional area and hence adjust the flowrate. This adjustment is performed with a thumbscrew, which is screwed into the casing, engaging the shoulder of the central body. The screw's setting is unaffected when the nozzle is dismantled and the central body removed.

B.2.2 Green dispensing nozzle

Green (1996) patented a post-mix dispenser that uses a series of narrow tubes to depressurise the flow. It is shown in Figure B.2.2. Preliminary experiments testing a similar depressurisation device (Nozzle 3) are described in Chapter 3. At the outlet, a ring of cold syrup is injected into the depressurised water flow, before reaching the target container.

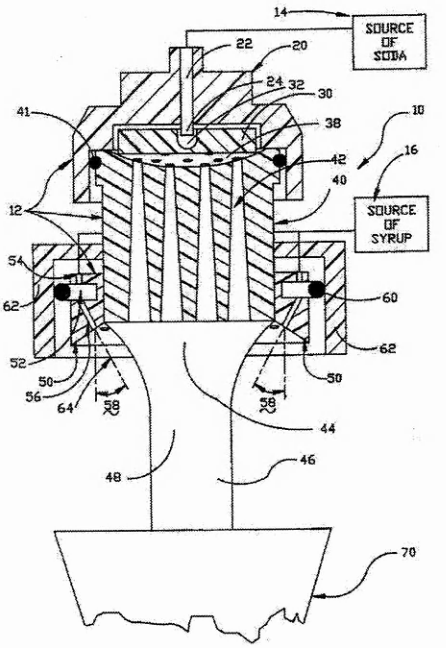

Figure B.2.2 Carbonated drink dispenser. Green (1996).

Pressurised saturated water flows downwards within the nozzle into a cavity [number 32 on Figure B.2.2], where the flow changes direction by 180°. The flow then briefly rises before falling into the dish-shaped neck section [40]. After reaching the neck section, the flow divides into a number of conical passages. These passages increase in diameter in the direction of the flow, reducing the velocity of the water.

The syrup flows through a number of delivery channels around the perimeter. The deliveries of the carbonated water and syrup are coordinated so that the water begins to fall from the neck section just before the syrup is injected. The syrup joins the flow of depressurised water at an angle so that the syrup intersects the free-falling flow of depressurised water. This provides maximum mixing before reaching the target container, minimising stratification and foaming.

B.3 Beer dispensers

This section describes a series of Guinness patents for the dispensing of beer, ale and stouts. They use a combination of a smooth restriction and turbulence generation sections, to produce the desired head size on a beer.

B.3.1 Ash (1961)

Ash (1961a and b) patented a beer depressurisation device, shown in Figure B.3.1. It consists of a restriction and a perforated disc with a number of fixed size, round apertures, with a diameter between 0.38 and 2.03mm. A sudden pressure drop is produced through the disc, releasing gas from solution, to produce a homogenous, fine and regular head. The aggregate area of the apertures determines the flowrate. When operating at 1.4 bar with six 1mm diameter holes, a flowrate of 60ml/second can be achieved. The disc is removable so that the aperture size can be selected for an appropriate flowrate and bubble size, according to the gas pressure, temperature and other dispensing conditions. The disc can be either up or downstream of the valve. If the restriction is upstream of the valve, the cross-sectional area of the passageway through the tap must be greater than the cross sectional area of the aperture, so as not to create a back pressure. To produce such a rapid pressure drop, the length of the restriction must not exceed 0.4mm.

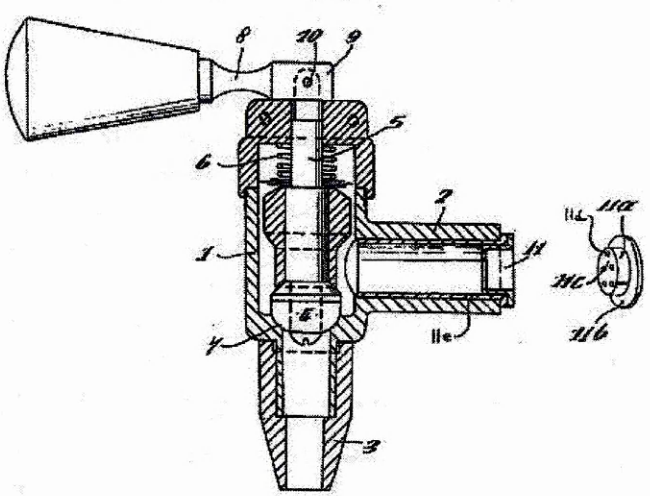

Figure B.3.1 Guinness dispense nozzle. Ash (1961b).

Another method of dispensing described by Ash (1961b) sent the flow through a throttling device like a plug cock. However, to produce the required rapid pressure drop, the plug cock had to be 'cracked' open and this was unable to produce an adequate flowrate.

B.3.2 Carnaghan (1964)

Carnaghan (1964) incorporated the principles of a perforated plate into a flow control valve, as shown in Figure B.3.2. The valve controls the amount of head produced and if desired, the flow can bypass the holes producing laminar flow. The dispenser has a tubular housing, with a plunger that moves axially within the housing, creating an annular flow passage. Changing the position of the plunger within the housing controls the head size on the beer. The plunger has a triangular cross section with three flats that centre the plunger within the housing, creating an annulus.

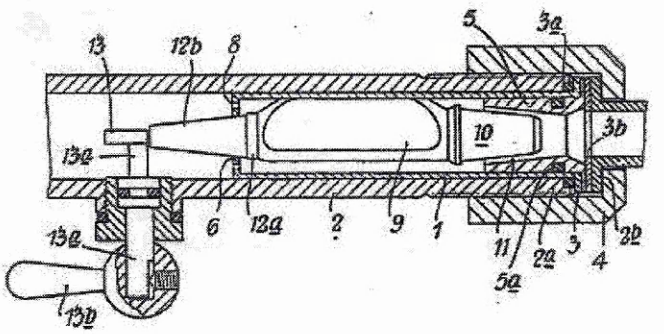

Figure B.3.2 Guinness dispense nozzle. Carnaghan (1964).

The housing is cylindrical with a tapered section at the inlet and a flange at the outlet. The outlet flange has a large central hole, surrounded by a number of smaller, symmetrically spaced 'cavitation' holes of less than 2.5mm inch in diameter. The plunger has a cylindrical centre section with tapered sections at either end. The downstream end of the plunger fits through the central hole in the flange at the end of the housing. The upstream taper of the plunger is centred within the upstream housing taper to create a restriction. It is shaped so that, whatever the plunger position, liquid passes through the annular space towards the main body of the plunger.

When the plunger is fully downstream, the tapered end of the plunger blocks the large central hole in the housing flange. This forces the flow through the cavitation holes, rapidly dropping the pressure and creating turbulence. This releases the gas from solution, producing a maximum sized head. In this position, the tapered inlet end of the plunger is withdrawn from the housing, creating no restriction. In contrast, when the plunger is fully upstream, the central hole at the end of the housing is opened, lessening the flow through the cavitation holes. The upstream end of the plunger enters the tapered housing section, creating a restriction and dropping the pressure. In this case the liquid flow is laminar, and the gas remains in solution forming a minimal head. With the plunger in an intermediate position, the head size can be controlled, creating a mixture of turbulent and non-disturbed flow. The dimensions of the device are chosen so that the rate of flow through it does not alter with the change of position of the plunger.

B.3.3 Painter and Thomasson (1969)

Painter and Thomasson (1969) combined the adjustable restriction, described by Carnaghan (1964), within a tap, as shown in Figure B.3.3. Again a large closure hole surrounded by cavitation holes is used. The restriction is a helix that moves in and out of the defining flow passage, increasing and decreasing the length of restriction.

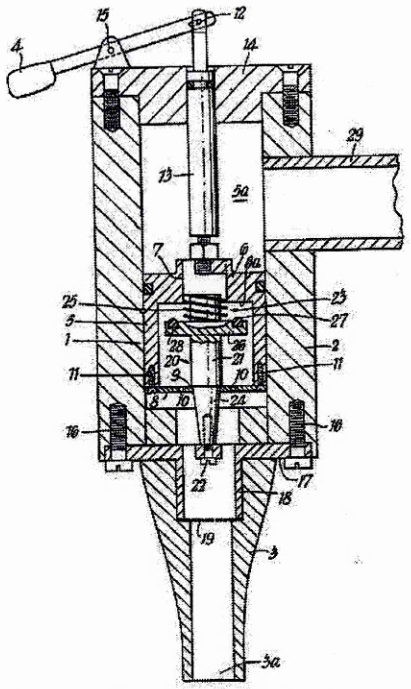

Figure B.3.3 Guinness dispense nozzle. Painter and Thomasson (1969).

A maximum head is achieved when the large central hole is closed, forcing the flow through the cavitation holes. In this state, the helix is removed from the flow passage and the pressure drop is solely across the cavitation holes. Lifting the plunger opens the central closure hole, reducing the flow through the cavitation holes. This creates a greater pressure drop occurring across the helix, reducing the amount of cavitation and head size. A minimum head size is produced with laminar flow when the closure hole is completely opened and the helix retracts into the flow passage, creating a pressure drop solely across the helix. The pressure distributions across this nozzle are described in Chapter 2.2.3.

B.3.4 Hildebrand and Yoakley (1972)

Hildebrand and Yoakley (1972) designed a simple dispense device for carbonated liquids, particularly beer, as shown in Figure B.3.4. An insert is placed into the flow path to create turbulence and cavitate the flow. The combination of a plate with cavitation holes followed downstream by a baffle produces a homogeneous head. The device is preferably placed downstream of a conventional dispensing tap, so it can be removed easily for cleaning.

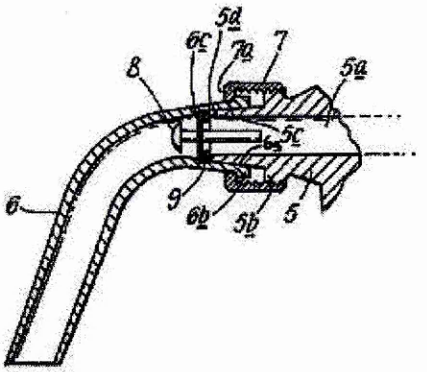

Figure B.3.4 Guinness dispense nozzle. Hildebrand and Yoakley (1972).

The cavitation plate has 3 holes with a diameter of 0.64 to 1.27mm, ideally 0.89mm. The holes are inclined inwards to produce a jet that strikes the baffle. This jet is then deflected back by the concave baffle producing turbulence, acting to homogenise the foam and provide an even head. The distance between the plate and the baffle should be no greater than the internal diameter of the flow passage. The distance of the baffle can be varied to control the turbulence and hence, the amount of foaming. The variation in distance can be achieved by having a range of devices or the device can be made adjustable by threading the internal boss on the cavitation plate. The insert is preferably made of stainless steel so it can withstand the corrosion caused by cavitation.

C Calibrations

This section shows the calibrations for all the experimental equipment used in this thesis.

C.1 Pressure measurement equipment

Pressure is fundamental to bubble formation. It was therefore measured carefully before and after depressurisation. The same Budenberg standard test pressure gauge, with a 0-100psi range, was used to measure the carbonator pressure and the air pressure. The nozzle inlet and outlet pressures were measured using Keller series 3 piezoelectric pressure transducers, with a working range of 0 – 10 bar absolute. They were identified as PT1 and PT2 respectively. PT2 failed during the project and was replaced with PT3.

A signal conditioning box was used to connect the pressure transducers via a power supply (set to 9V) to the voltmeter readout. The schematic circuit diagram is shown in Figure C.1.1. The readout was in Volts, which was subsequently converted to bar.

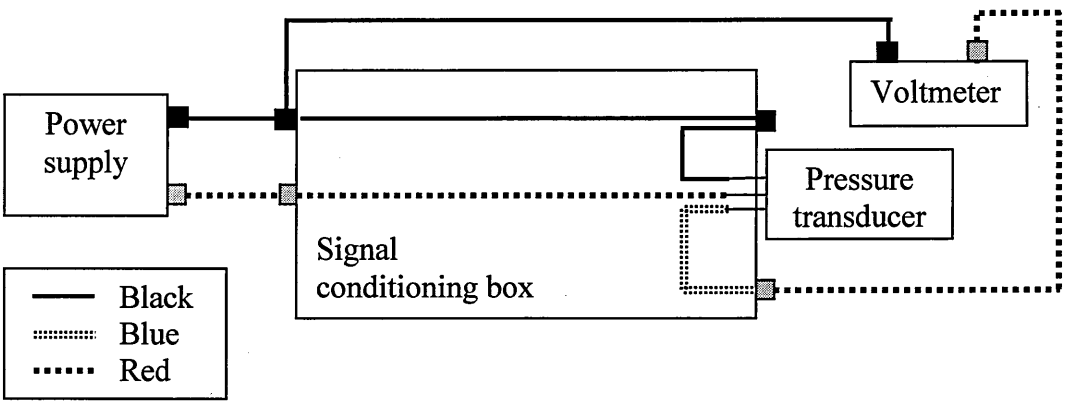

Figure C.1.1 Circuit diagram for connection of pressure transducer to voltage output.

The pressure transducers and the pressure gauge were calibrated using a Druck DPI 601 digital pressure indicator, for pressures up to 7bar. When taking the difference between two pressures, there was a slight offset, due to the output connections and wires. The pressure transducers were connected in turn and both calibrated through the same output system, when taking a pressure difference, a 0.1bar offset was produced. This offset was removed from the pressure difference results.

The calibrations of PT1, PT2 and PT3 are shown in Figures C.1.2 to C.1.4. The pressure gauge calibration is shown in Figure C.1.5. The calibrations were all linear.

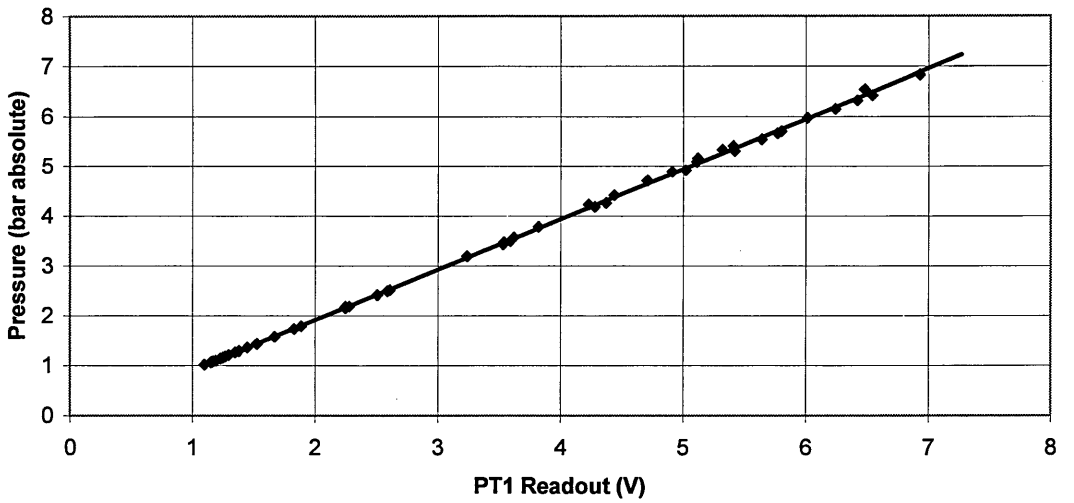

Figure C.1.2 Pressure transducer 1 calibration.

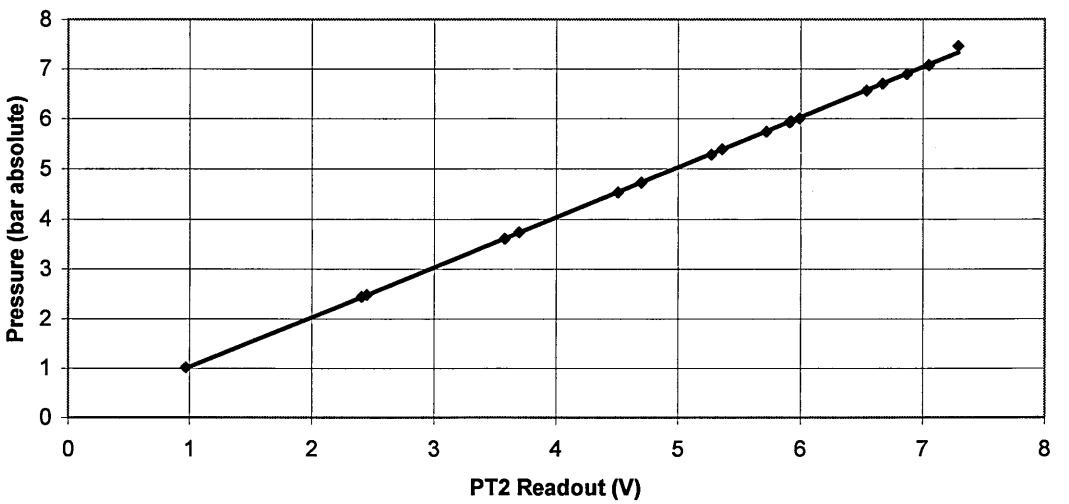

Figure C.1.3 Pressure transducer 2 calibration. (PT2 was later replaced by PT3).

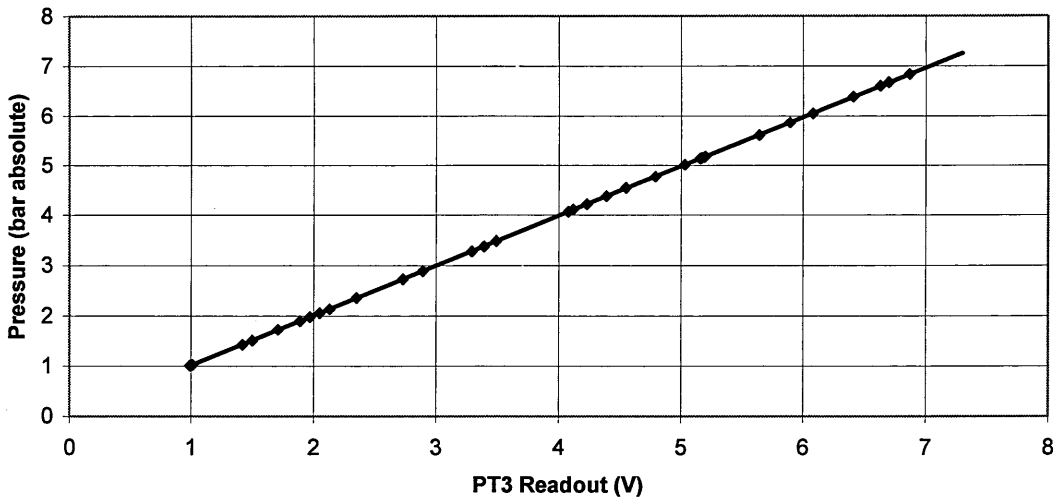

Figure C.1.4 Pressure transducer 3 calibration. (Replacement of PT2)

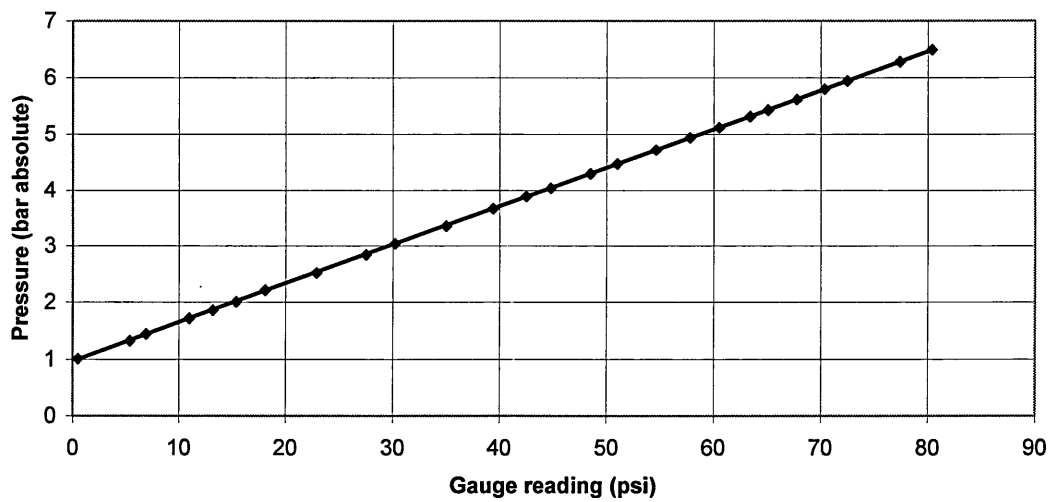

Figure C.1.5 Pressure gauge calibration

A summary of the calibrations is shown below, where P is the actual pressure in bar absolute.

PT1	P = 1.0088 (Reading) – 0.1012	Equation C.1.1
PT2	P = 1.0017 (Reading) + 0.0268	Equation C.1.2
PT3	P = 0.9921 (Reading) + 0.0211	Equation C.1.3
Pressure gauge	P = 0.0687 (Reading) + 0.961	Equation C.1.4

C.2 Temperature probes

Temperature measurement was fundamental to the dissolved gas experiments, as carbon dioxide solubility increases as temperature decreases. The laboratory

temperature was found to be constantly between 23 and 25°C. To reduce the effect of temperature on the experiment, a large sump tank was used to provide a constant temperature water supply.

PT100 PTFE insulated probes were used to measure the temperature of the flow before depressurisation (TC1) and at the nozzle outlet (TC2). A narrow type K industrial mineral insulated probe with a 1mm diameter was used at the coil outlet (TC3), to cause minimal disturbance to the flow, as the tube diameter was only 2.5mm. Each thermocouple had a digital readout. They were calibrated against a digital thermometer and probe using a S1220 System Teknik AB calibration block. The block had slots for each of temperature probes and was heated to a series of temperatures. The calibrations were all linear and are shown in Figures C.2.1 to C.2.3. Unfortunately the minimum temperature that could be calibrated was 20°C, however all of the experiments were performed above this temperature.

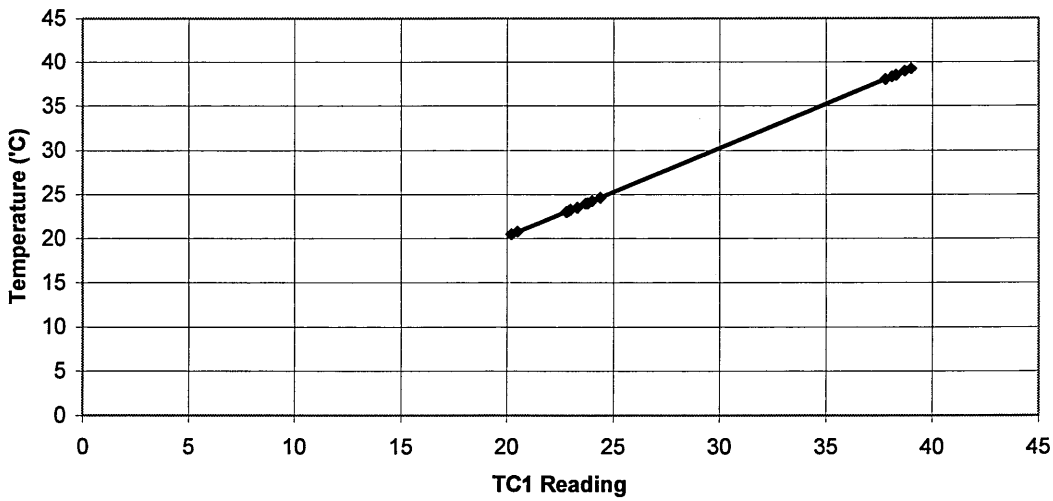

Figure C.2.1 Temperature probe 1 (TC1) calibration.

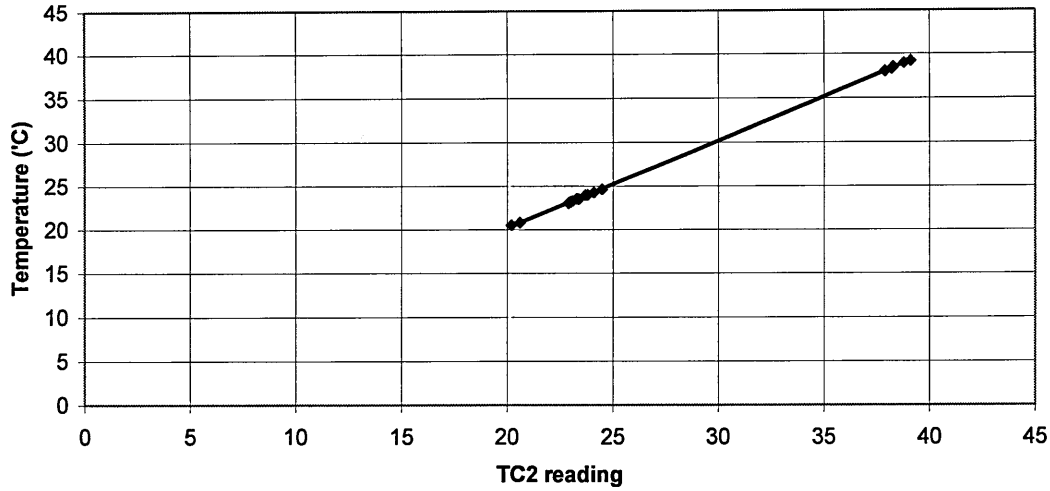

Figure C.2.2 Temperature probe 2 (TC2) calibration.

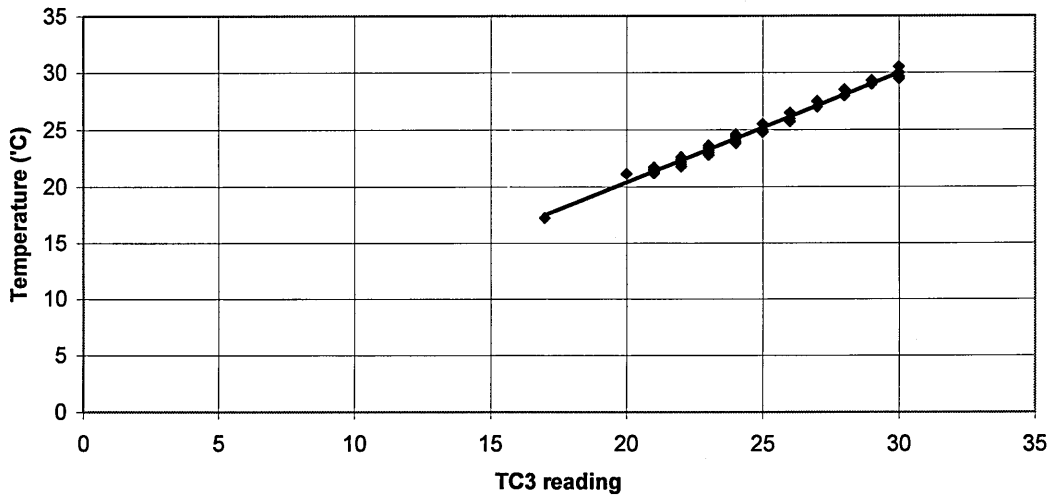

Figure C.2.3 Temperature probe 3 (TC3) calibration.

A summary of each of the temperature probe calibrations is shown below, where t is temperature (°C).

TC1	t = 0.9988 (Reading) + 0.2688	Equation C.2.1
TC2	t = 0.9977 (Reading) + 0.232	Equation C.2.2
TC3	t = 0.9609 (Reading) + 1.1631	Equation C.2.3

C.3 Rotameters

The air flowrate was measured using a Brooks Instrument, Model 1350, set of rotameters. The set consisted of a range of different sized tubes and floats to cover a range of flowrates. The flowrate was controlled with a valve that was integrated into the rotameter apparatus. Air was taken from the laboratory supply and regulated to

5.4bar(a) at the rotameter inlet. The pressure was measured using the Budenberg standard test pressure gauge. The pressure was set slightly higher than the water pressure, 5.3bar(a), so that the gas could be injected into the water flow in the mixed air and water experiments. A non-return valve was used after the rotameter to ensure that no water entered the rotameter. The basic layout of the air flowrate measurement apparatus is shown in Figure C.3.1.

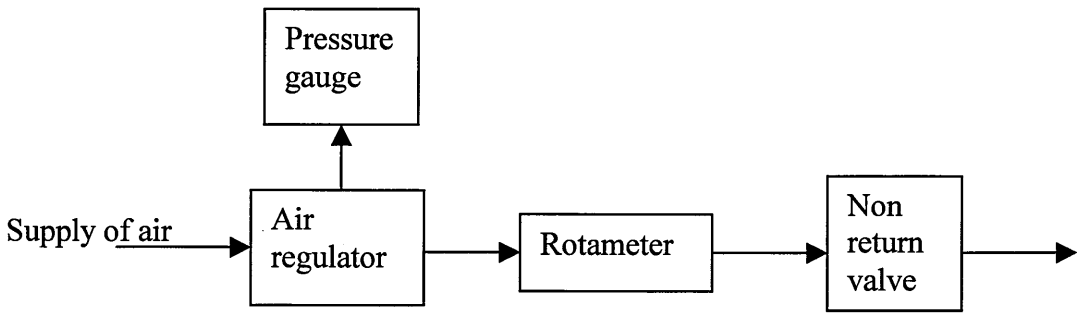

Figure C.3.1 Air flow measurement layout for experimentation.

Brook Instruments, the rotameter manufacturers, supplied a basic computer program to convert the maximum reading for each rotameter setup into a flowrate. The rotameter outlet temperature and pressure, and the fluid properties were all used to calculate the flowrate. Experimental calibrations were performed with each tube and float combination to validate the program's accuracy.

The experimental rotameter calibration used a slightly different equipment arrangement to the depressurisation experiments. The pressure after the rotameter remained high during the experiments due to the restriction of the depressurisation device. For the calibration, a needle valve was used to set the outlet pressure of the rotameter. The non-return valve was not used for the calibration. The calibration setup is shown in Figure C.3.2.

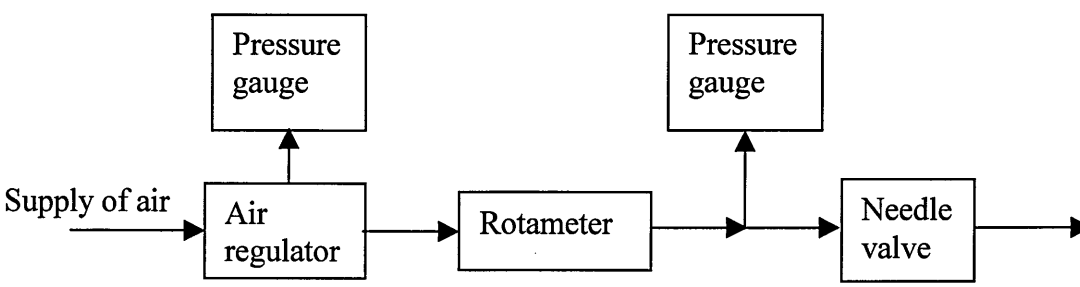

Figure C.3.2 Layout of the regulation and measurement of air supply during calibration.

The rotameter set consisted of 4 tubes and 4 floats that could be interchanged to measure a wide range of flowrates. The four tubes had different diameters. The narrowest tube was used to measure the lowest flowrates and widest for the highest flowrates. The tubes were named as follows, with the narrowest tube first: R-2-15-

AAA, R-2-15-A, R-2-15-C and R-6-15-B. There were four different ball floats to interchange into each of the tubes. The weights and their densities were as follows, with the lightest to measure the lowest flowrates first: Glass (2540 kg/m^3), Sapphire (4030 kg/m^3), Stainless Steel 316 (8040 kg/m^3) and Tantalum (1660 kg/dm^3). During the calibration, five different positions of the float within the tube were tested for each tube and float combination. The accuracy of the rotameter decreased as the ball sank lower into the tube.

Two different experimental calibration methods were used, which depended on the flowrate. A Bell prover was used to calibrate the higher flowrates. At the lower flowrates, a measuring cylinder was used that was filled with water and turned upside down in a tank of water, as shown in Figure C.3.3. Air was then bubbled into the measuring cylinder for a given length of time. The volume of air expelled within this amount of time was used to calculate the volumetric flowrate. Two different measuring cylinders were used to cover the range of flowrates, 100 and 500 ml. The uncertainty of this method was 1.5% of the flowrate, until the air flowrate became too high to accurately measure the time to fill the larger cylinder.

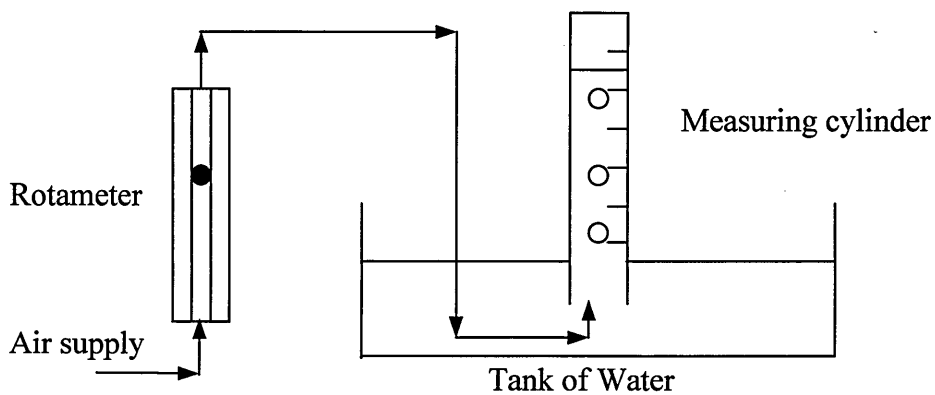

Figure C.3.3 Rotameter calibration procedure for low air flowrates.

C.3.1 Results

Calibrations were obtained for each tube and weight combination, and are shown in Figures C.3.4 to C.3.7. The figures compare the experimental calibrations with the computer program results. Both methods of calibration produced similar results with a maximum of ±10% deviation at the largest flowrates. The accuracy diminished at very low flowrates, particularly with the R-2-15-AAA tube, as tiny changes in the pressure changed the position of the float considerably.

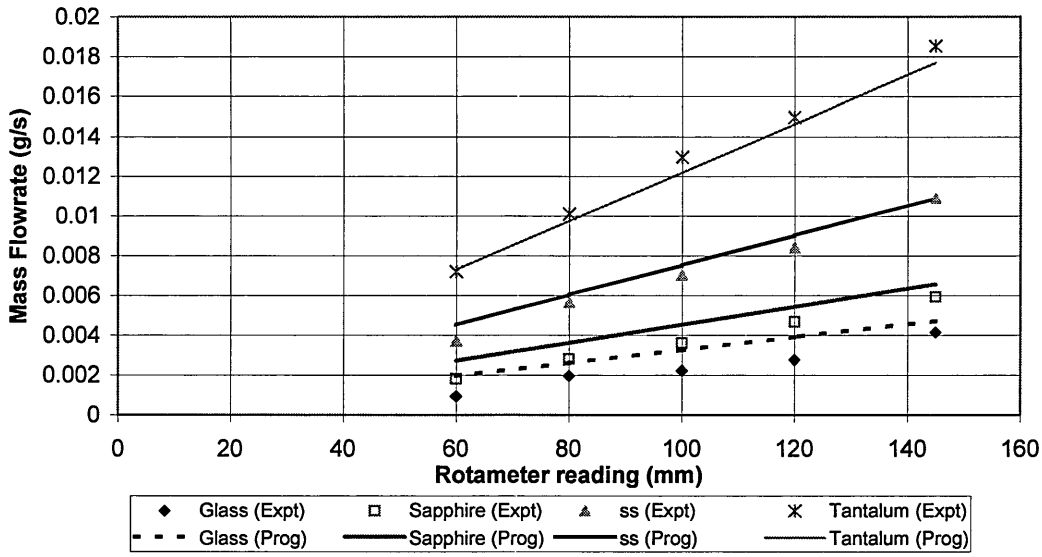

Figure C.3.4 Rotameter tube R-2-15-AAA calibration.

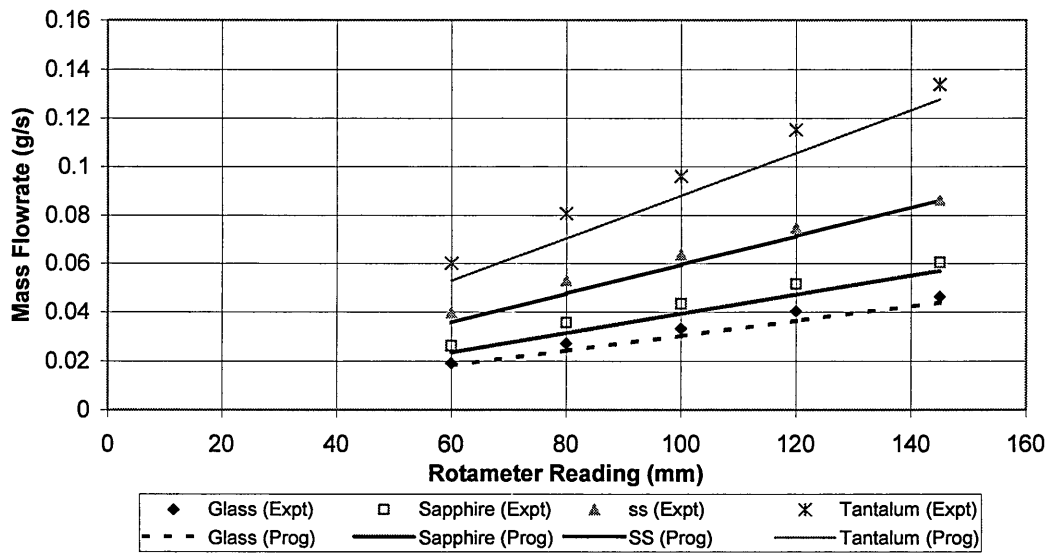

Figure C.3.5 Rotameter tube R-2-15-A calibration.

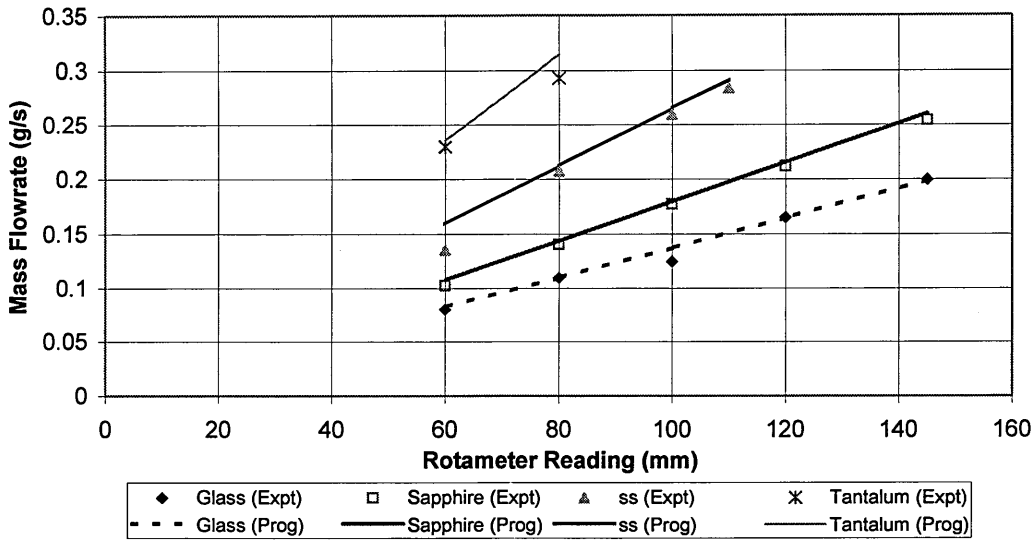

Figure C.3.6 Rotameter tube R-2-15-C calibration.

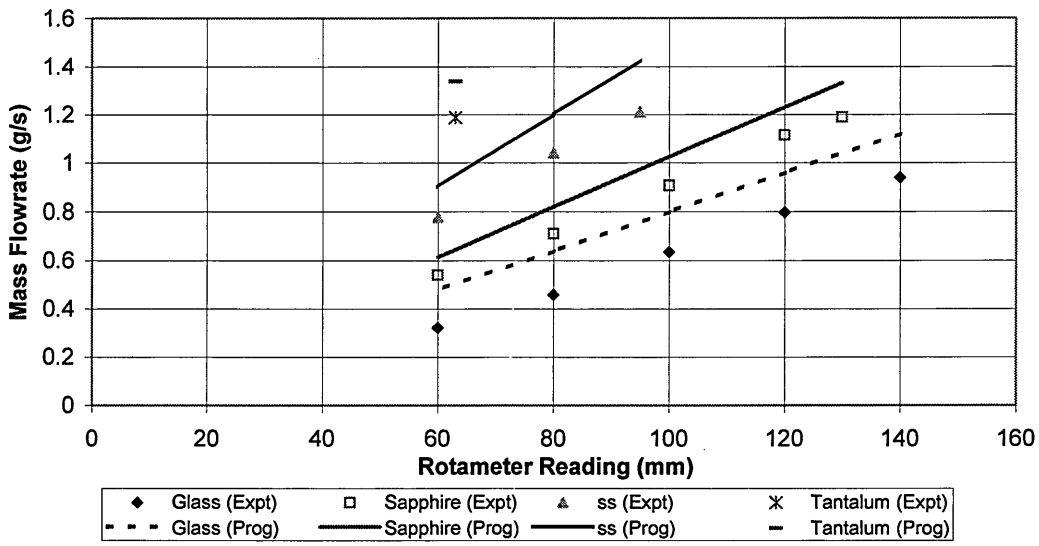

Figure C.3.7 Rotameter tube R-6-15-B calibration.

A summary of the equations produced from the experimental calibrations for various tube and float combinations is shown below. G (g/s) was the actual air flowrate and R the rotameter reading. The equations apply to an inlet pressure to the rotameter of 5.4Bar(a) and 5.3bar(a) at the outlet. The results in brackets are less accurate, as there were insufficient data to produce accurate trendlines.

R-2-15-AAA	Glass	$G = 1x10^{-7} R^2 + 1x10^{-5} R$	Equation C.3.1
	Sapphire	$G = 1x10^{-7} R^2 + 3x10^{-5} R$	Equation C.3.2
	316 SS	$G = 1x10^{-7} R^2 + 6x10^{-5} R$	Equation C.3.3
	Tantalum	$G = 4x10^{-8} R^2 + 0.0001 R$	Equation C.3.4

R-2-15-A	Glass	$G = -2x10^{-7} R^2 + 0.0003 R$	Equation C.3.5
	Sapphire	$G = -3x10^{-7} R^2 + 0.0005 R$	Equation C.3.6
	316 SS	$G = -9x10^{-7} R^2 + 0.0007 R$	Equation C.3.7
	Tantalum	$G = -1x10^{-6} R^2 + 0.0011 R$	Equation C.3.8
R-2-15-C	Glass	$G = 0.0007 R^2 + 1.0516 R$	Equation C.3.9
	Sapphire	$G = 0.0001 R^2 + 1.4598 R$	Equation C.3.10
	316 SS	$G = 0.0039 R^2 + 1.7689 R$	Equation C.3.11
	Tantalum	$(G = 3.1285 R)$	Equation C.3.12
R-6-15-B	Glass	$G = 8x10^{-7} R^2 + 0.0013 R$	Equation C.3.13
	Sapphire	$G = 2x10^{-7} R^2 + 0.0017 R$	Equation C.3.14
	316 SS	$G = 5x10^{-6} R^2 + 0.0021 R$	Equation C.3.15
	Tantalum	$(G = 0.0037 R)$	Equation C.3.16

In order to calculate the air flowrate, the rotameter outlet pressure was assumed to be the same as the inlet pressure to the depressurisation device. In the two-phase air and water experiments, the inlet pressure to the device was at least 95% of the rotameter inlet pressure. Hence, the experimental calibrations could be used to calculate the air flowrate. However, at low flowrates with the single-phase air experiments, the inlet pressure to the device was significantly less than the rotameter inlet pressure. The reduction in pressure, before the device would have been due to the flow resistance of the apparatus leading up to the nozzle being similar to the nozzle itself. The pressure losses would have been high across the non-return valve and between the float and tube of the rotameter itself. Hence, the pressure at the rotameter outlet was likely to have been less than the pressure used for the experimental calibrations and the calibrations would not apply. Therefore, low flowrates of the single-phase air were calculated solely by the computer program, using the inlet pressure to the depressurisation device. However, the rotameter outlet pressure was likely to have been greater than the device inlet pressure and the flowrate would have been underestimated.

C.4 Dissolved gas experiment calibrations

C.4.1 Flowrate calibrations

The water flowrate was measured in different ways, depending on the flow type. For the dissolved gas experiments, the flowrate was measured by timing the switching off and on cycles of the water pump to the saturator. A cycle started when the water pump to the saturator switched off, when the water level in the saturator was at a maximum. The pump was then switched on again when the level in the saturator went below a minimum level. Hence, a fixed volume of water passed each cycle.

To calibrate the flowrate, the mass of water that passed through the system each cycle was measured 30 times and averaged. The mass of water that passed each cycle was found to be 556 ±10g. Hence, equation C.4.1 was used to determine the water

flowrate. The uncertainty of equation C.4.1 was found to be approximately 2% of the measurement for carbonator pressures of between 1bar and 5.5bar absolute.

$$\text{Flowrate} = 556\text{g} / \text{Time of cycle} \qquad \text{Equation C.4.1}$$

The time between cycles decreased as the flowrate increased. At high flowrates the water pump was unable to refill the saturator fast enough and hence, gas was forced out of the outlet. The maximum flowrate for the outlet flow to contain gas-saturated water alone was found to be 100 ml/s. However a maximum flowrate of 80ml/s was used in this research.

During the water pump cycle, the saturator pressure fluctuated slightly. The minimum pressure was approximately 98.5% of the maximum pressure. For the majority of the cycle the pressure was at the minimum value but just after the water pump switched off, a maximum was reached. The minimum and maximum were recorded for each experiment, but the minimum was used for the calculations.

C.4.2 Saturator efficiency

The efficiency of the saturator was determined to ensure the accuracy of the dissolved gas concentration calculations. The saturator efficiency was defined as the ratio of the actual amount of carbon dioxide dissolved at the saturator outlet, to the amount of dissolved gas that should have been dissolved if the saturator was 100% efficient. The amount of carbon dioxide that should have been dissolved at the carbonator outlet was calculated using the solubility equation, equation C.6.3, at the carbonator pressure and temperature. The actual amount of carbon dioxide dissolved at the saturator outlet, was determined using the trapped method, as outlined in Chapter 4. The flow was trapped in the section before the depressurisation device, where the pressure was approximately 98% of the carbonator pressure.

The concentration of dissolved gas at the device inlet was found to be 7.5±0.3mg/ml. Using the solubility equation C.6.3, with the carbonator pressure, 5.3bar(a), and a temperature of 24°C, the amount of carbon dioxide that would have been dissolved if the saturator were 100% efficient was calculated to be 7.9mgCO_2/mlH_2O. Hence, for flowrates of less than 100ml/s, the average saturator efficiency was found to be 95%. The saturator efficiency is shown in Figure C.4.1.

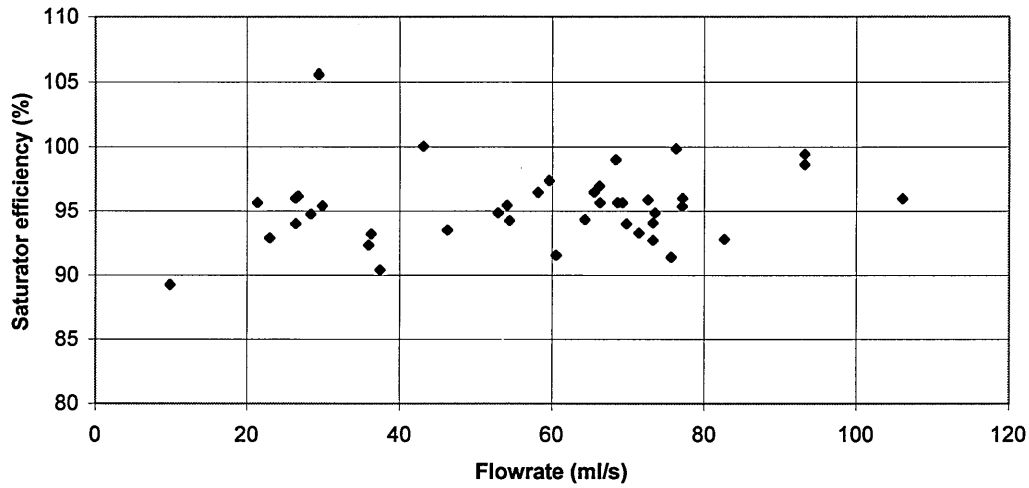

Figure C.4.1 The saturator efficiency variation with flowrate.

Figure C.4.1, shows that for flowrates of up to 100ml/s, the efficiency did not vary, despite the variation in residence time in the saturator. The maximum flowrate of the experiments was 80ml/s and therefore the saturator efficiency was taken to be 95%. The uncertainty of using the trapped method to calculate the dissolved carbon dioxide concentration was found to be approximately 5% of the calculated concentration.

C.5 Trapping tube calibrations

C.5.1 Trapping tubes volume

In the gas-saturated liquid experiments, a sample of the flow was trapped before and after the depressurisation device, so the concentration of gas dissolved in the flow could be determined. The volume of the tubes used to trap the flow was calibrated using a syringe to accurately measure the volume.

A syringe, of similar volume to the tube, was filled with water. The trapping tube being calibrated was evacuated of water and the attached syringe closed. The trapping section was positioned vertically, with the lowest valve of the section shut. The upper valve was then opened and water from the syringe injected into the section until the water level was visible in the tube, above the fittings. This was after the perspex block for the inlet measurement section and the nozzle outlet section, and after the initial trapping valve for the coil outlet section. The required volume to fill this section was noted from the syringe and the procedure repeated five times to determine a mean value. The trapping tube was then filled in stages with the syringe and volumes graduations marked on the tube. This was repeated several times to ensure accuracy and the graduations were eventually permanently marked on the tube. The section was then inverted to determine the volume of the fittings and perspex blocks at the other end of the tube. Water was added until the volume reached the last marking on the tube, so the total volume of the trapping section could be determined. The total volume of the trapping section before the depressurisation

device was found to be 19.6ml. The nozzle outlet section was found to be 20ml and the coil outlet section 1.99ml.

C.5.2 Trapping tube expansion

The polyurethane tube used to trap the outlet flow from the coils was found to expand under pressure. This would have affected the volumes used to calculate the concentration of carbon dioxide. It was impossible to perform accurate calculations to determine the tubes expansion, as the Youngs modulus of polyurethane is always stated as a range. The tubing manufacturer, SMC stated the Youngs modulus to be between 12-24MN/m^2. In the literature, Callister (1994) and Perry (1984), a range of 0.17-34.5MN/m^2 was reported. To determine accurately how much the tube expanded, a simple experiment was performed to measure the expansion.

A 1.1m length of tubing was filled with water to a height of 1m. This was subjected to a range of pressures of up to 5 bar(g). The pressure was applied via a Druck DPI digital pressure indicator, which was connected directly to the tube. A diagram of the apparatus is shown in Figure C.5.1. A non-return valve was used to ensure no water entered the pressure indicator. The height of water in the tube at each pressure was measured, in order to determine the new tube diameter. The original height of water at atmospheric pressure was marked on the tube. The height of this mark was measured at each pressure to determine if the tube extended longitudinally. This experiment was repeated 8 times.

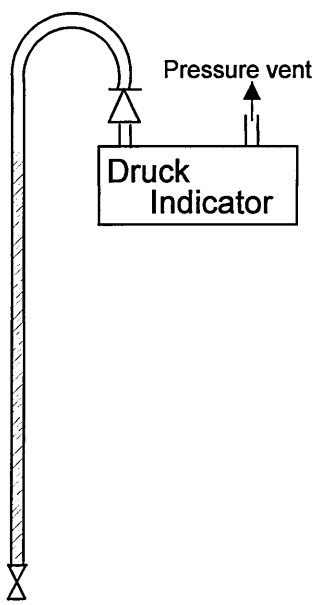

Figure C.5.1 Tube expansion experimental apparatus.

It was assumed that the tube diameter was uniform along its length and was 2.5mm at atmospheric pressure. Water was assumed to be incompressible and hence, the

volume of liquid in the tube remained constant. With these assumptions equations C.5.1 and C.5.2 were produced.

$$V_1 = V_2 \qquad \text{Equation C.5.1}$$

$$\frac{\pi d_1^2}{4} l_1 = \frac{\pi d_2^2}{4} l_2 \qquad \text{Equation C.5.2}$$

V_1 - volume of water at atmospheric pressure
V_2 - volume of water when under internal pressure
d_1, l_1 - tube diameter and length of water at atmospheric pressure
d_2, l_2 - tube diameter and length of water with an internal pressure

Consequently the tube diameter when under internal pressure was calculated from equation C.5.3, from the measured lengths of liquid and knowing the tube diameter at atmospheric pressure.

$$d_2 = \sqrt{\frac{d_1^2 l_1}{l_2}} \qquad \text{Equation C.5.3}$$

The diameter of the tube was found to expand linearly with pressure, up to a maximum 2.4% increase in diameter at 5bar (g). The variation in tube diameter with pressure is shown in Figure C.5.2.

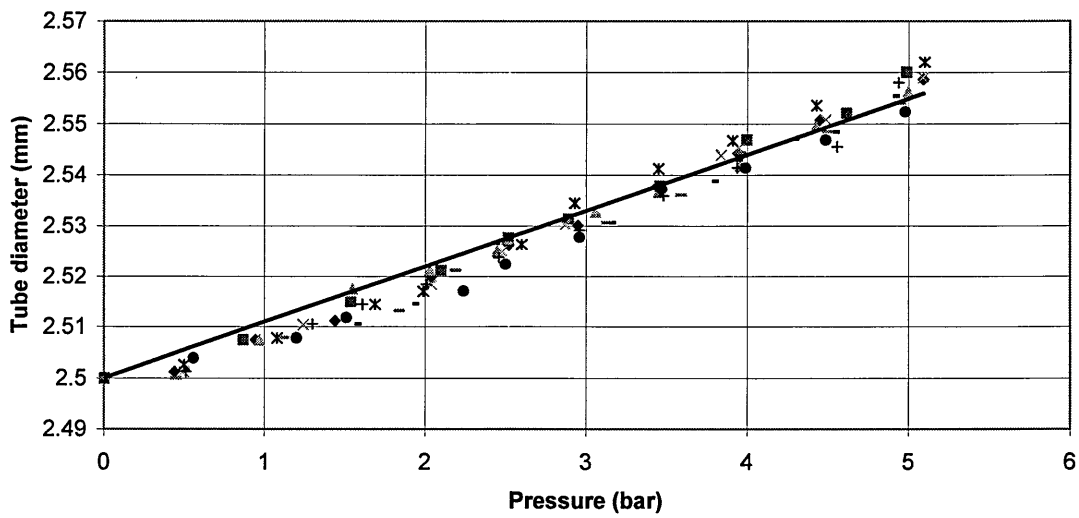

Figure C.5.2 Variation of tube diameter with pressure.

From a linear correlation of Figure C.5.2, equation C.5.4 was produced to calculate the tube diameter at different pressures. The 2.5 intercept of the equation corresponds to the original diameter of the tube at atmospheric pressure in millimetres

$$d_2 = 0.011\ P + 2.5 \qquad \text{Equation C.5.4}$$

d_2 - tube diameter under pressure (mm)
P - internal pressure (bar(g))

There was occasionally a slight difference in the height of water at atmospheric pressure, before and after pressurisation. A maximum difference of 3% to the total difference in height was seen. The difference was significantly less than this the majority of the time, so the effect was neglected.

The trapping tube length increased by a maximum of 0.2%. This was negligible compared to the increase in diameter and was therefore ignored.

From these results the volume of liquid read from the calibrated trapping tube in the experiments could be converted, to the actual tube volume using equation C.5.6.

$$\frac{V_1 4}{\pi d_1^2} = \frac{V_2 4}{\pi d_2^2} \qquad \text{Equation C.5.5}$$

$$V_2 = \frac{V_1 (0.011P + 2.5)^2}{2.5} \qquad \text{Equation C.5.6}$$

From this experiment the actual Youngs modulus of the polyurethane tubing was determined from the gradient of the stress versus strain correlation, shown as Figure C.5.3. The stress and strain of the tube were calculated from equations C.5.7 and C.5.8, taken from Harvey (1985) for a cylinder.

$$\text{Strain (e)} = \text{dilation } (\delta r) / \text{radius (r)} \qquad \text{Equation C.5.7}$$

$$Stress(\sigma_s) = \frac{pr}{2h} \qquad \text{Equation C.5.8}$$

σ_s - stress
p - internal pressure
h - wall thickness
r - tube radius

The linear gradient of Figure C.5.3, showed the Youngs modulus to be 30MN/m^2. This is higher than the manufacturer's range and is at the upper range reported in the literature.

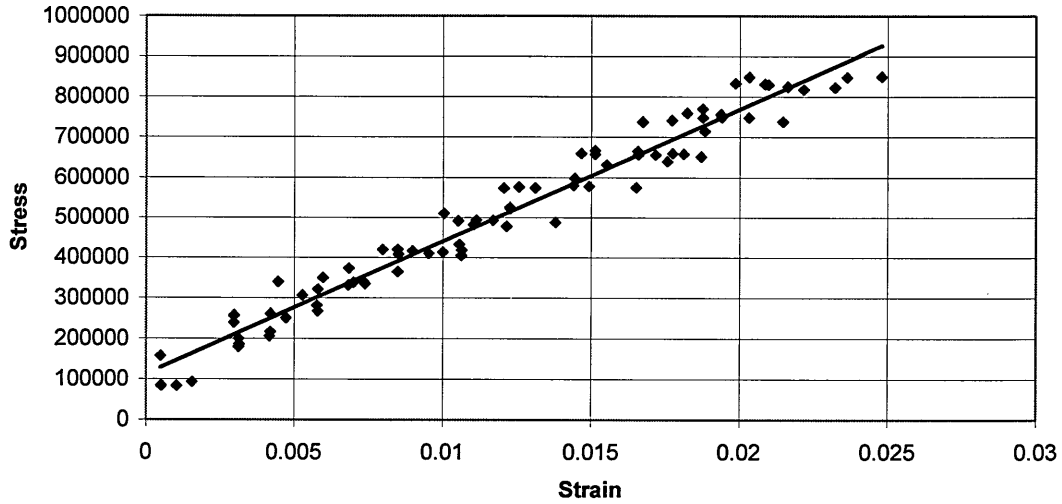

Figure C.5.3 Stress strain chart to calculate the Youngs modulus of the polyurethane tubing.

C.6 Solubility of carbon dioxide in water

The solubility of carbon dioxide in water at different temperatures and pressures was used to determine the concentration of dissolved gas in the gas-saturated flow experiments. Quinn and Jones (1945) showed a table, shown as Table C.6.1, for the solubility of carbon dioxide in water at different temperatures and pressures. Here, an equation has been produced to fit the data in the table, so that calculations in this thesis can be simplified.

P(psi)	t (F)												
(g)	32	36	40	44	48	55	60	65	70	75	80	85	90
15	3.46	3.19	2.93	2.7	2.5	2.2	2.02	1.86	1.71	1.58	1.44	1.35	1.27
20	4.04	3.73	3.42	3.15	2.92	2.57	2.36	2.17	2	1.84	1.69	1.58	1.48
25	4.58	4.27	3.92	3.61	3.35	3.04	2.69	2.48	2.29	2.1	1.93	1.8	1.7
30	5.21	4.81	4.41	4.06	3.77	3.31	3.03	2.8	2.58	2.37	2.18	2.03	1.91
35	5.8	5.35	4.91	4.52	4.19	3.69	3.37	3.11	2.86	2.63	2.42	2.26	2.13
40	6.37	5.89	5.39	4.97	4.61	4.05	3.71	3.42	3.15	2.89	2.67	2.49	2.34
45	6.95	6.43	5.88	5.43	5.03	4.43	4.06	3.74	3.44	3.16	2.91	2.72	2.56
50	7.53	6.95	6.36	5.89	5.45	4.8	4.4	4.05	3.73	3.42	3.16	2.94	2.71
55	8.11	7.48	6.86	6.34	5.87	5.17	4.74	4.37	4.02	3.69	3.4	3.17	2.99
60	8.71	8.02	7.35	6.79	6.29	5.53	5.08	4.68	4.31	3.95	3.64	3.39	3.2
70	9.86	9.09	8.33	7.7	7.13	6.27	5.76	5.3	4.89	4.49	4.14	3.86	3.63
80	11.02	10.17	9.31	8.61	7.98	7	6.43	5.92	5.46	5.02	4.62	4.31	4.06
90	12.18	11.25	10.3	9.52	8.82	7.74	7.11	6.54	6.04	5.55	5.12	4.77	4.49
100	13.34	12.33	11.29	10.43	9.66	8.4	7.79	7.18	6.62	6.08	5.6	5.22	4.91

Table C.6.1 Table shown in Quinn and Jones (1945), of the solubility of carbon dioxide in water, $mlCO_2$ / mlH_2O, with pressure in psi and temperature in degrees Fahrenheit.

Table C.6.1 shows the pressure in psi gauge and temperature in degrees Fahrenheit. Table C.6.2 shows the equivalent table converted with pressure in bar absolute and temperature in degrees Centigrade, as used in this thesis. The solubilities in Table C.6.1 are in $mlCO_2/ mlH_2O$, at 0°C and 1 atm. Table C.6.2 shows the solubility in $mgCO_2/ mlH_2O$. This was converted using the density of carbon dioxide, shown in Perry (1984), to be 1.9768 g/l (at 0°C and 1 atm).

P bar (a)	t °C 0.00	2.22	4.44	6.67	8.89	12.78	15.56	18.33	21.11	23.89	26.67	29.44	32.22
1.01	3.56					2.15	1.98						
2.05	6.84	6.31	5.79	5.34	4.94	4.35	3.99	3.68	3.38	3.12	2.85	2.67	2.51
2.39	7.99	7.37	6.76	6.23	5.77	5.08	4.67	4.29	3.95	3.64	3.34	3.12	2.93
2.74	9.05	8.44	7.75	7.14	6.62	6.01	5.32	4.90	4.53	4.15	3.82	3.56	3.36
3.08	10.30	9.51	8.72	8.03	7.45	6.54	5.99	5.54	5.10	4.69	4.31	4.01	3.78
3.43	11.47	10.58	9.71	8.94	8.28	7.29	6.66	6.15	5.65	5.20	4.78	4.47	4.21
3.77	12.59	11.64	10.65	9.82	9.11	8.01	7.33	6.76	6.23	5.71	5.28	4.92	4.63
4.12	13.74	12.71	11.62	10.73	9.94	8.76	8.03	7.39	6.80	6.25	5.75	5.38	5.06
4.46	14.89	13.74	12.57	11.64	10.77	9.49	8.70	8.01	7.37	6.76	6.25	5.81	5.36
4.81	16.03	14.79	13.56	12.53	11.60	10.22	9.37	8.64	7.95	7.29	6.72	6.27	5.91
5.15	17.22	15.85	14.53	13.42	12.43	10.93	10.04	9.25	8.52	7.81	7.20	6.70	6.33
5.84	19.49	17.97	16.47	15.22	14.09	12.39	11.39	10.48	9.67	8.88	8.18	7.63	7.18
6.53	21.78	20.10	18.40	17.02	15.77	13.84	12.71	11.70	10.79	9.92	9.13	8.52	8.03
7.22	24.08	22.24	20.36	18.82	17.44	15.30	14.06	12.93	11.94	10.97	10.12	9.43	8.88
7.91	26.37	24.37	22.32	20.62	19.10	16.61	15.40	14.19	13.09	12.02	11.07	10.32	9.71

Table C.6.2 Table, converted from Quinn and Jones (1945), for the solubility of carbon dioxide in water, with units of $mgCO_2/ mlH_2O$, with pressure in bar(a) and temperature in degrees Centigrade.

The data in Table C.6.2 was then converted into an equation to calculate the solubility of carbon dioxide in water, in terms of temperature and pressure. Pressure was initially plotted against solubility, for each temperature, as shown in Figure C.6.1. This produced a set of linear correlations for solubility in terms of pressure, for each temperature.

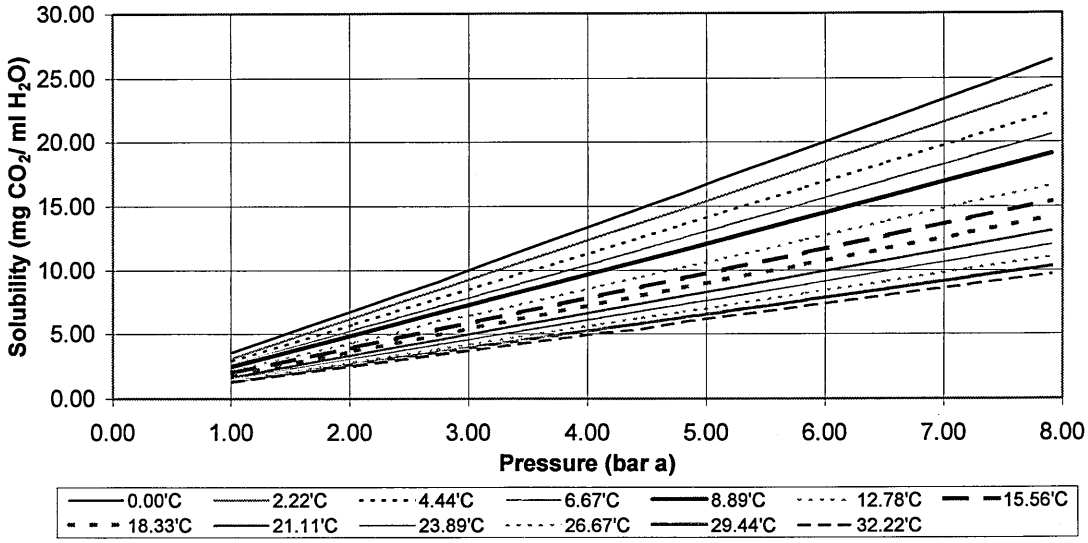

Figure C.6.1 Solubility of carbon dioxide in water against pressure for each temperature.

At 0°C	$C_G = 3.3373\ P$
At 2.22°C	$C_G = 3.081\ P$
At 4.44°C	$C_G = 2.8221\ P$
At 6.67°C	$C_G = 2.607\ P$
At 8.89°C	$C_G = 2.4153\ P$
At 12.78°C	$C_G = 2.1202\ P$
At 15.56°C	$C_G = 1.9478\ P$
At 18.33°C	$C_G = 1.794\ P$
At 21.11°C	$C_G = 1.6537\ P$
At 23.89°C	$C_G = 1.5188\ P$
At 26.67°C	$C_G = 1.3993\ P$
At 29.44°C	$C_G = 1.3047\ P$
At 32.22°C	$C_G = 1.2268\ P$

The coefficients of these equations were then correlated for temperature, using equation C.6.1, to produce an equation for the factor, f1. The correlation is shown as Figure C.6.2.

$$C_{G\,(T,P)} = f1(t)\ P \qquad \text{Equation C.6.1}$$

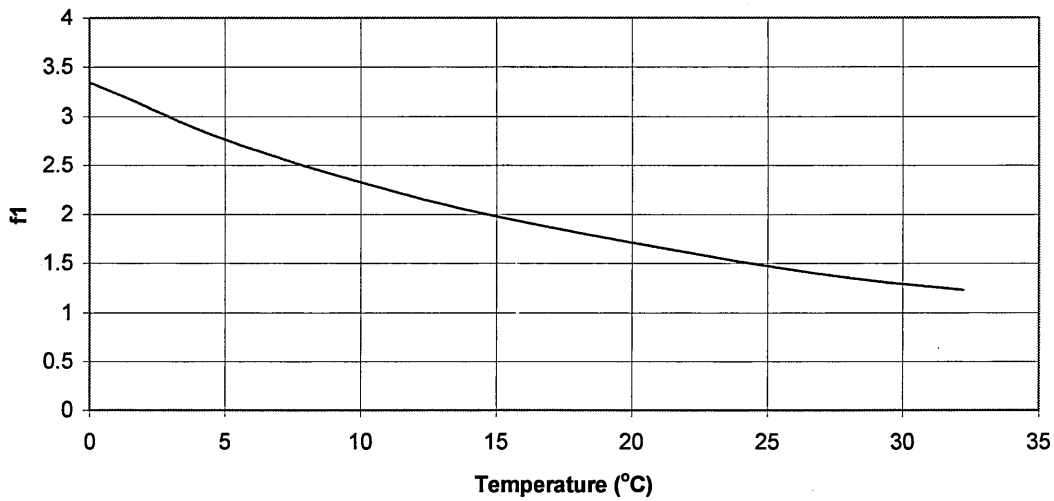

Figure C.6.2 Correlation of f1 against temperature.

Figure C.6.2 shows f1 versus temperature. A polynomial relationship was found to fit the data and is shown as equation C.6.2.

$$f1 = 0.0014152121\ t^2 - 0.1093249061\ t + 3.3027709023 \quad \text{Equation C.6.2}$$

Equation C.6.2 can then be combined with equation C.6.1, to produce equation C.6.3 for the solubility of carbon dioxide in water, in terms of temperature and pressure. The numbers were not rounded for greater accuracy.

$$\mathbf{C_G = P\ (0.0014152121\ t^2 - 0.1093249061\ t + 3.3027709023)} \quad \text{Equation C.6.3}$$

Equation C.6.3 was found to fit the data in Table C.6.2 with more than 98% accuracy.

C.7 Gas density conversion

C.7.1 Carbon dioxide

The density of carbon dioxide for various pressures is required for the dissolved gas concentration calculations. Perry (1984) stated the density of carbon dioxide to be 1.9768 g/l, at 0°C and 1 atmosphere. This was converted using the ideal gas law to calculate the density of carbon dioxide at any temperature and pressure, assuming k_G to be a constant. Equation C.7.1 was used to calculate k_G, for the density at 0°C and 1 atmosphere, with pressure in N/m^2 and temperature in degrees Kelvin.

$$\frac{P'}{\rho t'} = k_G \quad \text{Equation C.7.1}$$

$$k_G = \frac{101330}{1.9768 \times 273} = 187.76$$

$$\rho = \frac{P'}{187.76t'}$$ Equation C.7.2

This was then converted to the units used in this thesis to produce Equation C.7.3.

$$\rho = \frac{P}{0.00188t + 0.513}$$ Equation C.7.3

P - pressure (bar)
ρ - density (kg/m^3)
t - temperature (^{o}C)
k_G - constant

C.7.2 Air

Munday (1979) stated that the density of air at 20°C and 1bar is 1.19kg/m^3. This was converted for different temperatures and pressures using the same method as shown for carbon dioxide, with pressure in bar and temperature in degrees Centigrade.

$$\frac{P}{\rho T} = k$$ Equation C.7.4

$$k = \frac{1}{1.19 \times 20} = 0.042$$

$$\rho = \frac{P}{0.042t}$$ Equation C.7.5

D Dissolved gas concentration measurement techniques

The concentration of carbon dioxide dissolved in water was measured experimentally to determine the performance of a depressurisation device. The chosen method must not obstruct the flow, due to the ease of bubble formation, particularly at the outlet when the flow was supersaturated.

Several different methods to obtain a flow sample are described in the literature. Hayward (1961), Packham and Richards (1975) and Hall and Corlett (1997) all extracted a sample of the flow using a T-piece or syringe. These would cause a flow disturbance and encourage bubble formation, even if performed slowly and carefully. A simpler method to obtain a sample with minimal flow disturbance is to trap a section of flow by simultaneously closing two ball valves. This principle is outlined in Whalley (1990), as a method to determine the void fraction of the flow. Providing ball valves were used with the same flow path diameter, there would be minimal disturbance to the flow. The sample can then be removed or tested in situ.

Barker et al (1998) described four different methods to measure the concentration of dissolved carbon dioxide. They tested a commercially available orbisphere. This is an on-line probe that monitors the dissolved gas in drinks. It comprises a semi-permeable membrane and thermal conductivity detector. It is low maintenance and can withstand high pressures but is very expensive. A simple, cheaper pressure gauge was found to produce similar results. The vapour pressure of a bottle after carbonation was measured and the concentration of dissolved gas was then determined from a solubility chart relating to the measured temperature and pressure.

Titration can also be used to determine the concentration of dissolved gas. Using the following scheme:

$$CO_2 + H_2O \Leftrightarrow H_2CO_3 \Leftrightarrow H^+ + HCO_3^- \Leftrightarrow 2H^+ + CO_3^{2-}$$

Adding sodium hydroxide to a sample converts all the HCO_3^- to CO_3^{2-}, so the amount of CO_2 can be calculated. A back titration was also investigated by carbonating the sodium hydroxide to quench the carbon dioxide, converting it to the soluble carbonate ion, which remains in solution when depressurised. This was titrated against hydrochloric acid. This was not suitable for the experimental procedure used in this thesis, as the removal of the sample from the trapping tube and the addition of any chemical would have agitated the sample and encouraged the gas to be released. This method would be more suited to a batch process.

The pressure gauge method described by Barker et al (1998) was incorporated into the experimental method used. The flow was trapped between two ball valves with the same internal diameter as the tubing. Once trapped, the pressure and temperature were recorded, and the solubility of the gas was calculated. The total amount of gas trapped was calculated using the gas solubility and the ideal gas law.

Another method to determine the concentration of dissolved gas was also incorporated into the experimental procedure. This was adapted from methods outlined by Hayward (1961), Hall and Corlett (1997) and Packham and Richards (1975). Hayward (1961) described two instruments to measure the air content in oil. A vacuum was applied and the total volume of dissolved gas determined. Air is released very slowly but can be accelerated by agitation or spreading the oil as a thin film. It was found that more viscous oils took longer to release the gas. Hall (1997) modified the method from Hayward using a dual expansion method. A known volume of liquid was withdrawn from the flow over 30 seconds. The flow was then expanded in turn in two cylinders. The first expansion took more than 10 hours. Most of the gas was released within an hour after the second expansion.

Packham and Richards (1975) adapted the Van Slyke apparatus used for blood gas determination. This was achieved by lowering a reservoir to reduce the sample pressure. The reservoir was repeatedly raised and lowered to pass the water into another reservoir via a partially closed valve, creating high shear to liberate the gas. Once the bubbles stopped forming, the final volume of gas was measured. The fraction of carbon dioxide and oxygen was also determined. Aqueous potassium hydroxide (20%) was added to absorb the carbon dioxide. The volume of carbon dioxide was calculated from the change in volume. The amount of oxygen was found in a similar manner using alkaline pyrogallol to absorb the oxygen.

In this thesis the concentration of dissolved carbon dioxide was determined experimentally from a sample produced by trapping the flow between ball valves. The first method of determining the concentration was found by recording the trapped pressure and temperature. The total volume of gas trapped was found using the ideal gas law and the solubility of carbon dioxide. This was known as the trapped method.

A gas-tight syringe was attached to the trapped section so the flow could be depressurised and the total volume of gas at atmospheric pressure determined. The syringe was 'pulled' to create a vacuum to encourage the bubbles to form. This was known as the syringe method. The gas release was slow, so a standard experimental procedure was produced to release the maximum amount of gas and reduce experimental errors. The syringe was initially pulled and wedged open to a vacuum of 0.6 bar absolute for 15 minutes. The wedge was then removed and the system was returned to atmospheric pressure for 5 minutes to reach equilibrium and redissolve any gas that would be dissolved at atmospheric pressure. Sample experiments proved this method to release most of the gas, and leaving it for longer made negligible difference. Standardising the experiment reduced any errors.

E Coil equations

Many equations are in the literature to calculate the friction factor for single-phase flow in coils. The most applicable and practical equations are listed in this section. The equations were formulated with different inlet flow conditions and different diameters of tube and coil. A few equations were also found for two-phase flow which are also shown. Equations found to calculate the critical Reynolds number for the transition from laminar to turbulent flow are also shown. The friction factor equations shown all use the Fanning friction factor, as used in equation E.1.

$$\Delta P = 4f\frac{l}{d}\frac{\rho u^2}{2} \qquad \text{Equation E.1}$$

Several of the equations use the Dean number (Dn) which can be calculated from equation E.2.

$$Dn = \mathrm{Re}\left(\frac{d}{D}\right)^{0.5} \qquad \text{Equation E.2}$$

E.1 Single-phase flow

E.1.1 Coil friction factor equations - Laminar

Dean (1928)

This theoretically produced equation is suitable for Dn < 20.45. The equation was referenced in Srinivasan et al (1968), Larrain and Bonilla (1970), Van Dyke (1978), Manlapaz and Churchill (1980), Berger et al (1983). Manlapaz and Churchill (1980) stated the equation slightly differently, possibly a mistake.

$$\frac{f_c}{f_s} = 1 - 0.03058\left(\frac{Dn^2}{288}\right)^2 + 0.01195\left(\frac{Dn^2}{288}\right)^4 \qquad \text{Equation E.1.1.1}$$

White (1929)

The empirical equation is suitable for Dn = 11.6-2000+ and f_s / f_c = 1 for Dn < 11.6, but is not valid if f_c < 0.0024. The equation was referenced in Rogers and Mayhew (1964), Kubair and Kuloor (1966), Srinivasan et al (1968), Boyce et al (1969), Larrain and Bonilla (1970), Akagawa et al (1971), Mishra and Gupta (1979), Manlapaz and Churchill (1980) and Liu et al (1994).

$$\frac{f_s}{f_c} = 1 - \left(1 - \left(\frac{11.6}{Dn}\right)^{0.45}\right)^{1/0.45} \qquad \text{Equation E.1.1.2}$$

Adler (1934)

This formula derived theoretically, assuming a laminar boundary layer near the wall. It is suitable for large Dean numbers. The equation was referenced in Srinivasan et al (1968), Larrain and Bonilla (1970), Van Dyke (1978), Manlapaz and Churchill (1980), Berger et al (1983) and Liu et al (1994).

$$\frac{f_c}{f_s} = 0.1064 Dn^{0.5} \qquad \text{Equation E.1.1.3}$$

Prandtl (1954)

The empirical equation is suitable for 20< Dn< 1000. A slightly different version is shown in Manlapaz and Churchill (1980), with 0.29 not 0.37 this was presumed to be a mistake. The equation was also referenced in Kubair and Varrier (1961-62), Srinivasan (1968) and Van Dyke (1978).

$$\frac{f_c}{f_s} = 0.37 Dn^{0.36} \qquad \text{Equation E.1.1.4}$$

Ito (1959) - referenced in Mori and Nakayama (1967a), Srinivasan et al (1968) and Oguri (1995)

This empirical equation is applicable for 13.5 > Dn > 2000 and d/D < 50.

$$\frac{f_c}{f_s} = \frac{21.5 Dn}{(1.56 + \log_{10} Dn)^{5.73}} \qquad \text{Equation E.1.1.5}$$

Kubair and Varrier (1961-62)

The equation is suitable for Re = 2000 – 9000 and d/D = 0.037- 0.097. The equation was referenced in Kubair and Kuloor (1965) and Srinivasan et al (1968).

$$f_c = 0.7716 e^{3.553(d/D)} \mathrm{Re}^{-0.5} \qquad \text{Equation E.1.1.6}$$

Hasson (1963) - referenced in Barua (1963), Srinivasan et al (1968), Van Dyke (1978) and Liu et al (1994)

This empirical equation is suitable for 30 < Dn < 2000.

$$\frac{f_c}{f_s} = 0.0969Dn^{0.5} + 0.556$$ Equation E.1.1.7

Barua (1963)

This formula was theoretically derived for large Dean numbers. It was referenced in Srinivasan et al (1968), Van Dyke (1978) and Berger et al (1983).

$$\frac{f_c}{f_s} = 0.0918Dn^{1/2} + 0.509$$ Equation E.1.1.8

Mori and Nakayama (1965)

This equation was produced from an experimental and theoretical study. An approximation technique and produced equation for the first and second approximation. It is applicable for a wide range of Dn. The equation was referenced in Srinivasan et al (1968), Van Dyke (1978) and Berger et al (1983).

$$\left(\frac{f_c}{f_s}\right)_I = 0.1080Dn^{1/2}$$ Equation E.1.1.9a

$$\left(\frac{f_c}{f_s}\right)_{II} = \left(\frac{f_c}{f_s}\right)_I \frac{1}{1-3.253Dn^{-1/2}}$$ Equation E.1.1.9b

Kubair and Kuloor (1965)

This empirical equation was derived for non-isothermal fluids and is applicable for Re = 170-9000/Re_{crit}. The equation was also referenced in Srinivasan et al (1968).

$$f_c = 16\left[2.8 + 12\left(\frac{d}{D}\right)\right]\mathrm{Re}^{-1.15}$$ Equation E.1.1.10

Schmidt (1967)

The equation was referenced in Manlapaz and Churchill (1980).

$$\frac{f_c}{f_s} = 1 + 0.14\left(\frac{d}{D}\right)^{0.97}\mathrm{Re}^{\left(1-0.644\left(\frac{d}{D}\right)^{0.312}\right)}$$ Equation E.1.1.11

Ito (1969)

The equation is an improved and extended version of Adler's equation. The equation was referenced in Van Dyke (1978), Manlapaz and Churchill (1980) and Berger et al (1983).

$$\frac{f_c}{f_s} = 0.1033 Dn^{1/2}\left[\left(1+\frac{1.729}{Dn}\right)^{1/2} - \left(\frac{1.729}{Dn}\right)^{1/2}\right]^{-3} \qquad \text{Equation E.1.1.12}$$

Collins and Dennis (1975)

The equation was referenced in Van Dyke (1978).

$$\frac{f_c}{f_s} = 0.1028 Dn^{1/2} + 0.380 \qquad \text{Equation E.1.1.13}$$

Van Dyke (1978)

The equation was derived theoretically and is suitable for 20 < Dn < 200. The equation was referenced Manlapaz and Churchill (1980), Berger et al (1983) and Liu et al (1994).

$$\frac{f_c}{f_s} = 0.47136 Dn^{1/4} \qquad \text{Equation E.1.1.14}$$

Manlapaz and Churchill (1980)

The equation was referenced in Awwad et al (1995b), and Xin et al (1996). The following values of m should be used for the following values of Dn:

m=2 Dn< 20
m=1 20 < Dn < 40
m=0 Dn > 40

$$\frac{f_c}{f_s} = \left[\left(1-\frac{0.18}{\left[1+\left(35/Dn\right)^2\right]^{1/2}}\right)^m + \left(1+\frac{d/D}{3}\right)^2 \frac{Dn}{88.33}\right]^{1/2} \qquad \text{Equation E.1.1.15}$$

E.1.2 Coil friction factor equations - Turbulent

White (1932)

The equation is applicable for Re= 15,000 –100,000. The equation was also referenced in Kubair and Varrier (1961-62) and Srinivasan et al (1968). Kubair shows 0.0012 instead of 0.012. This was presumed a mistake.

$$f = 0.08\,\mathrm{Re}^{-0.25} + 0.012\left(\frac{d}{D}\right)^{0.5} \qquad \text{Equation E.1.2.1}$$

Ito (1959)

The first two equations were derived from the $1/7^{th}$ power velocity distribution law. The third from the logarithmic velocity distribution law.

A. The empirical equation is applicable for $0.034 < \mathrm{Re}(d/D)^2 < 300$. Below $\mathrm{Re}(d/D)^2 = 0.034$ the flow resembles straight pipe. The equation was also referenced in Rogers and Mayhew (1964), Mori and Nakayama (1965), Srinivasan et al (1968), Boyce et al (1969), Czop et al (1994), Awwad et al (1995b) and Xin et al (1996).

$$f_c = 0.076\,\mathrm{Re}^{-0.25} + 0.00725\left(\frac{d}{D}\right)^{0.5} \qquad \text{Equation E.1.2.2}$$

B. The empirical equation was deduced for large $\mathrm{Re}(d/D)^2$, and may be used for $\mathrm{Re}(d/D)^2$ exceeding 6. The equation was also referenced in Seban and Mclaughlin (1963), Rogers and Mayhew (1964), Mori and Nakayama (1967), Srinivasan et al (1968), Akagawa et al (1971) and Oguri (1995).

$$\frac{f_c}{f_s} = 1.00\left[\mathrm{Re}\left(\frac{d}{D}\right)^2\right]^{1/20} \qquad \text{Equation E.1.2.3}$$

Kubair and Varrier (1961-62)

This equation was obtained from experimental results and was suitable for Re = 9000-25000 and d/D = 0.037-0.097. This equation was also referenced in Srinivasan et al (1968).

$$f_c = 0.003538\,e^{1.887(d/D)}\,\mathrm{Re}^{0.09} \qquad \text{Equation E.1.2.4}$$

Mori and Nakayama (1967a)

This equation was also referenced in Srinivasan et al (1968). The first equation is suitable for normal practical use.

A. $$f_c = \frac{0.075}{\left[\mathrm{Re}\left(d/D\right)^2\right]^{1/5}}\left(1+\frac{0.112}{\left[\mathrm{Re}\left(d/D\right)^2\right]^{1/5}}\right)\left(\frac{d}{D}\right)^{1/2}$$ Equation E.1.2.5

The second equation is suitable for fairly large Reynolds numbers.

B. $$f_c = \frac{0.048}{\left[\mathrm{Re}\left(d/D\right)^{2.5}\right]^{1/6}}\left(1+\frac{0.068}{\left[\mathrm{Re}\left(d/D\right)^{2.5}\right]^{1/6}}\right)\left(\frac{d}{D}\right)^{1/2}$$ Equation E.1.2.6

Mishra and Gupta (1979)

The equation is applicable for d/D = 0.00289-0.15 and Re= 4500-100,000. The equation was also referenced in Das (1993).

$$f_c = 0.079\,\mathrm{Re}^{-0.25} + 0.0075\left(\frac{d}{D}\right)^{0.5}$$ Equation E.1.2.7

Ruffel (1979) - referenced in Czop et al (1994)

This equation is suitable for rough pipes.

$$f_c = 0.015 + 2.53\left(\frac{d}{D}\right)^{0.275}\mathrm{Re}^{-0.4}$$ Equation E.1.2.8

Czop et al (1994)

$$f_c = 0.024 Dn^{-0.1517}$$ Equation E.1.2.9

E.1.3 Coil critical Reynolds number equations

The critical Reynolds number in a coil applies when the flow changes from laminar to turbulent. It is shown in many different forms in the literature as a function of d/D.

Ito (1959)

This empirical equation, according to Liu, is the most accepted. It calculates the lower critical Reynolds number for a curved pipe. Good agreement with experimental results was achieved 15< D/d < 860. When D/d > 860, the critical Reynolds number coincides with a straight pipe. This was also referenced in Rogers and Mayhew (1964), Mori and Nakayama (1967a), Srinivasan et al (1968), Akagawa et al (1971), Mishra and Gupta (1979), Das (1993), Czop et al (1994) and Liu et al (1994).

$$\mathrm{Re}_{Crit} = 20000\left(\frac{d}{D}\right)^{0.32} \qquad \text{Equation E.1.3.1}$$

Kubair and Varrier (1961-62)

The equation was derived from experimental results for d/D 0.0005 to 0.103. This was referenced in Kubair and Kuloor (1965), Liu et al (1994) and Srinivasan et al (1968).

$$\mathrm{Re}_{Crit} = 12730\left(\frac{d}{D}\right)^{0.2} \qquad \text{Equation E.1.3.2}$$

Srinivasan et al (1968)

For d/D in the range 0.004 to 0.1. When d/D<0.00116, Re_{Crit} is the same as a straight pipe i.e. 2100. This was also referenced in Czop et al (1994), Liu et al (1994), Perry (1984) and Awwad et al (1995b).

$$\mathrm{Re}_{Crit} = 2100\left[1+12\left(\frac{d}{D}\right)^{0.5}\right] \qquad \text{Equation E.1.3.3}$$

Kutateldze and Borishanskii (1966) – referenced in Srinivasan et al (1968)

This equation is only valid for the limited range d/D 0.0417 to 0.1667.

$$\mathrm{Re}_{Crit} = 2300 + 12930\left(\frac{d}{D}\right)^{0.3} \qquad \text{Equation E.1.3.4}$$

Ward-Smith (1980) – referenced in Liu et al (1994)

This formula is for $d/D < 0.1$.

$$\mathrm{Re}_{Crit} = 2300\left(1 + 10\left(\frac{d}{D}\right)^{0.5}\right) \qquad \text{Equation E.1.3.5}$$

E.1.4 Spiral friction factor equations - Laminar

Kubair and Kuloor (1966) - referenced Srinivasan et al (1968)

These formulae were suitable for Re 200-3000, and are based on the diameter of the first and last turns of the spiral.

$$f_c = 16.1\left[e^{\left(3.554\frac{d}{D_{\max}}\right)} - e^{\left(3.554\frac{d}{D_{\min}}\right)}\right]\mathrm{Re}^{-0.5} \qquad \text{Equation E.1.4.1}$$

and

$$f_c = 0.7716\left[e^{\left(16.1\frac{d}{D_{av}}\right)}\right]\mathrm{Re}^{-0.5} \qquad \text{Equation E.1.4.2}$$

Kubair and Kuloor (1966) - referenced in Srinivasan et al (1968) and Ali and Seshadri (1971)

The equation used the arithmetic mean of the first and last turns of the spiral. They used the following equation to fit their own data for $300 < \mathrm{Re} < 7000$.

$$f_c = 12.74\left[\frac{d^2}{lD_{av}}\right]^{0.3}\mathrm{Re}^{-0.5} \qquad \text{Equation E.1.4.3}$$

E.1.5 Spiral friction factor equations - Turbulent

Kubair and Kuloor (1966) - referenced in Srinivasan et al (1968) and Ali and Seshadri (1971)

This equation for turbulent flow is based is on the authors experimental results. This was referenced in Srinivasan et al (1968) and Ali and Seshadri (1971).

$$f_c = 0.079\,\mathrm{Re}^{-0.25} + 0.1025\left(\frac{d}{D_{av}}\right)^{0.9} \qquad \text{Equation E.1.5.1}$$

E.1.6 Spiral critical Reynolds number equations

Kubair and Kuloor (1966) - referenced Srinivasan et al (1968) and Ali and Seshadri (1971)

This formula was modified from Kubair and Varrier's (1961-62) equation for coils, replacing the coil diameter with the average spiral diameter.

$$\mathrm{Re}_{Crit} = 12730\left(\frac{d}{D_{av}}\right)^{0.2} \qquad \text{Equation E.1.6.1}$$

Srinivasan et al (1968)

This equation was modified from Srinivasan's equation for coils, using the coil maximum diameter. This was also shown in Ali and Seshadri (1971).

$$\mathrm{Re}_{Crit} = 2100\left[1 + 12\left(\frac{d}{D_{\max}}\right)^{0.5}\right] \qquad \text{Equation E.1.6.2}$$

Ali and Seshadri (1971)

Ali found two critical Reynolds numbers in a spiral.

$$\mathrm{Re}_{critI} = 2100\left[1 + 4.9\left(\frac{d}{R_{\max}}\right)^{0.21}\left(\frac{p}{R_{\max}}\right)^{0.1}\right] \qquad \text{Equation E.1.6.3a}$$

$$\mathrm{Re}_{critII} = 2100\left[1 + 6.25\left(\frac{d}{R_{\min}}\right)^{0.17}\left(\frac{p}{R_{\min}}\right)^{0.1}\right] \qquad \text{Equation E.1.6.3b}$$

R_{max} - maximum radius of coil
R_{min} - minimum radius of coil
P - pitch of coil

E.1.7 Annular coil friction factor equations

Xin et al (1997)

This equation applies when Dn = 35-20000, d_o/d_i = 1.61 –1.67 and $D/(d_o - d_i)$ = 21 – 32

$$f = 0.02985 + 75.89 \frac{\left[0.5 - a\tan\left(\frac{Dn - 39.88}{77.56}\right)\Big/\pi\right]}{\left(\frac{D}{d_o - d_i}\right)^{1.45}} \qquad \text{Equation E.1.7.1}$$

d_o - inner diameter of outer tube
d_i - outer diameter of inner tube

E.2 Two phase flow

E.2.1 Coil friction factor equations

Rippel et al (1966)

This equation applies for a d=1.27cm, D=20.32cm coil.

For annular flow

$$\left(\frac{\Delta P}{\Delta l}\right)_{TP} = \left(\frac{\Delta P}{\Delta l}\right)_{G} + 4.44\lambda^{0.86}\frac{\rho_G u_2^{\,2}}{gd} \qquad \text{Equation E.2.1.1a}$$

For bubble and slug flow

$$\left(\frac{\Delta P}{\Delta l}\right)_{TP} = \left(\frac{\Delta P}{\Delta l}\right)_{G} + 31.3\lambda^{1.25}\frac{\rho_G u_2^{\,2}}{gd} \qquad \text{Equation E.2.1.1b}$$

For Stratified flow

$$\left(\frac{\Delta P}{\Delta l}\right)_{TP} = \left(\frac{\Delta P}{\Delta l}\right)_{G} + 3.20\lambda^{0.875}\frac{\rho_G u_2^{\,2}}{gd} \qquad \text{Equation E.2.1.1c}$$

λ = liquid volumetric fraction, $Q_L/(Q_L+Q_G)$

Akagawa et al (1971)

This empirical equation was for upward flow in coils of d/D = 1/11 and 1/22.7, when d was 9.92mm.

$$\frac{\Delta P_{TP(coil)}}{\Delta P_{L(straight)}} = \frac{f_{L(coil)}}{f_{L(straight)}} + 9.63\left(1+1.7\frac{d}{D}\right)\left(\frac{\mathrm{Re}_G}{\mathrm{Re}_L}\right)^{0.747} \mathrm{Re}_L^{-0.019} \qquad \text{Equation E.2.1.2}$$

Czop et al (1994)

A suggestion for the Martinelli parameter in turbulent, upflow in coils. Best results were achieved in conjunction with Chisholm (1967).

$$X = \left(\frac{1-x}{x}\right)^{0.924}\left(\frac{\mu_G}{\mu_L}\right)^{-0.07585}\left(\frac{\rho_G}{\rho_L}\right)^{0.5} \qquad \text{Equation E.2.1.3}$$

Awwad et al (1995a)

Using the Lockhart and Martinelli principle, incorporating an extra factor with the Froude number, Fr, to account for effect of liquid velocity. This was derived for horizontal coils.

$$\phi_L = \left(\frac{X}{9.63F_d^{0.61}}\right)\left(1+\frac{12}{X}+\frac{1}{X^2}\right)^{1/2} \qquad \text{Equation E.2.1.4}$$

where F_d is defined as

$$F_d = Fr\left(\frac{d}{D}\right)^{0.1} = \frac{u_L^2}{gd}\left(\frac{d}{D}\right)^{0.1} \qquad \text{Equation E.2.1.5}$$

Awwad et al (1995b)

Non-linear data regression was used to produce a slightly different version of the previous equation. The value of C and n depend on the value of F_d. When $F_d \leq 0.3$, C = 7.79 and n = 0.576. When $F_d > 0.3$, C = 13.56 and n = 1.3. F_d is as defined before.

$$\phi_L = \left(\frac{X}{C[F_d]^n}\right)\left(1+\frac{12}{X}+\frac{1}{X^2}\right)^{1/2} \qquad \text{Equation E.2.1.6}$$

Xin et al (1996)

For vertical coil flow when $F_d \leq 0.1$.

$$\frac{\phi_L}{\left(1+20/X+1/X^2\right)^{1/2}} = 1+\frac{X}{65.45F_d^{0.6}} \qquad \text{Equation E.2.1.7a}$$

For $F_d > 0.1$

$$\frac{\phi_L}{\left(1+20/X+1/X^2\right)^{1/2}} = 1+\frac{X}{434.8F_d^{1.7}} \qquad \text{Equation E.2.1.7b}$$

Where F_d is defined as, where β is the helix angle

$$F_d = Fr\left(\frac{d}{D}\right)^{1/2}(1+\tan\beta)^{0.2}$$

$$= \frac{u_L^{\,2}}{gd}\left(\frac{d}{D}\right)^{1/2}(1+\tan\beta)^{0.2} \qquad \text{Equation E.2.1.8}$$

E.2.2 Annular coil friction factor equations

Xin et al (1997)

For vertical coils, when d_o/d_i =1.61 – 1.67 and $D/(d_o-d_i)$ = 21-32.

$$\phi_L^{\,2} = 1+\frac{10.646}{X}+\frac{1}{X^2} \qquad \text{Equation E.2.2.1a}$$

For horizontal flow, using the Froude number, Fr, when d_o/d_i = 1.61-1.67 and d_o = 21.18mm and $D/(d_o-d_i)$ =21. The single-phase friction factor can be calculated, as shown before for the annular coil.

$$\phi_L = \left(1+\frac{0.0435X^{1.5}}{F}\right)\left(1+\frac{10.646}{X}+\frac{1}{X^2}\right)^{1/2} \qquad \text{Equation E.2.2.1b}$$

When $F = Fr^{0.9106}e^{0.0458(\text{In Fr})\text{^}2}$ and the Froude number is:

$$Fr = \frac{u_L^{\,2}}{g(d_o-d_i)} \qquad \text{Equation E.2.2.2}$$

F Determination of the coil fittings effects

F.1 Determination of the coil friction factor

The measured experimental pressure drop for the coils included the pressure drop due to the fittings as well as the coil. The effect of the fittings varied with coil length. A large proportion of the total pressure drop when the shortest coil was used would have been due to the fittings. The method shown below was used to determine the pressure drop due to the coil alone, for single-phase water flow.

The friction factor was assumed to be the same for each length of a particular coil diameter. By rearranging equation 2.3.1.2, used to calculate the frictional pressure drop in a straight pipe, the pressure drop can be shown to be proportional to the sum of the coil length, l_{coil}, and the equivalent length of the fittings, $l_{fittings}$. This is shown as equation F.1. For a particular coil diameter, the factors in the first bracket were assumed to remain constant. The correlation of pressure drop against coil length should therefore be linear and vary with flowrate. The intercept from the linear correlation would then correspond to the pressure losses due to the fittings, which would also vary with flowrate.

$$\Delta P = \left(\frac{4f\rho}{2d}\right)\left(l_{coil} + l_{fittings}\right)u^2 \qquad \text{Equation F.1}$$

The single-phase water pressure drop for particular flowrates in each coil was determined from Figure 6.2.1. Pressure drop was then plotted against tube length for a range of flowrates. This is shown in Figures F.1 and F.2, for the 0.029m and 0.079m diameter coils respectively. Linear correlations were produced for each flowrate and coil diameter. The gradients and intercepts are shown in Table F.1.

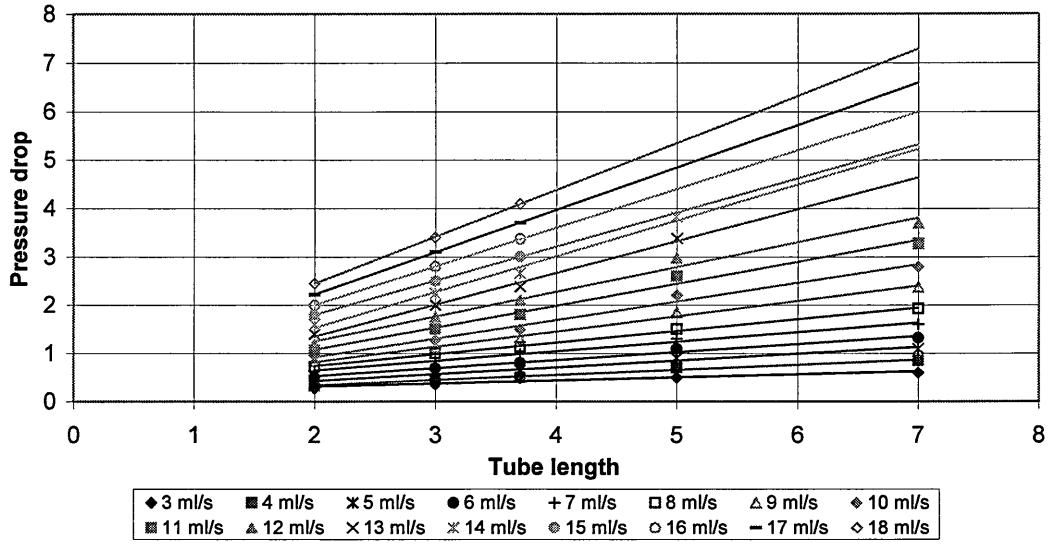

Figure F.1 Correlation of pressure drop versus tube length for a range of flowrates for D=0.029m.

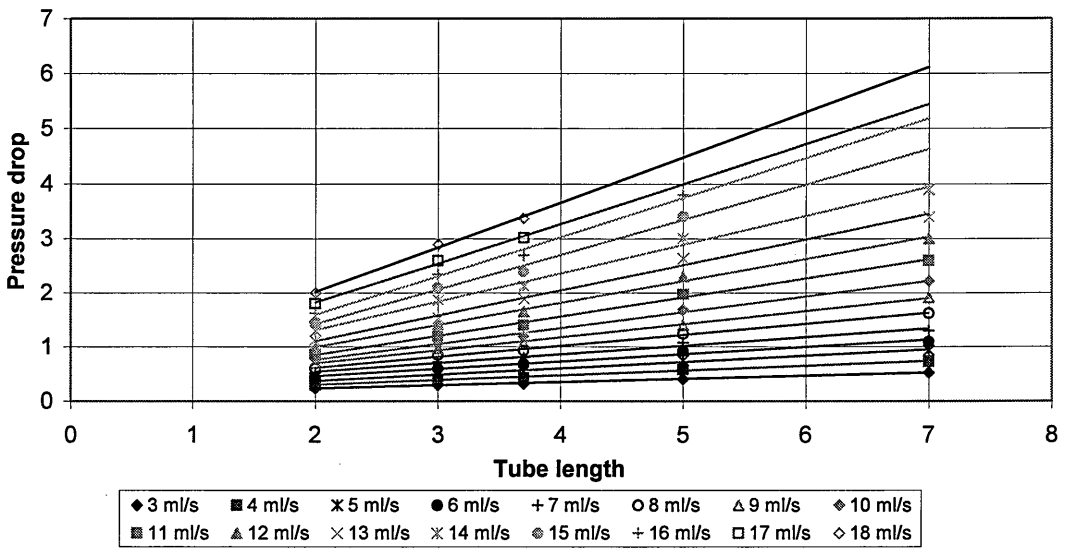

Figure F.2 Correlation of pressure drop versus tube length for a range of flowrates for D=0.079m.

Flowrate (ml/s)	Velocity (m/s)	Reynolds number	D=0.029m		D=0.079m	
			Gradient (Bar/m)	Intercept (Bar)	Gradient (Bar/m)	Intercept (Bar)
3	**0.61**	**1528**	0.0614	0.1917	0.0582	0.1192
4	**0.81**	**2037**	0.1003	0.1259	0.0867	0.1292
5	**1.02**	**2546**	0.1405	0.1442	0.1154	0.1444
6	**1.22**	**3056**	0.1662	0.1961	0.1354	0.1876
7	**1.43**	**3565**	0.1984	0.2487	0.1586	0.2273
8	**1.63**	**4074**	0.2422	0.2531	0.2026	0.2092
9	**1.83**	**4584**	0.315	0.1918	0.2396	0.2181
10	**2.04**	**5093**	0.3842	0.1536	0.292	0.1813
11	**2.24**	**5602**	0.4548	0.1633	0.3545	0.1404
12	**2.44**	**6112**	0.5108	0.2313	0.408	0.1811
13	**2.65**	**6621**	0.6572	0.0392	0.4684	0.1769
14	**2.85**	**7130**	0.7393	0.0503	0.5258	0.2631
15	**3.06**	**7639**	0.7055	0.3874	0.6411	0.1419
16	**3.26**	**8149**	0.8	0.4	0.7174	0.1604
17	**3.46**	**8658**	0.8774	0.4589	0.7238	0.3758
18	**3.67**	**9167**	0.9692	0.5061	0.8178	0.3884

Table F.1 The correlation data for pressure drop versus tube length for a range of flowrates, for both diameters of coil.

The intercept of the correlations corresponded to the loss of a 0m long coil and hence the losses due to the fittings. Using only the gradient of the correlations, as shown in Table F.1, enabled the pressure drop due to the coil alone to be found. The gradient represents the pressure drop per tube length and has been plotted against velocity for both the 0.029 and 0.079m coil diameters in Figure F.3. This was then used to determine the friction factors for each coil diameter.

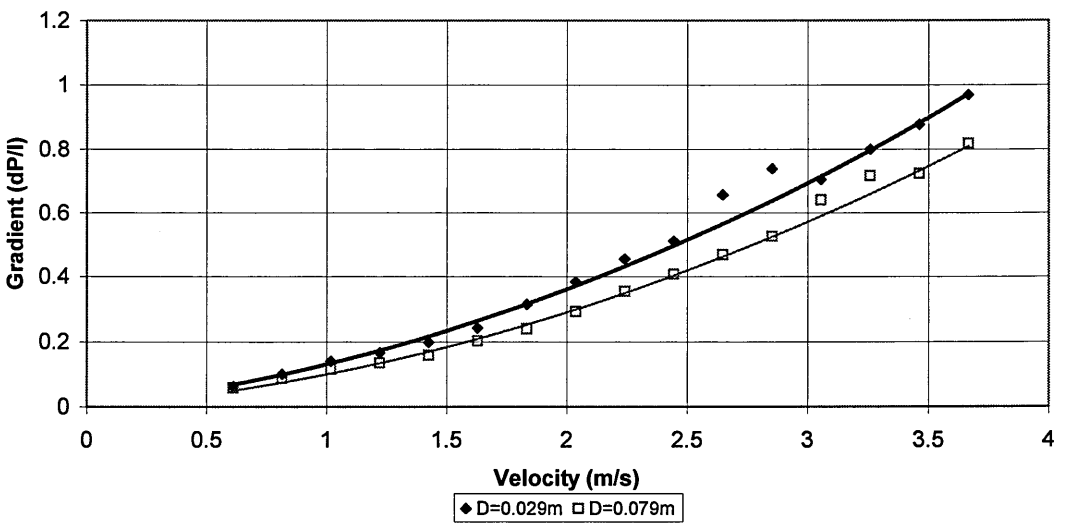

Figure F.3 Pressure drop per unit length versus velocity for both coil diameters for the single-phase water experiments.

F.2 Percentage of the total pressure drop attributable to the fittings

The percentage of the total pressure drop attributable to the fittings was found for each coil length. This was calculated by dividing the pressure drop due to the fittings, calculated using the method outlined above, by the total experimental pressure drop. This was found to vary with flowrate. Up to 50% of the total pressure drop with the 2m coil was found to be due to the fittings and up to 20% with the 7m coil. Figure F.4 shows the percentage effects of the fittings versus flowrate for the 5m long coils.

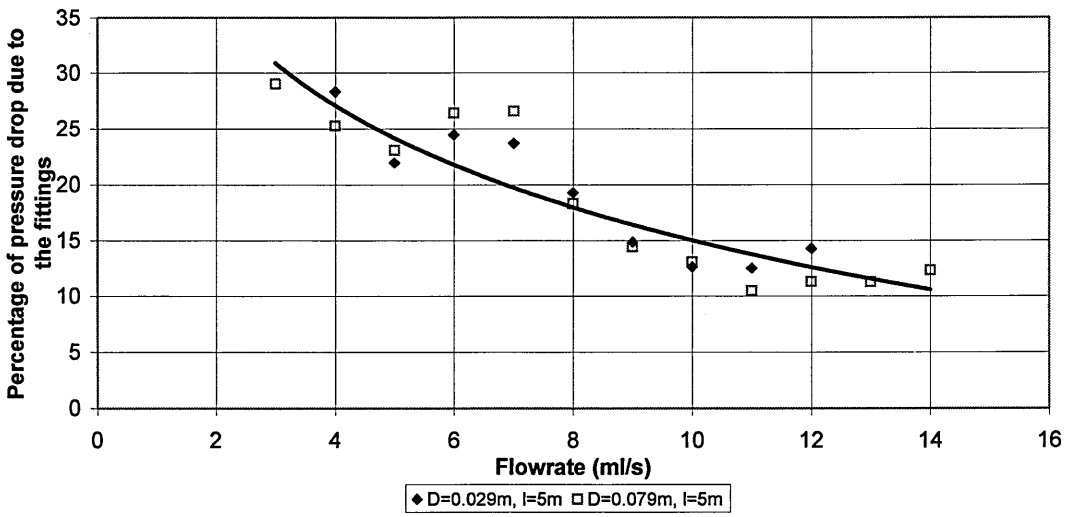

Figure F.4 The percentage of the total pressure drop, attributable to the fittings for various flowrates with the 5m long coils.

With the single-phase water experiments, a 5m long straight pipe and a 5m long 0.139m diameter coil, were tested. The effect of the fittings on these results were determined by finding the percentage of the total pressure drop attributable to the fittings, for the 5m long, 0.029m and 0.079m diameter coils. Figure F.4 shows that, the percentage effect of the fittings was similar for these coils. Hence, a correlation was produced by combining the results from the 5m long, 0.029m and 0.079m diameter coils to determine the mean percentage effect of the fittings. This correlation, as well as the correlations for the other coil lengths, are shown in Table F.2.

Length of tube (m)	Correlation
2	$\%\Delta P_{fitting} = -19.9 \ln Q + 71.7$
3	$\%\Delta P_{fitting} = -17.3 \ln Q + 60.8$
3.7	$\%\Delta P_{fitting} = -14.5 \ln Q + 48.1$
5	$\%\Delta P_{fitting} = -13.2 \ln Q + 45.4$
7	$\%\Delta P_{fitting} = -12.3 \ln Q + 34.0$

Table F.2 Equations to calculate the percentage of the total pressure drop attributable to the fittings.

G New equation for the friction factor in a coil

A new equation to calculate the friction factor within a coil was formulated, by assuming a coil to be a series of 90° bends. Coil losses have been assumed to be made up of the losses due a straight pipe of the same length and 90° bends. As the losses in bends and straight pipes are well documented in the literature, but not for coils, the approach could be used to calculate the losses in coils with any dimensions. In this thesis, the losses in bends are taken from Miller (1990). Similar results were obtained by treating a coil as a series of 180° bends.

The number of 90° bends in a coil, n_b, can be calculated from the coil length, l, and diameter, D. This is shown as equation G.1. The loss coefficient of a coil can then be directly calculated from the losses in 90° bends, as shown by equation G.2.

$$n_b = \frac{4l}{\pi D} \qquad \text{Equation G.1}$$

$$K_c = K_b \frac{4l}{\pi D} \qquad \text{Equation G.2}$$

where

n_b - number of 90° bends
K_b - loss coefficient of a bend (from Miller)
K_c - loss coefficient of a coil

Miller (1990) stated that the losses in a bend depend on its diameter. Figure G.1 shows how the loss coefficient in a bend, K_b, varies with the ratio of bend radius, r, to pipe diameter, d, for different bend angles.

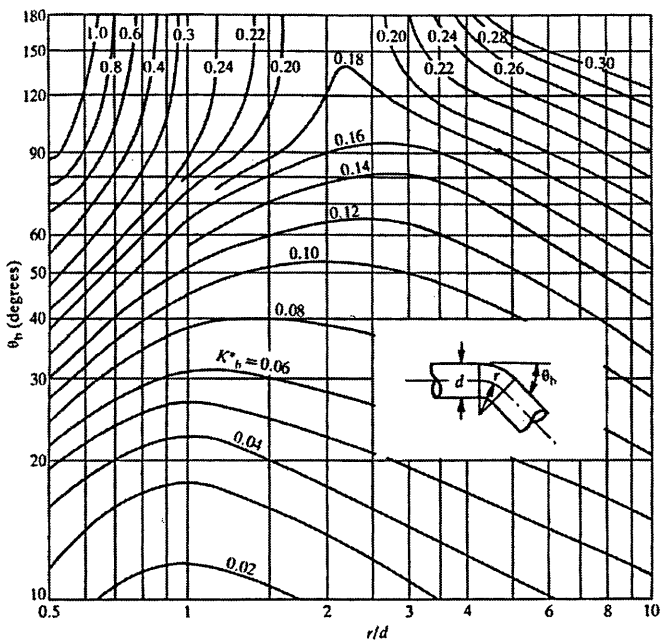

Figure G.1 Loss coefficients, K_b, for circular cross-sectional bends, Miller (1990).

As these calculations use the losses in 90° bends, Figure G.1 was redrawn for 90° bends alone. This was done by drawing a line across the 90° bends in Figure G.1 and replotting loss coefficient against the bend dimensions. Figure G.2 shows the bend dimensions converted to the ratio of tube diameter, d, to coil diameter, D, as used in this thesis. Correlating the data produced equation G.3, so the loss coefficient could be calculated in terms of d/D.

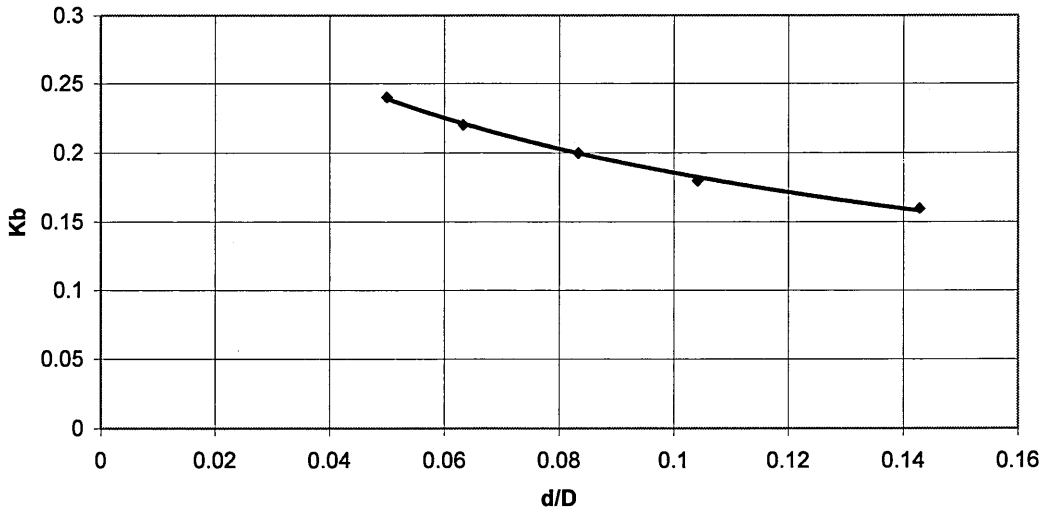

Figure G.2 Correlation of d/D versus the loss coefficient for 90° bends.

$$K_{b\ (high\ Re)} = -0.0768\ln(d/D) + 0.0089 \qquad \text{Equation G.3}$$

Figure G.1 applies to Reynolds numbers with the order of 10^6, which is far higher than the values of the present experiment. Miller showed a correction chart for variations in Reynolds number. This is shown as Figure G.3

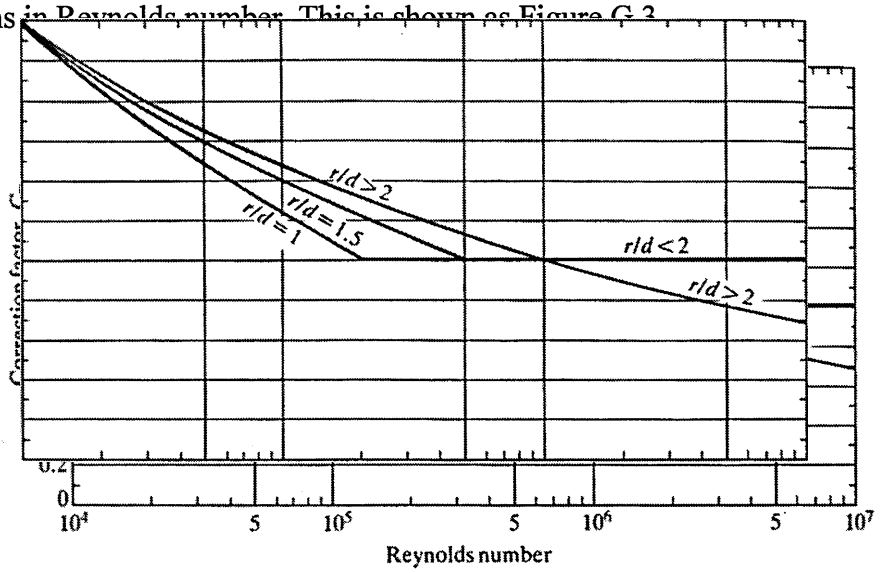

Figure G.3 Reynolds number correction factors. Miller (1990).

The experiments coils were all in the r/d>2 range. Equation G.4 shows a correlation of the correction factor in terms of the Reynolds number, for the r/d>2 range. The Reynolds numbers in Figure G.3 are greater than the experimental values calculated in this thesis, therefore equation G.4 was used to interpolate the values.

$$Re_{correct\ factor} = 9.9531\ Re^{-0.1653} \qquad \text{Equation G.4}$$

A large proportion of the losses due to a bend occur downstream of a bend. In coils these additional losses would not occur as there is another bend immediately afterwards. Miller stated correction factors for bend-bend interactions. For two bends at 180°, like in a coil, with no spacer between the bends and for both bends with r/d of 3, the correction factor was stated to be 0.71. The coils used had r/d values of greater than 3 but this was the nearest value stated in Miller.

A general equation can now be formed to calculate the losses in a 90° bend. This is shown as equation G.5.

$$\begin{aligned} K_b &= (-0.0768 \ln (d/D) + 0.0089) \times 9.9531\ Re^{-0.1653} \times 0.71 \\ &= Re^{-0.1653} (-0.7644 \ln (d/D) + 0.0886) \end{aligned} \qquad \text{Equation G.5}$$

The loss coefficient of the bends in a coil was found by combining equations G.2 and G.5, to produce equation G.6.

$$K_c = \left(Re^{-0.1653} \left(-0.5427 \ln\left(\frac{d}{D}\right) + 0.0629 \right) \right) \frac{4l}{\pi D}$$

$$K_c = \left(Re^{-0.1653} \frac{4l}{D} \left(-0.1727 \ln\left(\frac{d}{D}\right) + 0.02 \right) \right) \qquad \text{Equation G.6}$$

The total loss through a coil can then be calculated by summing the frictional loss in a straight pipe of the same length, equation G.7, and the loss through the equivalent number of 90° bends, equation G.6.

$$\Delta h_{straight} = 4 f_s \frac{l}{d} \frac{u^2}{2g} \qquad \text{Equation G.7}$$

$$\Delta h_{Total} = 4 f_s \frac{l}{d} \frac{u^2}{2g} + K_c \frac{u^2}{2g} \qquad \text{Equation G.8}$$

$$= 4 \frac{u^2}{2g} \frac{l}{d} \left(f_s + K_c \frac{d}{4l} \right) \qquad \text{Equation G.9}$$

Therefore the friction factor of a coil can be calculated:

$$f_c = f_s + \left(Re^{-0.1653} \frac{4l}{D} \left(-0.1727 \ln\left(\frac{d}{D}\right) + 0.02 \right) \right) \frac{d}{4l}$$

$$f_c = f_s + \left(Re^{-0.1653} \frac{d}{D} \left(-0.1727 \ln\left(\frac{d}{D}\right) + 0.02 \right) \right) \qquad \text{Equation G.10}$$

The equation is applicable for rough and smooth coils when equation G.11, from Miller (1990), converted for Fanning friction factor, is used to calculate the turbulent friction factor. When ε is the pipe roughness.

$$f_s = \frac{0.0625}{\left[\log\left(\varepsilon/3.7d + 5.74/\mathrm{Re}^{0.9}\right)\right]^2}$$ Equation G.11

The equation ignores interference effects. Ito (1960) stated that bend resistance varies with different velocity distributions in the approach pipe. The proximity of other fittings up and downstream could also affect the resistance. A considerable portion of the energy can be lost downstream of a tangent. Ito found that the distorted flow can persist up to 50 pipe diameters downstream of a bend, but most of the loss is within 30 diameters of the bend. This would affect the losses of a coil and hence, the equation may not be totally accurate.

H Test nozzle engineering drawings

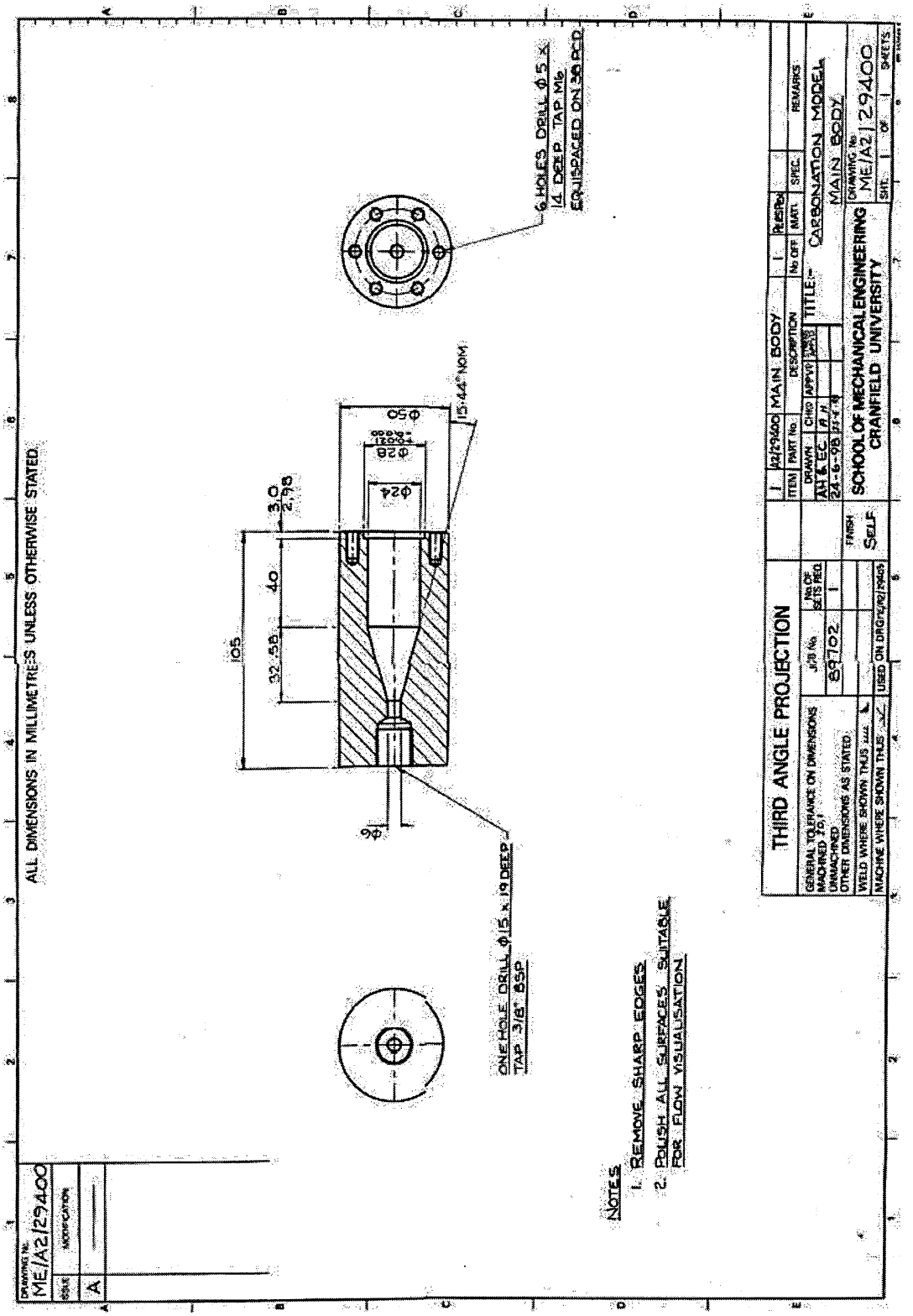

Figure H.1 Engineering drawing of the test nozzle – main body

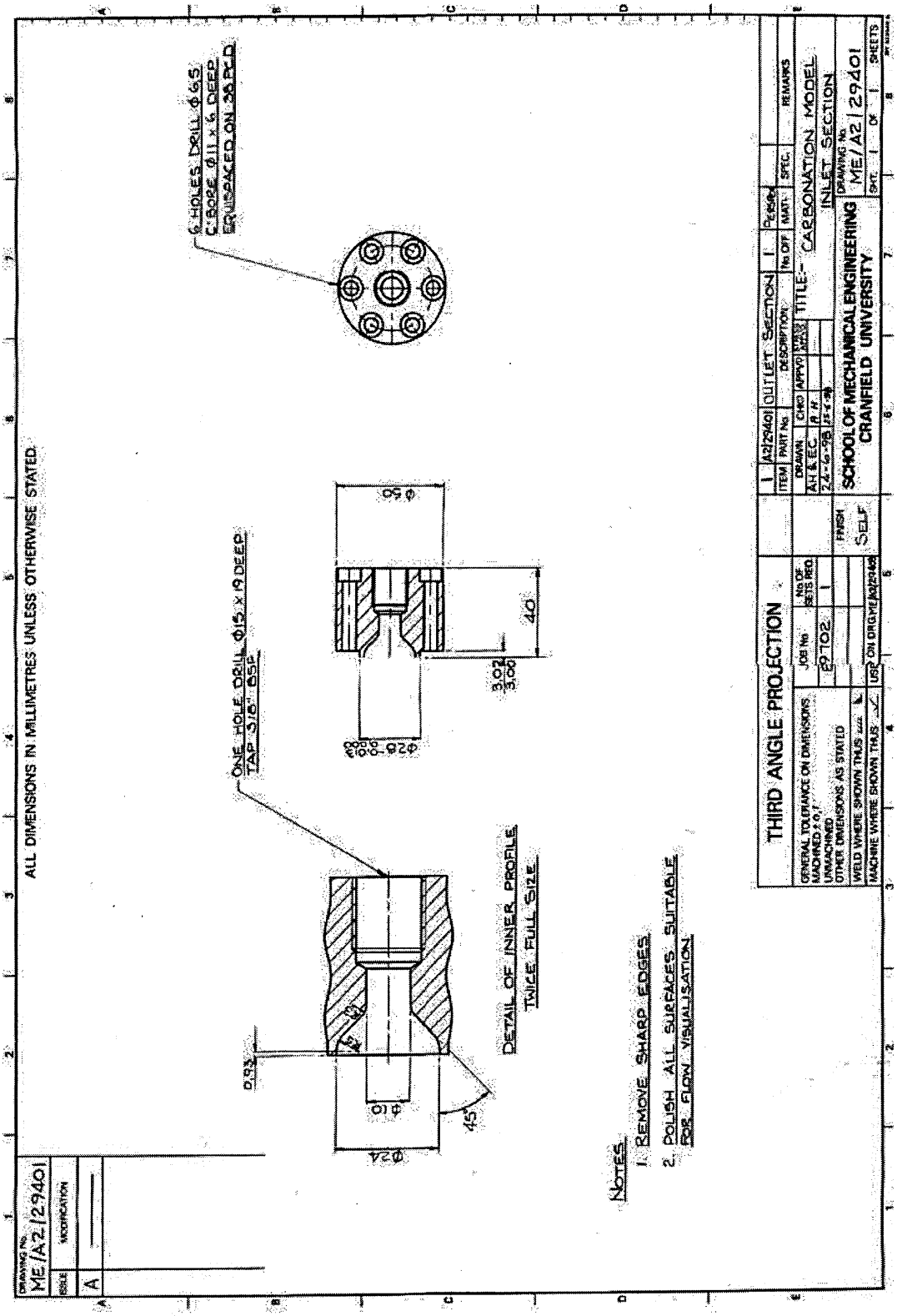

Figure H.2 Engineering drawing of the test nozzle – outlet section

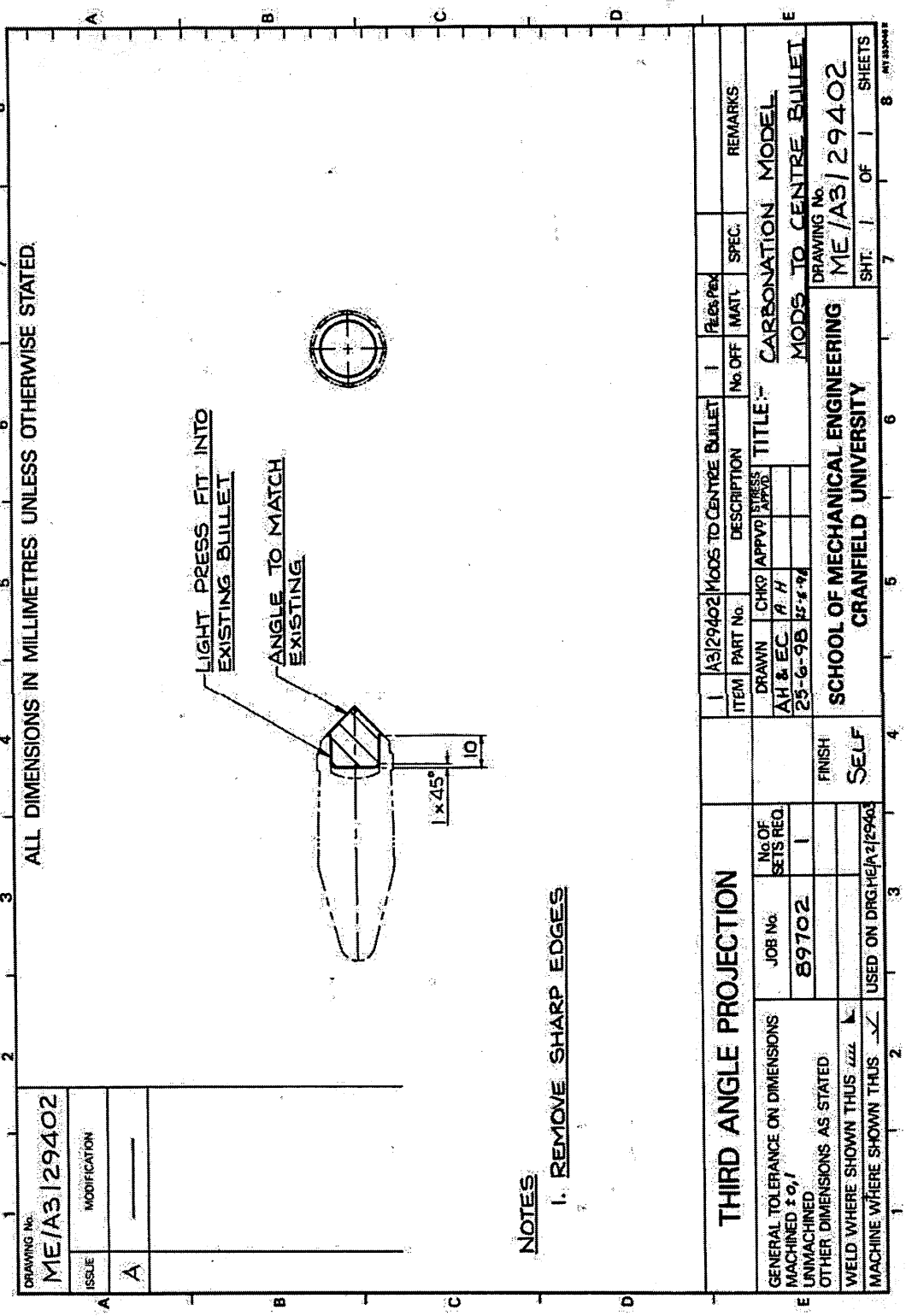

Figure H.3 Engineering drawing of the test nozzle – modifications to the central body

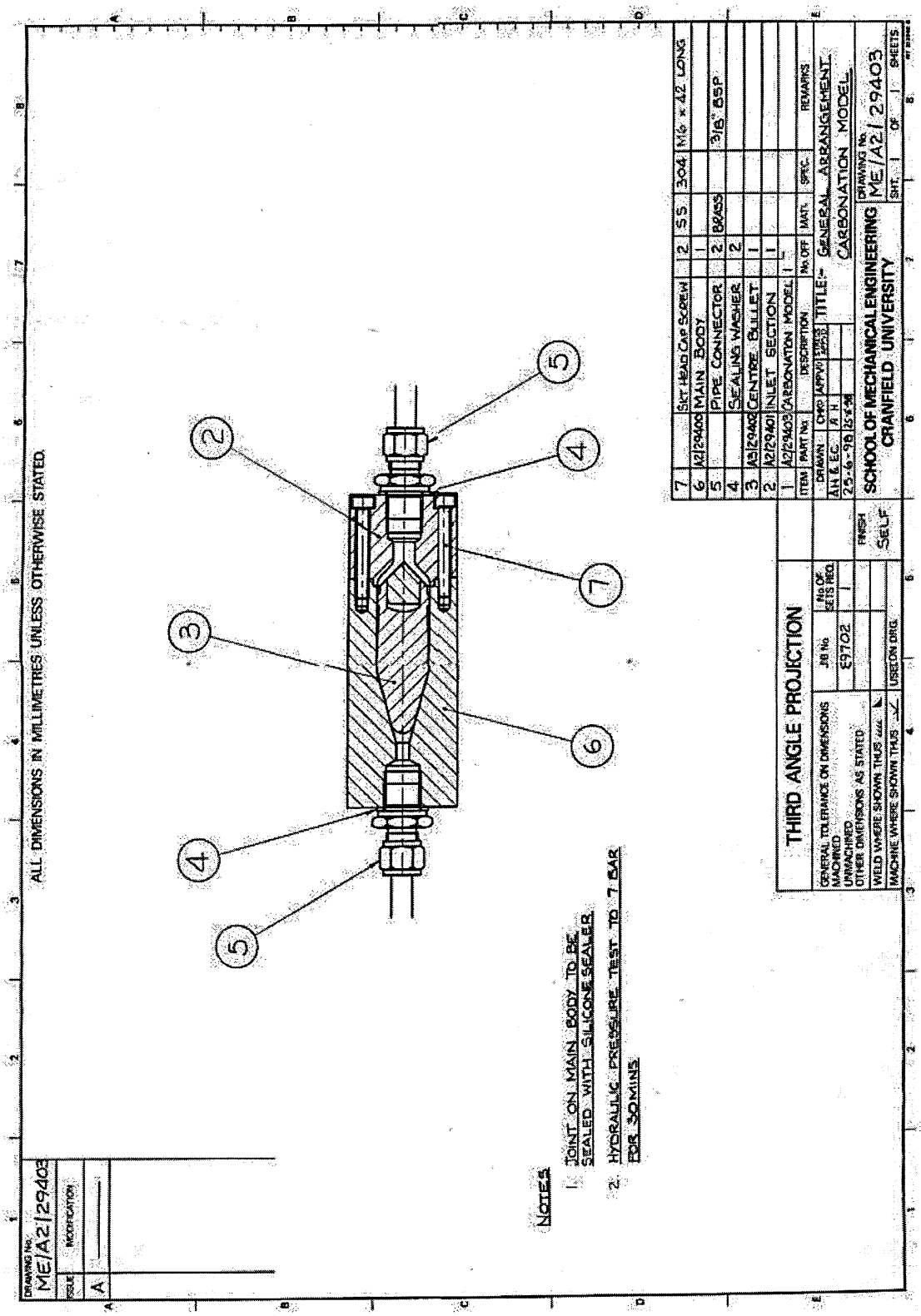

Figure H.4 Engineering drawing of the test nozzle – whole nozzle